NEW STRATEGIES IN THE EXPRESSION, PURIFICATION, AND RECONSTITUTION OF THE CYSTIC FIBROSIS TRANSMEMBRANE CONDUCTANCE REGULATOR FOR BIOCHEMICAL AND BIOPHYSICAL CHARACTERIZATION IN DIFFERENT LIPID ENVIRONMENTS

A Dissertation
Presented to
The Academic Faculty

By

Kerry M. Strickland

In Partial Fulfillment
Of the Requirements for the Degree
Doctor of Philosophy in the
School of Chemistry and Biochemistry

Georgia Institute of Technology

May 2020

NEW STRATEGIES IN THE EXPRESSION, PURIFICATION, AND RECONSTITUTION OF THE CYSTIC FIBROSIS TRANSMEMBRANE CONDUCTANCE REGULATOR FOR BIOCHEMICAL AND BIOPHYSICAL CHARACTERIZATION IN DIFFERENT LIPID ENVIRONMENTS

Approved by:

Dr. Ingeborg Schmidt-Krey, Advisor
School of Chemistry and Biochemistry
School of Biological Sciences
Georgia Institute of Technology

Dr. Bridgette Barry
School of Chemistry and Biochemistry
Georgia Institute of Technology

Dr. Raquel Lieberman
School of Chemistry and Biochemistry
Georgia Institute of Technology

Dr. Nael A. McCarty
Marcus Professor of Cystic Fibrosis
Emory University School of Medicine

Dr. Loren Williams
School of Chemistry and Biochemistry
Georgia Institute of Technology

Date Approved: [December 11, 2019]

To my friends and family.
Thank you for all of your support and love in this journey.

ACKNOWLEDGMENTS

TABLE OF CONTENTS

CHAPTER 2. ATP SIGNALING IN A REVISED HOMOLOGY MODEL OF CYSTIC FIBROSIS TRANSMEMBRANE CONDUCTANCE REGULATOR (CFTR)

CHAPTER 4. CFTR RECONSTITUTION AND FUNCTION

LIST OF TABLES

LIST OF FIGURES

Figure 1.10: Diagram of classes for CFTR mutations. The 346 currently identified disease-causing mutations are classified into one of the five above described classes. Each mutation class houses mutations that affect one of the following: protein production (class 1), protein processing (class 2), protein gating (class 3), protein conduction (class 4), or insufficient protein on the cell surface (class 5). However, many mutations can contribute to multiple classes of disfunction. The most common mutation, ΔF508, is classified as a class 2 mutation. — 24

Figure 1.11: Diagram of the current CF modulators and the tableted list of FDA-approved mutations. Currently, four different modulator therapies have been approved in single, double, or triple combination therapies and treat 39 of the 346 disease-causing mutations. These modulators are either potentiators, like ivacaftor (VX-770), or correctors, like lumacaftor (VX-809), tezacaftor (VX-661), and elexacaftor (VX-445). — 25

Figure 1.12: Electrostatic salt bridge triad identified in homology models of CFTR and molecular dynamics and confirmed by electrophysiological techniques. This catalytic triad has been investigated in the translation of ATP binding at the nucleotide binding domains (NBDs, NBD1 is pink, and NBD2 is blue) to the Transmembrane Domains (TMDs, TMD1 is gray, and TMD2 is green). This triad is investigated further in chapter II of this dissertation. — 27

Figure 1.13: Depiction of the Lasso motif in CFTR. The lasso motif (red) is a motif found in several members of the ABC transporter superfamily of proteins, in which the N-terminus tucks into the lipid bilayer. For orientation, Transmembrane Domain 1 (TMD1) is gray, nucleotide binding domain 1 (NBD1) is pink, TMD2 is green, and NBD2 is blue. PDB ID: 6MSM used to generate the figure. — 29

Figure 1.14: A structure of nanodisc formed by Membrane Scaffold Protein (MSP). An individual MSP (orange) wraps around an individual leaflet of the lipid bilayer (gray). Thus, two MSP molecules form a single nanodisc composed of a lipid bilayer. From the top-down view (A), the nanodisc in this image is of MSP1D1 and has a diameter of 9.7 nm. In the side-on view (B), a nanodisc has a height of approximately 5 nm. Images were built in Visual Molecular Dynamics (VMD) software from PDB ID: 6CM1 to show a top-down view (left) and side-on view (right) of a nanodisc. — 34

Figure 1.15: Depiction of the lipids first and commonly used to generate nanodiscs. All three lipids have the same head group (phosphatidylcholine) but differ in tail composition. The abbreviations are the following: 1,2-dimyristoyl-sn-glycero-3-phosphocholine (DMPC), 1,2-dipalmitoyl-sn-glycero-3-phosphocholine (DPPC), or 1-palmitoyl-2-oleoyl-sn-glycero-3-phosphocholine (POPC). — 35

pore architecture of CFTR. The Journal of General Physiology **144**, 159-179 . N=5 for K968A-CFTR. ***, P < 0.001 compared to WT.

yield. Immunoblotting for CFTR: Primary – 596 mouse anti-CFTR antibody, 1:1,500 and Secondary – LI-COR goat anti-mouse antibody, 1:10,000

gel stained with 0.5 µg/mL ethidium bromide. Theoretical gel for restriction digestion (left) was produced for ease of interpretation of experimental gel (right). Colony c3 was chosen as the source of pMSP1D1because the results of both restriction digestion experiments displayed anticipated banding patterns.

appears to be small liposomes. Samples were stained in 2% uranyl acetate. The scale bar corresponds to 50 nm.

three sterol derivatives—cholesterol (A), zymosterol (B), and CHS (C). These structural differences include the double bond between C-5 and C-6 of the B ring in cholesterol and CHS, but only a single bond in zymosterol. Zymosterol has a double bond present between C-8 and C-9 of the B ring, which is a single bond in cholesterol and CHS. Zymosterol also includes another double bond present between C-24 and C-25, which is a single bond in both cholesterol and CHS.

LIST OF SYMBOLS AND ABBREVIATIONS

°C	degrees Celsius
μL	microliter
μs	microsecond
2D	2-dimensional
3D	3-dimensional
Å	angstrom
ABC transporter	ATP binding cassette Transporter
ABCA	subclass A of human ABC transporters
ABCA4/ABCR	ABC transporter Subclass A number 4
ABCB	subclass B of human ABC transporters
ABCC	subclass C of human ABC transporters
ABCC7	ABC transporter Subclass C number 7/ CFTR
ABCD	subclass D of human ABC transporters
ABCD2/X-ALD	ABC transporter Subclass D number 2/ X-linked Adrenoleukodystrophy
ABCE	subclass E of human ABC transporters
ABCE1/OABP	organic anion binding protein/ABC transporter subclass E number 1
ABCF	subclass F of human ABC transporters
ABCF2	ABC transporter Subclass F number 2
ABCG	subclass G of human ABC transporters

ABCG2/BCRP	ABC transporter Subclass G number 2/breast cancer resistance protein
ADP	adenosine diphosphate
AFT	arginine-framed tripeptides
ALD	adrenoleukodystrophy protein
A-loop	particular loop structure in CFTR
AMP-PNP	adenylyl-imidodiphosphate
Arf1	ADP-ribosylation factor 1
atm	atmosphere
ATP	adenosine triphosphate
BCA	bicinchoninic acid
BHK	baby hamster kidney cells
BSA	bovine serum albumin
Ca^{2+}	calcium cation
CAL	CFTR-associated ligand protein
ccc	cross-correlation coefficient
CF	Cystic Fibrosis
CFF	Cystic Fibrosis Foundation
CFP	cyan fluorescent protein
CFTR	Cystic Fibrosis Transmembrane conductance Regulator
CFTRinh172	specific CFTR inhibitor

CHARMM36	Chemistry at Harvard Macromolecular Mechanics, force field
chCFTR	chicken CFTR
CHIP	a carboxy terminus HSP-70 interacting protein
CHO	Chinese hamster ovary cells
CHS	cholesteryl hemisuccinate
CNX	chaperone lectins calnexin
COPII	coat protein II
cRNA	complementary RNA
cryo-EC	electron cryo-crystallography
cryo-EM	electron cryo-microscopy
CTF	contrast transfer function
CV	coefficient of variation
cyclic AMP/cAMP	adenosine 3',5'-monophosphate
D110C	aspartic acid at position 92 in WT-hCFTR substituted with cysteine
D565/A566/D567	diacidic export motif in WT-hCFTR
D924	aspartic acid at position 924 in WT-hCFTR
D993	aspartic acid at position 993 in WT-hCFTR
DDM	n-dodecyl β-d-maltoside
DIBMA	diisobutylene maleic acid
DIBMALP	diisobutylene maleic acid lipid particles
DMEM	Dulbecco's Modified Eagle Medium

DMPC	1,2-dimyristoyl-sn-glycero-3-phosphocholine
DMSO	dimethyl sulfoxide
DNA	deoxyribonucleic acid
DPPC	1,2-dipalmitoyl-sn-glycero-3-phosphocholine
DTT	dithiothreitol
E267	glutamic acid at position 267 in WT-hCFTR
E543	glutamic acid at position 543 in WT-hCFTR
E92	glutamic acid at position 92 in WT-hCFTR
ECL1	extracellular loop 1
ECL2	extracellular loop 2
ECL3	extracellular loop 3
ECL4	extracellular loop 4
ECLs	extracellular loops
EDTA	ethylenediaminetetraacetic acid
EGTA	ethylene glycol-bis(β-aminoethyl ether)-N,N,N′,N′-tetraacetic acid
ER	endoplasmic reticulum
ERQC	ER quality control machinery
EtBr	ethidium bromide
F12	Ham's F12 nutrient mixture
F337	phenylalanine at position 337 in WT-hCFTR
FBS	fetal bovine serum
FC	fold change

fs	femtoseconds
GERAD	glycoprotein ER-associated degradation pathway
GGN20	alias for subclass F of ABC transporter family
GTPase	guanidine triphosphatase
hApo1	human apolipoprotein 1
hCFTR	human CFTR
HCl	hydrochloric acid
HDL	high-density lipoprotein complex
HEPES	4-(2-hydroxyethyl)-1-piperazineethanesulfonic acid
His-tag	histidine-based affinity chromatography tagging system
HOLE	program to explore pore dimensions in ion channel molecular structures
Hsp70	heat shock protein 70
Hsp90	heat shock protein 90
Hz	Hertz
ICL	intracellular loops
IPTG	isopropyl β- d-1-thiogalactopyranoside
IRES	internal ribosomal entry site
I-V	Current-Voltage relationship
K	Kelvin
K1060	lysine at position 1060 in WT-hCFTR
K1292	lysine at position 1292 in WT-hCFTR

K892C	lysine at position 892 in WT-hCFTR substituted with cysteine
K95	lysine at position 95 in WT-hCFTR
K968	lysine at position 968 in WT-hCFTR
KCl	potassium chloride
kHz	kiloHertz
L1135	leucine at position 1135 in WT-hCFTR
LmrA	ATP binding cassette (ABC) multidrug transporter found in *Lactococcus lactis*
LPR	lipid to protein ratio
M	molarity
mA	milliAmps
MβCD	methyl-beta-cyclodextrin
MD	molecular dynamics
MDFF	molecular dynamics flexible fitting
MDR	multidrug resistance
mg	milligrams
Mg^{2+}	magnesium cation
MgATP	ATP magnesium salt
$MgCl_2$	magnesium chloride
mL	milliliter
mM	millimolar
MOI	multiplicity of infection

MRP	multidrug resistance-associated protein
MRP1 (ABCC1)	multidrug resistance protein 1/ ABC transporter subclass C number 1
MRP7	multidrug resistance protein 7
MRP9	multidrug resistance protein 9
ms	milliseconds
MS	mass spectrometry
MsbA	lipid ABC exporter
MSD1	membrane spanning domain 1
MSP	membrane scaffold protein
mV	milliVolts
MWCO	molecular weight cut-off
MΩ	megaohm
N1138	asparagine at position 1138 in WT-hCFTR
N894	asparagine at position 894 in WT-hCFTR
N900	asparagine at position 900 in WT-hCFTR
Na^+	sodium cation
NaCl	sodium chloride
NaH_2PO_4	sodium phosphate monobasic
NAMD	Nanoscale Molecular Dynamics
NBD	nucleotide binding domain
NBD1	nucleotide binding domain 1
NBD2	nucleotide binding domain 2

NBF	nucleotide binding fold
ng	nanogram
NHERF-1	Na^+/H^+ exchanger regulatory factor proteins
NMDG	N-methyl-d-glycamine
NMDG-Cl	N-methyl-d-glucamine chloride salt
NTA	nitrilotriacetic acid
OST	oligosaccharyltransferase
P/S	penicillin/streptomycin
PBS	phosphate buffered saline
PBST	phosphate buffered saline plus Tween 20
pCDNA3.1	mammalian expression vector
pcDNA5/TO	vector for protein expression in T-Rex™ CHO cells
PDB	Protein Database
PDZ-binding domain	post synaptic density protein, *Drosophila* disc large tumor suppressor, and zonula occludens-1 protein
pGEMHE	oocyte expression vector
P-gp (ABCB1)	P-glycoprotein/ ABC transporter subclass B number 1
pH	log of $[H^+]$
P_i	inorganic phosphate
PIC	protease inhibitor cocktail
PKA	protein kinase A
PKC	Protein kinase C
PLB	planar lipid bilayer

PM	plasma membrane
P_o	open probablity
POPC	1-palmitoyl-2-oleoyl-sn-glycero-3-phosphocholine
pS	picoSiemens
PVDF	polyvinylidene difluoride
Q-loop	particular loop structure in CFTR
R1128	arginine at position 1128 in WT-hCFTR
R29/Q30/R31	one of 4 RXR motifs in WT-hCFTR
R303	arginine at position 303 in WT-hCFTR
R347	arginine at position 347 in WT-hCFTR
R516/Y517/R518	one of 4 RXR motifs in WT-hCFTR
R553/A554/R555	one of 4 RXR motifs in WT-hCFTR
R764/R765/R766	one of 4 RXR motifs in WT-hCFTR
R899	arginine at position 899 in WT-hCFTR
R933	arginine at position 933 in WT-hCFTR
Rab1a/Rab2	GTPase proteins important in secretory trafficking
R-domain	Regulatory domain
R_G	radius of gyration
RIPA	radioimmunoprecipitation Assay
RMSD	root mean square deviation
RPM	revolutions per minute
RT	room temperature
RTC	Ribosome-Sec61 translocon complex

RXR motif	ER retention/retrieval motif of membrane proteins
S341	serine at position 341 in WT-hCFTR
S422	serine at position 422 in WT-hCFTR
S660	serine at position 660 in WT-hCFTR
S670	serine at position 670 in WT-hCFTR
S686	serine at position 686 in WT-hCFTR
S686	serine at position 686 in WT-hCFTR
S700	serine at position 700 in WT-hCFTR
S700	serine at position 700 in WT-hCFTR
S712	serine at position 712 in WT-hCFTR
S737	serine at position 737 in WT-hCFTR
S753	serine at position 753 in WT-hCFTR
S768	serine at position 768 in WT-hCFTR
S790	serine at position 790 in WT-hCFTR
S795	serine at position 795 in WT-hCFTR
S813	serine at position 813 in WT-hCFTR
S898	serine at position 898 in WT-hCFTR
Sav1866	ABC transporter from *Staphylococcus aureus*
SDS-PAGE	sodium dodecyl sulfate-polyacrylamide gel electrophoresis
Sec24	protein involved in ER transport vesicles formation
Sec61	protein involved in membrane protein translocation
SEM	standard error of the mean

Sf9	immortalized cell line from *Spodoptera frugiperda*
SMA	styrene maleic acid
SMALP	styrene maleic acid lipid particles
SMA-QA	SMA with a quaternary ammonium
SMA-SH	SMA with exposed sulfhydryls
SMI	styrene maleimide
SMILPs	stryene maleimide lipid particles
SNARE	protein complex that mediates vesicle fusion
SPA	single particle analysis
SRP	signal recognition particle
SUR1	sulfonylurea receptors 1
SUR2	sulfonylurea receptors 2
T1134	threonine at position 1134 in WT-hCFTR
T338	threonine at position 338 in WT-hCFTR
T690	threonine at position 690 in WT-hCFTR
T787	threonine at position 787 in WT-hCFTR
T788	threonine at position 788 in WT-hCFTR
TAP	transporter associated with antigen processing
TBS	Tris-buffered saline
TBST	Tris-buffered saline with Tween-20
TEM	transmission electron microscopy
TES	2-[(2-Hydroxy-1,1-bis(hydroxymethyl)ethyl)amino]ethanesulfonic acid,

	N-[Tris(hydroxymethyl)methyl]-2-aminoethanesulfonic acid
TIP3P	water modeling system
TM1	transmembrane helix 1
TM10	transmembrane helix 10
TM11	transmembrane helix 11
TM12	transmembrane helix 12
TM2	Transmembrane helix 2
TM3	transmembrane helix 3
TM4	transmembrane helix 4
TM5	transmembrane helix 5
TM6	transmembrane helix 6
TM7	transmembrane helix 7
TM8	transmembrane helix 8
TM9	transmembrane elix 9
TMD	transmembrane domain
TMD1	transmembrane domain 1
TMD2	transmembrane domain 2
T-Rex CHO	modified CHO cell line for protein expression
Tris	tris(hydroxymethyl)aminomethane
U	Units
UDP	uridine diphosphate
UGGT	UDP-glycoprotein glucosyltransferase

V	volts
V350	valine at position 350 in WT-hCFTR
VMD	Visual Molecular Dynamics
WT	wildtype
x-loop	particular loop structure in CFTR
zCFTR	zebrafish CFTR
zSMA	derivative of SMA
zSMALP	derivative of SMALPs
ΔF508	mutant version of CFTR, deletion of phenylalanine at position 508 in WT-hCFTR
ΔR$_{708\text{-}835}$CFTR	mutant version of WT-hCFTR

SUMMARY

Membrane proteins are difficult to study in solution due to the use of detergent to protect the hydrophobic portion of the protein that interacts with the fatty acid tails of the lipid bilayer. However, a recent technology called nanodiscs provides a packaged lipid bilayer system in which membrane proteins can be studied in solution in a lipid environment and thus without the use of detergent. Nanodiscs have revolutionized the study of membrane proteins, even difficult and complex membrane proteins. A particularly challenging membrane protein, the Cystic Fibrosis Transmembrane conductance Regulator (CFTR), has shown to be very sensitive to the detergent and lipid environment, especially during purification and reconstitution. This dissertation explored new methods of expression, purification, reconstitution, functional assays, and structurally important lipids for human CFTR. The development of multiple expression systems improved detergent purification methods and increased the yield of functional CFTR. The utilization of nanodiscs technology has provided a method of measuring changes in CFTR's ATPase activity dependent on the environment and may provide a new method for determining structure-induced changes to CFTR that are dependent on the environment. The identification of possibly key structural lipids in detergent-solubilized CFTR and some preliminary investigation into the annular lipid environment of CFTR was completed by lipidomics mass spectrometry. This dissertation also utilized both traditional and nontraditional molecular modeling methods to refine a CFTR homology model and study a key interaction in the translation of ATP binding in the nucleotide binding domains (NBDs) to the transmembrane domains (TMDs).

CHAPTER I

INTRODUCTION

1.1. INTRODUCTION.

1.1.1. Publications resulting from this chapter.

Parts of this chapter will be published in *Methods in Molecular Biology* on the reconstitution of membrane proteins. Other parts of this chapter will be published in downstream manuscripts.

1.2. MEMBRANE PROTEINS.

Membrane proteins are essential for maintaining physiological processes and are the main target of pharmaceutical drugs. Studying membrane proteins can be challenging due to the hydrophobic region of the protein that interacts with the fatty acid tails of the lipid bilayer. Detergents can protect the hydrophobic region of membrane proteins from the aqueous environment by housing those regions in a non-physiological environment. However, studying membrane proteins in a lipid environment, the more physiologically relevant environment, has traditionally been more difficult. New technologies, discussed below, have improved traditional challenges and revealed the importance of the lipid environment to membrane proteins (1). Understanding the role the lipidic environment plays in maintaining or altering membrane protein structure and function can improve our understanding of drug design (2).

1.2.1. Adenosine triphosphate (ATP) binding cassette (ABC) transporters.

The adenosine triphosphate (ATP) binding cassette (ABC) transporters represent a superfamily of mainly membrane proteins, expressed in both prokaryotes and eukaryotes.

Of the 49 known human ABC transporters, almost 50% are involved in the regulation of

the lipid bilayer (3, 4). The human ABC transporters are organized into 7 subclasses—

ABCA, ABCB, ABCC, ABCD, ABCE, ABCF, and ABCG (Table 1.1) (5). While each

Table 1.1: Table of Human ABC transporter subclasses—ABCA through ABCG. For each subclass a common alias, the number of genes currently identified, a general functional, and an example member is listed.

Subclasses	Alias	Number of genes	General function	Examples (alternate name, disease relevance)
ABCA	ABCI	12	Mostly lipid trafficking	ABCA4 (ABCR, Stargardt Disease)
ABCB	MDR/TAP	11	Mostly multidrug resistance	ABCB1 (P-glycoprotein, P-gp, drug inefficacy)
ABCC	MRP	13	Mostly toxin excretion	ABCC1 (Multidrug resistance-associated protein 1, MRP1, drug inefficacy) ABCC7 (Cystic Fibrosis Transmembrane conductance Regulator, CFTR, cystic fibrosis)
ABCD	ALD	4	Fatty acid transport	ABCD2 (X-linked adrenoleukodystrophy, X-ALD)
ABCE	OABP	1	Organic anion efflux	ABCE1 (Organic anion binding protein, OABP)
ABCF	GGN20	3	Immune response	ABCF2 (drug-resistant cancer)
ABCG	white	5	Sterol transport	ABCG2 (Breast Cancer Resistance Protein, BCRP, chemotherapeutic resistance)

Adapted from Vasiliou, V., et al. (2008). "Human ATP-binding cassette (ABC) transporter family." Human Genomics **3**(3): 281.

of the subclasses has a particular architecture, all have the following motifs in the nucleotide binding domains (NBDs), or nucleotide binding folds (NBFs): the Walker A motif and the Walker B motif, and the ABC signature motif, which is located upstream of the Walker B motif in the primary sequence (6). Most of these human subclasses, all but ABCE and ABCF, contain two transmembrane domains (TMDs). The TMDs contain anywhere from 6-12 membrane-spanning helices, allowing access to the substrate-binding site from only one side of the membrane at a time (3) (Figure 1.1A). The movement of bound substrates across the membrane is powered by the cooperative binding of ATP at two sites in the interface of the NBDs, forming a head-to-tail dimer, and possibly the hydrolysis of ATP at either both sites or only one site (7-15) (Figure 1.1B), although the notion that ATP hydrolysis powers substrate movement has been contested recently (16). An ATP binding site that can hydrolyze ATP is known as a consensus site, and an ATP binding site that cannot hydrolyze ATP is known as a degenerate site (14, 17) (Figure 1.1B). ATP binding, and possibly hydrolysis, initiates conformational changes translated through the interface of NBDS and TMDs (8) (Figure 1.1A). For many ABC transporters this transmission interface utilizes cross-matched intracellular loops (ICLs) with the NBDs to translate conformational changes to the corresponding TMDs (7, 9) (Figure 1.1A); however, the mechanism of transport, including how ABC transporters transition from an open state to a closed state and how ATP is hydrolyzed, is still debated. First, the reaction path of ATP hydrolysis has been elusive (6, 18, 19), until a recent study proposed a three-step mechanism of hydrolysis (16) (Figure 1.2). Second, whether ATP is hydrolyzed symmetrically or even with every transport cycle is still unknown (17). Third, the model for ATP binding and release is
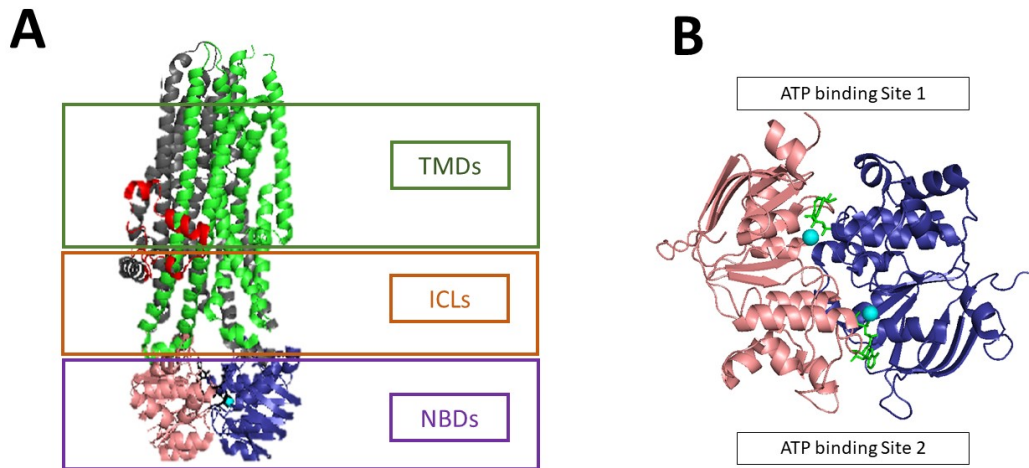
Figure 1.1: Model of an ABC transporter in a lipid bilayer and ATP-binding at the NBD interface. (A) The general architecture of most human ABC transporters is shown. The Transmembrane Domains (TMDs), boxed in forest green, exist in the lipid bilayer and are the site of substrate binding. The intracellular loops (ICLs), boxed in orange, translate conformation changes by ATP binding and hydrolysis at the nucleotide binding domains (NBDs), boxed in purple. TMD1 is gray, TMD2 is green, NBD1 is pink, and NBD2 is blue. Some ABC transporters contain a unique motif known as the lasso motif (red). (B) The interface of NBDs bound with ATP (green) and coordinated Mg^{2+} (cyan) is shown. Both images were developed using PDB ID: 6MSM.
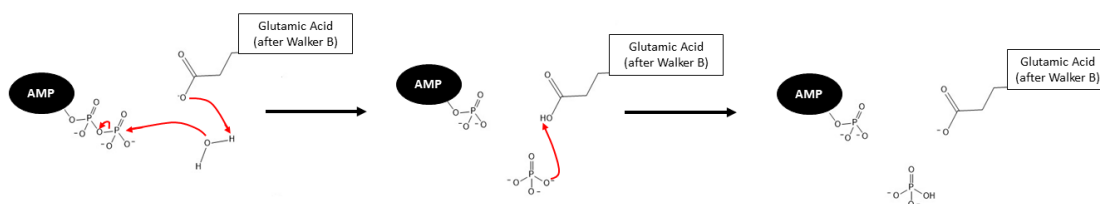
Figure 1.2: The currently proposed ATP hydrolysis reaction path of ABC transporters. While the mechanism of ATP hydrolysis in ABC transporters has been elusive, recent computational studies of the acidic residue just after the Walker B motif predict the above hydrolysis mechanism. For hCFTR, this acidic residue is glutamic acid.

highly contested. While many models have been proposed, it is becoming more accepted that a "one model fits all ABC transporters" theory may not be accurate (17). Initially, the alternating access model, proposed in 1966 by Jardetzky (20), was modified to propose a transport mechanism of P-glycoprotein (P-gp) (21) and then for LmrA (22) (Figure 1.3). This mechanism was the most accepted theory, with structural and biophysical data from multiple ABC transporters supporting this mechanism (7, 8, 13, 21, 23-26). In the alternating access model, ATP binding in the NDBs forms a tight dimer, which opens the high-affinity substrate binding site. ATP binding then induces a conformational change in the TMDs, opening the substrate binding site to the other side of the cell. ATP hydrolysis induces a structural change to release the substrate—possibly inducing a lower affinity binding site—and disrupts the NBD dimer, allowing the release of adenosine diphosphate (ADP) and inorganic phosphate (P_i) (7, 17, 21, 22). For eukaryotic ABC transporters, this conformational change is typically from the inward-facing conformation, where the substrate binding site is accessible intracellularly to outward-facing, where the substrate binding site is accessible extracellularly (19, 21, 27, 28). There were two other mechanistic theories that emerged later to accommodate other structural and biochemical data. These models were the switch model, also called the tweezers-like (12) or processive clamp (29) models, and the constant contact model (6). In the switch model, substrate binding prepares the NBDs for ATP binding. Once ATP binds in the interface of the NBD dimer, the TMDs undergoes a conformational change, exposing the substrate to the other side of the membrane. ATP hydrolysis allows for the release of the NBD dimer and also ADP (30, 31) (Figure 1.3). While this model has structural, biochemical, and other biophysical data in support (32), there is mounting

evidence in support of the constant contact model (14, 33-36). In the constant contact model, the NBDS remain dimerized as ATP binding at one site can induce structural changes to allow substrate binding and conformational changes in the TMDs to provide the substrate access to the opposite side of the membrane (31, 33) (Figure 1.3). Controversial new data suggest that ATP hydrolysis is not sufficient for "the power stroke" of ABC transporters (16), and thus other mechanisms are gaining support (37). With the mounting evidence for each mechanistic model and the variety of substrates for individual ABC transporters across the superfamily, both eukaryotic and prokaryotic known proteins, the concept that one proposed mechanism might work for all ABC transporters would be fallible (17). This is especially true for the Cystic Fibrosis Transmembrane conductance Regulator (CFTR)—the only chloride ion channel ATP in the ABC transporter superfamily, since substrate-induced conformational changes are unlikely in this case.

1.3. CYSTIC FIBROSIS TRANSMEMBRANE CONDUCTANCE REGULATOR (CFTR).

CFTR, also known as ABCC7 or MRP7 (multidrug resistance protein 7), is a chloride ion channel regulated by the phosphorylation of a large intrinsically disordered domain called the Regulatory-domain (R-domain) and ATP binding in both a consensus ATP site and a degenerate ATP site (38). Thus, CFTR is the only chloride ion channel in the ABC transporter superfamily, and as the name suggests, this channel protein is of great medical importance.

1.3.1. CFTR architecture.

CFTR was first identified as an ABC transporter by the characteristic motifs when the

gene was discovered in 1989 (38). CFTR is a monomeric protein of 1480 amino acids composed of 5 domains. Four of the domains are consistent with most ABC transporters—TMD1, NBD1, TMD2, and NBD2; however, CFTR has a linking region connecting NBD1 to TMD2, called the R-domain. While many ABC transporters have linking regions (39, 40), CFTR has the largest at about 240 residues and is the only ABC transporter known to be tightly regulated by phosphorylation of this linker (41, 42). Like other ABC transporters, CFTR contains two ATP binding sites. Unlike most ABC transporters, which have a somewhat strict stoichiometric ratio of ATP consumption to substrate transported, CFTR forms a diffusive pore at the surface of the cell (43). CFTR classically contains ICLs that cross-interact with the NBDs, as well as extensive flexible extracellular loops (ECLs). One of these loops, ECL4, is glycosylated during CFTR biogenesis and is used in tracking CFTR maturation in the cell (44) (Figure 1.4). Both termini of CFTR have key structural features found in other ABC transporters. The first is the PDZ-binding domain located at the C-terminus, which aids in trafficking and anchoring CFTR to the cell surface (45-47). The second is the lasso motif (48), which has been found in a few other ABC transporters, including multidrug resistance protein 1 (MRP1) and sulfonylurea receptors 1 and 2 (SUR1 and SUR2) (49-51) and might aid in trafficking (52, 53).

1.3.2. CFTR biogenesis and trafficking.

During its biogenesis, CFTR undergoes several post- and co-translational modifications. These modifications play critical roles in the folding of CFTR and, thus, its trafficking through the endoplasmic reticulum (ER) and Golgi and, finally, insertion into the plasma membrane (PM).
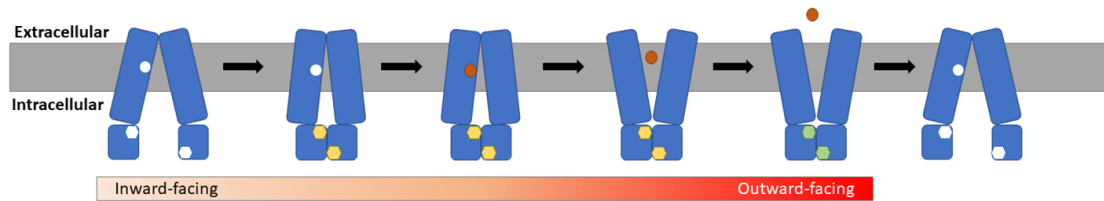
Figure 1.3: Scheme of the proposed mechanistic models of ABC transporters. There are three commonly accepted mechanisms for substrate transport in ABC transporters—alternating access model, switch model, and constant contact model. In the alternating access model, ATP binding induces conformational changes that allow for substrate binding. Substrate binding induces conformational changes in the transmembrane domains (TMDs) that open the substrate pocket to the opposite side of the membrane. ATP hydrolysis and release cause conformational changes to release the substrate and prepare the protein for a new transport cycle. In the switch model, substrate binding induces conformational changes and allows for ATP binding. ATP binding induces conformational changes to release the substrate, and ATP hydrolysis and release prepares the protein for a new transport cycle. In the constant contact model, ATP binding at only one site can open the substrate binding pocket and ATP hydrolysis and release at only one binding site prepares the protein for the next transport cycle.
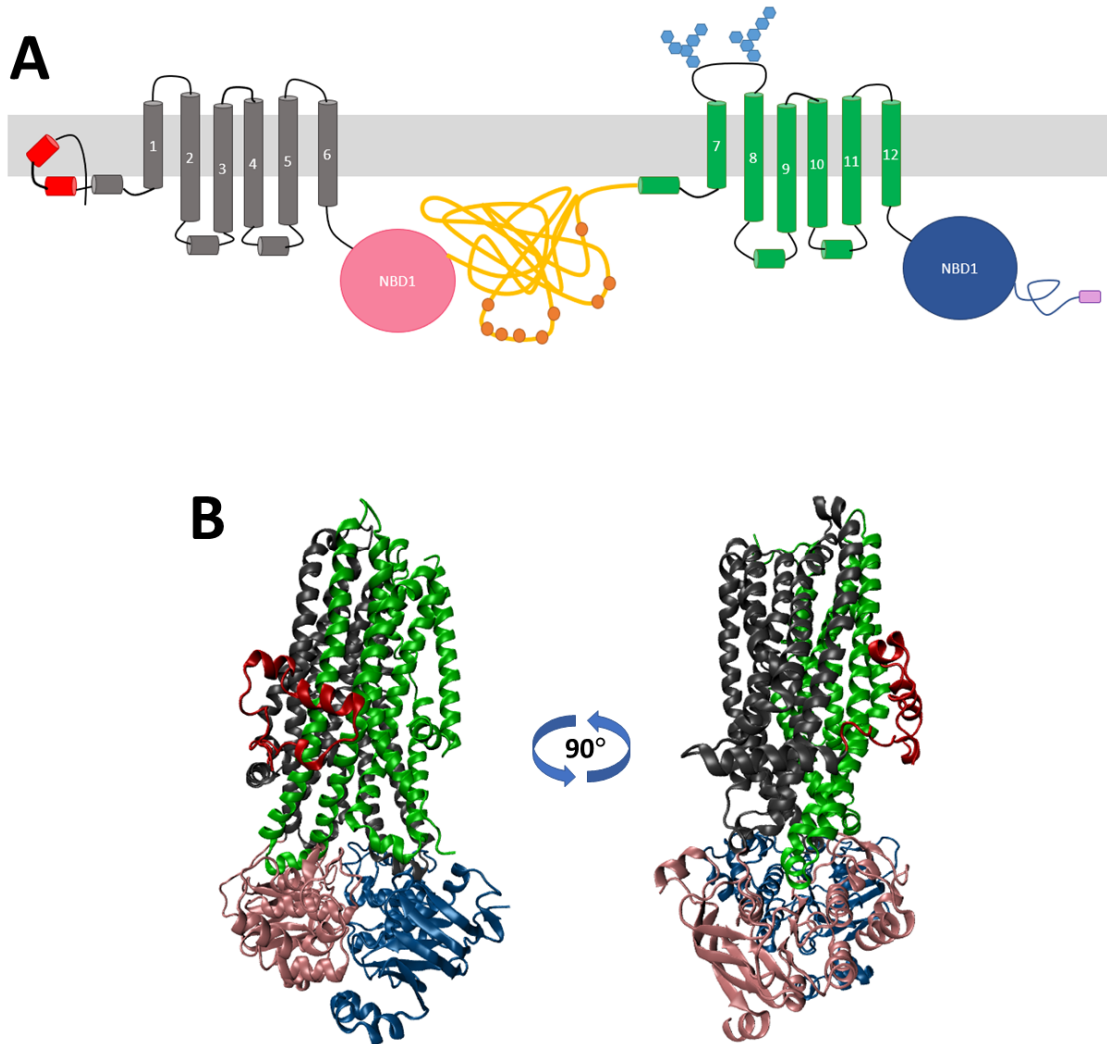
Figure 1.4: Two different representations (schematic and cartoon) of CFTR architecture. Structural domains depicted in both styles (schematic-top and cartoon-bottom): the lasso motif (red), TMD1 (gray), NBD1 (pink), TMD2 (green), and NBD2 (blue). (A) In the schematic representation, several more features of CFTR are displayed. The R-domain (yellow) is phosphorylated at several sites (orange circles), extracellular loop 4 (ECL4) is glycosylated at two sites (cyan hexagons), and the C-terminus contains the PDZ binding domain (purple box). (B) The cartoon representation was built using PDB ID: 6MSM and is one of the recently released structures of CFTR.

1.3.2.1. CFTR CO-TRANSLATIONAL FOLDING.

During the synthesis of TMD1, the emergence of the signal sequence on transmembrane helix 1 (TM1) from the ribosome is believed to be inefficient at being recognized by the signal recognition particle (SRP) due to two charged residues—E92 and K95 (54). The inefficient recognition of this signal sequence prevents a C-*trans* orientation of CFTR but does possibly promote initial location to the ER and Sec61. The signal sequence on transmembrane helix 2 (TM2) that interacts with SRP does promote proper insertion of the N-terminal flanking sequence into the ER through Sec61, thus forming the ribosome-Sec61 translocon complex (RTC) (N-*trans* orientation) (54). Proper insertion of TM1 is then believed to be mediated by extracellular loop 1 (ECL1) (54). Next, both transmembrane helix 3/ transmembrane helix 4 (TM3/4) and transmembrane helix 5/ transmembrane helix 6 (TM5/6) are believed to be inserted into Sec61 as helical hairpins due to the short extracellular loop 2 (ECL2) and extracellular loop 3 (ECL3) (54, 55). NBD1 and the R-domain are believed to fold in the cytosol co-translationally (55, 56). While little is known about the "folding" of the R-domain due to its intrinsically disordered nature, much has been done to understand the folding mechanism of NBD1 because the most common disease-relevant mutation occurs in this domain (ΔF508). First, studies showed that NBD1 experiences consecutive folding of each subdomain, the first being the N-terminal ATP-binding subdomain (57). The next domains to be folded are the α-helical subdomain and the α/β-core subdomain, which most likely use the first formed domain as a scaffold; however, the folding order of these subdomains is still debated (58). Other studies have shown that in order to prevent steric clashing during translation of NBD1 and the R-domain, the ribosome must transiently detach from the

RTC (56, 59, 60). Whether the same or a different translocon is used for translation of TMD2 is unknown. Transmembrane helix 7 (TM7) directs membrane targeting and translocation of extracellular loop 4 (ECL4), while TM8 terminates translocation causing redirection of ICL3 into the cytosol. This mechanism only occurs in conjunction with TM7, which is a cooperative property specific to CFTR (55, 61, 62). The remaining transmembrane helix 9/ transmembrane helix 10 (TM9/10) and transmembrane helix 11/ transmembrane helix 12 (TM11/12) are believed to be inserted into the translocon similarly to TM3/4 and TM5/6 as helical hairpins (55, 62). Finally, NBD2 is believed to fold co-translationally, very similarly to NBD1 (56). Once each major domain has folded, CFTR must also undergo significant domain reorganization to achieve the native architecture of the mature protein through at least two distinct folding events (63).

1.3.2.2. CFTR FOLDING AND MATURATION.

Throughout the process of CFTR folding, both co-translationally and post-translationally, CFTR must pass through at least four checkpoints of the ER quality control machinery (ERQC) (Figure 1.5). The first checkpoint precedes the first domain reorganization event, which requires CFTR to be released from the RTC and the related chaperones (64, 65). At this first checkpoint, before the release of RTC, CFTR emerges from the ribosome as a nascent polypeptide and interacts with cytosolic chaperones such as heat shock protein 70 (Hsp70) and heat shock protein 90 (Hsp90) and several co-chaperones (58, 63). These chaperones play critical roles in both folding and partitioning between wildtype (WT-CFTR) and mutant, misfolded CFTR (64, 66-71). Any misfolded mutant CFTR is trapped by these chaperones and signaled for degradation through the E3 ubiquitin ligase CHIP ((carboxyl) c-terminal of Hsp70 Interacting Protein) pathway

(72). Once successfully passing this checkpoint, CFTR is released from the RTC and related chaperones and allowed to move to the second checkpoint. The second checkpoint involves the proper folding of CFTR through N-linked glycosylation and processing in the ER. Before the release of CFTR from the ribosome, nascent CFTR receives core N-glycosylation (14-unit oligosaccharide—two N-acetylglucosamine, nine mannose, and three glucose residues) in the lumen of the ER by OST (oligosaccharyltransferase) at two residues N894 and N900 of ECL4, each containing a glycosylation consensus sequence DXS/T (62, 73). The release of CFTR from the RTC, after checkpoint 1, initiates glycosylation processing in which the partially glycosylated structure is recognized by chaperone lectins calnexin (CNX) and the calreticulin ER lumenal chaperones that assist in CFTR folding (74-76). At this step, misfolded CFTR is targeted to UDP (Uridine diphosphate)-glycoprotein glucosyltransferase (UGGT), which induces the re-glycosylation process (77). Lengthy processing time at this stage indicates improper folding, and CFTR could be trafficked to the glycoprotein ER-associated degradation (GERAD) pathway (66). However, proper folding of CFTR leads to the third checkpoint, which involves the arginine-framed tripeptides (AFTs) pathway. CFTR's ability to be exported from the ER to the Golgi is confirmed by the following four retention/retrieval (RXR) motifs: R29/Q30/R31, R516/Y517/R518, R553/A554/R555, and R764/R765/R766 (78). Failing this checkpoint, due to the exposure or accessibility of these motifs, causes the imprisonment of CFTR in the ER (79). The fourth and final checkpoint is critical for exiting the ER and relies on the specific export diacidic motif D565/A566/D567), allowing CFTR packaging into coat protein (COP) II-coated vesicles, specifically with Sec24, at the ER exit site (80). Mutation of this motif almost

completely prevents CFTR processing to the Golgi, especially in the absence of low temperature correction (80-82).
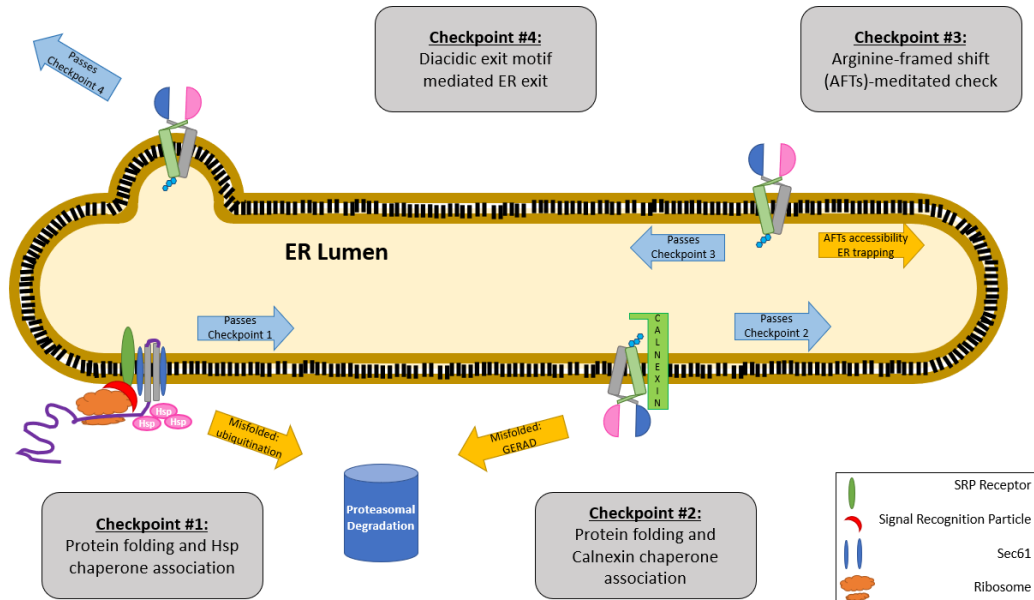
Figure 1.5: Simplified depiction of the four CFTR folding checkpoints. In the ER, CFTR will proceed through four processing checkpoints. These checkpoints occur both co-translationally and post-translationally and ensure properly folded CFTR can exit the ER and proceed to the Golgi. At one of these checkpoints, CFTR is glycosylated, known as Band B, and can be distinguished from CFTR that is glycosylated further in the Golgi (Band C).

Adapted from Farinha, C. M., and Canato, S. (2017) From the endoplasmic reticulum to the plasma membrane: mechanisms of CFTR folding and trafficking. Cellular and Molecular Life Sciences 74, 39-55

1.3.2.3. CFTR TRAFFICKING TO THE PLASMA MEMBRANE (PM).

Once it passes these checkpoints, CFTR is trafficked to the plasma membrane, either by traditional or non-traditional processes. First, CFTR is transported in COPI vesicles to the trans-Golgi either through typical traffickers like Arf1, Rab1a/Rab2, or Golgi SNARE. As CFTR moves through the Golgi, the core-glycosylation (high-mannose oligosaccharide structures sensitive to endoglycosidase H, known as Band B in reference to its apparent molecular weight by SDS-PAGE) is modified with the removal of some glycan units and the addition of more complex units, like fucose, neuraminic acid, or sialic acid. After this glycosylation event, CFTR has matured (now appearing as Band C) (83). Another well-accepted theory, however, is that CFTR experiences a mode of anterograde trafficking between the ER and Golgi. In some cell types, CFTR is dependent on the late-endosomal target-SNARE syntaxin 13 pathway (84, 85). Finally, CFTR is delivered to the plasma membrane from the trans-Golgi network, experiencing three distinct processes of balancing CFTR levels at the plasma membrane—anterograde trafficking, endocytosis, and recycling. These processes are regulated by a variety of interacting partners with CFTR. The incorporation of CFTR into clathrin-coated vesicles is dependent on a small sequence motif on the C-terminal tail. There are two types of endocytic motifs—tyrosine-based (NPXY or YXXφ) or dileucine-based (D/EXXXLL/I and DXXLL). CFTR has two confirmed endocytic motifs—the YDSI (at 1424) and the LL motifs (at 1430); however, FVLI (at 1413) is not believed to be an endocytic motif but is needed for CFTR maturation (86-88). These signals are recognized by the assembly polypeptide-2 system that forms a complex with clathrin to promote the internalization of CFTR (89). Another route of CFTR recycling is regulated by small GTPases of the

Rab family (88, 90). Furthermore, while these are mechanisms to balance CFTR levels by recycling, there are also mechanisms to anchor CFTR to the plasma membrane, including the PDZ domain proteins. The C-terminus of CFTR contains a consensus PDZ binding motif (DTRL), which binds to multiple Na^+/H^+ exchanger regulatory factor proteins (NHERF-1, NHERF-2, and NHERF-3) and to CFTR-associated ligand protein (CAL). Interactions with the proteins stabilize CFTR expression at the cell surface (91-98).

1.3.3. Biochemical and biophysical studies of CFTR.

Since the identification of the CFTR gene, it has been the hope that understanding the function of CFTR will establish how each mutant version is linked to the disease Cystic Fibrosis (CF). One of the key features of CF is the abnormally high sweat chloride levels of patients; thus, it was suspected that CFTR is a chloride ion channel or that CFTR might regulate the expression of a chloride ion channel (38). Some of the first functional studies of CFTR identified it as a chloride ion channel regulated by adenosine 3',5'-monophosphate (cyclic AMP, cAMP) signaling (43, 99-102). Later studies showed that cAMP-mediated stimulation induced the phosphorylation of CFTR in its R-domain (42, 102-108). Moreover, further studies identified the need for ATP binding at the NBD interface (107, 109-114) to allow for chloride ion pore formation in the TMDs of CFTR.

1.3.3.1. R-DOMAIN PHOSPHORYLATION.

The R-domain contains nine consensus protein kinase A (PKA) phosphorylation sites (R-R/K-X-S*/T*, where the asterisk indicates the phosphorylated residues) at resides S660, S686, S700, S712, S737, S768, T788, S795, and S813 (Figure 1.6). Also, to note, there is one phosphorylation site outside of the R-domain in NBD1 (S422) (105). If all

10 of these sites are mutated, S753 was found to be phosphorylated (115). Phosphorylation studies of purified R-domain peptide show that only five sites are phosphorylated by PKA (S660, S700, S737, S795, S813), and two sites (S686 and S700) can be phosphorylated by protein kinase C (PKC) (106, 116); however, whole-cell experiments suggest that stimulation of PKC enhances phosphorylation of CFTR by PKA (102, 117). While each of these sites can be phosphorylated, not all sites contribute equally to the activation of CFTR. In fact, phosphorylation at S737 (in oocytes) or S768 shows an inhibitory effect on CFTR (118-120) in the presence of all other phosphorylated residues; however, when all possible residues are mutated to alanine, these residues show stimulatory effects (121). Residues S660, S737, S795, and S813 have been proposed to contribute the most to CFTR regulation by showing the most dramatic reduction in current when mutated to alanine (122). Only when all 11 sites discussed earlier, as well as four other residues (S670, T690, T787, S790) are mutated to alanine, is CFTR no longer regulated by PKA (123). Mutation of these sites individually, or multiple sites, reduced the rate of channel opening without changing the

650	dqfsaerrn**S**	iltetlhrfs	670	legdapv**S**wt	etkkqsfkqt	690	gefgekrkn**S**
700	ilnpinsirk	f**S**ivqktplq	720	mngieedsde	plerrl**S**lvp	740	dseqgeailp
750	risvistgpt	lqarrrq**S**vl	770	nlmthsvnqg	qnihrkt**T**as	790	trkv**S**lapqa
800	nlteldiysr	rl**S**qetglei	820	seeineedlk	ecffddmesi	840	pavtt

Figure 1.6: Sequence of the R-domain highlighting the positions of phosphorylation. There are nine phosphorylation sites (bolded and underlined), all with varying levels of functional consequences to CFTR.

channel closing rate, but also reduced the affinity of CFTR for binding ATP; thus, phosphorylation of the R-domain regulates the interaction of ATP with the NBDs (108, 124). Complete deletion of the R-domain produces a non-functional CFTR channel (103); however, partial deletion (residues 708-835) produces a CFTR channel ($\Delta R_{708-835}$CFTR) with similar biophysical properties, minus regulation by PKA and reduced (1/3) open probability (P_o) or the fraction of time a channel is open during a recording (103, 108, 125). In these specific $\Delta R_{708-835}$CFTR mutant channels, incubation with AMP-PNP (adenylyl-imidodiphosphate) could not stabilize CFTR's open state. The instability of the open state in the $\Delta R_{708-835}$CFTR mutant indicates the possibility that the R-domain also plays a role in stabilizing ATP binding in the NBDs. In this mutant phosphorylation no longer regulates CFTR, only binding of MgATP can (125).

1.3.3.2. ATPase ACTIVITY.

After phosphorylation, WT-CFTR channels are activated by the binding of ATP to the NBDs. Specific motifs in both NBDs not only indicated ATP binding and hydrolysis but also that CFTR was a member of the ABC transporter superfamily. These motifs, which exist is both NBDs, are the Walker A motif (G-X-X-G-X-G-K-s/t), the Walker B motif (R-X-X-X-X-X-X-X-h-h-h-h-D) and the ABC signature motif (L-S-G-G-Q) and forms two ATP binding sites. (38). ATP binding site 2 is composed of the Walker motifs of NBD2 and the ABC signature motif of NBD1 and is known as the consensus site in CFTR. As mentioned before, the other ATP binding site (ATP binding site 1) is known as the degenerate site with respect to ATP hydrolysis and is composed of the Walker motifs of NBD1 and the slightly altered ABC signature (L-S-H-G-H) of NBD2 (38, 48, 126-128) (Figure 1.7). Studies of CFTR's single-channel behavior reveal that after

A

	Walker A	Walker B	ABC signature
NBD 1	GSTGAGKT	RAVYKDADLYLLD	LSGGQ
NBD 2	GRTGSGKS	RSVLSKAKILLLD	LSHGH
Motif Sequence	GXXGXGKs/t	RXXXXXXXhhhD	LSGGQ

B
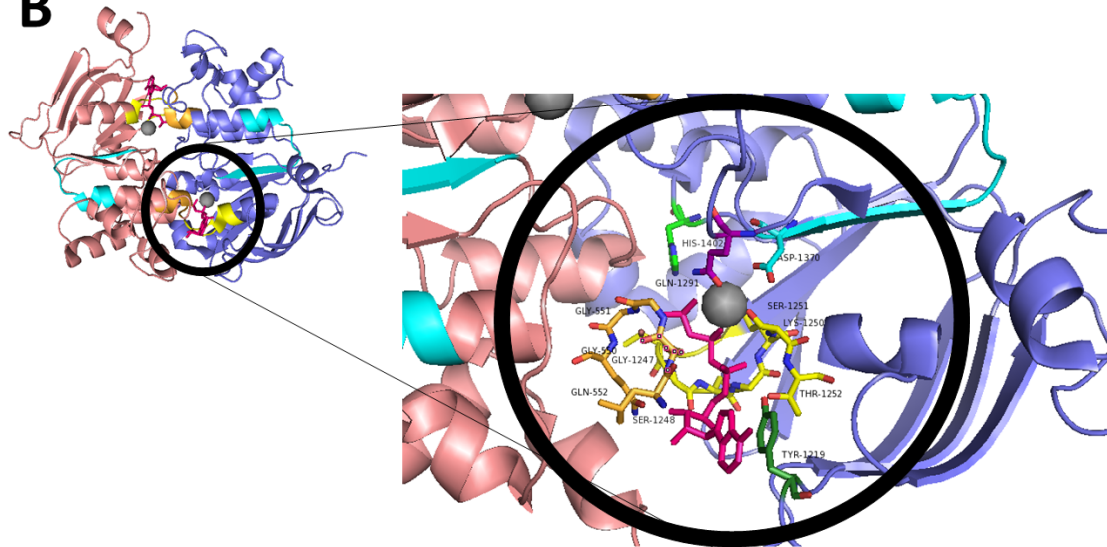
Figure 1.7: Diagram of ATP (magenta) binding sites at the interface of the nucleotide binding domain 1 (NBD1, pink) and nucleotide binding domain (NBD2, blue). As discussed in Figure 1.1, there are two ATP binding sites in ABC transporters formed from the Walker A, Walker B, and ABC Signature motifs in the nucleotide binding domains. (A) The sequences of these motifs for hCFTR are tabled. (B) The consensus site (ATP binding site 2, marked by the black circle) is discussed further. Highlighted in this figure is the Walker A of NBD 2 (yellow) and ABC Signature of NBD 1 (orange) , which form the ATP binding site stabilized by several residues of NBD2: Y1219 in A-loop (dark green), H1402 in H-loop (light green), Q1292 of Q-loop (purple), and D1320 of Walker B in NBD2 (cyan). A coordinated Mg^{2+} is gray.
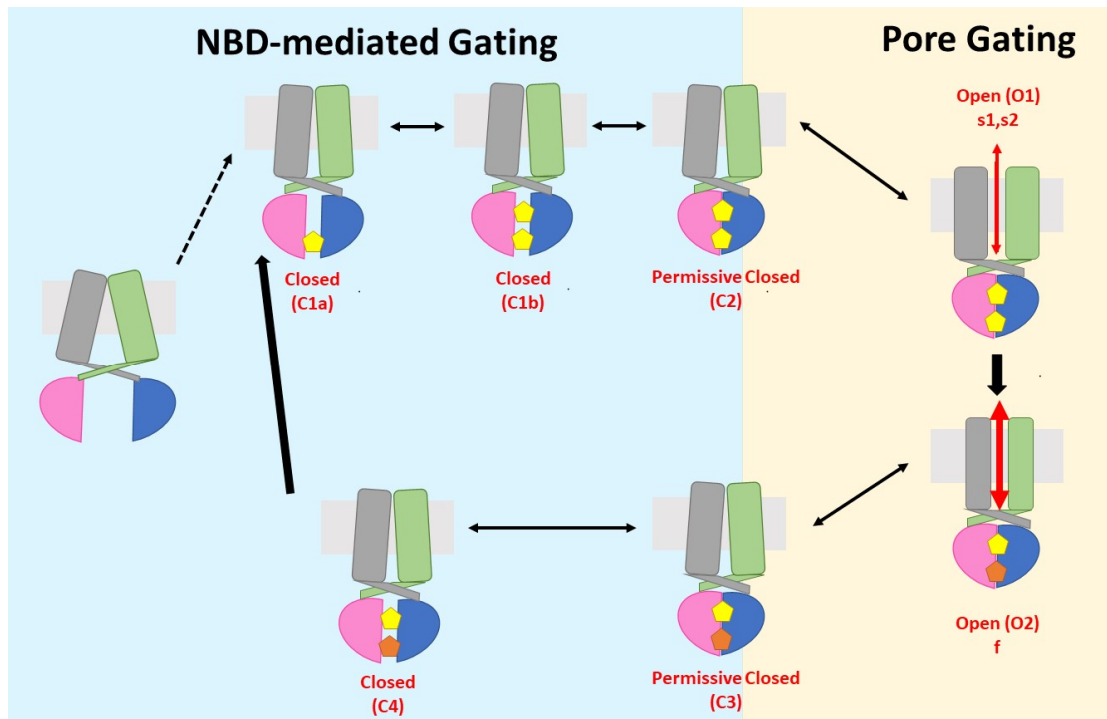
Figure 1.8: Scheme of CFTR gating and opening cycle. CFTR is a chloride ion channel regulated by phosphorylation of the R-domain. After phosphorylation of the R-domain, the fully open pore is regulated by two different gating stages. The NBD-mediated gating (blue background) occurs with the binding of one ATP molecule (yellow) at a consensus site and one ATP molecule (yellow) at a degenerate site in the nucleotide binding domains (NBDs; NBD1 is pink, and NBD2 is blue). Then the pore is regulated by pore gating (pink background) in which CFTR has several subconductance states (s1 and s2, thin red arrow) but will process to a fully conducting pore (f, thick red arrow). Hydrolysis of ATP (yellow) at the consensus site and the release of ADP (orange) and inorganic phosphate causes the channel to close by inducing conformational changes in the Transmembrane Domains (TMDs, TMD1 is gray, and TMD2 is green).

phosphorylation, increasing the concentration of MgATP leads to a decreased mean closed time, but no change in mean open time. These data suggest a minimal model of at least two closed states and a single open state (C_1, C_2, O_1) (124). Further characterization of the single-channel behavior of CFTR shows another short-lived subconductance state (O_2) and asymmetric transitions between these states in the CFTR gating cycle (124). These data, and more, reveal that CFTR has a very complex gating cycle, transitioning between multiple states (Figure 1.8) (124, 129, 130). Several studies have shown that the presence of MgATP before phosphorylation cannot activate CFTR, but the addition of only MgATP after the removal of PKA and ATP does activate CFTR channels (124). Nevertheless, in the case of deleting part of the R-domain, CFTR still retains ATPase activity and some channel activity (125). In the initial studies of purified recombinant NBD1 and NBD2, both have ATPase activity without the presence of TMD1, TMD2, or the R-domain (113, 131). While ATPase activity assays are used to demonstrate functional CFTR, especially in the case of purified protein, the reconstitution of the purified protein into planar lipid bilayers reveals substantial details about the chloride channel function of CFTR discussed below (48, 132-134).

1.3.3.3. CHLORIDE ION PORE.

The earliest electrophysiological studies of CFTR revealed its high anion selectivity over cations (99, 132); however, there is much less selectivity between anions (99, 135). Several experiments have shown that Cl^- might not be the only physiologically relevant anion that permeates through CFTR, including bicarbonate (135, 136) and possibly glutathione and thiocyanate (137, 138). Thus, it is generally accepted that the minimum pore diameter of CFTR is around 5 Å (139). For Cl^-, CFTR demonstrates a linear I-V

relationship under symmetrical conditions, with one of the lowest single-channel conductances of any channel ranging from 6 pS to 10 pS, depending on buffer conditions, Cl^- concentration, and temperature (104, 132, 140, 141). When phosphorylated CFTR is reconstituted into planar lipid bilayers and is in the presence of ATP, the open probability (P_o) of WT-CFTR is measured to be ~0.3 to ~0.5, depending on buffer conditions, with the observation of the aforementioned subconductance states (112, 132, 142, 143). Further exploration of these subconductance states reveals that mutations not only in the TMDs (144-148) but also in the NDBs can affect the frequency of these states (143, 149). As high-resolution structures of CFTR were unavailable until recently, identifying key residues that lined the pore of CFTR was accomplished through a combination of site-directed mutagenesis, cysteine accessibility studies, and introduction of various pore blockers, with the evaluation of changes to CFTR by electrophysiology. Detailed reviews of these studies identified several key residues in TM1, TM6, TM11, and TM12 (124, 150, 151), many of which were confirmed in the several newly released structures of CFTR (126, 128) (Figure 1.9). A narrow region in the pore of CFTR, first identified by electrophysiology in combination with the techniques mentioned above, most likely composes the selectivity filter. In this region are residues S341 (TM6), T338 (TM6), and F377 (TM6) (139, 152). Every study investigating the chloride pore, ATP binding, and phosphorylation builds on our understanding of how mutations in each domain of CFTR affect the function of this protein and its clinical relevance.
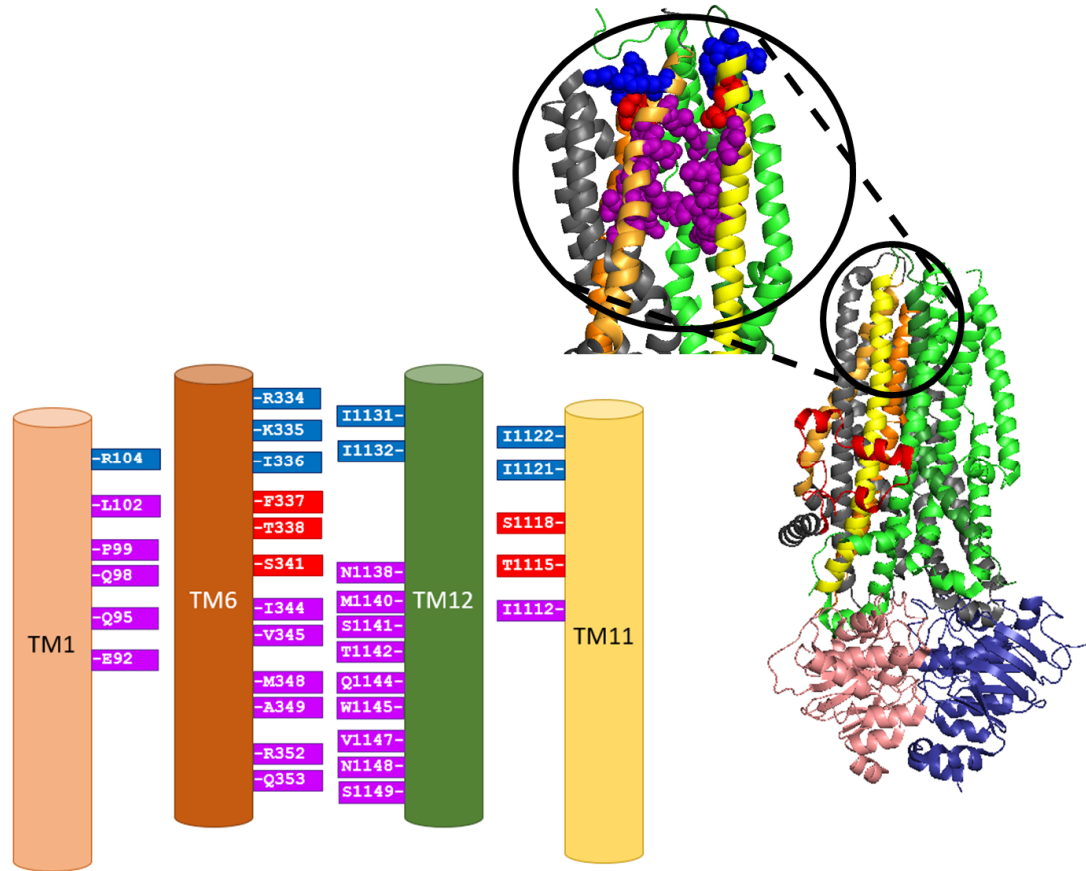
Figure 1.9: Depiction of residues believed to be important in pore formation of CFTR. A full structure of CFTR (right) highlights the general architecture of CFTR with TMD1 in gray, NBD1 in pink, TMD2 in green, and NBD2 in blue. The black circle highlights four transmembrane helices, TM1 as pale orange, TM6 as orange, TM12 as forest green and TM11 as yellow, and the residues on those helices that are important in pore formation. Residues accessible from the extracellular side are blue, from the intracellular side are purple, or both are red.

Adapted from Linsdell, P. (2014) Functional architecture of the CFTR chloride channel. Mol Membr Biol. 2014 Feb;31(1):1-16.

1.3.4. Disease-relevance of CFTR.

More than 2000 mutations have been identified within the gene of CFTR (http://www.genet.sickkids.on.ca/), and 346 of those mutations are identified as CF-causing (cftr2.org/mutations_history). These mutations are categorized into five different classes—production mutations (class I), processing mutations (class II), gating mutations (class III), conductance mutations (class IV), and amount/localization mutations (class V)(153) (Figure 1.10). In recent years, four different CFTR modulator therapies have been released for many processing, gating, and conductance mutations and some production and amount/localization mutations. These CFTR modulators are single, double, and triple combination therapies known clinically as Kalydeco® (Ivacaftor/VX-770), Orkambi® (ivacaftor/VX-770 and lumacaftor/VX-809), Symdeko® (ivacaftor/VX-770 and tezacaftor/VX-661), and Trikafta® (ivacaftor/VX-770; tezacaftor/VX-661; and elexacaftor/VX-445) (Figure 1.11). These compounds are classified as either correctors—molecules that enable proper folding or trafficking—or potentiators—molecules that increase PKA regulated chloride channel gating of CFTR (154). Currently, many mutations are being treated with these modulators, but not all mutants are impacted by these compounds, especially in the production and amount/localization class of mutations. Single mutations in CFTR can impart complex molecular defects suggesting recategorization of mutation classes to allow current therapies to be tested on orphan mutations. This reclassification can also enable connecting the functional consequences of these mutations with the structure of CFTR (155).
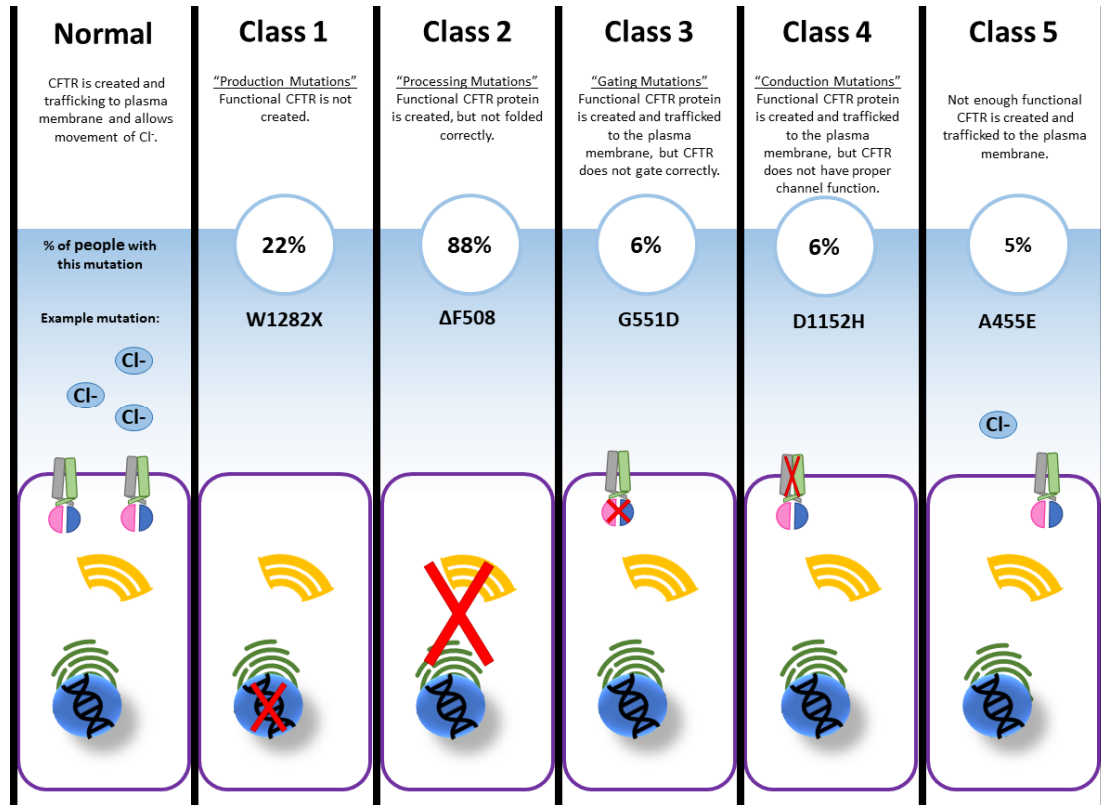
Normal	Class 1	Class 2	Class 3	Class 4	Class 5
CFTR is created and trafficking to plasma membrane and allows movement of Cl-.	"Production Mutations" Functional CFTR is not created.	"Processing Mutations" Functional CFTR protein is created, but not folded correctly.	"Gating Mutations" Functional CFTR protein is created and trafficked to the plasma membrane, but CFTR does not gate correctly.	"Conduction Mutations" Functional CFTR protein is created and trafficked to the plasma membrane, but CFTR does not have proper channel function.	Not enough functional CFTR is created and trafficked to the plasma membrane.

Figure 1.10: Diagram of classes for CFTR mutations. The 346 currently identified disease-causing mutations are classified into one of the five above described classes. Each mutation class houses mutations that affect one of the following: protein production (class 1), protein processing (class 2), protein gating (class 3), protein conduction (class 4), or insufficient protein on the cell surface (class 5). However, many mutations can contribute to multiple classes of disfunction. The most common mutation, ΔF508, is classified as a class 2 mutation.

Adapted from cftr2.org/mutations_history and https://www.cff.org/Care/Clinician-Resources/Network-News/August-2017/Know-Your-CFTR-Mutations.pdf.

Kalydeco ® (VX-770)

2789+5G→A	G551D	G1069R	D1270N
711+3A→G	A1067T	S1255P	D110H
3849+10kbC→T	S1251N	D110E	R352Q
3272-26A→G	R74W	R347H	S945L
P67L	L206W	D579G	R1070W
R117C	A455E	R117H	D1152H
F1074L	S977F	F1052V	S549N
E193K	G551S	R1070Q	G1349D
E831X	E56K	S549R	G178R
	G1244E	K1060T	

Symdeko® (VX-770+VX-661)

ΔF508/ΔF508	L206W	D110E	D1270N
2789 +5G→A	A455E	R347H	D110H
3272-26A→G	S977F	D579G	R352Q
711+3A→G	D1152H	R1070W	S945L
3849+10kbC→T	F1074L	F1052V	R117C
	E56K	E831X	R74W
	E193K	E193K	K1060T
	P67L	A1067T	

Orkambi® (VX-770+VX-809)

ΔF508/ΔF508

Trikafta® (VX-770+VX-661+VX-445)

ΔF508/ΔF508	ΔF508/xxxx

Figure 1.11: Diagram of the current CF modulators and the tableted list of FDA-approved mutations. Currently, four different modulator therapies have been approved in single, double, or triple combination therapies and treat 39 of the 346 disease-causing mutations. These modulators are either potentiators, like ivacaftor (VX-770), or correctors, like lumacaftor (VX-809), tezacaftor (VX-661), and elexacaftor (VX-445).

1.4. CFTR STRUCTURES.

Structural characterization of CFTR is of great importance as structures can aid in understanding the complex molecular defects imposed by single mutations, elucidating the complex transitions from different closed and open states, and clarifying the chloride channel function of CFTR as a member of the ABC transporter superfamily.

1.4.1. Initial full-length CFTR structures.

Two structures of hCFTR were solved by 2D (two-dimensional) electron

crystallography—one in 2004 at a resolution of 20 Å and one in 2011 at a resolution of 9Å (156, 157). Both structures confirmed the general architecture of CFTR predicted in an initial gene discovery study (38). The first study showed two different global conformations, and the second study revealed an outward-facing conformation of CFTR without the presence of ATP or phosphorylation. The traditional terms of outward- and inward-facing for ABC transporters are used to describe general conformations states of CFTR, especially when a conformation lacks a fully conducting pore. In the interim of waiting for more structures of CFTR, several homology models of CFTR were developed.

1.4.2. CFTR homology models.

Several structures of ABC transporters were released, providing a variety of scaffolds for homology models (9, 158). The first of these models investigated the molecular interface of the most common mutation (ΔF508) and key interactions necessary to reestablish channel function (159, 160). The next several homology models investigated the transitions of CFTR from the inward-facing conformation to the outward-facing conformation and the formation of a fully conducting pore (130, 161-165). These models not only confirmed several key interactions but unveiled new interactions significant to CFTR's conformational transitions. One of these interactions includes E543 in the X-loop of NBD1 and K968 in ICL3, which our lab investigated further (166) (Figure 1.12). While these models were built keeping functional information in mind and rigorously evaluated, the NBDs are anticipated to have similar structures across ABC transporters, but the variety of substrates of ABC transporters compared to the chloride channel function of CFTR results in skepticism for the validity of the models.
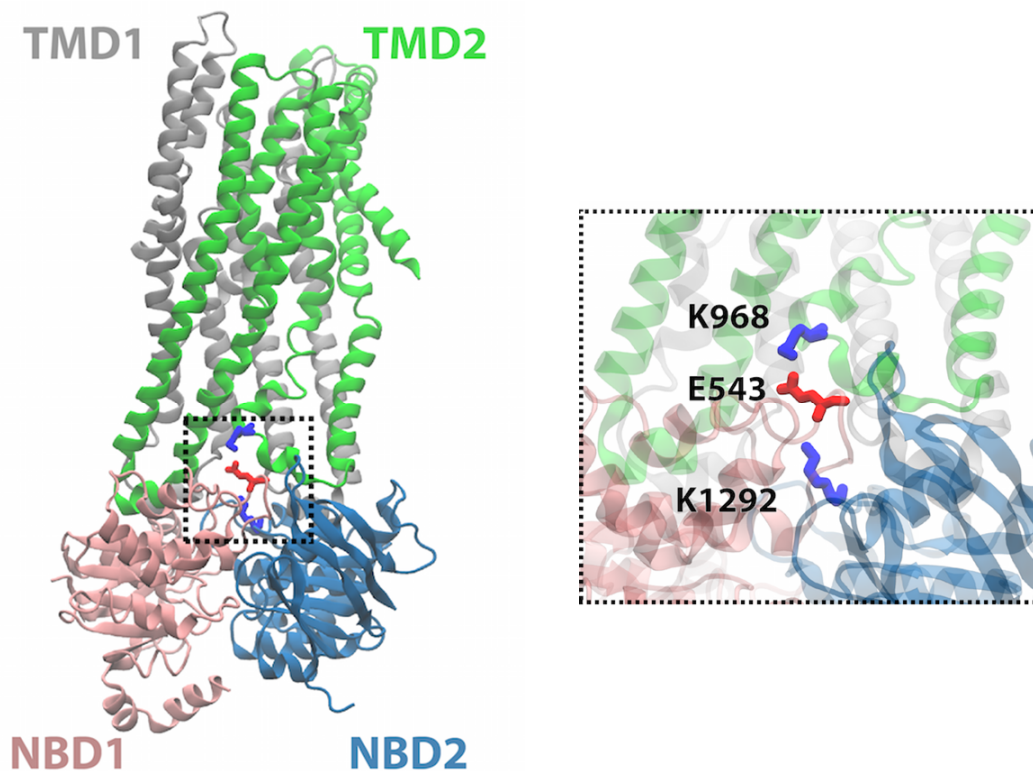
Figure 1.12: Electrostatic salt bridge triad identified in homology models of CFTR and molecular dynamics and confirmed by electrophysiological techniques. This catalytic triad has been investigated in the translation of ATP binding at the nucleotide binding domains (NBDs, NBD1 is pink, and NBD2 is blue) to the Transmembrane Domains (TMDs, TMD1 is gray, and TMD2 is green). This triad is investigated further in chapter II of this dissertation.

Republished from Strickland, K. M., Stock, G., Cui, G., Hwang, H., Infield, D. T., Schmidt-Krey, I., McCarty, N. A., and Gumbart, J. C. (2019) ATP-Dependent Signaling in Simulations of a Revised Model of Cystic Fibrosis Transmembrane Conductance Regulator (CFTR). The Journal of Physical Chemistry B 123, 3177-3188.

1.4.3. Recent CFTR structures.

In three years, eight structures of 3 orthologs of detergent-solubilized CFTR were released from two laboratories in a broad range of resolutions—all solved by single particle electron cryo-microscopy (cryo-EM, see below). The first structures were of ATP-free, dephosphorylated zebrafish CFTR (zfCFTR) (inward-facing conformation) at a resolution of 3.7 Å and hCFTR under the same conditions at a resolution of 3.9 Å. In both structures, the NBDs were of significantly lower resolution, and thus, crystal structures of the NBDs were used to construct the final models (48, 126). From the same lab, the phosphorylated, ATP-bound structures (outward-facing) of zfCFTR and hCFTR were solved at resolutions of 3.4 Å and 3.2 Å (127, 128). All four of these structures revealed that CFTR contains a structural motif called the lasso motif. The lasso motif is found in several other ABC transporters (SUR1, SUR2, and MRP1) in which the N-terminus loops into the lipid bilayer (Figure 1.13). These structures also exhibit a rearrangement of TM7 and TM8 and a kink in TM8, which is not seen in other similar ABC transporters. The functional consequence of the rearrangement and the kink in TM8 is still highly unclear and continues to be debated (167-169). The release of two more structures of hCFTR with different potentiators bound, Vertex potentiator VX-770 (resolution at 3.3 Å) or Galapagos potentiator GLPG1837 (resolution at 3.2 Å), showed both potentiators bound in the pocket created by the kink in TM8 (170). Whether this identified binding pocket is the physiological binding pocket for either or both of these potentiators or if these potentiators are correcting detergent-induced structural deformations has yet to be investigated. From a different lab, two other structures of recombinant thermostabilized chicken CFTR (chCFTR), one dephosphorylated, ATP-

absent (inward-facing) structure (resolution at 4.3Å) and one phosphorylated, ATP-bound (outward-facing) structure (resolution at 6.6 Å) also have been released. These structures show TM8 to be fully helical (171), and thus do not present the significant rearrangement of TM 7 and TM8 nor the kink in TM8. There are other peculiar structural characteristics in TM7 for these structures in which TM7 is almost orthogonal to the fatty acid tails of the lipid bilayer. As more structures are released, the kink in TM8 has been thought to be detergent-induced and not physiological (172).
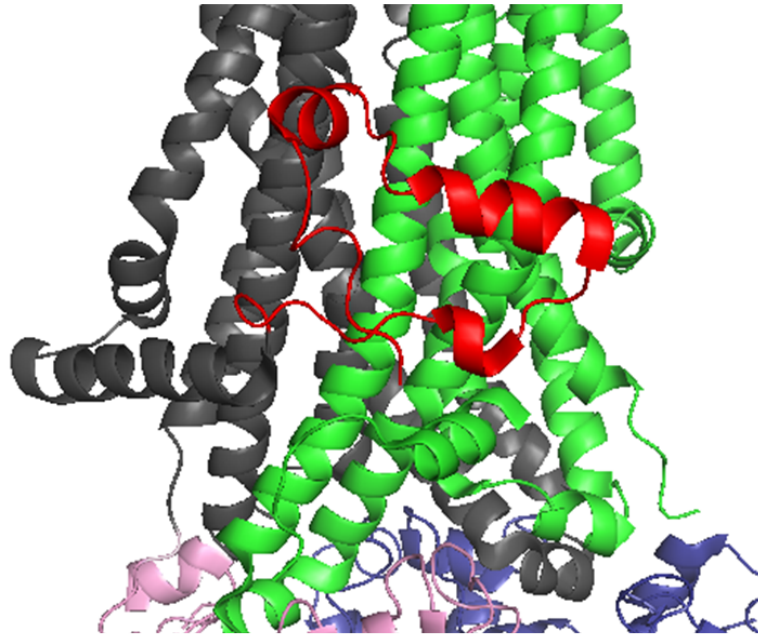
Figure 1.13: Depiction of the Lasso motif in CFTR. The lasso motif (red) is a motif found in several members of the ABC transporter superfamily of proteins, in which the N-terminus tucks into the lipid bilayer. For orientation, Transmembrane Domain 1 (TMD1) is gray, nucleotide binding domain 1 (NBD1) is pink, TMD2 is green, and NBD2 is blue. PDB ID: 6MSM used to generate the figure.

Table 1.2: Current released CFTR structures and the conditions of protein.

Protein	Organism	Res	Environment	Modifi-cation	State	Method	Year	Expression system
hCFTR	human	20 Å	Lipids	-		2D electron crystallography	2004	BHK cells, stables
hCFTR	human	11 Å	Lipids	-	Closed (?), outward-facing, dephosphorylated, apo-ATP	2D electron crystallography	2011	BHK cells, stables
zfCFTR	zebrafish	3.7 Å	Detergent (LMNG, digitonin, CHS)	-	Closed, inward-facing, dephosphorylated, apo-ATP	Single Particle	2016	Sf9 virus, HEK cells
hCFTR	human	3.9 Å	Detergent (LMNG, digitonin, CHS)	-	Closed, inward-facing, dephosphorylated, apo-ATP	Single Particle	2017	Sf9 virus, HEK cells
zfCFTR	zebrafish	3.4 Å	Detergent (LMNG, digitonin, CHS)	E1372Q	Closed, outward-facing, phosphorylated, ATP-bound	Single Particle	2017	Sf9 virus, HEK cells
chCFTR	chicken	4.3 Å	Detergent (DMNG, digitonin)	ΔRI/1404S/1441X	Closed, outward-facing, dephosphorylated, ATP-present	Single Particle	2018	BHK cells, stable
chCFTR	chicken	6.6 Å	Detergent (DMNG, digitonin)	ΔRI/1404S/1441X	Closed, outward-facing, phosphorylated, ATP-present	Single Particle	2018	BHK cells, stable
hCFTR	human	3.2 Å	Detergent (LMNG, digitonin, CHS)	E1371Q	Closed, outward-facing, Phosphorylated, ATP-bound	Single Particle	2018	Sf9 virus, HEK cells
hCFTR	human	3.3 Å	Detergent (LMNG, digitonin, CHS)	E1371Q	Closed, outward-facing, Phosphorylated, ATP-bound, VX-770-bound	Single Particle	2019	Sf9 virus, HEK cells
hCFTR	human	3.2 Å	Detergent (LMNG, digitonin, CHS)	E1371Q	Closed, outward-facing, Phosphorylated, ATP-bound, GLPG1837-bound	Single Particle	2019	Sf9 virus, HEK cells

1.4.4. Need for more CFTR structures.

While these structures have provided invaluable information, confirming many interactions identified previously by functional experiments, there is still a need for additional structures to understand the function of CFTR fully. All high-resolution structures published to date are of protein entirely solubilized in detergent (Table 1.2). Current studies have shown that the solubilization detergent or stabilization detergent dramatically alters CFTR ATPase activity, even after reconstitution into lipids (133); in fact, the choice of reconstitution lipid affects the ATPase activity (134). Thus, it is likely that structures of CFTR in a lipid environment could be very different from those in detergent. Additionally, all of the various transition states of CFTR in opening and closing and the disease-causing mutations have yet to be explored in terms of a detailed structural description. These data suggest the need for more structures and simulations of these structures to connect CFTR structure and function.

1.5. MEMBRANE PROTEINS AND LIPIDS.

The importance of the lipid environment in maintaining membrane protein structure has been recognized; however, studying purified membrane proteins reconstituted into a lipidic environment has been limited to relatively large structural complexes—bicelles and sheets—due to the nature of lipids (173). Many recent advancements in small lipid bilayer complexes have been and are continuing to be developed, thus improving our understanding of the importance of the lipid bilayer on membrane protein structure and function by improving membrane protein stabilization during purification and reconstitution (174-177).

1.5.1. Advancements in purifying and studying membrane proteins in lipid bilayers.

Studying membrane proteins in a lipidic environment has presented many challenges, especially for functional assays, due to the structures that lipid bilayers form—bicelles and sheets (173). Thus, studying some individual membrane proteins in a lipid environment was almost impossible until recently. The use of amphipathic polymers to stabilize the hydrophobic portions of the membrane proteins or lipids in an aqueous environment has dramatically improved studies of individual membrane proteins (178). Nanodiscs use amphipathic polymers to protect the hydrophobic tails of lipid molecules while keeping the entire protein-lipid complex soluble in an aqueous environment (179, 180). Depending on the type of amphipathic polymer and technique used, a membrane protein can be solubilized and purified in detergent before reconstitution into a lipid bilayer, or the membrane protein and the surrounding annular lipid environment can be solubilized and purified directly for biochemical or structural analysis (1, 181).

1.5.2. "Standard" nanodiscs.

The first type of nanodisc, termed "standard nanodiscs," was developed in 1998 in Dr. Steven Sligar's lab by modifying the human Apolipoprotein-1 (hApo1)—a naturally occurring protein that packages lipid molecules into high-density lipoprotein complex, known as HDL (182). Replacing the large globular N-terminal domain of hApo1 with a Histidine tag (His-tag) and cleavage site left a ~200 amino acid peptide polymer that spontaneously folds into α-helices referred to as the Membrane Scaffold Protein (MSP) (183). Incubation of MSP with detergent-solubilized lipids leads to the spontaneous formation of the nanodisc (Figure 1.14) of regular diameter as the detergent is being removed (183). The length of MSP determines the diameter of the nanodisc. The first developed MSP constructs are still the most commonly used and create nanodiscs with

either 9.7 nm or 11.9 nm diameter (184). Although the diameter can be increased and decreased by altering the length of MSP (185-187), changing the length of MSP will ultimately change the number of lipids accommodated upon insertion and thus will require optimization of the Lipid-to-Protein ratio (LPR) in each experiment (183, 185). Originally, nanodiscs were formed from one of three common lipid types—1,2-dimyristoyl-sn-glycero-3-phosphocholine (DMPC), 1,2-dipalmitoyl-sn-glycero-3-phosphocholine (DPPC), or 1-palmitoyl-2-oleoyl-sn-glycero-3-phosphocholine (POPC) (183, 184) (Figure 1.15); however, now nanodiscs are being generated from different types of lipids and lipid combinations with relative ease (188). There are a few restrictions in forming these nanodiscs. The first is that the LPR and temperature during nanodisc formation are highly dependent on lipid type and its phase transition temperature (179, 187). Nanodiscs form most easily and consistently when the mixture is incubated at temperatures above the phase transition temperature (179, 187). The most likely explanation for this is that lipids behave as a liquid above the phase transition temperature and as gel-like below the phase transition temperature, thus preventing the necessary interactions for forming nanodiscs (179, 187). It is also important that all detergent from membrane protein solubilization and lipid solubilization must be completely removed, either by absorption of the detergent using BioBeads™ or by dialysis (Figure 1.16). The incomplete removal of detergent will also prevent nanodisc formation, and thus the amount of BioBeads™ or length of incubation must be optimized (179). While at first MSP was limited to reconstituting detergent purified membrane proteins, methods have been identified to solubilize membrane proteins with their native lipid environment (189, 190), albeit still using detergent to disrupt the membrane. As

newer amphipathic polymers are discovered, the opportunity to solubilize the membrane without detergent will be a major advantage to studying membrane proteins both structurally and functionally (181).
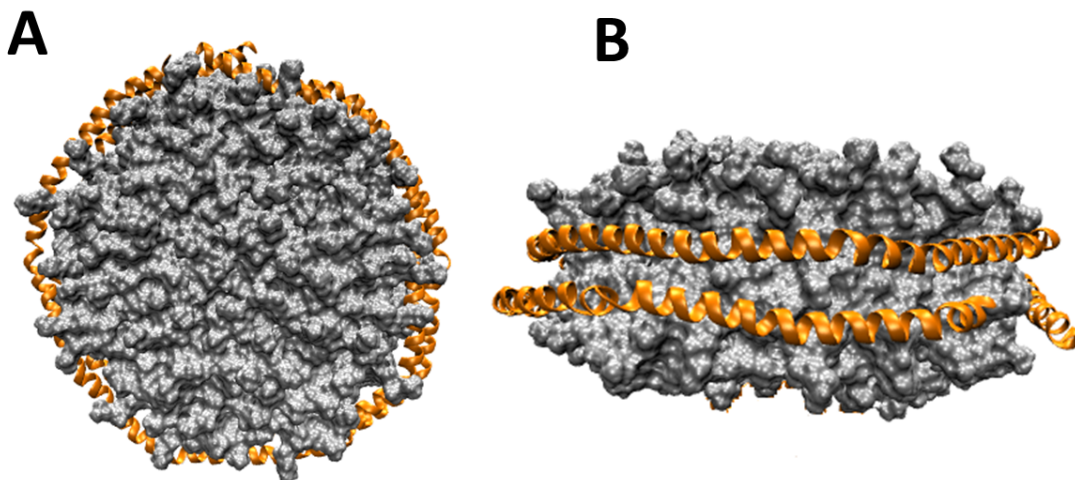
Figure 1.14: A structure of nanodisc formed by Membrane Scaffold Protein (MSP). An individual MSP (orange) wraps around an individual leaflet of the lipid bilayer (gray). Thus, two MSP molecules form a single nanodisc composed of a lipid bilayer. From the top-down view (A), the nanodisc in this image is of MSP1D1 and has a diameter of 9.7 nm. In the side-on view (B), a nanodisc has a height of approximately 5 nm. Images were built in Visual Molecular Dynamics (VMD) software from PDB ID: 6CM1 to show a top-down view (left) and side-on view (right) of a nanodisc.

Figure 1.15: Depiction of the lipids first and commonly used to generate nanodiscs.
All three lipids have the same head group (phosphatidylcholine) but differ in tail
composition. The abbreviations are the following: 1,2-dimyristoyl-sn-glycero-3-
phosphocholine (DMPC), 1,2-dipalmitoyl-sn-glycero-3-phosphocholine (DPPC), or 1-
palmitoyl-2-oleoyl-sn-glycero-3-phosphocholine (POPC).
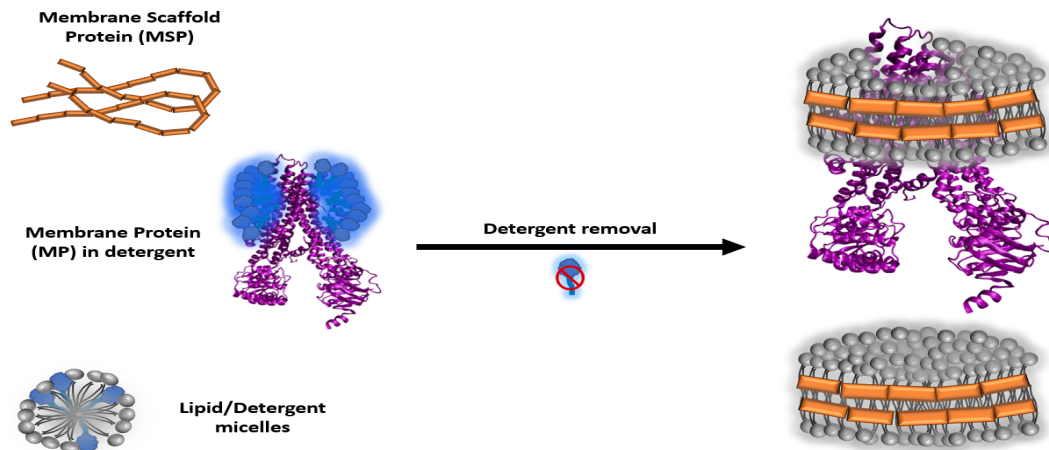
Figure 1.16: Schematic of nanodisc formation. The incubation of the membrane
protein (MP) of interest, membrane scaffold protein (MSP) and lipids (DMPC, DPPC,
POPC, etc.) in a particular ratio with the removal of detergent, either via BioBeads[TM]
or dialysis, will form membrane protein-loaded nanodiscs (full nanodiscs) or lipid-only
nanodiscs (empty nanodiscs).

1.5.3. Native nanodiscs.

The term "native nanodiscs" is used to describe the solubilization of a membrane protein with its native lipid environment using a synthetic polymer (191). While the term is used in a more global capacity to describe any discoidal bilayer system containing a membrane protein and its native lipid environment, the first native nanodisc utilized the synthetic styrene-maleic acid (SMA) polymer to solubilize small portions of the native lipid environment around the membrane protein of interest into uniformly sized discoidal particles (191, 192) (Figure 1.17). Initially, these lipid-bound SMA particles were called styrene-maleic acid lipid particles (SMALPs) (192); they also are called lipodisqs when formed from the commercially available SMA called Lipodisq® (193).
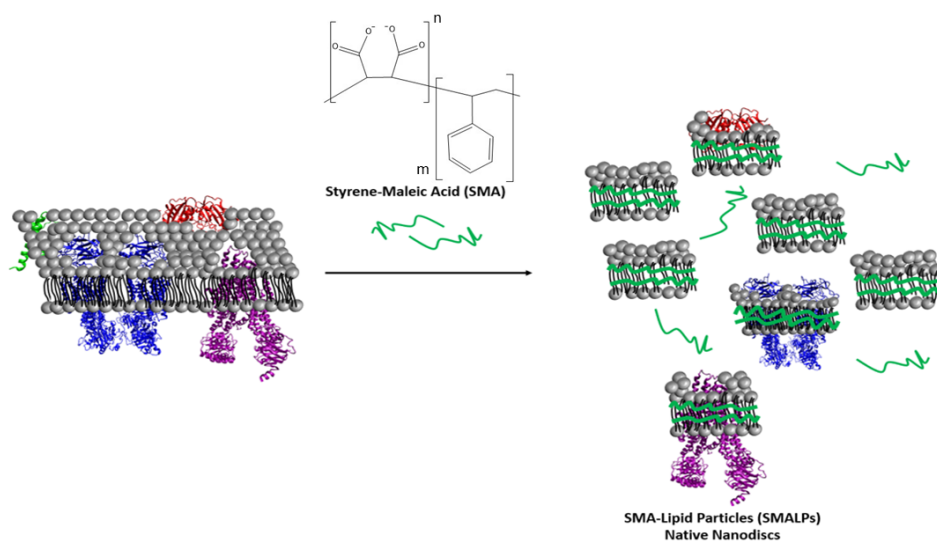
Figure 1.17: Schematic of native nanodiscs formation. Cell membranes containing several endogenous membrane proteins and CFTR incubated with Styrene Maleic Acid (SMA) polymer. SMA will self-insert into the membrane and form native nanodiscs. The membrane protein or membrane proteins of interest can be separated from endogenous membrane proteins using affinity chromatography. The following PDB IDs were used to generate this image: 5UAR, 5IRZ, 6F46, and 1HRK.

1.5.3.1. STYRENE-MALEIC ACID LIPID PARTICLES (SMALPs).

SMA is a synthetic copolymer formed by radical polymerization of maleic anhydride and styrene and then hydrolysis of the maleic anhydride moiety (Figure 1.18) (192). Several different ratios of styrene to maleic acid copolymers are available, with 2:1 and 3:1 being the most common and available commercially under the brand name Lipodisq®, as well as in ratios of 3:1, 2.3:1, and 1.2:1 under the SMALP brand name (194). Computational simulations of SMA in the proximity of a lipid bilayer show that styrene inserts into hydrophobic tails of the lipids in about 20 ns (195). After about 400 ns, the SMA polymer is completely inserted into the membrane. Unlike MSP, SMA solubilizes the membrane by wrapping around the membrane without a clear orientation (195). SMA requires particular buffer conditions for SMALP formation, which can introduce many disadvantages for specific membrane proteins (194). First, the presence of divalent cations, like Mg^{2+} or Ca^{2+}, as well as low pH, inhibit the formation of SMALPs (194, 196, 197). Several studies show SMA preferentially binds lipids in a fluid phase over a
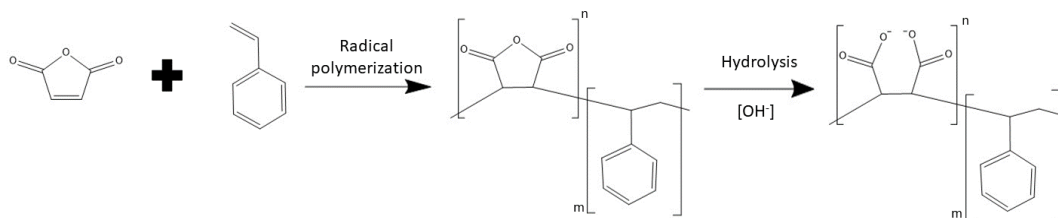
Figure 1.18: Reaction diagram of SMA formation. Styrene and maleic anhydride monomers are mixed and polymerized, forming a polymer of varying uniformity. The final step in the formation of SMA is the hydrolysis of maleic anhydride to maleic acid under basic conditions. The final SMA polymer is used to solubilize membrane proteins and surrounding lipids embedded from the lipid bilayer.

gel phase or an ordered phase (198). Several other studies show SMA solubilizes certain types of lipids preferentially over others, including cholesterol (199, 200). Thus, SMA might not be as efficient at solubilizing a cholesterol-heavy lipid environment, causing preferential SMALP formation of non-cholesterol-associated membrane proteins. However, several varieties of SMA have been developed to combat some of these disadvantages, especially those related to the buffer conditions.
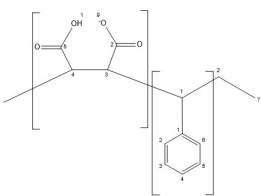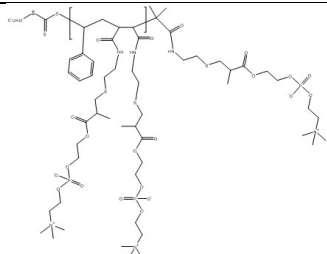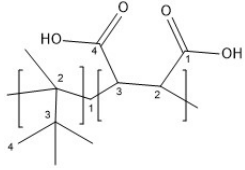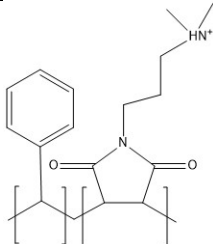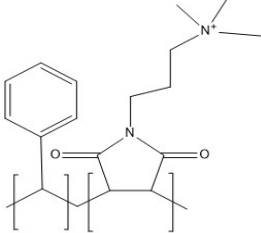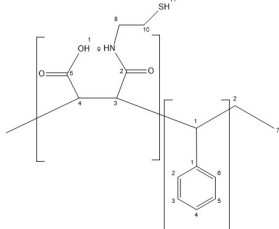
1.5.3.2. OTHER COPOLYMER VARIANTS.

Since the first production of SMA, many copolymers have been identified that can form nanodiscs providing their unique advantages and disadvantages; this discussion is summarized in Table 1.3. The first of these new polymers, called zSMA, modified the carboxyl groups of the SMA copolymer to phosphatidylcholine groups (201); thus, lipid particles formed from this copolymer are referred to as zSMALPs. The zSMA copolymer shows dramatically improved buffer compatibilities for a pH range of 4-10 and a divalent cation concentration of up to 20 mM. The ability of zSMA to solubilize membrane proteins from *E. coli* shows dramatic improvement over the first SMA copolymer for two membrane proteins (201). Further efforts to improve the first SMA copolymer led to the development of the diisobutylene maleic acid copolymer (DIBMA) (202). DIBMA forms similarly shaped discoidal particles to SMA and MSP, called DIBMA lipid particles (DIBMALPs), but with a slightly larger diameter at about 20 nm (202). DIBMALPs have one definite advantage to both SMALPs and standard nanodiscs. The DIBMA copolymer lacks UV-absorbing rings, allowing for more accurate spectrometry results of the incorporated membrane protein (202). DIBMA has another advantage over SMA, as DIBMA is not as sensitive to divalent cations. However, DIBMA is not as effective at

solubilizing membrane proteins from *E. coli* membranes as the commonly used detergent DDM (n-dodecyl β-d-maltoside) (202).

DIBMA and zSMA are not the only new variants developed. Another new variant is the styrene maleimide (SMI) copolymer, forming SMI lipid particles (SMILPs) (203). Interestingly, SMILPs are slightly smaller in diameter than DIBMALPs at 11 nm, but similar in size to the standard nanodisc diameter. The SMI copolymer is even more tolerant of divalent cations than any predecessor, showing lipid solubilization at up to 100 mM for both Ca^{2+} and Mg^{2+}. SMI can solubilize membrane proteins from *E. coli* membranes as well as detergent (DDM) at physiologically low pH. SMI is much improved over the SMA copolymer; however, SMI is not as efficient at solubilizing membrane proteins from *E. coli* membranes at neutral pH as SMA and detergent (DDM) (203). The copolymer showing the most dramatic improvement to the disadvantages of the first SMA copolymer is styrene maleimide quaternary ammonium (SMA-QA) (204). Nanodiscs formed by this copolymer show no sensitivity to divalent cations (up to 200 mM) or too low, neutral or high pH, and this copolymer shows the ability to control the diameter of the nanodiscs by regulating the ratio of polymer to lipid; however, the ability of this copolymer to solubilize membrane proteins remains to be tested (204). One of the most recent, yet attractive, copolymers developed again modifies the first SMA copolymer by forming an amide bond on the carboxylic moiety of the maleic acid through the addition of cystamine. This new polymer, called SMA-SH, does not improve the buffer condition solubility of SMA, but it does allow for membrane protein purification strategies and a plethora of fluorescent studies (205, 206). These polymer variants and advantages and disadvantages are summarized in Table 1.3.

Table 1.3: Structures of SMA derivatives and current characterization. The use of polymers to solubilize membrane proteins and package lipids into nanodiscs is a relatively new technology, and each polymer provides a unique set of advantages.

Polymer	Structure	Advantages	Disadvantages
SMA (Styrene Maleic Acid)		• Original polymer • Heavily characterized • Commercially available	• Precipitates in the presence of divalent cations • pH sensitive • Preferential lipid binding
zSMA		• pH range of 4-10 • Divalent cation concentration <20mM	• Not commercially available • UV-absorbing moiety
DIBMA (Diisobutylene Maleic Acid)		• Large particle diameter (20 nm) • No UV-absorbing moiety	• Lipid preference
SMI (Styrene Maleimide)		• Divalent cation concentration <100 nM • Good lipid solubilization at low pH	• Poor lipid solubilization at high pH
SMA-QA (Styrene Maleimide Quaternary Ammonium)		• Divalent cation concentration <200 mM • No pH sensitivity • Size is controllable	• Has not been tested for membrane protein solubilization
SMA-SH		• Modified cystamine allows for purification strategies and fluorescent studies.	• No improvements on buffer conditions from SMA

1.5.4. Downstream studies of membrane proteins in nanodiscs.

Using traditional biochemical and biophysical techniques to study individual membrane proteins in a lipid bilayer has been difficult. The use of nanodiscs, both the original and native, has vastly increased the number of studies providing both functional and structural data for membrane proteins. This nanodisc technology is especially crucial for membrane proteins involved in lipid regulation and synthesis (179).

1.6. CONCLUSIONS.

The improved technologies of nanodiscs have created an entirely new environment for studying membrane proteins and allows for the investigation of a multitude of new questions about the importance of the lipid environment for membrane proteins. This work describes the initial optimization strategies for building the foundation to investigate the importance of the environment for the very complex, but medically relevant membrane protein CFTR. The following chapters describe the optimization of three different expression cell systems of CFTR and two different affinity chromatography tagging systems. As CFTR has a complex biogenesis, the determination of an appropriate cell expression system and the location of tag for affinity chromatography is highly important for the purification of properly folded, functional CFTR. For our purified CFTR, both the channel function and the ATPase activity were evaluated. In other studies, the ATPase activity of CFTR depended on the detergent used for solubilization, even after reconstitution into a lipid environment (133). Another study reported that CFTR ATPase activity also depends on the lipid environment as studied by destabilized proteoliposomes, which are destabilized by the presence of detergent (134). We hypothesize that we will also see reduced ATPase activity of CFTR in detergent as

compared to in a lipid environment. Because of the differences in ATPase activity, we also hypothesize that the channel activity of CFTR will vary depending on the lipid environment. From one of the aforementioned detergent-solubilized structures of human CFTR, several lipid tail-like densities and a cholesterol-shaped electron density can be seen. This suggests that these lipids play an important structural role for CFTR. We determined the co-purified lipids in our detergent-solubilized purified CFTR sample. These newly released detergent-solubilized structures provide new structural information on CFTR, but before the release of these structures, structural studies relied on homology models. We hypothesized that a homology model could be refined by flexibly fitting in low-resolution maps of the protein determined from 2D lipid crystals. We analyzed these new models with traditional and non-traditional molecular dynamics methods and discussed more in the next chapter.

CHAPTER II

ATP SIGNALING IN A REVISED HOMOLOGY MODEL OF CYSTIC FIBROSIS TRANSMEMBRANE CONDUCTANCE REGULATOR (CFTR)

2.1.   INTRODUCTION.

2.1.1. Publications resulting from this chapter.

Reprinted with permission from Kerry M. Strickland, Gorman Stock, Guiying Cui, Hyea Hwang, Daniel T. Infield, Ingeborg Schmidt-Krey, Nael A. McCarty, and James C. Gumbart (2019) **ATP-Dependent Signaling in Simulations of a Revised Model of Cystic Fibrosis Transmembrane Conductance Regulator (CFTR)**. *J Phys Chem B*. 123(15):3177-3188. Copyright (2019) American Chemical Society.

2.1.2. Individual contributions to the work.

Original concept proposed by Dr. JC Gumbart. Initial simulations designed and prepared by Gorman Stock with guidance from Dr. Gumbart. Final simulations prepared and run by Dr. Hyea "Sunny" Hwang. I analyzed simulation data in preparation for the manuscript in conjunction with Dr. Gumbart. Dr. Guiying Cui initially designed and performed the electrophysiological experiments, while I further analyzed electrophysiological data using a variety of software tools. I wrote the manuscript and edited after reviewer recommendations and have updated the chapter here for inclusion in the thesis.

2.1.3. Introduction.

Ever since the discovery of the cystic fibrosis transmembrane conductance regulator (CFTR) gene in 1989 (38), the corresponding protein, CFTR, has been studied intensely

due to its role in the disease cystic fibrosis (CF). CF is a debilitating disease that significantly diminishes the quality and length of life of affected individuals. With nearly 2000 mutations identified in the gene of human CFTR (http://www.genet.sickkids.on.ca/app) and more than 300 currently identified as disease-causing (207) understanding the structure−function relationship of this protein is critical for overcoming these defects of function. Studying CFTR has been particularly challenging, as it functions as a channel instead of a transporter, making it unique among the proteins in the ABC (ATP-binding cassette) transporter superfamily (208). ABC transporters represent a family of transmembrane proteins with typically four domains: two nucleotide-binding domains (NBDs) and two transmembrane domains (TMDs) (209). ABC transporters, either importers or exporters, move a preferred substrate in a single direction across the membrane with a strict relationship between the amount of substrate transported and ATP consumed. The energy of ATP binding at (typically) two distinct sites in the NBDs is used to enable conformational change in the TMDs; hydrolysis of ATP leads to transport of the substrate across the membrane (210). CFTR, on the other hand, evolved to use ATP to form a diffusive pathway for chloride ions; it is the only member of the ABC transporter superfamily known to act as a channel with no strict stoichiometry between ATP usage and substrate transport. CFTR uses a modified "alternating access" transport mechanism (211) in which a pore opens in the TMDs on the time scale of a second (114). In the alternating access model, the substrate has access to the binding site from inside the cell (inward-facing state) or from outside the cell (outward-facing state) but not both at the same time (20). In contrast, in CFTR, the outward-facing state is no longer closed to the inside, but instead, it can form a

channel connecting both sides. One of CFTR's NBDs bears a degenerate ATP-binding site, a feature found in some ABC exporters (212), and thus, CFTR can only hydrolyze ATP at one of the two binding sites. CFTR also possesses a unique ~240-residue regulatory domain (R-domain) between NBD1 and TMD2 (38). Flexible linker domains are found in some other ABC transporters (39, 40); however, the R-domain of CFTR is the largest found to date. Furthermore, it is the only linker known to tightly regulate the protein based on its phosphorylation state (41, 42). The majority of what is presently known about CFTR has been gained through a variety of biophysical techniques. Most prominent among these techniques, due to the channel function of CFTR, is electrophysiology, which was used to characterize and classify many clinically relevant mutations as they were identified (43, 213, 214). Electrophysiology combined with mutagenesis led to the identification of numerous functionally important residues (124). However, until recently, high resolution structural data, necessary to confirm the locations of these residues, lagged far behind functional data on CFTR, in spite of considerable effort. In 2004 and in 2011, a 20 Å and a 9 Å structure of CFTR were published, respectively (156, 157). In both cases, CFTR was crystallized two-dimensionally, and its structure was determined using electron cryo-microscopy (cryo-EM). Both structures confirmed the general topology of CFTR but did not reveal specific residue positions. Within the last several years, four 3–4 Å resolution structures of CFTR have been solved by single-particle cryo-EM: an inward-facing zebrafish CFTR (zCFTR) (48), an outward-facing zCFTR (127), an inward-facing human CFTR (hCFTR) (126), and an outward-facing hCFTR (128), although none of them display an open pore. While these structures and models provide information on a few conformations of CFTR, its

complex gating cycle suggests there are numerous transitory states (215). Molecular dynamics simulations have the potential to reveal these otherwise "invisible" states, simultaneously providing more information on the transitional interactions formed and broken to translate structural information from one domain to another. Prior to the release of the 3–4 Å resolution structures of CFTR, structures of several other ABC transporters were solved (7, 14, 158, 216). These structures were used as templates for several CFTR homology models (130, 159, 161-165). While the homology of the NBDs across transporters is relatively high due to their conserved functions of ATP binding and hydrolysis, the TMDs are quite diverse due to the manifold substrates transported. To address this variability, experimental data on CFTR have been incorporated as hard constraints during homology-model building in efforts to capture the unique pore characteristics of CFTR (130, 164). Nonetheless, concerns about the validity of these models remain, since they were based upon the structures of distantly related paralogs. In this study, we have further refined an existing homology model of CFTR, that from Rahman *et al.* (130), by applying molecular dynamics flexible fitting (MDFF) to fit it to a cryo-EM map of CFTR (157, 217). Extended simulations of the best fit structure displayed the formation of a complete pore, albeit one that is not yet conductive. These simulations also revealed a novel pair of salt bridges involving three residues in the NBDs and intracellular loops (ICLs), which were transiently formed during the channel opening process and thus would not be represented in the static cryo-EM structures. Both salt bridges were experimentally confirmed to be functionally relevant, pointing to a putative allosteric mechanism for signaling the state of ATP occupancy in the NBDs to the pore.

2.2.   METHODS.

2.2.1. Flexible fitting.

The starting model of CFTR was taken from the 2013 homology-model study performed by Rahman *et al.* (130). Briefly, this outward-facing model was constructed by aligning the human CFTR sequence with the Sav1866 crystal structure (PDB 2HYD) in Modeler (7, 218). Additional experimental constraints, consisting of known interactions lining the pore of CFTR, e.g., salt bridges, were also used to refine the model (130). Here, we further refined the open-channel CFTR homology model using molecular dynamics flexible fitting (MDFF) (217, 219) and a cryo-EM map of CFTR reported in 2011 (130, 157). This map contains 12 copies of the protein arranged in two tightly packed crystal planes, which we refer to as the crystallographic map. In addition to the full map, MDFF was also performed on a second map created by averaging the 12 copies of the protein in the crystallographic map, referred to as the average map. For each of the two maps, the homology model was rigid-body docked using the Situs package (220), after which MDFF was performed using NAMD (221). The fitting was carried out with secondary-structure restraints. For the crystallographic map, the homology model was replicated and translated to match the 12 proteins apparent within the EM map. To prevent distortions at the edges of the map, symmetry restraints were applied to all 12 copies using the crystallographic symmetry parameters (222). MDFF simulations were set up as recommended in the MDFF tutorial (http://www.ks.uiuc.edu/Training/Tutorials/science/mdff/tutorial_mdff.pdf); alternative simulation parameters were not attempted. Fitting was run until the root-mean-square deviation of the backbone stopped increasing, roughly 2 ns each. Fitting to the crystallographic map increased the cross-correlation coefficient (ccc) from 0.26 to 0.40;

fitting to the averaged map increased it from 0.46 to 0.56, comparable to the values obtained in Simhaev *et al.* for a different model (0.50–0.53) (223). Even a perfect fit is not expected to yield a ccc of 1.0, as there is extraneous density due to, e.g., bound detergent molecules. Although the crystallographic-map fit contains 12 copies, the symmetry restraints are increased over the course of the simulation to such a degree that, by the end, the copies are in identical conformations (Simulation System Construction). Careful consideration went into the placement of ATP in our refined model. The degenerate binding site of CFTR was modeled after the human CFTR NBD1 homodimer crystal structure (PDB: 2PZE) (224). The crystal structure was aligned to NBD1 of the model by comparing their ABC binding motifs, namely, the ABC signature sequence, Walker A, and Walker B motifs. The corresponding ATP in the crystal structure was placed into the fits by this alignment. Because the NBD1 homodimer structure does not contain a canonical binding site, we used the crystal structure of human ABCB6 (PDB: 3NH9) (225) to model the second ATP in a procedure similar to the first. The three models, namely, the original homology model along with the two fitted models, were each inserted into a POPC lipid membrane slab generated using VMD (Visual Molecular Dynamics) (226). This membrane slab was roughly 140 Å by 75 Å and, after deleting lipids that overlapped with the protein, contained 344 lipid molecules. This system was then solvated above and below the membrane with ~72,000 water molecules. Na^+ and Cl^- ions were added at a concentration of 0.15 M to mimic biological conditions and to neutralize the system. The total atom count of each system was roughly 280,000 atoms.

2.2.2. MD simulations and analysis.

All simulations were performed using the NAMD Molecular Dynamics package (221).

The CHARMM36 force field (227-229) was utilized along with TIP3P water (230). Periodic boundary conditions were imposed. Constant pressure at 1 atm and temperature at 300 K were maintained during the simulations. A 12 Å cutoff with a force-based switching function beginning at 10 Å was employed for van der Waals interactions. A time step of 2 fs was used for all simulations, with long-range electrostatic interactions calculated every other time step using the particle-mesh Ewald method (231). Systems were equilibrated in stages as follows (232). First, all atoms except those in the lipid tails were restrained, allowing the tails to melt for 0.5 ns. Then, all of the atoms belonging to the protein were restrained, allowing the rest of the membrane to relax for an additional 0.5 ns. Next, only the backbone of the protein was restrained, allowing the side chain positions to relax for 0.5 ns. Finally, the systems were run at equilibrium fully unrestrained. Both fits as well as the original homology model were run for 100 ns in each of the three ATP states described, namely, with 0, one, or two ATP bound at the NBDs. In addition, the crystallographic-fit simulations were extended for 200 ns more, giving a total of 300 ns.

2.2.3. Pore analysis.

Pore analysis was performed using the modified Fortran code HOLE (233) and the Python package MDanalysis (234). The analysis was run with default parameters, i.e., an end-point radius of 22.0 Å, a search direction of the z-axis perpendicular to the membrane, a sample point distance of 0.2 Å, and no center point of the pore specified. The program uses the following van der Waals radii: 1.85 Å for carbon atoms, 1.65 Å for oxygen atoms, 2.00 Å for sulfur atoms, 1.75 Å for nitrogen atoms, 1.00 Å for hydrogen atoms, and 2.10 Å for phosphorus atoms. All trajectories were divided into 1 ns snapshots

that were then supplied to HOLE. The program output the pore radius as a function of position along the pore axis. To ensure faster calculation, only the TMDs and some of the surrounding lipids were included in the analysis. Finally, we employed a modified radius of gyration (R_G) method to analyze the splaying of the TMDs. While normally R_G is a three dimensional quantity, here we only considered the in-plane (x and y) distribution of the protein-backbone atoms. The trajectories were aligned along the z-axis prior to measuring the modified R_G.

2.2.4. Preparation of oocytes and cRNA.

Mutant constructs of human CFTR were generated using site-directed mutagenesis via the Quikchange protocol (Agilent Technologies, La Jolla, CA) of the original (wildtype) WT-hCFTR gene in the pGEMHE vector (graciously provided by Dr. D. Gadsby, Rockefeller University). Mutations were confirmed by sequencing the entire open reading frame before cRNA generation. A 2−10 ng aliquot of CFTR cRNAs was injected into *Xenopus laevis* oocytes, and incubation occurred at 17 °C in modified Liebovitz's L-15 media supplemented with HEPES (pH 7.5), penicillin, and streptomycin. Oocytes were typically incubated between 48 and 96 h after cRNA injections before recording. Animal handling methods and oocyte collection are in accordance with National Institute of Health (NIH) guidelines, as well as with protocols approved by the Institutional Animal Care and Use Committee (IACUC) of Emory University.

2.2.5. Electrophysiology.

Oocytes were shrunk in hypertonic solution; then, the vitelline membrane was manually removed. Pipettes used for inside-out macropatch recordings were pulled from borosilicate glass (Sutter Instrument Co., Novato, CA) and had resistances between 1 and

2 MΩ after being filled with chloride-containing pipet solution: 150 mM NMDG-Cl, 5 mM MgCl$_2$, 10 mM TES (pH 7.5). To activate surface-expressed channels, the cytoplasmic side of excised patches was exposed to solution containing the following: 150 mM NMDG-Cl, 1.1 mM MgCl$_2$, 2 mM Tris−EGTA, 10 mM TES, 1 mM MgATP (adenosine 5′-triphosphate magnesium), and 1 μL/mL (127.6 U/mL) of PKA (pH 7.5). All macropatch recordings, at RT (22–23 °C), were performed using an Axopatch 200B amplifier operated by pClamp 8.2 software; data were filtered at 100 Hz with a four-pole Bessel filter and acquired at 2 kHz. The following voltage protocol was applied every 5 s: hold at Vm = 0 mV, then step to +100 mV for 50 ms followed by a ramp down to −100 mV over 300 ms prior to returning to 0 mV.

2.2.6. Source of reagents.

The medium L-15 was obtained from Gibco/BRL (Gaithersburg, MD), and the PKA catalytic subunit was obtained from Promega (Madison, WI). Stock CFTR$_{inh}$172 was initially prepared as 50 mM in Dimethyl Sulfoxide (DMSO). All chemicals were diluted to the stated final concentration in recording solution immediately before use.

2.2.7. Statistical analysis.

Unless noted in the figure legend or body of text, statistical analysis values are the mean ± SEM. For data, a *t*-test for unpaired or paired measurements in Sigmaplot 12.3 (San Jose, CA) was used to evaluate statistical significance; only values of $P < 0.05$ were considered significantly different as denoted as follows: represented by * are values of $P < 0.05$, represented by ** are values of $P < 0.01$, and represented by *** are values of $P < 0.001$.

2.3. RESULTS.

2.3.1. MDFF fitting of the homology model to the cryo-EM map of crystallized CFTR.

Many groups have tried to circumvent the previous lack of structural knowledge by making homology models of CFTR using structures of closely related ABC transporters (159, 161-165, 235), including one from our work (130). To refine the Rahman *et al.* homology model (130), molecular dynamics flexible fitting (217) simulations were run on the outward-facing structure, which resulted from 10 ns of targeted MD (130), utilizing the 9 Å resolution cryo-EM map of wild-type human CFTR from Rosenberg *et al.* (157). The map may represent an artificially stabilized state of CFTR due to its crystallization (223), which differs from the single-particle cryo-EM used for the higher resolution structures recently released (48, 126-128); nonetheless, it is used here, as it represents a physically possible conformation that can aid improvement of existing homology models. Furthermore, all cryo-EM maps to date have been determined for CFTR in detergent, which may also alter its accessible conformations. MD simulations of a cryo-EM determined or fitted CFTR in a native-like membrane can allow it to relax to a more physiologically relevant state. Two approaches were used in fitting the Rahman *et al.* homology model to the map. In the first approach, we imposed crystallographic conditions matching the dimensions of the cryo-EM map, i.e., 12 copies of the protein with crystallographic symmetry restraints between them (see Methods). In the second approach, a single copy of CFTR was fit to a spatially averaged map provided by R. Ford (*personal communication*). Thus, two fitting approaches produced two new conformations of the homology model; we will refer to the first as the "crystallographic-fit model" and the second as the "averaged-fit model", named after the corresponding

maps to which they were fit. As mentioned above, the homology model was built with constraints on experimentally supported interactions specific to the open state of CFTR (130). The fitting of the model to either map lost one to three of these interactions (Table 2.1), although the map may represent a transient closed state of CFTR (223). In the crystallographic-fit model, S341, a pore-lining residue near the gate/selectivity filter of CFTR (152), is in close proximity to TM12 residues L1135 and N1138, which is characteristic of the closed state (see Figure 2.1). It should be noted that the 2D protein crystals used to determine the cryo-EM map were composed of nonphosphorylated CFTR in the absence of ATP (157), yet both phosphorylation and ATP binding are necessary for the opening of the channel (106, 112, 236-238). Therefore, it is not surprising that fitting an open-state homology model of CFTR to the cryo-EM map effectively "closed" the channel in the absence of ATP. In this pose, the NBDs are dimerized despite the lack of ATP, possibly a consequence of the 2D crystal packing in the cryo-EM experiments (157). However, this pose of CFTR may represent a physiological state of CFTR wherein the NBDs transiently interact, but the interaction of the NBDs without ATP is not sufficiently stable to open the CFTR pore (239, 240); this state may be equivalent to the "strained transitional" closed conformation described by Rahman *et al.*, which is permissive to opening but not yet open (130). The idea of an intermediate closed state has also been recently proposed by Simhaev *et al.* (223). In that study, two homology models of CFTR, those from Corradi *et al.* (162) and from Dalton *et al.* (164), were flexibly fitted into the Rosenberg *et al.* cryo-EM map (157) and simulated in the apo-ATP state. Analysis of the MD simulations of these new models also demonstrated a lack of pore formation in the absence of ATP. This suggests that

ATP binding to the NBDs stimulates significant conformational changes to enable pore formation.

Table 2.1: Experimentally validated interactions in the original homology model and fitted structures. *Numbers in brackets are references for the listed interactions.*

Residues	Interaction	Homology	Averaged	Crystallographic
S605-A1374	[1] Cross-link ≤8Å	✓	✓	✓
S549-S1248	[1] Cross-link ≤8Å	✓	✓	✓
S434-D1336	[1] Cross-link 8Å≤d≤16Å	✓	✓	✓
S549-A1374	[1] Cross-link 8Å≤d≤16Å	✓	✓	✓
E267-K1060	[2] Salt Bridge ≤4Å	✓	-	-
R347-D924	[3] Salt Bridge ≤4Å	✓	-	-
R352-D993	[4] Salt Bridge ≤4Å	✓	✓	-
M348-T1142	[5] Cross-link ≤13Å	✓	✓	✓
T351-T1142	[5] Cross-link ≤13Å	-	✓	✓

[1] M. Mense, P. Vergani, D. M. White, G. Altberg, A. C. Nairn, and D. C. Gadsby. In vivo phosphorylation of CFTR promotes formation of a nucleotide-binding domain heterodimer. EMBO J., 25:4728–4739, 2006.

[2] A. Billet, J. P. Mornon, M. Jollivet, P. Lehn, I. Callebaut, and F. Becq. CFTR: effect of ICL2 and ICL4 amino acids in close spatial proximity on the current properties of the channel. J. Cyst. Fibros., 12:737– 745, 2013.

[3] J. F. Cotten and M. J. Welsh. Cystic fibrosis-associated mutations at arginine 347 alter the pore architecture of CFTR: Evidence for disruption of a salt bridge. J. Biol. Chem., 274:5429–5435, 1999.

[4] G. Cui, Z.-R. Zhang, A. R. W. O'Brien, B. Song, and N. A. McCarty. Mutations at arginine 352 alter the pore architecture of CFTR. J. Membr. Biol., 222:91–106, 2008.

[5] E. Y. Chen, M. C. Bartlett, T. W. Loo, and D. M. Clarke. The 508 mutation disrupts packing of the transmembrane segments of the cystic fibrosis transmembrane conductance regulator. J. Biol. Chem., 279(38):39620–39627, 2004.
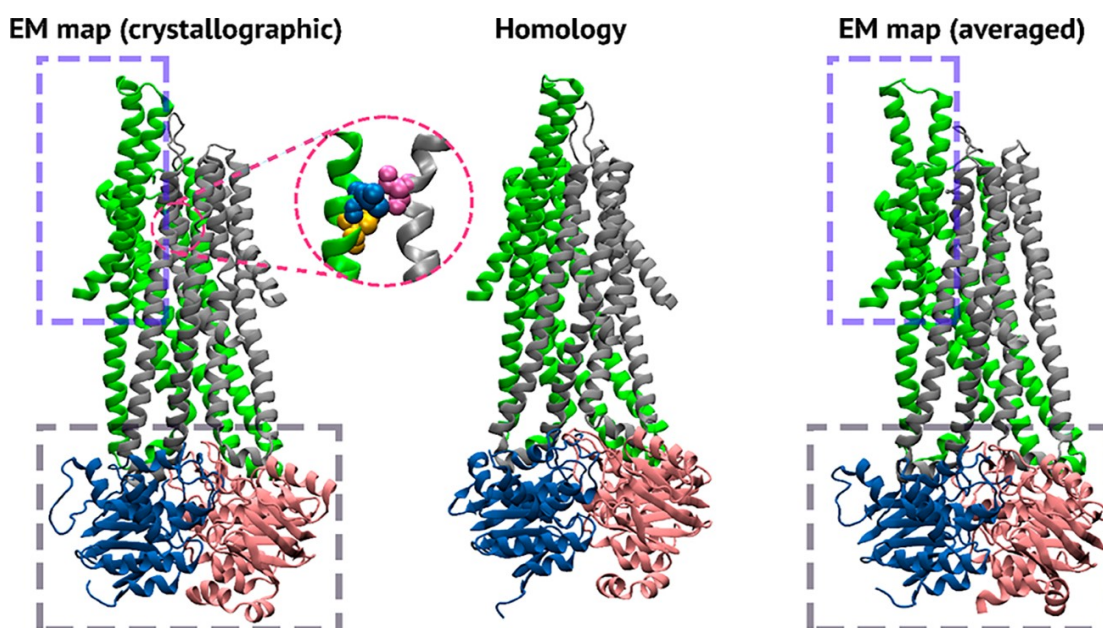
Figure 2.1: Cartoon depictions of our two MDFF-fitted structures ("crystallographic" on the left and "averaged" on the right) and the Rahman et al. homology model that served as the starting point for MDFF. The domains are colored as follows: NBD1, pink; NBD2, blue; TMD1, gray; TMD2, green. A slight twist of the NBDs relative to the original model is indicated by the gray rectangles in the refined models. The additional curvature of TMs 7 and 8, as compared to the homology model, is highlighted by the purple rectangles. The pink circle magnifies the proximity of residue S341 (pink) on TM6 and L1135 (blue) and N1138 (yellow) on TM12.

Reference: K. S. Rahman, G. Cui, S. C. Harvey, and N. A. McCarty. Modeling the conformational changes underlying channel opening in CFTR. PLoS One, 8(9):1–13, 2013.

2.3.2. ATP-stabilized dimerization of NBDs is improved in fitted models as compared to the original homology model.

A wealth of evidence indicates that CFTR channel opening is preceded by ATP-stabilized dimerization of the NBDs (241, 242). This was supported by targeted molecular dynamics simulations of the Rahman *et al.* homology model (130), which described a conformational wave starting with dimerization of the NBDs and leading to pore dilation. Our initial models generated from MDFF feature loosely dimerized NBDs, while the TMDs present a closed channel. We reasoned that simulating these models in the presence or absence of ATP may allow us to observe conformational changes relevant to channel gating of CFTR. To identify novel fitting-induced behavior, we simulated three distinct initial models, namely, the original Rahman *et al.* homology model (130) as well as our two MDFF-derived models. For each of these models, we generated the following three states: "bound" (two ATP docked between the NBDs; see Methods), "semi" (one ATP at the noncanonical binding site), and apo (no ATP). Thus, a total of nine states were each simulated for at least 100 ns. The dimerization of the NBDs has been quantified as the distance between the centers of masses of the NBDs and has been plotted for the bound simulations in Figure 2.2. Docking of ATP at both sites led to tighter NBD dimerization in both the averaged- and crystallographic-fit models when compared to the original homology model. Simulations of P-glycoprotein have led to the hypothesis that the adenine moiety of each ATP forms stabilizing hydrophobic interactions with the X-loop of an NBD (243). We see similar interactions between the X-loop of NBD1 and the ATP in the consensus site in the simulation of the crystallographic-fit model but not the

averaged-fit model; such an interaction is also seen in the cryo-EM structure of ATP-

bound hCFTR (128). In neither case were interactions between the X-loop of NBD2 and

the ATP in the degenerate site observed.
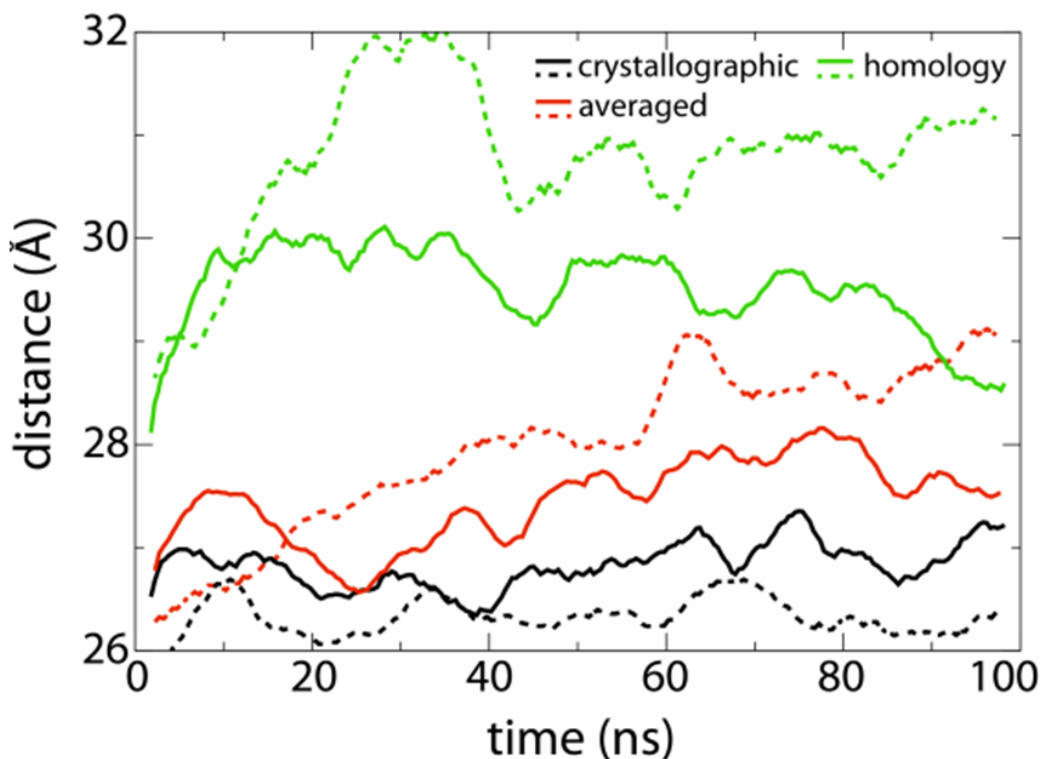
Figure 2.2: Plot of NBD-NBD distance for the three different CFTR homology models simulated with ATP bound. The separation was calculated by taking the difference in centers of mass of the α-carbons in each NBD. Both refined models, averaged and crystallographic, display tighter NBDs dimerization than the original Rahman et al. homology model. The dashed line and the solid line each represent a different trial.

Reference: K. S. Rahman, G. Cui, S. C. Harvey, and N. A. McCarty. Modeling the conformational changes underlying channel opening in CFTR. PLoS One, 8(9):1–13, 2013).

2.3.3. Analysis of simulations shows the development of a partial pore in the crystallographic-fit model.

It is expected that ATP binding at both sites will induce the opening of a pore in CFTR (244, 245). We searched for such a pore in the three models with the program HOLE applied every 1 ns to our simulation trajectories (233). Even though a fully conducting pore (radius larger than 1.8 Å across the entire length of CFTR) could not be seen in any of the nine systems within 100 ns, partial pore opening was observed for the crystallographic-fit model when compared to the original model but not for the averaged-fit model. To facilitate observing possible differences between the models, the pore radius near the residue F337 at the extracellular vestibule, which is one helical turn beyond S341 and noted as a bottleneck previously (157), was used for comparison (Figure 2.3). Upon simulating the original Rahman *et al.* homology model (130) with the addition of ATP, the originally reported pore quickly collapsed near F337 with a radius below 2 Å; however, a consistent increase in pore radius in the ATP-bound state of the crystallographic-fit model was observed during the simulation. This increase in pore radius is due to a coupled motion of TMs 9 and 12. In the simulation of the averaged-fit model, TM9 starts farther from the protein center, which allows TM12 to collapse inward, preventing the formation of a pore (see Figure 2.5). Repeated 100 ns runs of the bound and apo states for each model produced similar results (see Figure 2.4). The pore analysis also revealed alternative pathways through the extracellular region of CFTR. For example, the pathway described in Rahman *et al.* (130) was between residue S341 and T1134 on TMs 6 and 12, whereas, in our simulation of the crystallographic-fit model, a distinct pathway between TMs 1 and 12 is observed. These pathways are consistent with
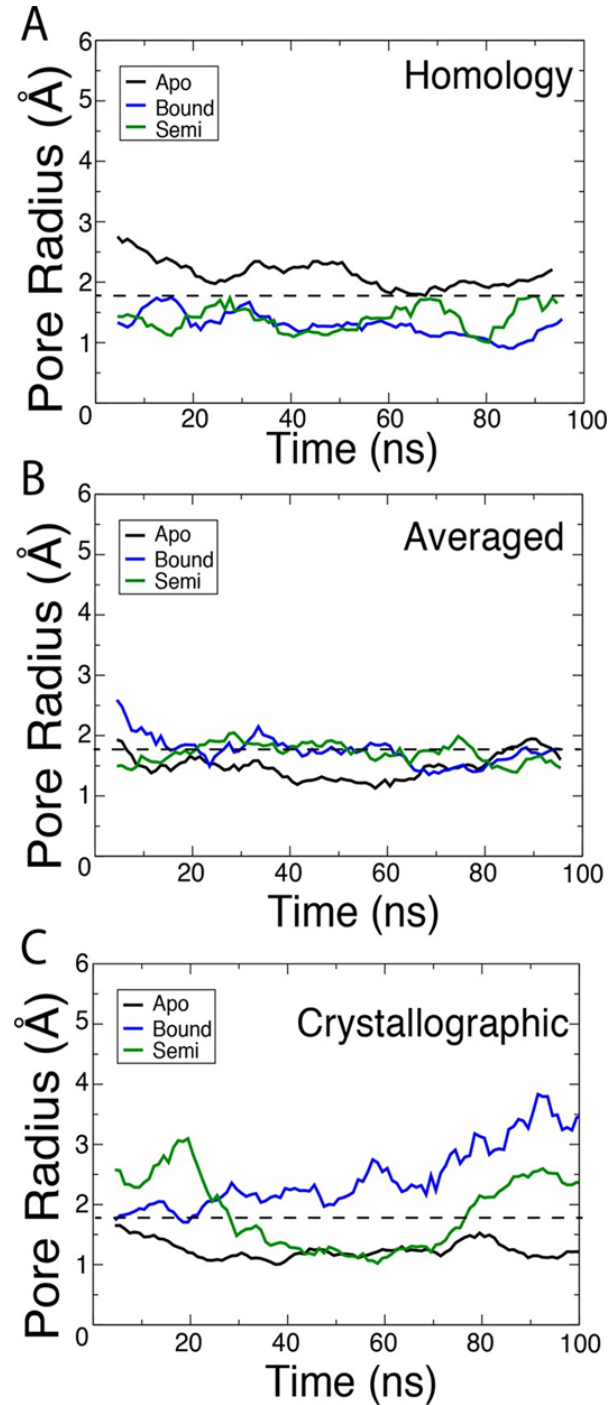
Figure 2.3: Pore analysis of the three different CFTR homology models simulated in ATP-apo (black), ATP semibound (green), and ATP-bound states (blue). The pore radius plotted for each model was evaluated near F337. The dashed line indicates the radius of a chloride ion (1.8 Å). Only the crystallographic-fit model shows widening in both bound and semibound states. See Figure 2.4 for repeated runs of the bound and apo states of each model.

59
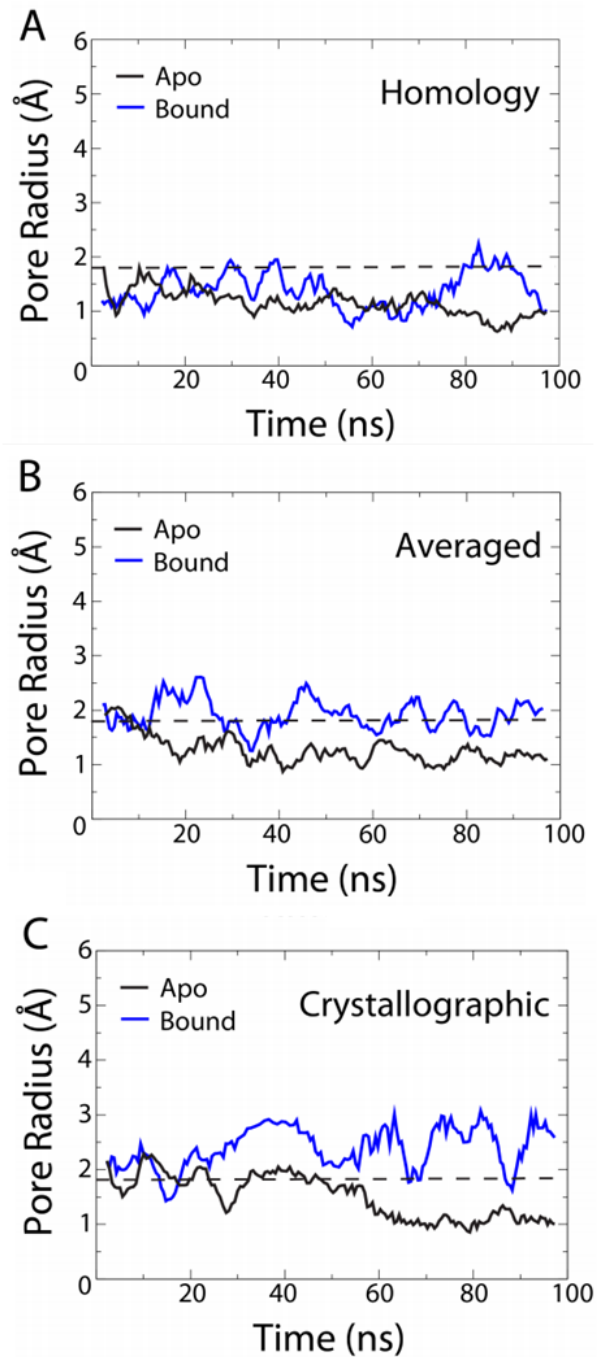
Figure 2.4: Pore analysis of the second runs of the three different CFTR homology models in ATP-apo (black) and ATP-bound states (blue). The pore radius plotted for each model was evaluated near F337. The dashed line indicates the radius of a chloride ion (1.8 Å). Only the crystallographic-fit model shows widening in both bound and semi-bound states.

60
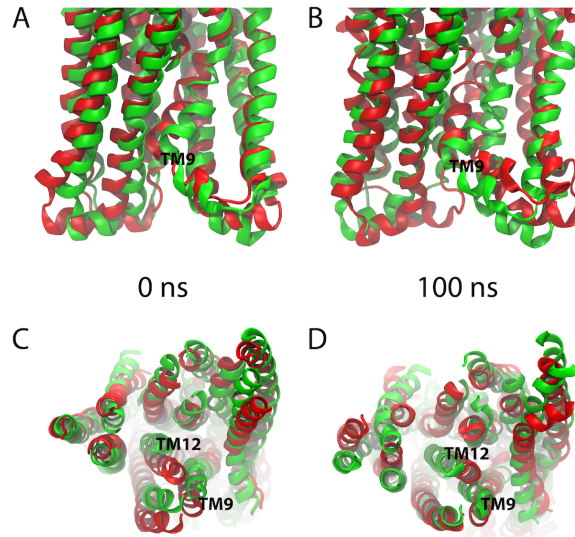
Figure 2.5: Comparison of the averaged-fit (red) and crystallographic-fit (green) models for the first run of each. (A,B) Comparison at 0 (A) and 100 ns (B) viewed from the membrane plane (the intracellular side is on the bottom). TM9 is indicated. (C,D) Comparison at 0 (C) and 100 ns (D) viewed from the extracellular side. TM9 and TM12 are indicated.

the findings based upon both the Mornon *et al.* (165) and Corradi *et al.* (162) homology models. Additionally, the Corradi study reported two lateral tunnel openings forming at the NBD and ICL cytoplasmic clefts. Multiple water-accessible pathways are also consistent with results of 0.1−1.2 µs-long simulations of both secondary and primary active transporters, which are found to be generally leaky for water (246). In the simulation analysis described above, the radius of the partial pore formed depends greatly on the positions of side chains, and thus, the precision of the pore reported may exceed the accuracy of the CFTR homology model. Therefore, an alternate metric was developed to focus on the outer radius of the channel. This metric, akin to a two-dimensional radius of gyration, R_G (see Methods), is plotted in Figure 2.6. A higher R_G value is indicative of more splayed TMDs, which may correlate with a more open pore in CFTR (247, 248).

We partitioned the TMDs along the channel axis into three slices, each including two to three turns of the TM helices, and measured R_G for each over all of the 100 ns simulations (data points taken every 0.2 ns). We then asked whether any of the simulations exhibited time-dependent changes in R_G that would be consistent with channel opening as the pore domain of CFTR shifts from inward-facing to outward-facing. Only R_G for the simulation of the crystallographic-fit model showed substantial dependence on the ATP occupancy state in two independent runs. This dependence is most pronounced for the slice most distant from the membrane on the extracellular side, shown in Figure 2.6 and Figure 2.7, as may be expected (R_G for the other two slices are given in Figure 2.8).
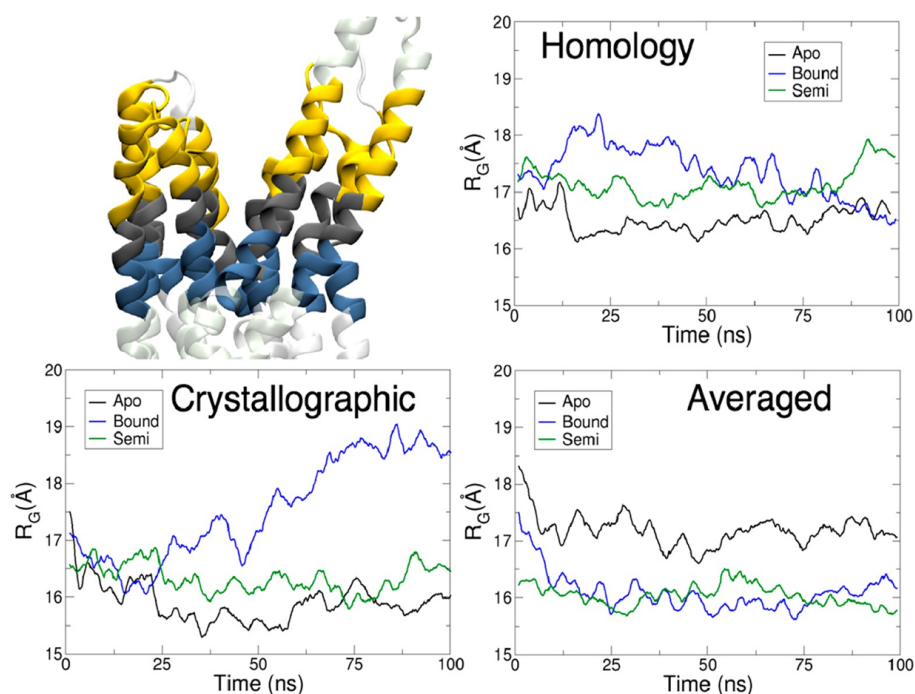
Figure 2.6: Radius of gyration (R_G) analysis for the three CFTR homology models simulated in ATP-apo, ATP-semibound, and ATP-bound states. (upper left) Cartoon representation of the TMDs of the crystallographic-fit CFTR (extracellular side at the top). The TMDs have been divided on the basis of their position along the pore axis into three sections. R_G for the upper section (yellow) is plotted here for the indicated structures, and the middle (gray) and bottom (blue) sections are plotted in Figure 2.7 and 2.8. The crystallographic-fit model shows significant widening for the uppermost section in the ATP-bound state.
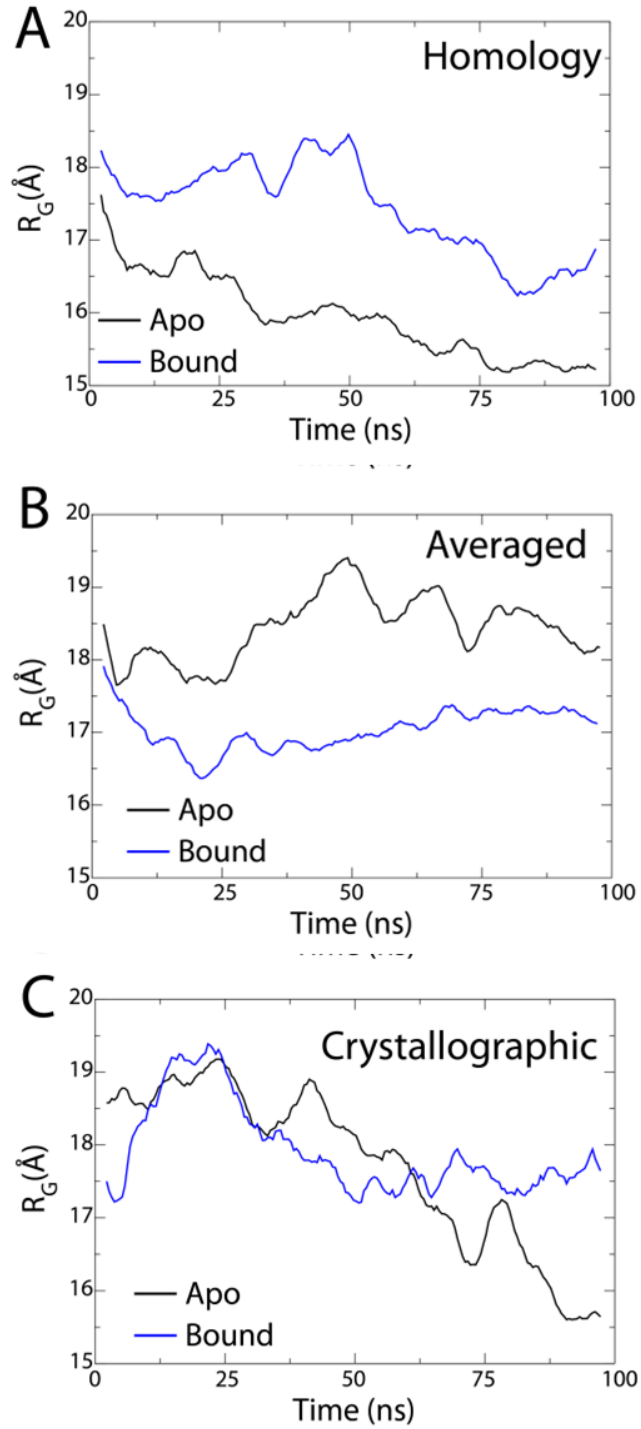
Figure 2.7: Radius of gyration (R_G) vs. time for slice 1 from the second runs of the Rahman et al. homology (A), averaged-fit model (B), and crystallographic-fit model (C).
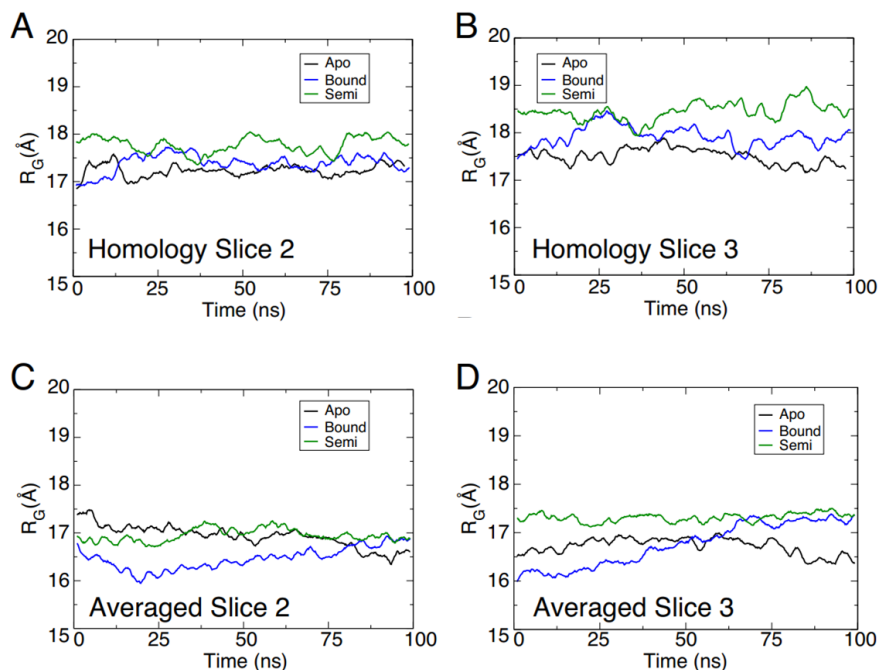
Figure 2.8: Radius of gyration (R_G) vs. time for slices 2 and 3 from the first runs of the Rahman et al. homology model (A,B) and averaged-fit model (C,D).

Reference: Rahman, K. S., Cui, G., Harvey, S. C., and McCarty, N. A. (2013) Modeling the Conformational Changes Underlying Channel Opening in CFTR. 8, e74574.
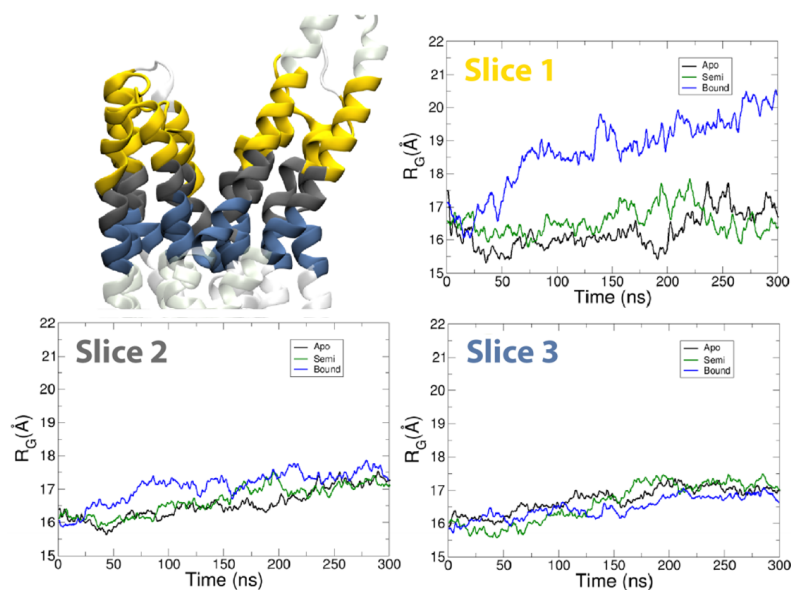
Figure 2.9: Radius of gyration (R_G) vs. time for the first crystallographic-fit run, extended to 300 ns. The graphs labeled Slice 1-3 correspond to the colored sections of the figure in the top left.

2.3.4. Extended simulations of the crystallographic-fit model display a complete pore in the ATP-bound state.

Given that only the crystallographic-fit model shows any ATP dependence, both in partial pore formation and in adopting a putative outward-facing conformation within 100 ns, simulations of all three ATP occupancies of this model were extended to 300 ns (second runs for the bound and apo states were also extended to 300 ns). The difference in R_G between the bound state and apo/semi states grew continuously over the entire 300 ns simulation (see Figure 2.9). Examination of the pore evolution in CFTR over this
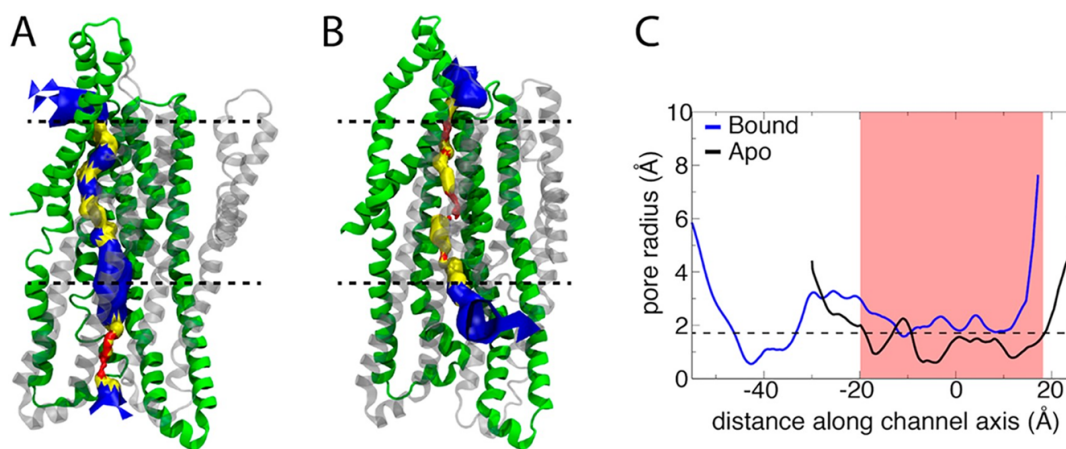
Figure 2.10: Pore analysis of the crystallographic-fit model in (A) ATP-bound and (B) ATP-apo states after 280 ns of simulation each. TMD1 is shown in gray, transparent and TMD2 is in green; NBDs are not shown. In parts A and B, the pore in CFTR is shown according to the following color scheme: radius >2.3 Å is blue, 1.15−2.3 Å is yellow, and <1.15 Å is red. The dashed lines indicate the position of the membrane. (C) Plot of pore radius as a function of position along the channel axis (normal to the membrane) for both bound (blue) and apo (black) states at 280 ns. The shaded area indicates the position of the membrane, and the dashed line at 1.8 Å is the radius of a chloride ion. Second runs of the bound and apo states are shown in Figure 2.11.
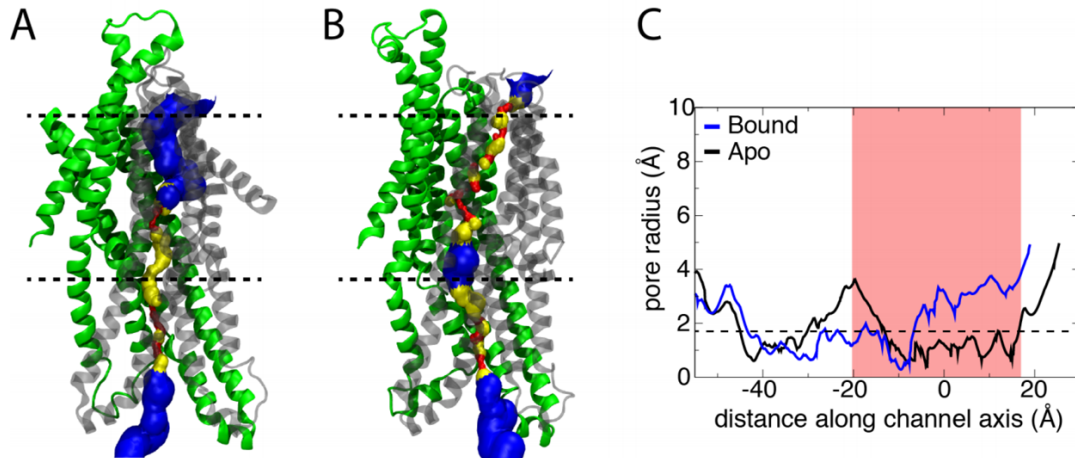
Figure 2.11: Pore analysis of the second 300-ns runs of the crystallographic-fit model in (A) ATP-bound and (B) ATP-apo states. TMD1 is shown in grey, transparent and TMD2 is in green; NBDs are not shown. In (A) and (B), the pore in CFTR is shown according to the following color scheme: radius > 2.3 Å is blue, 1.15-2.3 Å is yellow, and < 1.15 Å is red. The dashed lines indicate the position of the membrane. (C) Plot of pore radius as a function of position along the channel axis (normal to the membrane) for both bound (blue) and apo (black) states at 300 ns. The shaded area indicates the position of the membrane, and the dashed line at 1.8 Å is the radius of a chloride ion.

longer time scale reveals a complete pore in only the first run of the bound-state model at around 280 ns (Figure 2.11), albeit one that is still watertight on the intracellular side at the level of the tetrahelix bundle (235). At the same 280 ns time point, the apo state shows a different, mostly closed pathway (radius of 1−1.5 Å; Figure 2.10), which diverges laterally at the intracellular side of the membrane. The physiological relevance of this lateral pathway for exiting ions, if any, is uncertain. The second run of the bound state also displays an expanded pore in the transmembrane region, although not a complete one (see Figure 2.11). The pore is lined by TMs 4−9 and 12 at various points along its path through CFTR; structurally, it forms due to a radially outward shift of TMs 7−9 and 12 (Figure 2.12). The pore is continuously solvated, but we never observe an ion
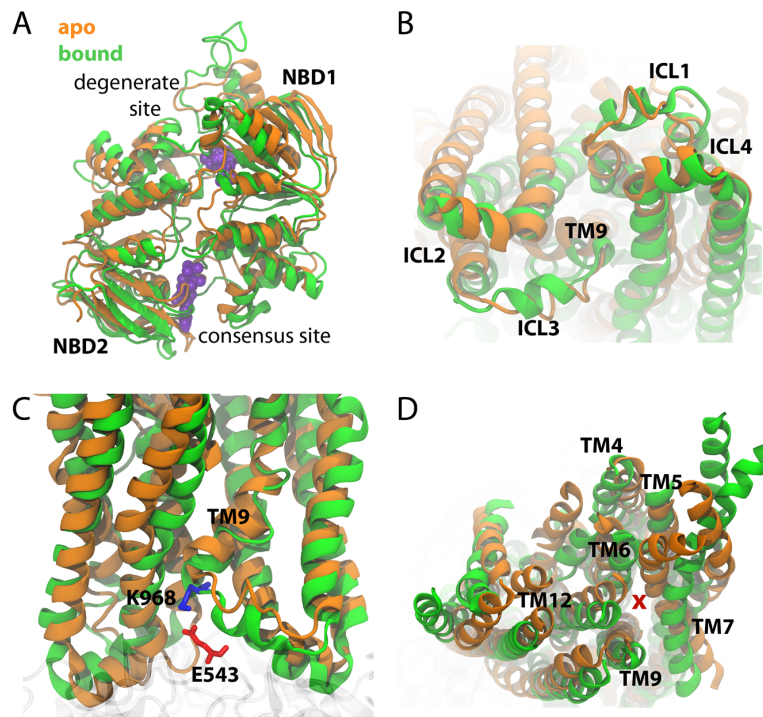
Figure 2.12: Differences between ATP-bound (green) and ATP-apo (orange) states of CFTR. Structures are taken after 280 ns of the first run starting from the crystallographic-fit model (see also Fig. 2.10). (A) NBDs viewed from the cytoplasm. ATP molecules in the bound state are shown in purple. (B) ICLs viewed from the cytoplasm in the same orientation as the NBDs in (A). The bottom of TM9, connected to ICL3, is also indicated. (C) Side-view of ICLs (bottom) and TMDs with one of the discovered salt bridges highlighted. (D) TMDs viewed from the extracellular side. The red x marks the position of the putative initial pore.

inside of it. Arginines, such as R303, R933, R347, and R1128, are present in the pore, which could provide a favorable electrostatic environment for chloride ions. However, the radius is only slightly above the 1.8 Å threshold for a desolvated chloride ion for much of its length, and therefore, we do not expect it to be conductive yet. On the basis of a comparison of the ATP-apo and ATP bound states, we hypothesize a causal chain of events leading to channel opening: (1) binding of ATP induces a tighter association of the NBDs (Figure 2.12), (2) the ATP-bound NBDs stabilize the ICLs (Figure 2.12), (3) the close association of NBDs and ICLs permits additional interactions, e.g., the observed

salt bridge between E543 (NBD1) and K968 (ICL3), which shifts the position of TM9, among others (Figure 2.12), and (4) this shift of TMs at the cytoplasmic side induces a corresponding one at the extracellular side, opening a pore (Figure 2.12).

2.3.5. Comparison of the Crystallographic-Fit Model with a Recent 3.2 Å Resolution Outward-Facing Human CFTR Structure.

The recent advancements in the field of single particle cryo-EM have led to multiple structures of CFTR in the resolution range 3–4 Å in different conformations. We compare our crystallographic-fit model to the phosphorylated, ATP-bound outward-facing conformation of hCFTR, which surprisingly did not possess an open pore as expected (128). We found an overall root-mean-square deviation for the backbone of 5.8 Å. In equilibrium MD simulations, fluctuations of 2–4 Å from a crystal structure are regularly observed, e.g., as seen for ABC transporters Sav1866 and MsbA (249, 250); while 5.8 Å is beyond these observations, it should be noted that both structures may represent distinct physiological states. Many features of the ATP-bound outward-facing structure of hCFTR (128) align with our crystallographic-fit model of human CFTR, such as the bending of TM6 at residue V350. While the positions of most of the TMs in the crystallographic-fit model match the 3.2 Å resolution structure closely, TM 6 is noticeably shifted in the crystallographic-fit model (RMSD 6.5 Å; see Figure 2.13). This is most likely due to the arrangement of TMs 7 and 8. TM8 in the hCFTR structure is broken into three short helices, a feature only seen in the recently published structures of CFTR (48, 126-128) and not found in structures of related ABC transporters. The helical portion of TM8 located at the extracellular side occupies a more central position within CFTR than in the crystallographic-fit model, displacing TMs 6 and 7. The functional
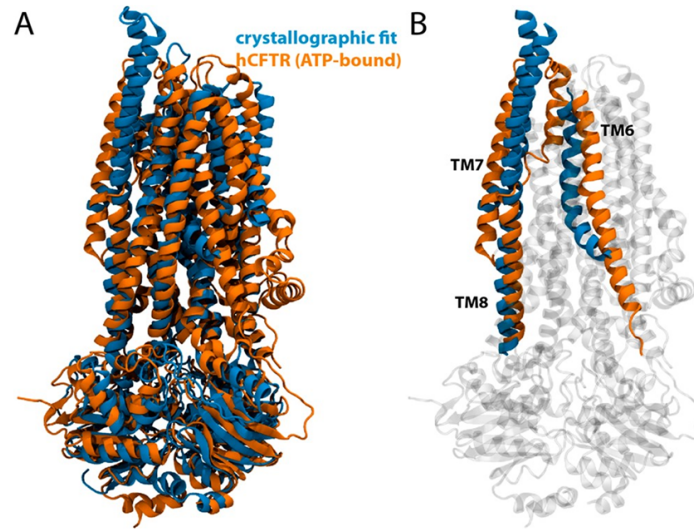
Figure 2.13: Structural comparison of the outward-facing hCFTR structure (PDB ID 6MSM) in orange and the hCFTR outward-facing crystallographic-fit model in blue. (A) Aligned structures. The root-mean-square deviation between the structures is 5.8 Å. (B) The alignments of TM6, TM7, and TM8 are highlighted to show major differences.
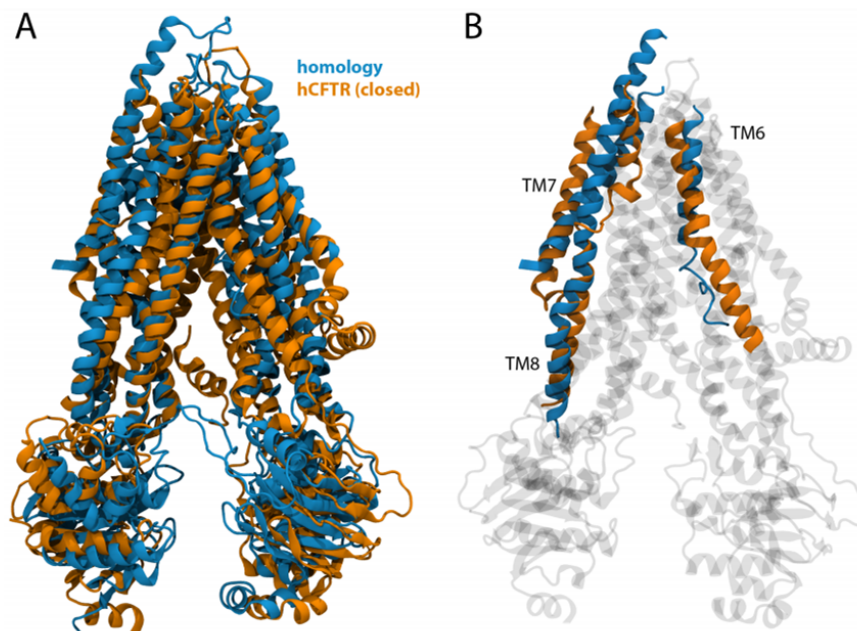
Figure 2.14: Comparison between the Rahman et. al. homology model (blue) and closed-state cryo-EM structure of human CFTR (orange; PDB 5UAK). The full structures are shown in (A) and TMs 6, 7, and 8 are highlighted in (B).

Reference: K. S. Rahman, G. Cui, S. C. Harvey, and N. A. McCarty. Modeling the conformational changes underlying channel opening in CFTR. PLoS One, 8(9):1–13, 2013).

relevance of this broken TM8 is still being investigated, especially through MD simulations (167). Similar differences are seen in comparing the closed-state homology model of Rahman *et al.* (130) with the 3.9 Å resolution structure of inward-facing hCFTR as well (Figure 2.14) (126). Despite these positional differences in the TMDs, the agreement between the ICLs and NBDs after alignment of the whole structure and model is better, with the ICLs having an RMSD of 4.2 Å and the NBDs 3.7 Å for the outward-facing structures. To further validate the crystallographic-fit model, three key open-state salt bridges were examined, namely, R347–D924 (147), R352–D993 (146, 251), and E267–K1060 (47). All three pairs form salt bridges in the outward-facing hCFTR structure (128). In simulations of the bound state of the crystallographic-fit model, a salt bridge between R347 and D924 is only seen once in 300 ns in one run, one between R352 and D993 forms for the first 30 ns in one run and is stable over 300 ns in the other, and, finally, one between E267 and K1060 is present over nearly the entire 300 ns of one run and the first 110 ns in the other. In contrast, in Simhaev *et al.*, all pairs of residues are within 2.5–6 Å over the course of 20 ns MDFF runs (223). These interactions, identified in many CFTR homology models (130, 159-162, 164, 252), have been validated through rigorous electrophysiology studies (146-148). Specifically, the first two interactions, R347–D924 and R352–D993, have been characterized, especially in our work (146, 148). Interestingly, the last of these interactions (E267 and K1060) was found via homology modeling and was subsequently verified experimentally (161, 235). Charge-reversal mutation of either residue lowers the opening rate of CFTR in response to ATP but not the stability of the open state, suggesting that the interaction plays an important role in maintaining the architecture of the ATP binding site in the apo state (235). In

70

addition, K1060 is the site of a disease-associated mutation (K1060T) (253). Although

this interaction was initially discovered on the basis of homologous residues in the

prokaryotic transporter MsbA, a multiple sequence alignment of these regions shows that

these residues are unique to CFTR among ABCC proteins (see Figure 2.15).

```
ICL2 E267 in red

ABCC7    nnlnkfdeglalahfvwiaplqvallmgliwellqasafcglgflivlalfqaglgrmmm
ABCC4    ndvnkfdqvtvflhflwagplqaiavtallwmeigisclagmavliillplqscfgklfs
ABCC5    ndgqrmfeaaavgsllaggpvvailgmiynviilgptgflgsavfilfypammfasrlta
ABCC12   sdsyslfeaalfcplpatipilmvfcaayaffilgptaligisvyvifipvqmfmaklns
ABCC11   gdvnylfegvcygplvlitcaslvicsissyfiigytafiailcyllvfplavfmtrmav
         :   : :      :                    : : : .     ::.        ::

ABCC7    kyrdqragkiserlvitsemieniqsvkaycweeamekmienlrqtelkltrkaayvryf
ABCC4    slrsktatftdarirtmnevitgiriikmyaweksfsnlitnlrkkeiskilrssclrgm
ABCC5    yfrrkcvaatdervqkmnevltyikfikmyawvkafsqsvqkireeerrilekagyfqsi
ABCC12   afrrsailvtdkrvqtmnefltcirlikmyaweksftntiqdirrrerkllekagfvqsg
ABCC11   kaqhhtsevsdqrirvtsevltciklikmytwekpfakiiedlrrkerkllekcglvqsl
         :          . *:    .*.:   *: :*  * *  : : : : ..:*. *     :.. .:

ABCC7    nssafffsgffvvflsvlpyalikg-iilrkifttisfcivlrmavtrqfpwavqtwyds
ABCC4    nlasffsaskiivfvtfttyvllgsvitasrvfvavtlygavrltvtlffpsaiervsea
ABCC5    tvgvapivvviasvvtfsvhmtlgfdltaaqaftvvtvfnsmtfalk-vtpfsvkslsea
ABCC12   nsalapivstiaivltlschillrrkltapvafsviamfnvmkfsia-ilpfsikamaea
ABCC11   tsitlfiiptvatavwvlihtslklkltasmafsmlaslnllrlsvf-fvpiavkgltns
         .           .  : . : :  :      *  ::    : :::   * :::    ::


ICL4 K1060 in red

ABCC7    kdiailddllpltifdfiqlllivigaiavvavlqpyifvatvpvivafimlrayflqts
ABCC4    kdighlddllpltfldfiqtllqvvgvvsvavavipwiaiplvplgiififlrryflets
ABCC5    kdmdevdvrlpfqaemfiqnvilvffcvgmiagvfpwflvavgplvilfsvlhivsrvli
ABCC12   kdmdeldvrlpfhaenflqqffmvvfilvilaavfpavllvvaslavgffillrifhrgv
ABCC11   gdleqldqllpifseqflvlslmviavllivsvlspyillmgaiimvicfiyymmfkkai
         *:  :*  **:    *:    : *.  : :   : * .:    : :    .

ABCC7    qqlkqlesegrspifthlvtslkglwtlrafgrqpyfetlfhkalnlhtanwflylstlr
ABCC4    rdvkrlesttrspvfshlssslqglwtiraykaeercqelfdahqdlhseawflflttsr
ABCC5    relkrldnitqspflshitssiqglatihaynkgqeflhryqelldnqapfflftcamr
ABCC12   qelkkvenvsrspwfthitssmqglgiihaygkkescity----------hllyfncalr
ABCC11   gvfkrlenysrsplfshilnslqglssihvygktedfisqfkrltdaqnnylllflsstr
         .*:::.   :** ::*: .*::**   ::.:              : :   : *

ABCC7    wfqmriemifviffiavtfisiltt-gegegrvgiiltlamnimstlqwavnssidvdsl
ABCC4    wfavrldaicamfviivafgslilaktldagqvglalsyaltlmgmfqwcvrqsaevenm
ABCC5    wlavrldlisialitttglmivlmhgqippayaglaisyavqltglfqftvrlasetear
ABCC12   wfalrmdvlmniltftvallvtlsfssistsskglslsyiiqlsgllqvcvrtgtetqak
ABCC11   wmalrleimtnlvtlavalfvafgisstpysfkvmavnivlqlassfqatarigleteaq
         *: :*:: :    .   . : :         .   : :.  : : . :*  .. . :.:
```

Figure 2.15: Sequence alignment of CFTR and related proteins. The sequence
segments in the alignment correspond to ICL2 (top) and ICL4 (bottom). Residues E267
and K1060, which appear to contribute to a salt bridge, are highlighted in red.

2.3.6. Identification and Experimental Validation of a Salt Bridge between ICL3 and NBD1. ABC transporters use flexible loop motifs to couple their domains, two of which are the Q- and X-loops. The Q-loop is adjacent to the ATP binding site and is known to facilitate NBD−NBD dimerization upon ATP binding as well as NBD−ICL coupling (254). It has also been suggested that one byproduct of the ΔF508 mutation is a conformation of the Q-loop that inhibits NBD dimerization (255). The X-loop is a flexible motif present at the interface between the NBDs and the ICLs, the latter of which are each composed of two long helices and one short helix arranged in a horseshoe shape (Figure 2.12) (256). The flexible Q- and X-loops are contact points to the ICLs and likely play an important role in conferring motion from the NBDs to the TMDs. In simulations
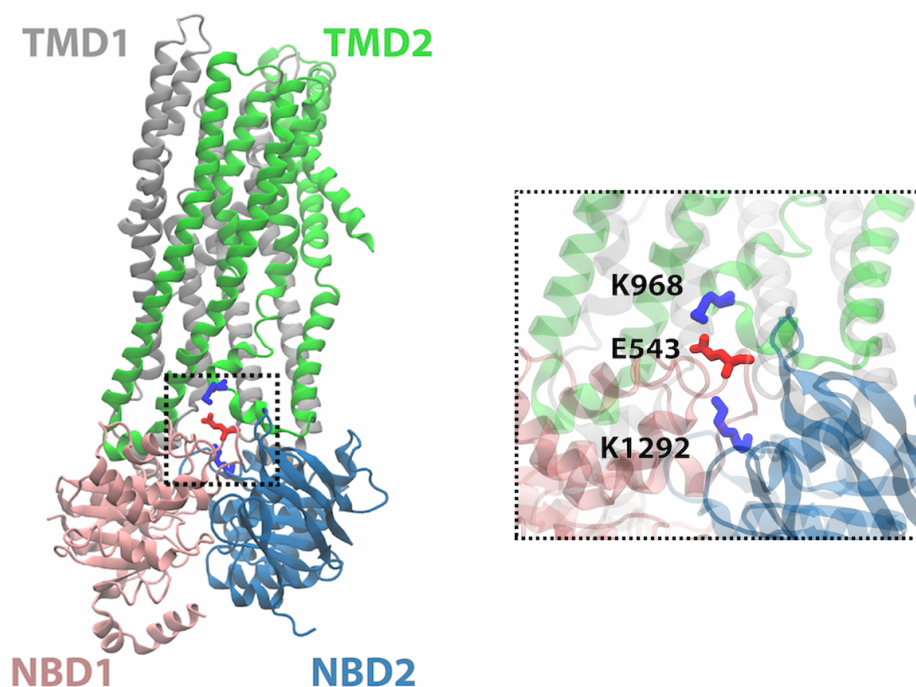
Figure 2.16. Snapshot of the bound crystallographic-fit trajectory after 200 ns (top), focusing on the interface between NBDs and ICLs (bottom). The domains of CFTR are labeled accordingly, and E543, K968, and K1292 are shown as sticks and colored by residue type (acidic in red and basic in blue).

of the crystallographic-fit model, E543 of NBD1 (X-loop) forms alternating salt bridges with K968 (ICL3) and K1292 of NBD2 (Q-loop); all three residues are shown in Figure 2.16. The former interaction has been observed in other homology models (130, 163) but not the latter. Over the 300 ns simulations of the bound state, E543 formed a salt bridge with K968 36% of the time (73% in the second run) and with K1292 26% of the time (0% in the second run; Figure 2.17). In one of the ATP-bound simulations, E543 appeared to alternate between interacting with K968 and K1292. The E543−K968 salt bridge was also present in the semi-bound simulation (80%) and for part of one of the apo simulations (37%), prior to the separation of the NBDs. The E543−K1292 salt bridge was only observed near the end of one of the apo simulations and was not observed at all in the semi-bound simulation. To determine the functional relevance of the E543−K968 and E543−K1292 salt bridges, the behaviors of CFTR channels bearing mutations at these sites were recorded in electrophysiology experiments. The single mutants E543Kand K968A-CFTR exhibited a significantly longer (E543K) or slightly shorter (K968A) mean activation time—defined as the time required for currents to reach a plateau in response to ATP + PKA—as compared to WT-CFTR (Figure 2.18). The mean activation time for the charge swapped double mutant (E543K/K968E-CFTR) was similar to WT-CFTR channels, exhibiting rescue. Even though the single mutant K1292E-CFTR had a mean activation time similar to WT-CFTR, the K1292E mutation in conjunction with the E543K mutation, as a charge swapped double mutant, partially rescued the long mean activation time seen in the E543K-CFTR mutant (Figure 2.18). While both charge-swapped double mutants E543K/ K1292E- and E543K/K968E-CFTR can at least partially rescue the mean activation time of the E543K mutant, the
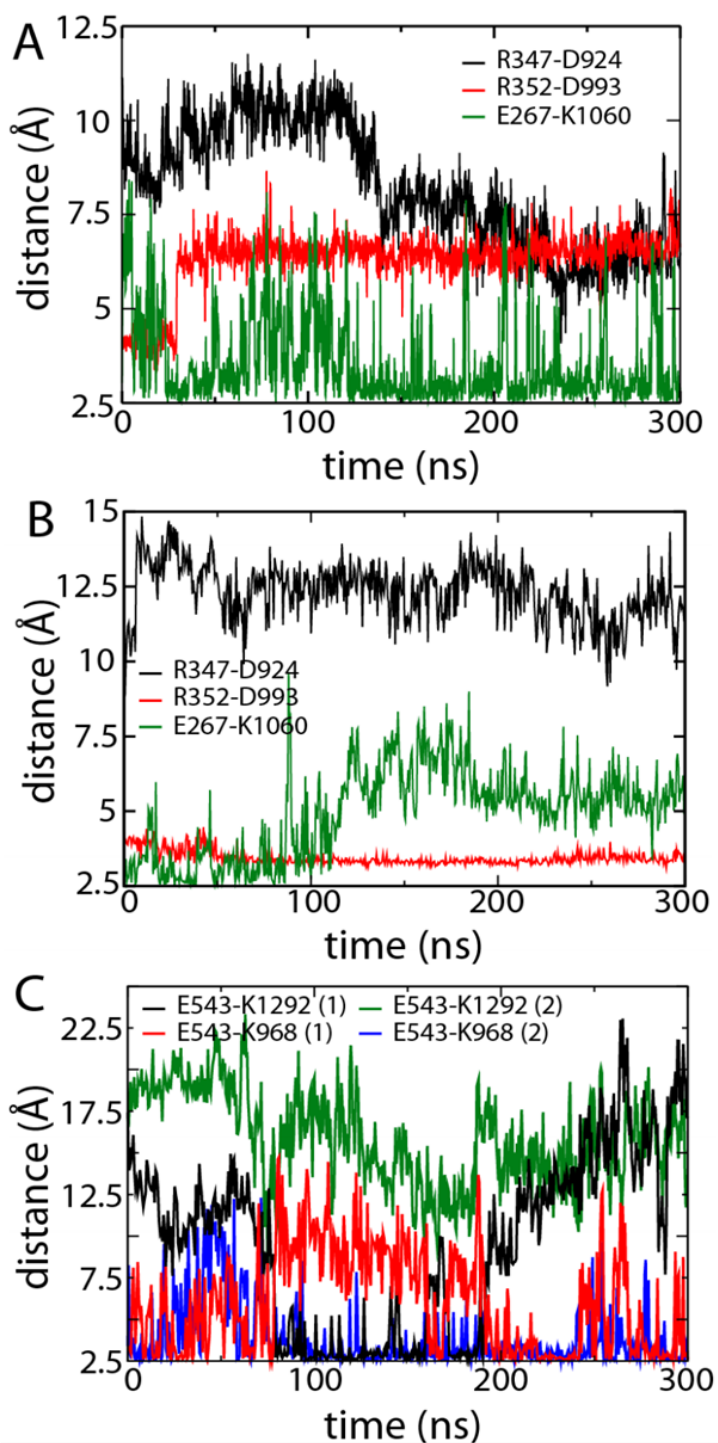
Figure 2.17: Salt-bridge distances over time for the crystallographic-fit ATP-bound simulation. Three experimentally verified salt bridges are tracked over time in (A) run 1 and (B) run 2. (C) Two salt bridges newly discovered and experimentally confirmed here for both runs.

latter has a greater effect (Figure 2.18). These data suggest that E543 interacts with both

K968 and K1292. It should be noted that, for CFTR to transition from the closed to the

open state, the R-domain must be phosphorylated. Although the homology model in our

simulation does not contain the R-domain, there are many other steps necessary for the

transition that could be observed. To investigate the effects of these residues on the

opening of CFTR after phosphorylation, we explored the reactivation of CFTR channels

with ATP alone. For this experiment, we used the following protocol: WT-CFTR and
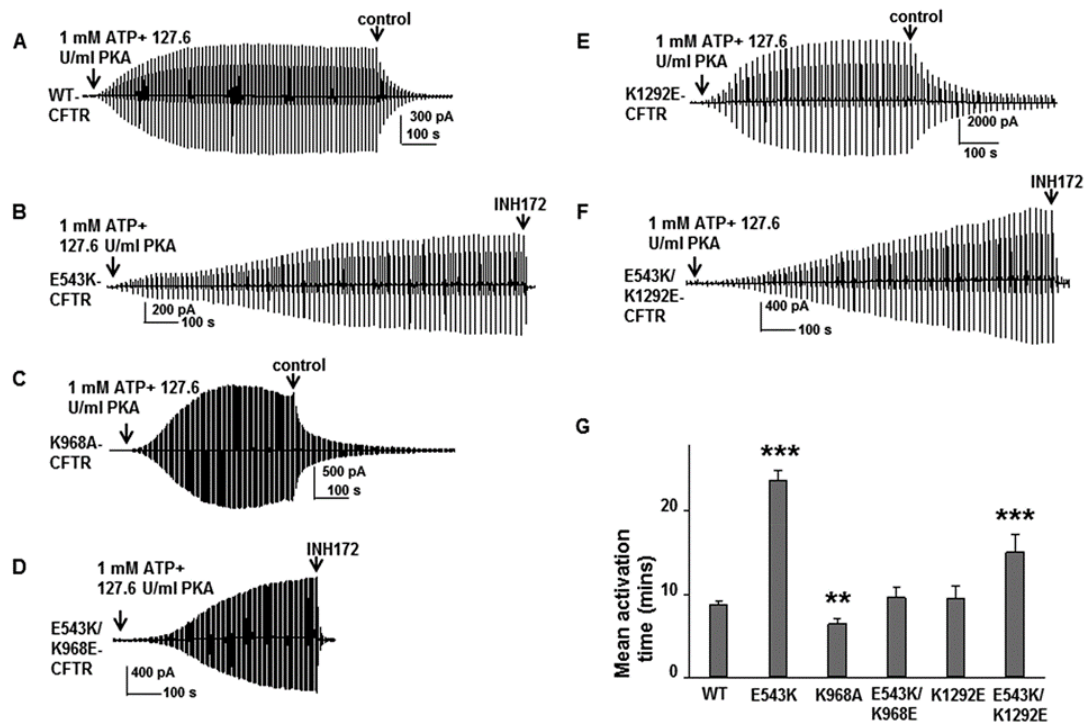
Figure 2.18: Mean activation time changed in mutants compared to wt-CFTR. Sample traces of inside-out macropatch currents of (A) WT-, (B) E543K-, (C) K968A-, (D) E543K/K968E-, (E) K1292E-, and (F) E543K/K1292E-CFTR recorded under the experimental conditions listed in the panels. Control, 150 mM Cl⁻ intracellular solution; INH172, 10 µM CFTRinh172. (G) Summary data for mean activation time for WT and mutants. Statistical data are as follows: n = 30 for WT; n = 11 for E543K; n = 7 for K1292E; n = 18 for K968A; n = 11 for E543K/K968E; n = 10 for E543K/K1292E. ***, P < 0.001 compared to WT; **, P < 0.01 compared to WT-CFTR.

mutated channels the by 127.6 U/mL PKA and 1 mM MgATP; channels were allowed

to close briefly by washout of ATP and PKA; channels were then reactivated by addition

of 1 mM MgATP alone; channels were then deactivated again by washout of ATP

(Figure 2.19). We attempted to fit both the reactivation and deactivation rates of the WT-

CFTR channel, the single E543K- mutant, the single K968A- mutant channel, and the

E543K/K968E-CFTR double mutant channel. However, mutation at these residues

caused the macroscopic opening and closing transitions, upon applying or washing out
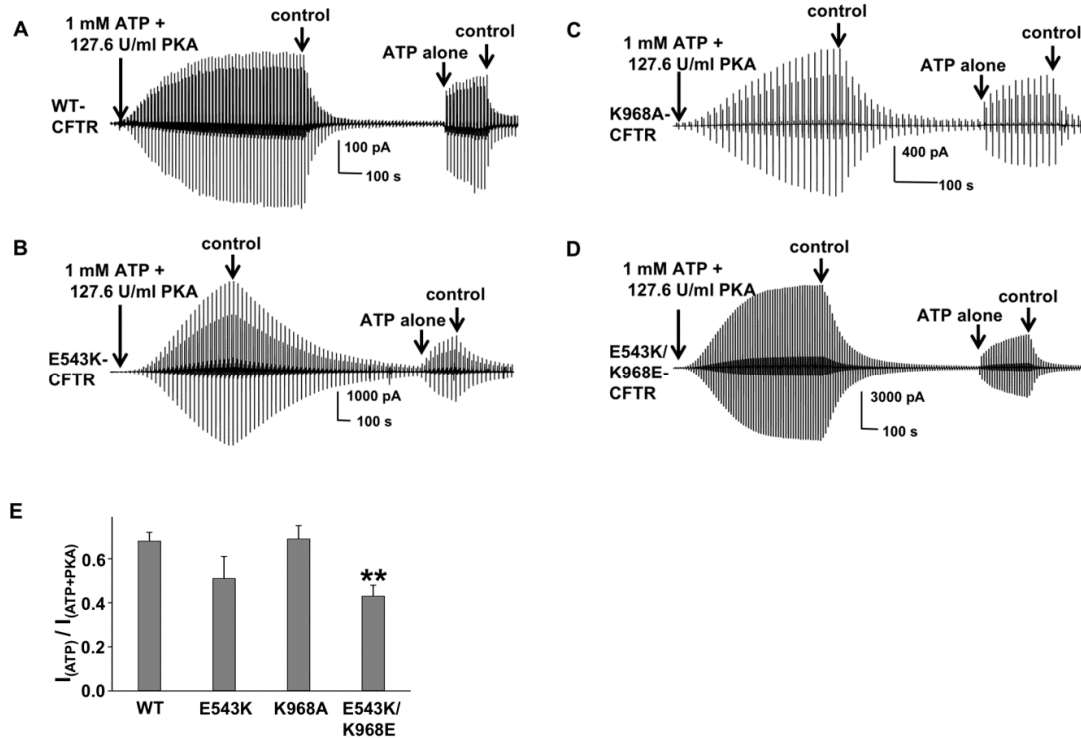
Figure 2.19: 1 mM MgATP reactivated WT and mutant CFTR after channels were fully activated by ATP + PKA. (A) WT-CFTR was fully activated with 1 mM MgATP and 127.6 U/ml PKA, deactivated by removal of ATP and PKA using control solution, and then reactivated by 1 mM MgATP alone. Representative current traces for E543K (B), K968A (C), and E543K/K968A-CFTR (D) were recorded with the same experimental conditions as WT-CFTR. Summary data are shown in E. Y axis indicate the ratio of maximum current in ATP alone ($I_{(ATP)}$) divided by maximum current in ATP and PKA ($I_{(ATP+PKA)}$). Statistical data are follows: n=4 for WT; n= 6 for E543K; n=8 for K968A; n=6 for E543K/K968E. **, P < 0.01 compared to WT.

ATP, to be quite irregular, compared to the behavior of WT-CFTR channels with the same protocol, making quantitative fits impossible (Figure 2.20). In spite of this inability to quantify, it is nonetheless evident that disrupting the interaction between E543 and K968 greatly perturbs the macroscopic channel behavior such that neither single nor double exponentials efficiently fit the reactivation data; however, the double E543K/K968E mutant began to restore WT macroscopic behavior. The combined electrophysiology data lead us to conclude that the K968−E543−K1292 triad contributes to the transition from the closed state to the open state. The charge-swapping double mutations were unable to completely rescue WT-CFTR channel behavior, suggesting that all three residues interact during gating. Another possibility is that, due to instability of the loop, any mutation may alter its structure. This same phenomenon was previously seen for electrostatic interactions in extracellular loop 1 (251). The final remaining question we addressed was whether these interactions also contribute to the steady-state channel function after CFTR is fully activated. Comparing the steady-state behavior to WT-CFTR channels, K968A-CFTR channels behaved very similarly, with regular closed and open states, a very rare subconductance state, and similar mean burst durations (Figure 2.21). Moreover, K968A-CFTR exhibited a significantly lower open probability as compared to WT-CFTR, which is supported by a previous study (235). These data suggest that the above electrostatic interactions contribute very little in modulating the steady-state behavior of CFTR channels and may contribute mostly to opening and/or closing transitions, but more experiments are needed to confirm.
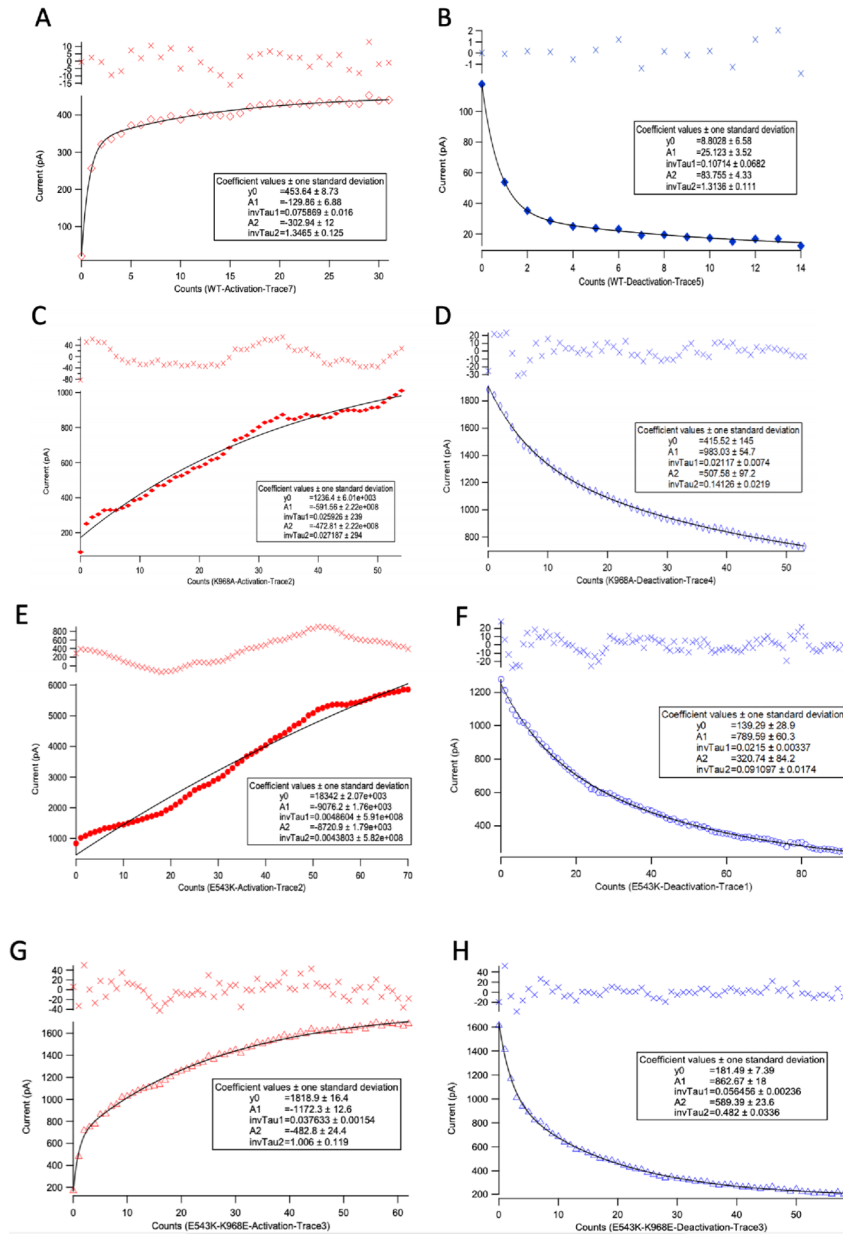
Figure 2.20: Representative fits of the ATP-induced activation of phosphorylated CFTR and deactivation after washout of ATP. All activation and deactivation data were fit in Igor using a double exponential (without an X-offset), as follows: (A) WT-CFTR activation, (B) WT-CFTR deactivation, (C) K968A-CFTR activation, (D) K968A-CFTR deactivation, (E) E543K-CFTR activation, (F) E543K-CFTR deactivation, (G) E543K/K968E-CFTR activation, and (H) E543K/K968E-CFTR deactivation. The differences between the raw data and the double exponential fit were calculated and plotted above each fit. Goodness of fit was also analyzed by Chi-square value. The activation traces for each single mutant (K968A-CFTR or E543K-CFTR) were impossible to fit using a double exponential function; however, the double mutant (E543K/K968E-CFTR) seems to partially restore to WT-CFTR channel behavior, although not completely, thus enabling the data to be fit.
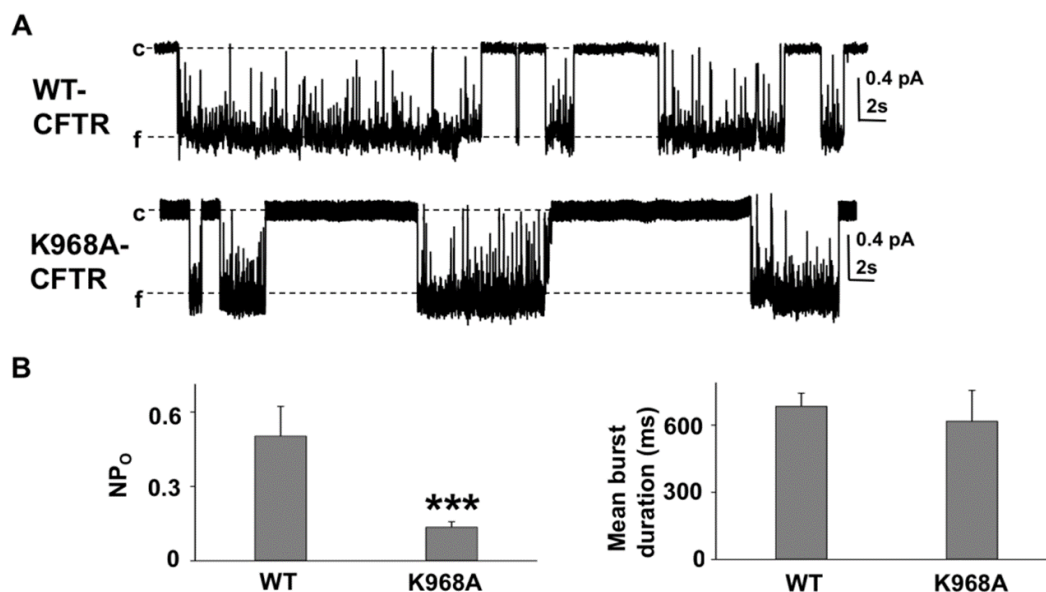
Figure 2.21: K968A exhibited similar single-channel behavior to WT-CFTR. (A)
Representative Single channel current traces of WT- and K968A-CFTR were recorded
using inside-out patch with 150 mM Cl− intracellular solution in the presence of 1 mM
MgATP with 127.6 U/ml PKA at membrane potential -100 mV. (B) Open probability
of K968A is significantly lower than WT-CFTR. (C) K968A exhibits similar mean burst
duration as WT-CFTR (WT-CFTR data cited from previous publication Cui, G.,
Rahman, K. S., Infield, D. T., Kuang, C., Prince, C. Z., and McCarty, N. A. (2014)
Three charged amino acids in extracellular loop 1 are involved in maintaining the outer
pore architecture of CFTR. The Journal of General Physiology **144**, 159-179 . N=5 for
K968A-CFTR. ***, $P < 0.001$ compared to WT.

2.4.   DISCUSSION.

Recent advancements in the field of cryo-EM have led to an influx of new structures at higher resolutions than previously attainable without relying on crystallization. Within the last three years, four structures of CFTR have been published using single-particle cryo-EM techniques (48, 126-128). These structures have provided valuable information on the closed state and the conformational changes induced by phosphorylation and ATP binding; however, none of them, including the outward-facing structures, displays a complete conducting pore. It is possible that the ATP-bound zebrafish and human CFTR structures both represent a state similar to the aforementioned "strained transitional" state of CFTR (130), and additional signals or steps are required before a pore will form on a much longer time scale than simulated here. Such putative transitional states of CFTR can be explored with MD simulations, combined with experimental confirmation of key interactions observed. Before the release of the four 3–4 Å resolution cryo-EM structures of CFTR, several homology models were built to ameliorate the dearth of structural information. Here, we refined one of those models from Rahman *et al.* (130) by flexibly fitting it to two versions of a low-resolution cryo-EM map (157), one with the full 12-fold crystallographic symmetry of the map and one averaged to a single copy. We found that fitting to the crystallographic map produced a more functionally relevant model than fitting to the averaged map, likely due to the maintenance of the crystal contacts, which further restrict fluctuations at a resolution below that of the map itself. Our study complements that of Simhaev *et al.* (223), who used the same map to refine two homology models of CFTR from Corradi *et al.* (162) and from Dalton *et al.* (164). Fitting was followed by simulations of each model for at least 100 ns in different ATP-

occupancy states. Similar to Simhaev *et al.* (223), we observed that even without ATP the NBDs collapse. When comparing the ATP-bound states simulated here, we found that the crystallographic-fit model exhibits increased NBD dimerization when compared to the original homology model as well as the opening of a partial pore at F337. The radius of gyration also shows a significant widening of the extracellular side of the protein in the crystallographic-fit model in the ATP-bound state compared to the apo state. Upon extension of the simulations from 100 to 300 ns, the crystallographic-fit model revealed the formation of a complete pore at 280 ns of one run (Figure 2.10) and an expanded partial pore in the other run (Figure 2.11), similar to the pore identified in other homology models (165). We note that, although the existence of a pore is a promising sign, the simulations are still far from converged, which would require a time scale orders of magnitude larger to fully describe CFTR's gating cycle. We also compared our crystallographic-fit model to the outward-facing hCFTR structure (128). We found that some elements of CFTR aligned moderately well between our crystallographic-fit model and the hCFTR structure, such as the ICLs (RMSD 4.2 Å) and NBDs (RMSD 3.7 Å). However, the structural differences in the TMDs are greater. These differences most likely stem primarily from a kink in TM8 seen only in the recently published structures of CFTR but not represented in CFTR structures resolved under different conditions (171). However, as mentioned previously, the outward-facing structure of hCFTR could represent a "strained transitional" state and, thus, has possibly not yet signaled for pore formation. These transitional states can be further characterized through MD simulations and confirmed through experimentation. In addition to the transition from a strained state to one with a pore over the 300 ns simulation of the

crystallographic-fit model, salt bridges were observed between E543 in the X-loop of NBD1 and K968 in ICL3 as well as between E543 and K1292 in the Q-loop of NBD2. These interactions, although previously suggested by other homology models (130, 163), have not been experimentally tested until now. Mutagenesis and electrophysiology show that disrupting the E543−K968−K1292 electrostatic triad significantly alters the macroscopic rate of channel activation, with E543K having the largest effect (see Figure 2.18). Therefore, we suggest that this triad is part of a structural relay from the NBDs to the TMDs signaling ATP occupancy and leading to pore formation, as observed in the simulations. Preliminary experiments suggest that, once signaling has occurred, the steady-state behavior is not strictly dependent on the triad. In the outward-facing hCFTR structure, neither the E543−K968 nor the E543−K1292 salt bridge is seen, although only slight movements of a loop would be required for them to form (side chain distances of 8.2 and 10.0 Å, respectively). Future simulations and experiments will be used to further elucidate the signaling mechanisms in CFTR, especially under different phosphorylation conditions.

CHAPTER III

CFTR EXPRESSION AND PURIFICATION

3.1. INTRODUCTION.

CFTR, only expressed in vertebrates, has a complex biogenesis requiring multiple proteins that aid in folding, proper insertion into the membrane, and post-translational processing of CFTR (58, 63, 257). Because of the complexity of CFTR biogenesis, the cell type chosen for CFTR expression for purification and location of the affinity tag is critical for a high yield of highly homogenous CFTR. Currently, several cell types are being used for CFTR expression and can be dependent upon the CFTR ortholog. Due to the complexity and instability of human CFTR, only eukaryotic cells have been used successfully in expression for purification. Purification of membrane proteins, especially ABC transporters, is highly dependent on the detergent solubilization step, including the choice of detergent and method of solubilization (258-260). CFTR is no different. CFTR ATPase function appears to be highly dependent on the detergent used for solubilization and stabilization, which cannot be rescued by reconstitution into lipids (133). In this chapter, we describe attempts and successes at expression and purification of human CFTR in three different cells types—Sf9 (ovary cells of *Spodoptera frugiperda*), BHK (Baby Hamster Kidney cells), and CHO (Chinese Hamster Ovary cells) – evaluating the overall quality of protein expression and purification. In the following chapters, CFTR function, both ATPase activity and channel function are evaluated.

3.1.1. Individual contributions.

3.1.1.1. Sf9 EXPRESSION SYSTEM.

The initial CFTR construct for protein expression in the Sf9 cell system was designed by Dr. Canhui Li and Dr. Mohabir Ramjeesingh of the Dr. Christine Bear Lab at the School of Medicine, University of Toronto, Canada and gifted to Dr. Brandon Stauffer of the McCarty Lab at the School of Medicine at Emory University in Atlanta, GA. I was initially taught cell culture and viral expression techniques for Sf9 cells by Dr. Youngman Kwon in the Kang Lab at Georgia State University in Atlanta, GA, and Dr. Nidhi Williams of Atlanta, GA. I performed the final bacmid transfection, viral infection, and CFTR protein expression from the Sf9 cells.

3.1.1.2. BHK EXPRESSION SYSTEM.

Stably transfected BHK-CFTR-10xHis cell line was gifted to McCarty Lab by Dr. John Hanrahan of the Department of Physiology at McGill University in Montreal, Canada. I maintained and designed cell culture protocols for transitioning to suspension culture and preformed and optimized protein purification.

3.1.1.3. CHO EXPRESSION SYSTEM.

CFTR-3xFLAG-tag construct gifted to Dr. Guiying Cui of McCarty Lab by Dr. Hong Joeng of the lab of Dr. Eric Sorscher in the School of Medicine at Emory University. Cloning of CFTR-3xFLAG insert into T-Rex™ pcDNA5/TO plus an IRES-CFP vector performed by the Custom Cloning Division within the Emory Integrated Genomics Core. I developed the stably transfected CHO-CFTR-3xFLAG-ECL4 line, with help from the Winship Flow Cytometry Core within the Pediatrics Department at Emory University and from Mr. Brian Dobosh (Tirouvanziam lab). Further optimization and protein purification was completed by me.

3.1.2. Publications resulting from this chapter.

Optimization of CFTR protein purification will be published in downstream publications, as CFTR purification is a new technique to both the McCarty and Schmidt-Krey labs.

3.2. METHODS.

3.2.1. Sf9 expression system.

3.2.1.1. MOLECULAR CLONING FOR hCFTR EXPRESSION IN SF9 CELLS.

Original plasmid (hCFTR with a c-terminal 10xHis-tag in pFastBacDual) (Figure 3.1) was provided by the Bear lab, as noted above. Amplification of plasmid was completed by transformation into XL 10-Gold *E. coli* cells on 75 µg/mL LB agar plates. Plasmid (given number pCF340 in the McCarty lab) was purified by miniprep (ZymoPure MiniPrep Kit) and CFTR sequence confirmed by full-length sequencing of hCFTR (Genewiz©, https://www.genewiz.com/en). Two stabilizing mutations, D110C and
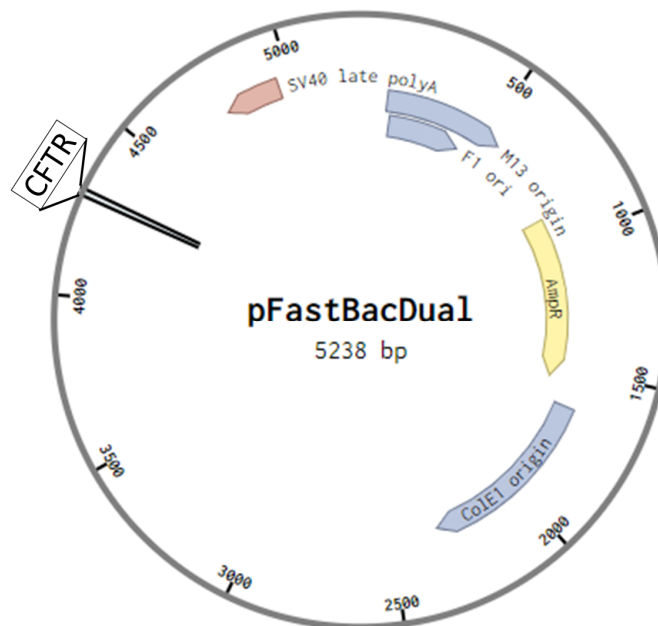
Figure 3.1: Plasmid map of WT-hCFTR in pFastBacDual vector. This plasmid was used for wt-hCFTR expression in Sf9 cells, but also for the generation of mutant hCFTR constructs and expression in Sf9 cells.

85

K892C, were introduced into WT-hCFTR (McCarty pCF546) using the Emory Integrated Genomics Core (EIGC). Full-length sequencing of hCFTR constructs were completed before the generation of bacmid.

3.2.1.2. MAINTENANCE OF SF9 CELLS.

Gibco® Sf9 cells from Invitrogen were thawed quickly in 37°C water bath and resuspended in 5 mL of SF-900™ II SFM media. To expand and infect cells, DMSO must be removed immediately upon resuspension. To remove DMSO, cells were pelleted at 800 g for 5 minutes at RT, and the supernatant removed. Cells were resuspended in 5 mL of new warmed SF-900™ II SFM media and transferred to 50 mL of media in a sterile 250 mL Corning media bottle. Cells were grown in a non-humidified, air-regulated incubator at 27°C with a loosened cap, shaking at 150 RPM. Cells were counted using a hemocytometer every two days and split at a density of 1×10^7 cells/ mL. To make frozen cell stocks, cells were pelleted at 800 g for 5 minutes at RT and then resuspended in freezing solution (30% FBS, 10% DMSO, and 60% SF-900™ II SFM media) and frozen at a density of 3×10^6 cells/mL to -80°C. Frozen cells were stored in liquid nitrogen.

3.2.1.3. BACULOVIRUS PRODUCTION.

A general outline can be seen in Figure 3.2. In accordance with instructions for the Bac-to-Bac Baculovirus Expression system (Invitrogen™), purified plasmid was transformed into DH10Bac *E.coli* for bacmid production and colonies were screened on LB-agar plates with 50 µg/mL kanamycin, 7 µg/mL gentamicin, 10 µg/mL tetracycline, and 100 µg/mL Bluo-gal and 40 µg/mL IPTG (Blue-white Screening). Colonies were selected based on positive blue/white screening, amplified, and purified in accordance with the ZR BAC DNA™ Miniprep Kit protocol (Zymo®). Purified bacmid was screened first by

PCR amplification of inserted gene followed by full-length sequencing of the WT and mutant hCFTR construct (Genewiz©, https://www.genewiz.com/en). Promising constructs were used for baculovirus production. Sf9 cells were plated at ~50% confluency in Grace's Insect Media, Unsupplemented (ThermoFischer™), and incubated for 1 hour before transfection. Sf9 cells were transfected for 5 hours at 27°C in Grace's Insect Media, Unsupplemented, using a Bacmid:Cellfectin ratio of 1 (µg) DNA: 8 (µL) Cellfectin® II, which was preincubated for 30 minutes at RT. Cells were allowed to recover and produce virus for 72 hours in Sf-900™ II media. Virus-containing media was removed, supplemented with 2% FBS (Fetal Bovine Serum), and stored at 4°C protected from light (for short-term storage). Viral colonies were selected and purified via plaque assay, and then the viral titer was determined also using plaque assay. Briefly, cells were plated at ~25% confluency in a 6-well plate and incubated overnight at 27°C before treatment with virus for 1 hour at RT. Virus-containing media was removed from infected cells, and cells were covered in 1% agarose in 1X Sf-900™ II media solution. The plates were incubated at 27°C, humidified until the number of plaque colonies did not change over 48 hours; then, viral colonies were either purified or titered. When purifying a viral colony, a sterile glass pipette was used to stab the agarose, and the agarose plug was transferred to a sterile microcentrifuge tube containing 0.5 mL of SF-900™ II SFM media supplemented with 2% FBS. This was mixed by vortexing, before 0.1 mL of plaque purified virus was plated into each well of a 6-well plate containing adherent Sf9 cells at 75-80% confluency and incubated for 72 hours. The media was collected, and the cell debris was pelleted by centrifugation at 500 g for 5 minutes at RT. The supernatant was transferred to a sterile 15 mL conical tube supplemented with 2%

FBS and was stored at 4°C away from light. During titering, plaque colonies were stained in 0.5 mL Neutral Red solution for 2 hours at RT and solution removed before counting colonies. To calculate the titer, the number of plaques per dilution was counted, multiplied by the dilution factor and divided by the volume of inoculation virus. Amplification of a plaque-purified p1 viral colony started with cells in a 6-well plate (2 x 10^6 cells/mL) which were infected at an MOI (multiplicity of infection) of 0.1 before being harvested at 48 hours. The cells were pelleted at 500 g for 5 minutes at RT and the supernatant was collected (p2 viral stock). The p2 viral stock was stored at 4°C supplemented with 2% FBS. The titer of p2 viral stock was determined using the plaque assay. For long term-storage, any viral stock was stored at -80°C protected from light.
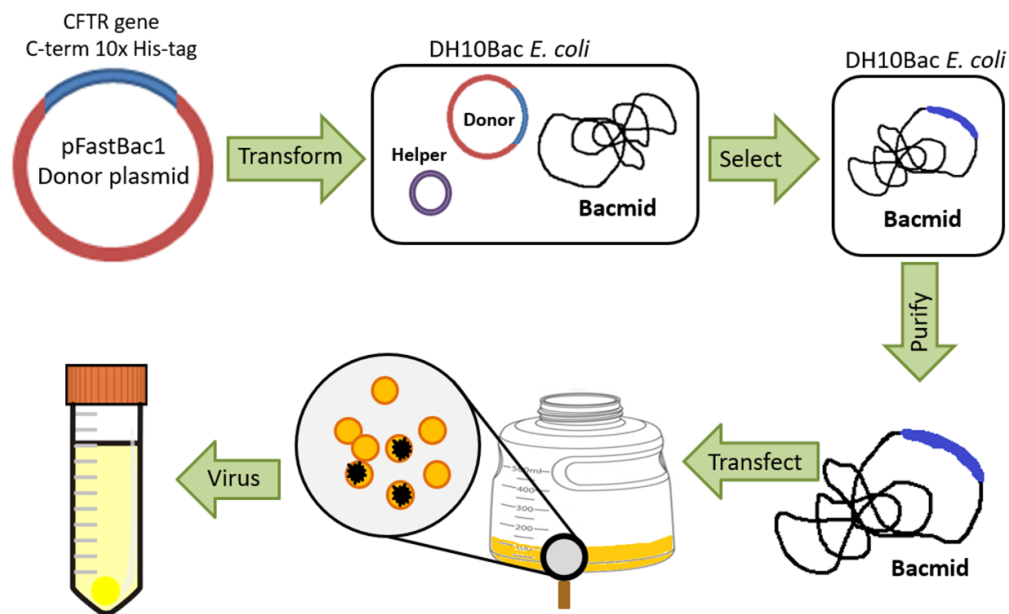
Figure 3.2: Depiction for the overall flow of baculovirus production. The purified donor plasmid is transformed into DH10Bac *E. coli*. Bacteria containing the recombined CFTR-containing bacmid will survive antibiotic selection and can be further screened using Blue-White screening. CFTR-containing bacmid is transfected into Sf9 cells to generate Baculovirus (within media). Baculovirus can be used to infect Sf9 cells for CFTR protein production and purification.

3.2.1.4. INFECTION OF SF9 CELL SUSPENSION CULTURE.

Sf9 cells were plated in a 10 cm dish at 1.8×10^7 cells at RT for 30 minutes. The media was removed and replaced with SF-900™ II SFM media supplemented with 1% FBS before adherent cells were infected at a multiplicity of infection (MOI) of 20 for 48 hours.

3.2.1.5. PROTEIN EXPRESSION SCREENING VIA WESTERN BLOT ANALYSIS.

Infected Sf9 cells were pelleted at 1000 g for 10 minutes at 4°C and the cell pellet was resuspended in RIPA buffer containing 1x protease inhibitor cocktail (cOmplete EDTA-free PIC Roche©). Infected cells were lysed on ice for 10 minutes at 4°C, and the cellular debris was pelleted at 1000 g for 10 minutes at 4°C. The total protein concentration was measured using Pierce™ Bicinchoninic Acid (BCA) microplate assay in accordance with the manufacturer's protocol. Equivalent total amounts of protein (50-150 µg) for each sample were mixed with 1x Laemmli sample buffer (prepared in house) supplemented with 50 mM DTT (Dithiothreitol) and then incubated at 37°C for 30 minutes. All samples and the ladder (Precision Plus Protein™ Dual Color Standards Marker Bio-Rad) were loaded into a Mini-PROTEAN® TGX™ precast 4-15% acrylamide: bisacrylamide SDS-PAGE. The gel was run at 150V for 45 minutes and then transferred overnight at 4°C at 60 mA onto a nitrocellulose membrane. All blots were blocked in 5% milk in TBST (Tris-buffered saline and Tween® 20) for 1 hour at RT, and then stained with 1:1,500 mouse anti-CFTR 596 antibody in TBST with 5% BSA overnight at 4°C, followed by 1:1,000 goat anti-mouse antibody conjugated to HRP (Sigma) in TBST with 5% BSA for 1 hour at RT with three 15 minute washing steps after each antibody stain with TBST. Western blotting detection was determined using Amersham™ ECL™ Western Blotting Detection reagents, and blots were imaged on a Bio-Rad ChemiDoc™ XRS+ system.

3.2.1.6. HIS-TAG ACCESSIBILITY DETERMINATION.

Infected Sf9 cells were collected by titration and pelleted at 1000 g for 10 minutes at 4°C. Cells were resuspended in 0.5 mL Roche Buffer A (50 mM NaH_2P0_4, pH 8.0, 0.3 M NaCl) and lysed using a Dounce Homogenizer. Large cellular debris was pelleted by centrifugation at 1000 g for 10 minutes at 4°C. The supernatant was prepared for resin-binding by the addition of DDM and imidazole to make a final concentration of 0.1% DDM and 0.5 mM imidazole in Roche A buffer solution. The prepared supernatant was mixed with 50 µL Roche© His-resin overnight at 4°C. The resin was "packed" in Ultrafree® PVDF 0.5 µm centrifuge filter (Millipore-Sigma®) at 100 g for 1 minute at 4°C and the flow-through was collected. The resin was washed in 150 µL Roche A supplemented with 0.1% DDM and 0.5 mM imidazole. CFTR was eluted from the resin with 50 µL Roche B (50 mM NaH_2P0_4, pH 8.0, 0.3 M NaCl, and 0.25 M imidazole) by centrifugation at 100 g for 1 minute at 4°C.

3.2.2. BHK-CFTR-10xHis Expression System.

3.2.2.1. MAINTENANCE OF BHK-CFTR-10xHIS CELLS.

BHK cells were stably transfected with recombinant hCFTR containing a 10x His-tag on the C-terminal end, as previously described (102). BHK cells were maintained adherently by splitting in the range of 1:5 to 1:20 at 100% confluency into DMEM/F12 50:50 (Dulbecco's Modified Eagle Medium: Nutrient Mixture F-12) plus 10% FBS with 1% Penicillin/Streptomycin and 0.5 mM Methotrexate (BHK-CFTR complete media). Frozen cell stocks were prepared in 10% DMSO, 30% FBS, and 60% DMEM/F12 50:50 at a density of 3 x 10^6 cells/ mL and cooled to -80°C, and then transferred to liquid nitrogen for long term storage.

3.2.2.2. HIS-TAG ACCESSIBILITY DETERMINATION.

Cells plated on 10 cm^2 plates were collected by trypsinization and pelleted at 1000 g for 10 minutes at 4°C. The cells were resuspended in 0.5 mL Roche Buffer A (50 mM NaH$_2$PO$_4$, pH 8.0, 0.3 M NaCl) and lysed using a Dounce Homogenizer. Large cellular debris was pelleted by centrifugation at 1000 g for 10 minutes at 4°C. Then the supernatant was prepared for resin-binding by the addition of DDM and imidazole to make a final concentration of 0.1% DDM and 0.5 mM imidazole in Roche A buffer solution. The prepared supernatant was mixed with 50 µL Roche$^©$ His-resin overnight at 4°C. The resin was packed in an Ultrafree$^®$ PVDF 0.5 µm centrifuge filter (MilliporeSigma™) at 100 g for 1 minute at 4°C and the flow-through was collected. The resin was washed in 150 µL Roche A supplemented with 0.1% DDM and 0.5 mM imidazole. CFTR was eluted from the resin with 50 µL Roche B (50 mM NaH$_2$PO$_4$, pH 8.0, 0.3 M NaCl, and 0.25 M imidazole) by centrifugation at 100 g for 1 minute at 4°C.

3.2.2.3. TRANSITION OF ADHERENT BHK-CFTR-10xHIS CELLS TO SUSPENSION CULTURE.

Cells plated on two T75 flasks were grown to confluency. Once confluent, cells were washed in PBS and incubated in 0.25% trypsin-EDTA for 90 seconds before being removed. The cells were incubated for another 90 seconds before being resuspended in 12 mL of BHK-CFTR complete media in the same plastic T75 flask. This method was repeated over 4 days, or until cells began forming 3 dimensional (3D) structures. Once the cells began forming 3D structures, the cells were transitioned into suspension flasks. The adherent cells were washed in the T75 flasks with PBS before incubation in 0.25% trypsin for 30 seconds. The cells were washed again in PBS and rested without solution

for another 30 seconds before being resuspended in BHK-CFTR complete media. Cells from two T75 flasks were transferred to a 1 L suspension culture flask filled with 500 mL of BHK-CFTR complete media supplemented with 0.1% Pluronic® F68 (Gibco®). The suspended cells were fed within 24 hours of transition with 550 mL of complete media supplemented with 0.1% Pluronic® F68 and spiked with 0.5 mM Methotrexate (final concentration) 12 hours before purification.

3.2.2.4. CFTR PURIFICATION FROM BHK-CFTR-10xHIS CELLS.

BHK cells were pelleted either in 50 mL conical tubes at 1000 g for 5 minutes at 4°C or in 750 mL bottles at 4000 g for 30 minutes with slow braking at 4°C. The cell pellet mass was measured, and all volumes described are for 1 g total mass. The cell pellet was resuspended in 10 mL of 8 mM HEPES-Na, pH 7.2, 0.8 mM EDTA, 1 mM DTT and PIC (1 mM PMSF, 20 µM Leupeptin, 3 µM Chymostatin, 3mM Benzamidine, 0.2 mM AEBSF, 10 µM E-65, 10 µM Bestatin, and 10 µM Pepstatin). The cells were lysed using a Dounce Homogenizer with 20 strokes from the loose pestle and then from the tight pestle. The cell lysate was mixed with 1/7th volume of 2M sucrose in 8 mM HEPES-Na, pH7.2, 0.8 mM EDTA, and 1 mM DTT and incubated on ice for 10 minutes. Large cellular debris was pelleted twice by centrifugation at 1000 g for 10 minutes, 4°C. The supernatant was ultracentrifuged at 100,000 g for 1 hour at 4°C with slow braking. The membrane pellet was washed in 5 mL of 50 mM Tris-HCl, pH 7.5, 0.5 M NaCl, and 10% glycerol by resuspension using a Dounce Homogenizer—three strokes with the loose pestle and then three strokes with the tight pestle. The resuspended pellet was ultracentrifuged again at 100,000 g for 1 hour at 4°C with slow braking. The membrane pellet was washed in 1 mL of 50 mM Tris-HCl, pH 8.0, 0.2 M NaCl, and 10% glycerol

92

and resuspended using a Dounce Homogenizer. The resuspended membranes were moved to an ice-cold beaker in a cold room, and enough 50 mM Tris-HCl, pH 8.0, 0.2 M NaCl, 2.5 mM $MgCl_2$, 10% glycerol, and 1 mM ATP was added dropwise to make a final volume of 10mL. CFTR was solubilized by adding 10% DDM/ 2% CHS (10% n-dodecyl-β-D-maltoside/ 2% cholesterol hemisuccinate) to make a final concentration of 0.1% DDM/ 0.02% CHS dropwise over 30 minutes with gentle mixing using a 5mm stir bar, while still on ice. Solubilized CFTR was separated from insoluble material by ultracentrifugation at 100,000 g for 30 minutes at 4°C with slow braking. Only native, solubilized CFTR was extracted from the supernatant and incubated with equilibrated HisPure™ Ni-NTA (nitrilotriacetic acid) resin (0.5 mL) (Thermo Fischer Scientific) for 1 hour at 4°C with rotating. The resin was packed in a gravity flow column and washed in increasing amounts of imidazole (10 mM, 25 mM, 75 mM and 125 mM) in 50 mM Tris-HCl, pH 7.5, 0.15 M NaCl, 2.5 mM $MgCl_2$, and 10% glycerol. CFTR was phosphorylated on the column with 10 U/mL Promega® PKA in 10 mM ATP in the first wash for 10 minutes at 4°C. CFTR was eluted from the column using 0.45 M imidazole in 5x resin volume in 1 mL fractions, and selected elution fractions were pooled and concentrated using Amicon® 100,000 MWCO (molecular weight cut-off) filters at 1000 g for 20 minutes at 4°C. The concentrated elution fractions were injected onto the ÄKTA™ Purifier (GE Healthcare Life Sciences) with a Superdex™ 200 10/300 GL column (GE Healthcare Life Sciences), and CFTR was isolated by size exclusion. CFTR was expected to elute at approximately 11 mL, in agreement with chromatography standards (Figure 3.3), and did successfully.
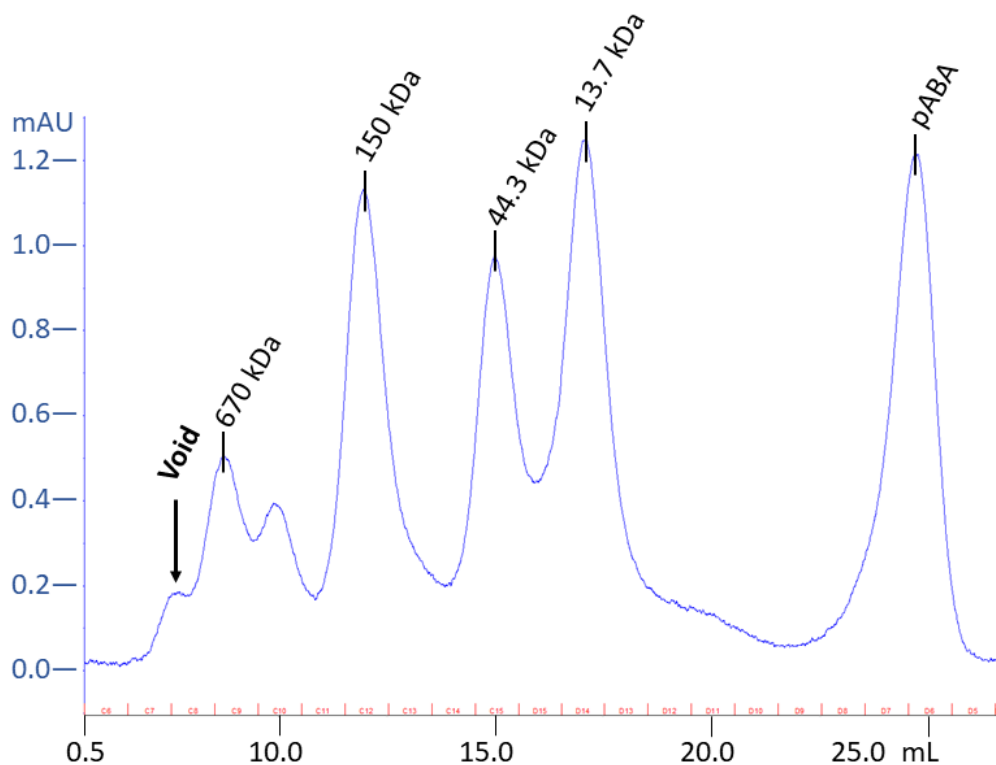
Figure 3.3: Size Exclusion Chromatography (SEC) Standards on Superdex™ 200 10/300 GL column. Molecular Weight standards for SEC were loaded onto Superdex™ 200 10/300 GL column and run at a flow rate of 0.25 mg/mL. Based on these standards and the molecular weight of CFTR (~170 kDa), CFTR and is anticipated to elute at 11 mL. CFTR-nanodiscs would be much larger, eluting at <11 mL but >9 mL.

3.2.2.5. ANALYSIS OF CFTR PURIFICATION.

Each sample was mixed with 6x Laemmli Sample Buffer (prepared in house) to a final of 1x and 50 mM DTT and immediately loaded, with a heated ladder, into either a MINI-PROTEAN® TGX™ precast 4-15% acrylamide: bisacrylamide SDS-PAGE or a hand-cast 8% acrylamide: bisacrylamide discontinuous SDS-PAGE. The gel was run at 150V for 45 minutes or 1 hour, depending on the gel type. Precast SDS-PAGE gel was transferred overnight at 4°C at 60 mA onto a nitrocellulose membrane. To improve the

CFTR signal on the nitrocellulose membrane, the membrane was fixed in 50% methanol at 4°C for 30 minutes and dried at 37°C for 30 minutes (261). The membrane was blocked in LI-COR Intercept blocking buffer for 1 hour at RT, stained in 1:1,500 mouse anti-CFTR 596 antibody in Intercept blocking buffer plus 0.1% Tween® 20 (Bio-Rad) overnight at 4° and in 1:10,000 LI-COR IRDye® 680 IR goat anti-mouse antibody in Intercept blocking buffer and 0.1% Tween® 20 for 1 hour at RT with three 15 minute washing steps with PBST after each antibody. The membranes were imaged on a LI-COR Odyssey® 9120 Infrared Imaging system. For the hand-cast discontinuous SDS-PAGE, gels were silver stained in accordance with Pierce Silver Stain manufacturer's protocol. All protein concentrations were determined using the Pierce™ BCA protein concentration assay.

3.2.3. T-Rex™ CHO expression system.

3.2.3.1. MOLECULAR CLONING.

The insert (construct nucleotide 905 to 5461) was cloned from the provided construct of WT-hCFTR in pCDNA3 which contains a glycine linker (3x) C-terminally and N-terminally to the 3xFLAG-tag within the extracellular loop 4 (ECL4), between construct nucleotides 3,598 and 3,712 (CFTR nucleotide 2,694 and 2,695 or CFTR amino acids S898 and R899). The addition of the tag increased the molecular weight by an additional 114 nucleotides (38 amino acids), making the final CFTR construct 4,557 nucleotides, or 1518 amino acids, in length. The vector was cloned from the provided T-Rex™ pcDNA5/TO construct containing WT-hCFTR plus an IRES-eCFP reporter system (construct nucleotide 1 to 1,040 and 5,484 to 11,420). The final construct, McCarty lab construct name pCF595, is 11,534 nucleotides and contains a CMV promoter with

Tetracycline operator, the WT-hCFTR construct with 3xFLAG-tag in ECL4, an IRES-eCFP reporter system, a hygromycin resistance gene, the BGH polyA tail, the SV40 promoter and origin, the pUC origin, and an ampicillin resistance gene (Figure 3.4). This construct was transformed into XL 10-Gold® Ultracompetent cells in accordance with the manufacturer's protocol. Several bacterial colonies were selected and grown in 5 mL of LB-Miller (Difco™) broth with 75 µg/mL ampicillin. Bacteria were pelleted and plasmid was purified using ZymoPURE™ Miniprep Kit. The purified plasmids were
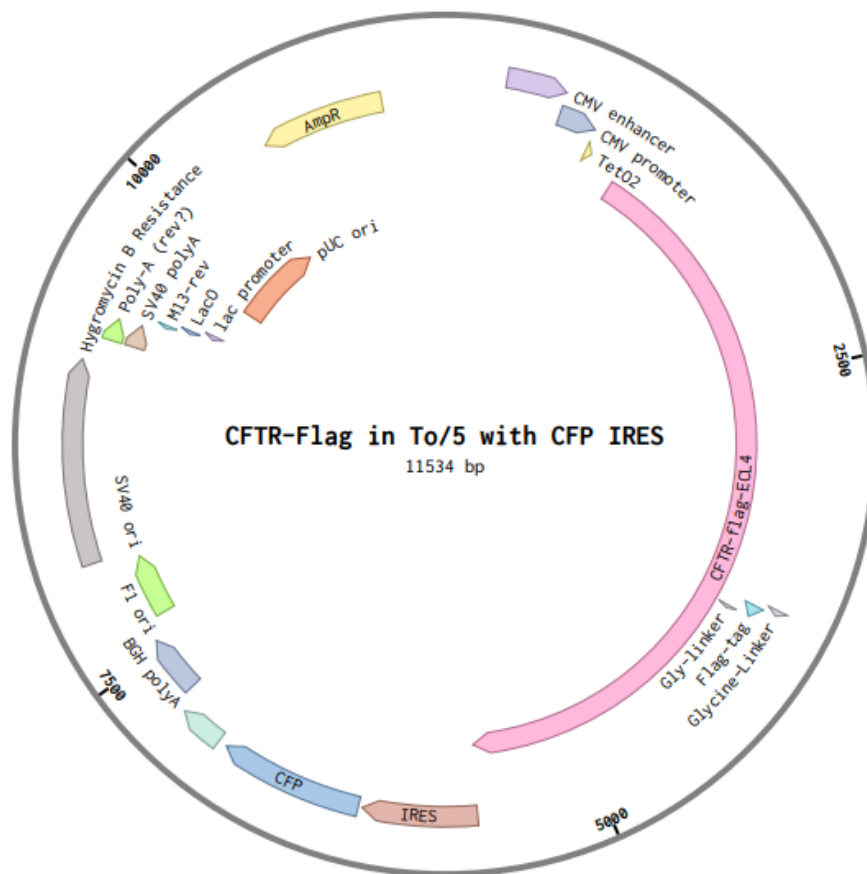
Figure 3.4: Plasmid map of WT-hCFTR with a 3x-FLAG-tag in ECL4 for stable transfection of T-Rex™ CHO cells. WT-hCFTR with a 3x FLAG-tag in extracellular loop 4 (ECL4) cloned from this construct and inserted into pcDNA5/TO containing an internal ribosomal entry site (IRES) and cyan fluorescent protein (CFP) for transfection and protein production reporting in T-Rex™ CHO cells.

screened via restriction digestion (Figure 3.5). Briefly, 5 µg of pCF595 was digested

with 2 units of *PvuI* (New England BioLabs® (NEB)) in NEB buffer 3.1 for 1 hour at

37°C. Restriction digests were analyzed on a 1% agarose gel stained with 0.5 µg/mL

ethidium bromide (EtBr) and imaged on a Bio-Rad ChemiDoc™ XRS+ system. Results

of the restriction digest informed the decision of a single bacterial colony for large-scale

amplification and plasmid purification using Maxiprep (ZymoPURE™). The CFTR

construct in the final purified plasmid was confirmed by full-length sequencing through

GeneWiz©.
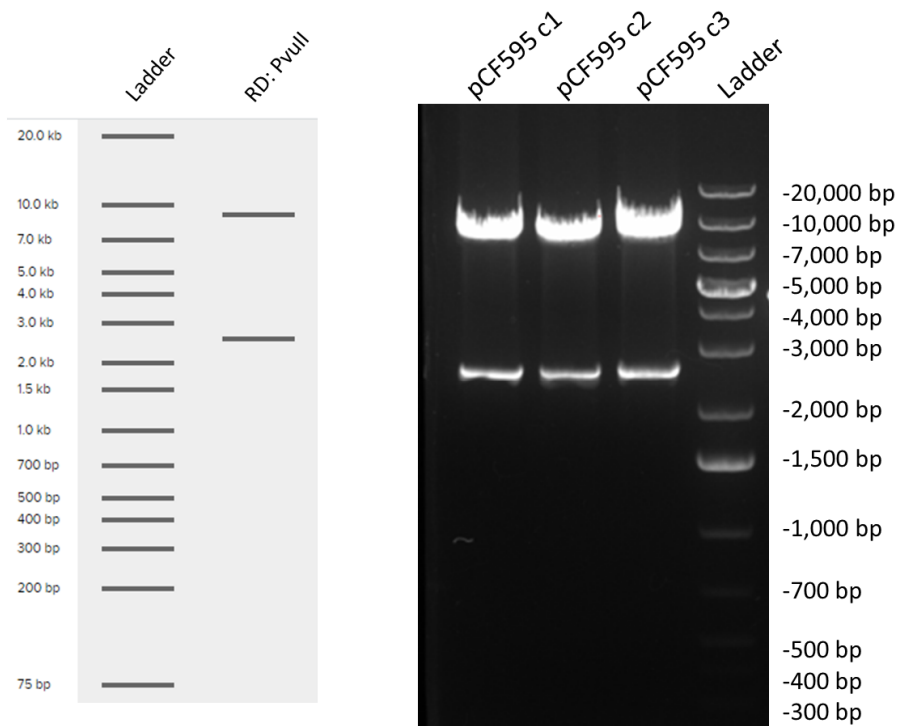
Figure 3.5: Restriction digestion of pCF595 (McCarty Lab). Results of restriction digestion, using *PvuI*, of pCF595 purified from three different bacterial colonies (c1, c2, c3) on a 1% agarose gel stained with 0.5 µg/mL ethidium bromide. Theoretical gel (left) was produced for ease of interpretation of experimental gel (right). Proper insertion and digestion will display two bands, one at just under 10 kbp and one between 3 kbp and 2 kbp. All three colonies (c1, c2, and c3) show expected digestion bands.

97

3.2.3.2. MAINTENANCE OF T-REX™ CHO CELLS.

T-Rex™ CHO cells (Thermo Fischer Scientific) were thawed and plated in a T25 flask

in Ham's F12, 10% FBS, 2 mM L-glutamine, 1% P/S and 10 µg/mL blasticidin (CHO

complete media) and allowed to grow to confluency. At confluency, cells were split at a

range of 1:5 to 1:20 into a new T25 flask containing CHO complete media. Frozen cells

were prepared in 10% DMSO, 45% conditioned CHO complete media (media exposed

to growing cells), and 45% new CHO complete media at a density of 3×10^6 cells/ mL

and cooled to -80°C and then transferred to liquid nitrogen for long term storage. Stably

transfected CHO-CFTR-3xFLAG cells were maintained using the same general methods

as T-Rex™ CHO cells, except CHO-CFTR-3xFLAG cells, which were grown in CHO

complete media plus 0.45 mg/mL hygromycin (CHO-CFTR complete media).

3.2.3.3. GENERATION OF STABLY TRANSFECTED T-REX™ CHO CFTR

EXPRESSION SYSTEM.

To confirm that a 3x-FLAG-tag in ECL4 would not interfere with CFTR biogenesis, the

generated CFTR-pCDNA3 construct was transfected into BHK cells (data not shown).

Optimal conditions for transfection of T-Rex™ CHO cells with pCF595 were determined

to be 1:2 ratio with a 12-hour transfection in a T25 flask. A hygromycin kill curve of T-

Rex™ CHO cells showed that after 4 days in 450 µg/mL hygromycin, approximately

50% of cells were dead (Figure 3.6). Transfected cells were induced with 1 µg/mL

tetracycline, and flow cytometric parameters were optimized using the Emory Flow

Cytometry Core (Figure 3.7). With optimized parameters, induced cells were separated,

singly, into two 96-well plates and allowed to grow for 3 days without selection. Once

growth was observed for most wells, the selection agent, hygromycin, was added at 450

µg/mL for 5 days (Figure 3.7). Over several weeks, confluent wells were transferred to a T25 flask and allowed to grow to confluency before the evaluation of protein expression and determination of induction conditions.
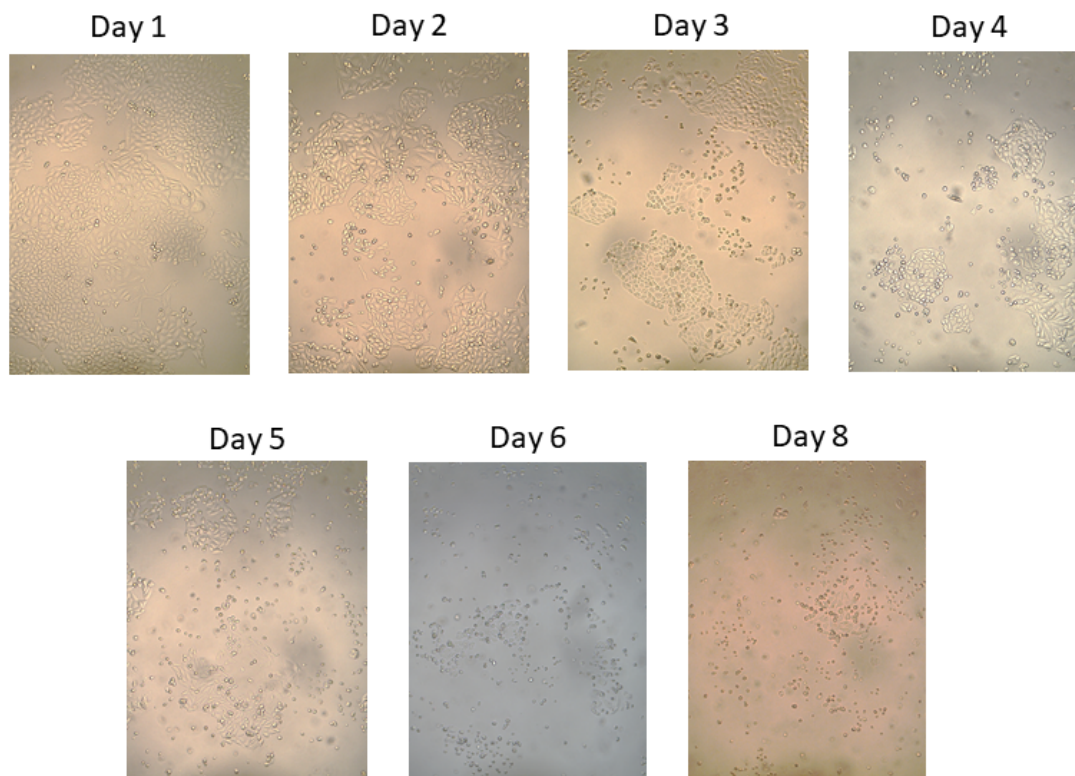
Figure 3.6: Microscopy of a T-Rex CHO cell kill curve at 450 µg/mL hygromycin. The concentration of selection agent that will show some cell death at 4 days and complete cell death after 8 days must be determined before the generation of a stable cell line by selection agent. A range of hygromycin concentrations was tested (0 µg/mL to 1.5 mg/mL) and a concentration of 450 µg/mL hygromycin fits this profile. Depicted in this figure is the concentration of 450 µg/mL, which displays cell death on Day 4, but the most on Day 8.
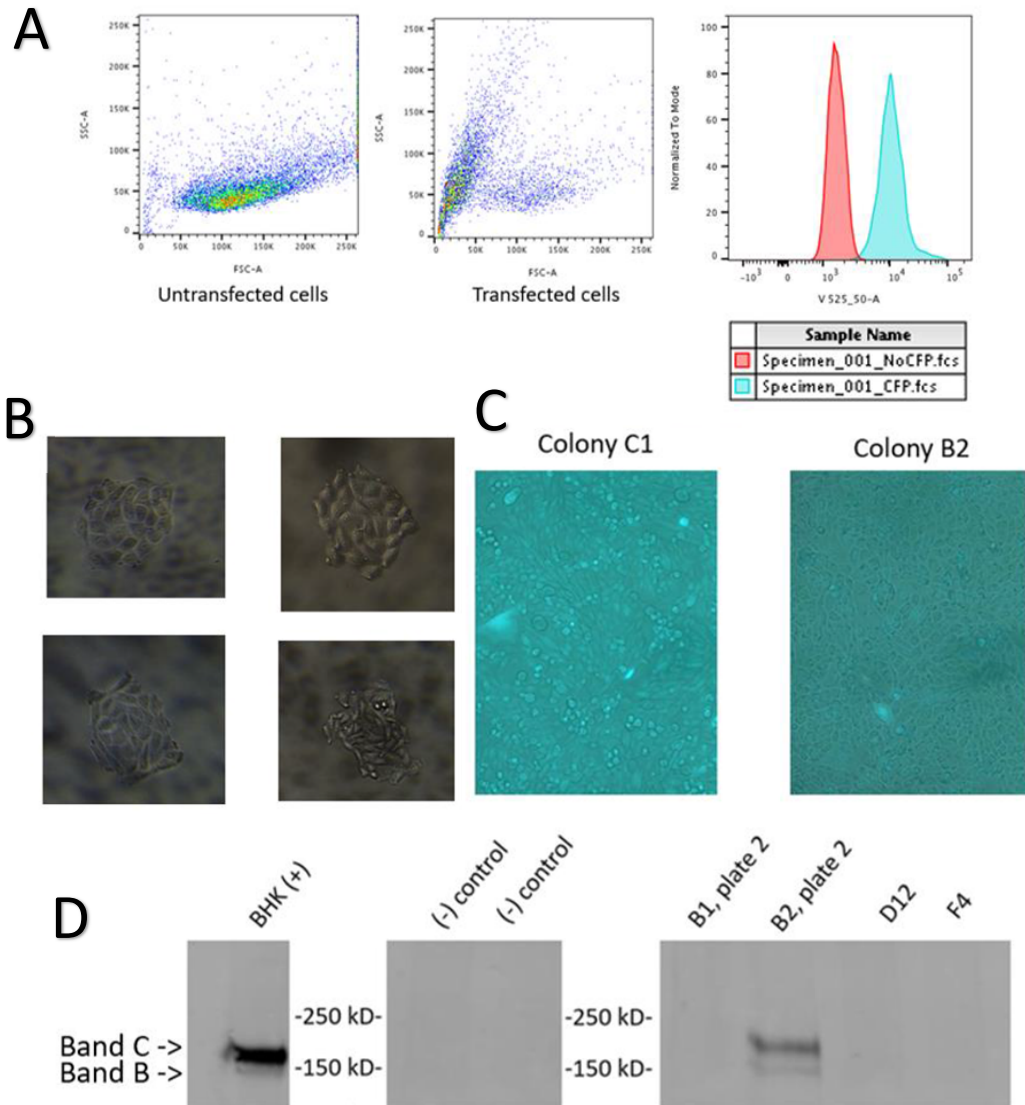
Figure 3.7: Generation of stably transfected T-Rex™ CHO cells with inducible CFTR-3xFLAG. The pcDNA5/TO containing an inducible WT-hCFTR cloned with a 3x-FLAG-tag in ECL4 and a CFP-reporting system was transiently transfected into T-Rex™ CHO cells. (A) T-Rex CHO cells were induced and were single-cell sorted by flow cytometry using the CFP reporting-system. The first plot of untransfected cells and the second of transfected cells show increased cell debris and death reported by the large side-scatter signal (SSC-A). The third plot shows the fluorescent channel separation of transfected cells from untransfected cells. (B) Representative individual colonies several days after sorting shows growth. (C) Images of two colonies that express CFTR, as well as the CFP-reporting system. (D) Western blot shows CFTR expression in colony B2, but not in several other colonies screened (D12 and F4). The first negative control is parental T-Rex™ CHO cells, and the second negative control is uninduced B2 colony. Immunoblotting for CFTR: Primary – mouse anti-CFTR 596 antibody, 1:1,500 and Secondary – IRDye® 680RD goat anti-mouse antibody, 1:10,000 (LI-COR).

100

3.2.3.4. ANALYSIS OF CFTR EXPRESSION AND PURIFICATION.

Induced stably transfected T-Rex™ CHO cells were pelleted at 1000 g for 10 minutes at 4°C and resuspended in RIPA buffer with protease 1x inhibitor cocktail (cOmplete EDTA-free PIC Roche©). Cells were incubated for 10 minutes at 4°C and cellular debris was pelleted at 1000 g for 10 minutes at 4°C. Total protein was measured using Pierce™ BCA microplate assay in accordance with the manufacturer's protocol. Equivalent amounts of protein (50-150 µg) were mixed with 1x Laemmli sample buffer (prepared in house) with 50 mM DTT and incubated at 37°C for 30 minutes. Samples and ladder, pre-heated (Precision Plus Protein™ Dual Color Standards Marker, Bio-Rad), were loaded into Mini-PROTEAN® TGX™ precast 4-15% acrylamide: bisacrylamide SDS-PAGE gels. Alternatively, an equivalent volume of each sample was mixed with 6x Laemmli Sample Buffer (prepared in house) to a final concentration of 1x and 50 mM DTT and immediately loaded, along with a pre-heated ladder, into Mini-PROTEAN® TGX™ precast 4-15% acrylamide: bisacrylamide SDS-PAGE or hand-cast 8% acrylamide: bisacrylamide discontinuous SDS-PAGE gels. The gel was run at 150V for 45 minutes or 1 hour, respectively. Precast SDS-PAGE was transferred overnight at 4°C at 60 mA onto a nitrocellulose membrane. To improve the overall CFTR signal on a nitrocellulose membrane, the membrane was fixed in 50% methanol at 4°C for 30 minutes and dried at 37°C for 30 minutes (261). The membrane was blocked in LI-COR Intercept blocking buffer for 1 hour at RT, stained in 1:1,500 mouse anti-CFTR 596 antibody in Intercept blocking buffer plus 0.1% Tween® 20 overnight at 4° and in 1:10,000 IRDye® 680RD goat anti-mouse antibody in Intercept blocking buffer and 0.1% Tween® 20 for 1 hour at RT with three 15-minute washing steps with PBST after each antibody. The membranes

were imaged on a LI-COR Odyssey® 9120 Infrared Imaging system. For the hand-cast discontinuous SDS-PAGE, gels were silver stained in accordance with Pierce Silver Stain manufacturer's protocol. All protein concentrations were determined using the Pierce™ BCA protein concentration assay.

3.2.3.5. *CFTR PURIFICATION FROM STABLY TRANSFECTED T-REX™ CHO CELLS.*

Adherent stably transfected CHO-CFTR-3xFLAG cells were seeded into 1 L suspension culture flask at 0.5×10^6 cells/mL in CHO-CFTR complete media plus 0.01% Pluronic® F68. Cells were grown to 500×10^6 cells/mL and induced with 10 ug/mL tetracycline for 12 hours. CHO cells were pelleted in 50 mL conical tubes at 1000 g for 5 minutes at 4°C. The cell pellet mass was measured, and all volumes listed in reference to 1 g initial mass. The cell pellet was resuspended in 10 mL of 8 mM HEPES-Na, pH 7.2, 0.8 mM EDTA, and 1 mM DTT. The cells were lysed using a Dounce Homogenizer with 20 strokes using the loose pestle and then again with the tight pestle. The cell lysate was mixed with $1/7^{th}$ volume of 2M sucrose in 8 mM HEPES-Na, pH7.2, 0.8 mM EDTA and 1 mM DTT and incubated on ice for 10 minutes. Large cellular debris was pelleted by centrifugation twice at 1000 g for 10 minutes at 4°C. The supernatant was ultracentrifuged at 100,000 g for 1 hour at 4°C with slow braking. The membrane pellet was washed in 5 mL of 50 mM Tris-HCl, pH 7.5, 0.5 M NaCl, and 10% glycerol by resuspension using a Dounce Homogenizer (3 strokes with the loose pestle and three strokes with tight). The resuspended pellet was ultracentrifuged again at 100,000 g for 1 hour at 4°C with slow braking. The membrane pellet was washed in 1 mL of 50 mM Tris-HCl, pH 8.0, 0.2 M NaCl, and 10% glycerol and resuspended using a Dounce Homogenizer. The resuspended membranes were moved to an ice-cold beaker in the cold room, and enough

50 mM Tris-HCl, pH 8.0, 0.2 M NaCl, 2.5 mM MgCl$_2$, 10% glycerol, and 1 mM ATP was added dropwise to make a final volume of 10 mL per initial cell pellet gram. To solubilize CFTR, 10% DDM/ 2% CHS solution was added dropwise over 30 minutes, to make a final concentration of 0.1% DDM/ 0.02% CHS with gentle mixing using a 5 mm stir bar. Solubilized CFTR was separated from insoluble material by ultracentrifugation at 100,000 g for 30 minutes at 4°C with slow braking. Only native, solubilized CFTR was extracted from the supernatant and incubated with Anti-FLAG® M2 Affinity Gel (0.01 mL) for 1 hour at 4°C with rotating. The resin was packed in a gravity flow column and washed in 50 mM Tris-HCl, pH 7.5, 0.15 M NaCl, 2.5 mM MgCl$_2$, and 10% glycerol. CFTR was eluted from the column using 2 column volumes (CV) of 0.1 mg/mL 3x FLAG® peptide and selected elution fractions were pooled and concentrated using Amicon® 100,000 MWCO filters by centrifugation at 1000 g for 20 minutes at 4°C. Concentrated elution fractions were injected into the ÄKTA™™ Purifier and CFTR was isolated by size exclusion on a Superdex™ 200 10/300 GL column. CFTR was anticipated to elute at about 12 mL, which also agrees with chromatography standards.

3.3.   RESULTS.

3.3.1. Expression of CFTR by baculoviral infection of Sf9 cells.

*3.3.1.1.*PRODUCTION OF MUTANT AND WT-hCFTR CONTAINING BACMID.

Full length sequencing of hCFTR in pFastBacDual construct showed the correct sequence for expression in Sf9 cells, albeit with a non-standard single codon repeat for the His-tag, instead of alternating codons. Bacmids purified after plasmid transformation into DH10Bac *E. coli* (Blue/White Screening) (Figure 3.8), and PCR amplification of the gene of interest region showed the correct size of WT and mutant hCFTR sequence

incorporation into Bacmid (Figure 3.9).
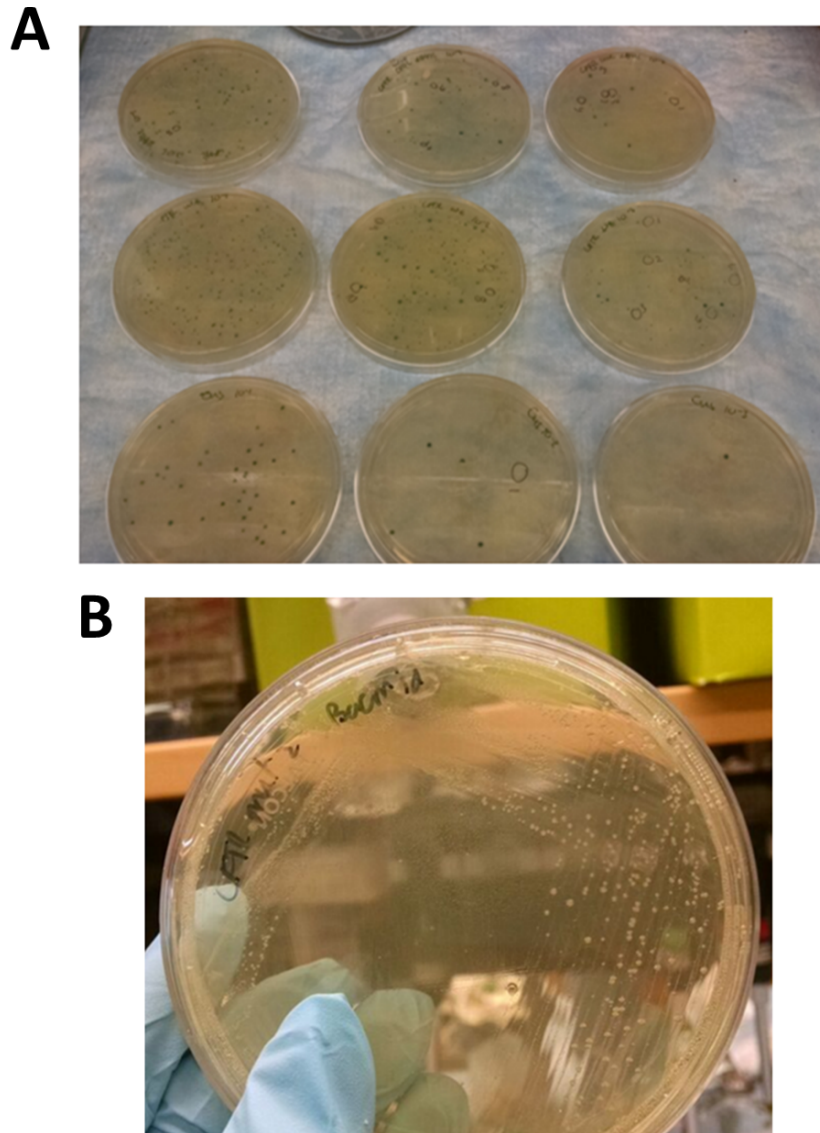
Figure 3.8: Images of representative agar plates utilizing Blue/White screening to confirm successful bacmid production after transformation. (A) Initial transformants plated on LB-agar plates with 50 µg/mL kanamycin, 7 µg/mL gentamicin, 10 µg/mL tetracycline, and 100 µg/mL Bluo-gal and 40 µg/mL IPTG. Colonies that have been transformed with plasmid and have correctly produced recombinant bacmid are white. (B) Selected colonies from the first plate were restreaked on new LB-agar plates (containing previously mentioned additives) to confirm the homogeneity of each selected colony.
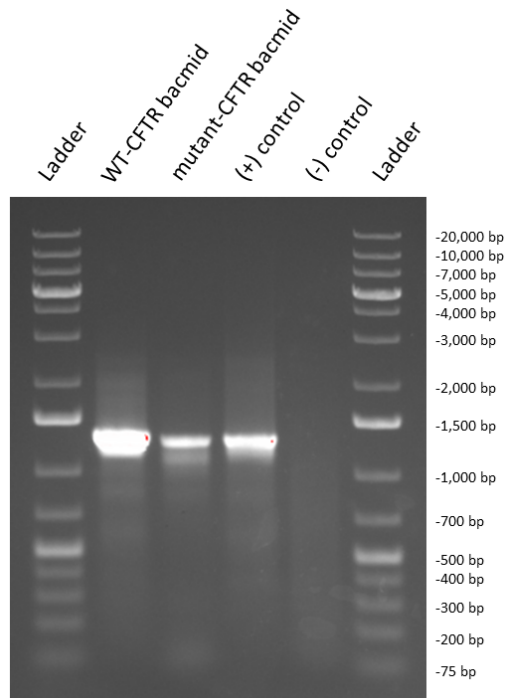
Figure 3.9: PCR amplification of a section of CFTR from purified WT-CFTR and mutant CFTR bacmid. Primers, designed in house, were used to amplify a specific region of CFTR from purified bacmid to confirm CFTR gene insertion into bacmid. The positive control is the WT-CFTR plasmid (pCF340, McCarty Lab) and the negative control is ABCC4 in pGEMHE construct. Both mutant and WT Bacmid show similar size bands to positive control suggesting the proper insertion of CFTR into the bacmid.

3.3.1.2. TRANSFECTION OF SF9 CELLS WITH BACMID TO PRODUCE

BACULOVIRUS.

Positive infection of Sf9 cells was observed via an increase in cell size and the generation of many vesicles within the cells (Figure 3.10). The titer of both p1 and p2 plaque-purified viral colonies was determined via plaque assay and neutral red staining. The levels of CFTR expression per viral colony was determined by Western blot using a CFTR specific antibody; however, a His-tag antibody could not detect the same CFTR expressed protein on a Western Blot (Figure 3.11). The lack of detection of a Hist-tag by Western blot suggested difficulty in the purification of CFTR using His-tag affinity chromatography.

105
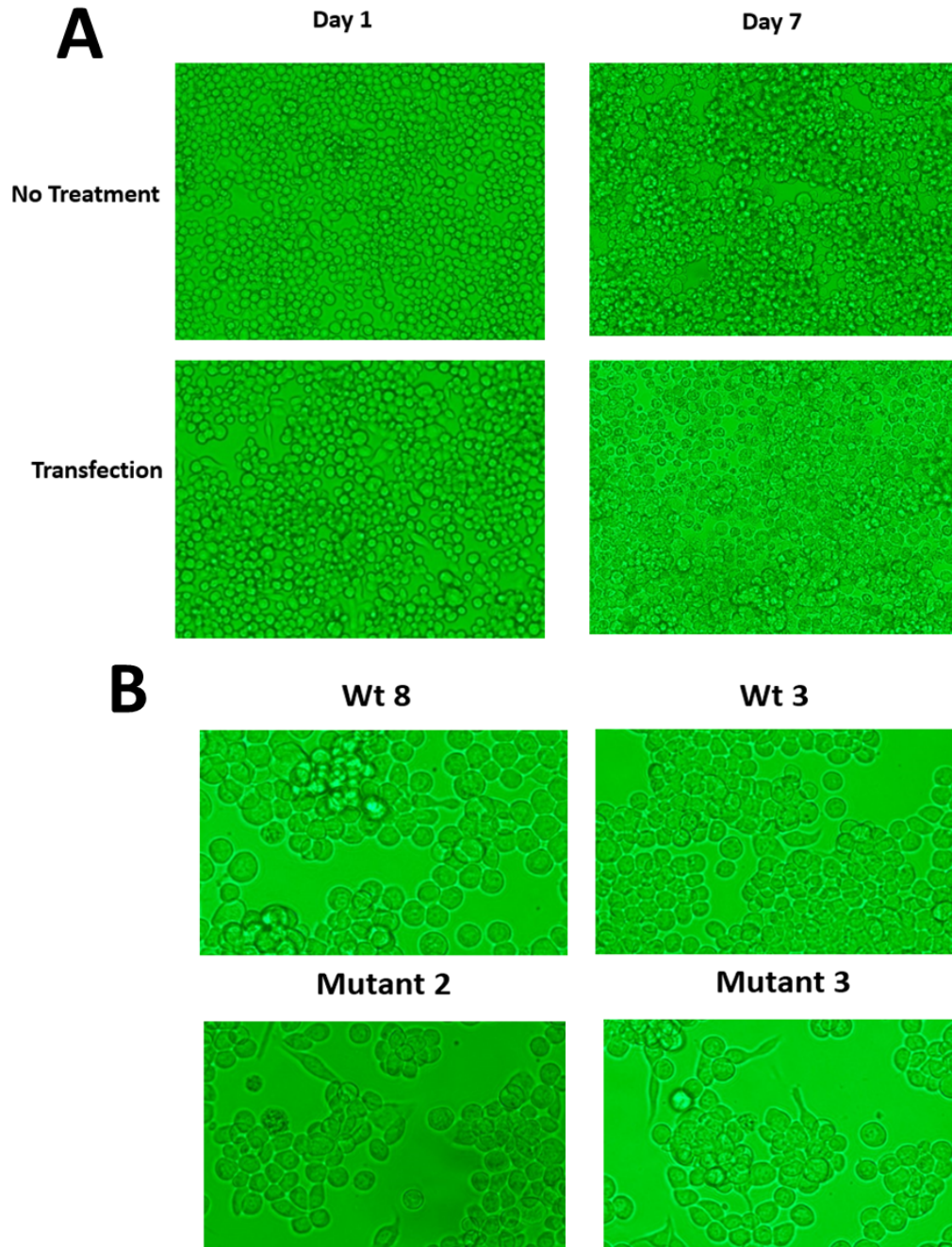
Figure 3.10: Images of transfected Sf9 cells to confirm viral infection and baculovirus production. (A) Images are comparing Sf9 cells that were transfected with bacmid (WT) to produce baculovirus. After 7 days, transfected Sf9 cells will appear larger in size when compared to untransfected cells and will contain many intracellular vesicles. Infected Sf9 cells will eventually leave a region of no cell growth or a plaque under plaque assay conditions. Individual plaques are collected and can be used to infect more copious amounts of cells. (B) Visualization of Sf9 cells infected with plaque-purified p1 virus for WT-CFTR (Wt 8 and Wt 3) or mutant CFTR (mutant 2 or mutant 3, D110C/K892C). Again, cells infected by baculovirus are identified by swelling and the presence of small vacuoles.
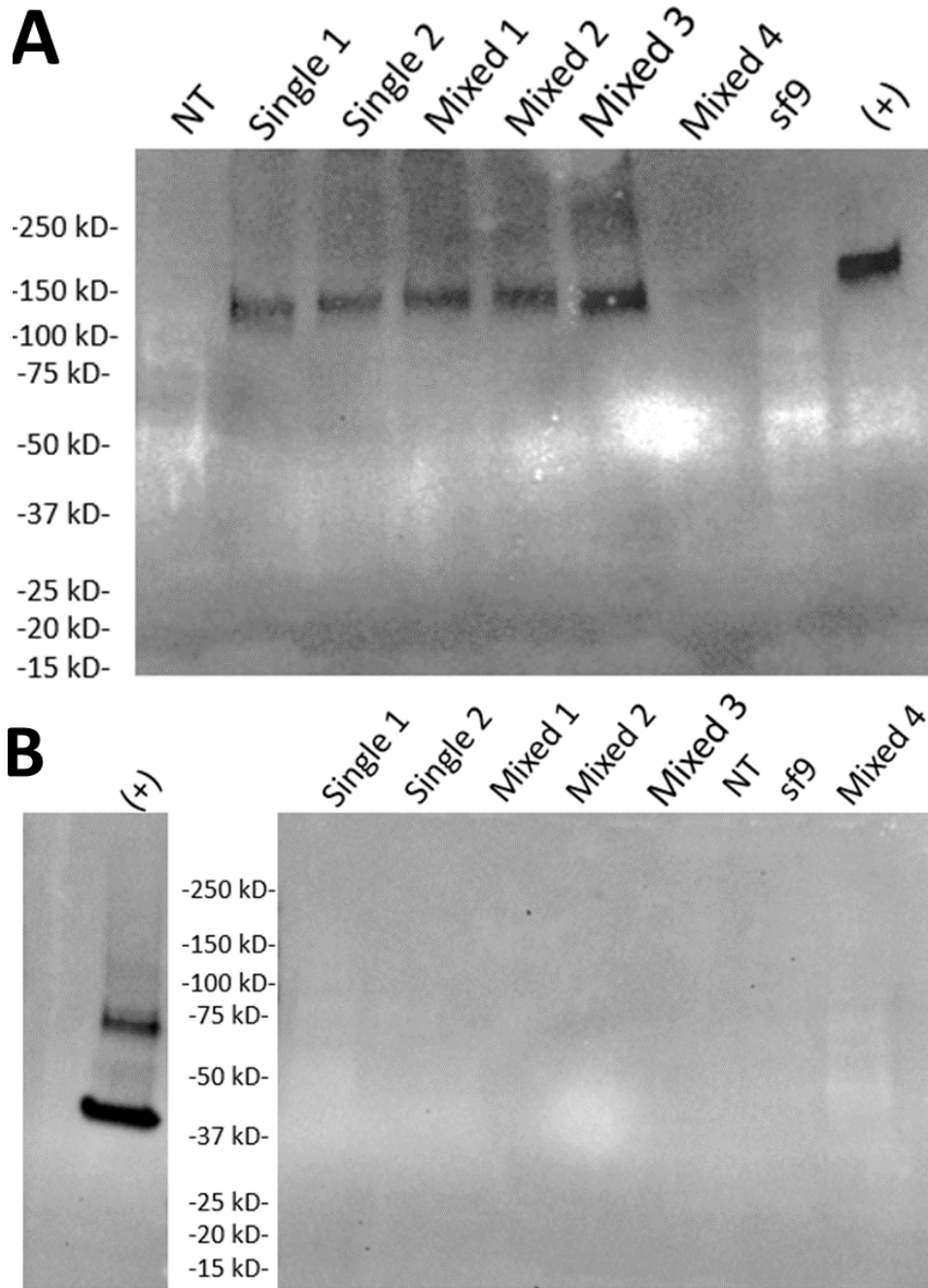
Figure 3.11: Western blot analysis to determine high-expressing WT-CFTR p1 viral stock. High-expressing CFTR plaque purified p1 viral stocks, single 1 and single 2, or mixed plaques, mixed 1, mixed 2, mixed 3, and mixed 4, were determined by western blot analysis using an anti-CFTR antibody (A), but were not detected by anti-His-tag antibody (B). Positive controls are CFTR expressed in BHK cells (A) and His-tagged sphingomyelinase, purified (B). Immunoblotting for CFTR: Primary – mouse anti-CFTR 596 antibody, 1:1,500 and Secondary – goat anti-mouse antibody conjugated to HRP, 1:1,000. Immunoblotting for His-tag: Primary – rabbit anti-His-Tag antibody, 1:1,000 and Secondary – goat anti-rabbit antibody conjugated to HRP, 1:1,000.

3.3.1.3. HIS-TAG IS NOT ACCESSIBLE IN CFTR PRODUCED BY SF9 CELLS.

A crude purification testing the accessibility of the His-tag on baculoviral expressed

CFTR showed no binding to Roche$^{©}$ cOmplete His-tag resin indicating the inability to

purify CFTR expressed in the Baculovirus system via the incorporated His-tag (Figure

3.12).
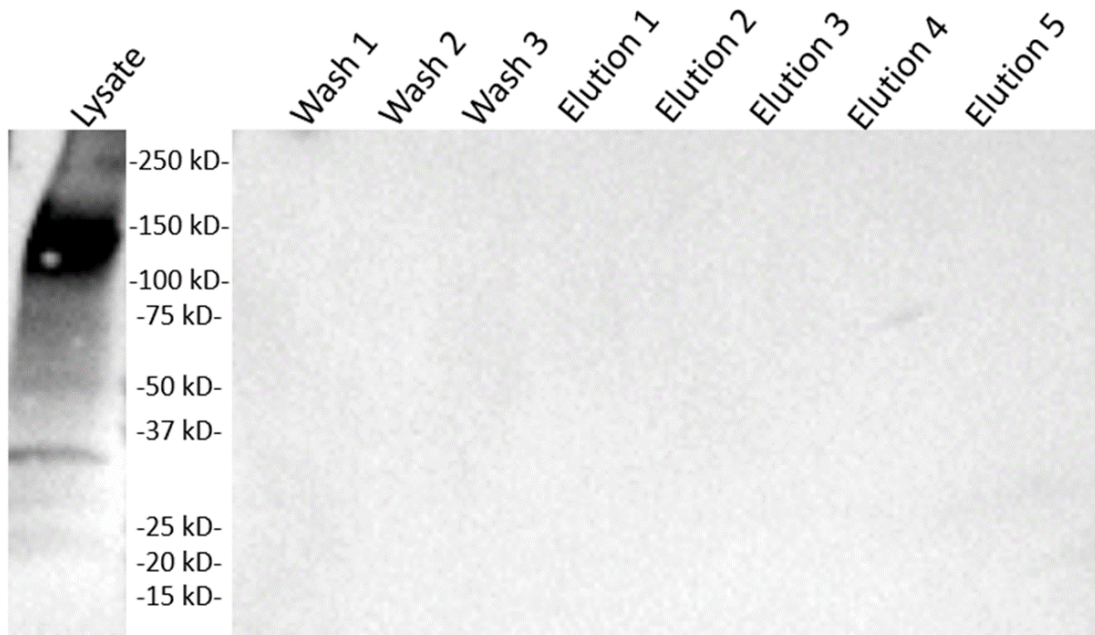
Figure 3.12: Western blot analysis of crude CFTR purification from infected Sf9 cells expressing WT-hCFTR. Sf9 cells were infected with a high CFTR expressing p1 virus (WT, mixed 3) at an MOI of 20. Infected cells were lysed in Roche A buffer and 0.1% DDM. CFTR could not be separated from the lysate using His-tag affinity resin, confirming the inaccessibility of His-tag. Immunoblotting for CFTR: Primary – mouse anti-CFTR 596 mouse antibody, 1:1,500 and Secondary – goat anti-mouse antibody conjugated to HRP, 1:1,000**.**

3.3.2. CFTR purification from the BHK-CFTR-10xHis expression system.

3.3.2.1. HIS-TAG OF RECOMBINANT CFTR IS ACCESSIBLE IN BHK-CFTR-10xHIS CELL LINE.

Because CFTR expressed in Sf9 cells showed the inability to use the His-tag for separation of CFTR from endogenous proteins under crude purification conditions, a new cell expression system was tested. A crude purification of CFTR using Roche© cOmplete His-Tag Resin from the stably transfected BHK cells showed that the His-tag was accessible (Figure 3.13). The accessibility of the His-tag on CFTR tested and confirmed in this cell expression system means the possibility of purifying CFTR for downstream applications.
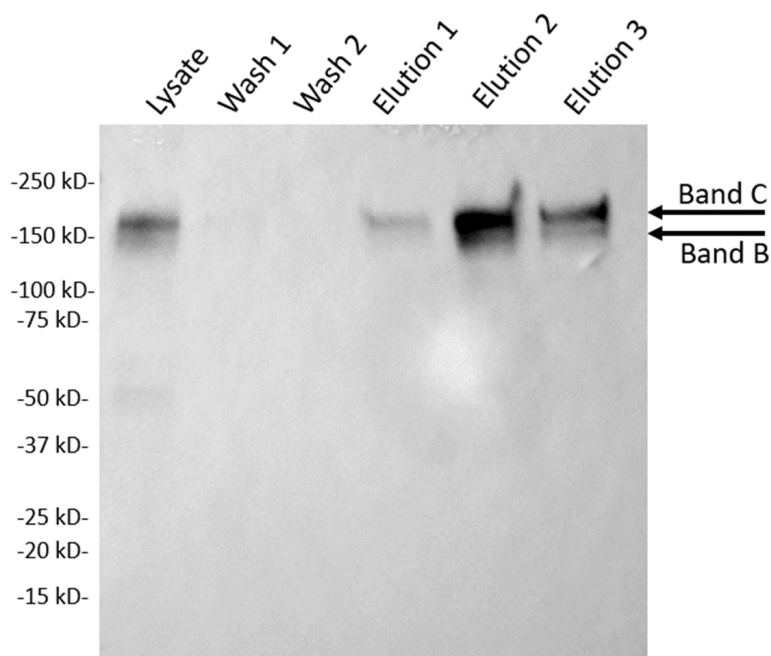
Figure 3.13: Western blot analysis of crude CFTR purification from BHK cells stably transfected to express WT-hCFTR. Stably transfected BHK cells expressing WT-hCFTR were lysed in Roche A buffer and 0.1% DDM. CFTR was separated from the endogenous protein in the lysate using His-tag affinity resin. The ability to separate CFTR confirms the accessibility of the His-tag in this cell expression system. Immunoblotting for CFTR: Primary – mouse anti-CFTR 596 antibody, 1:1,500 and Secondary – goat anti-mouse antibody conjugated to HRP, 1:1,000**.**

3.3.2.2. TRANSITION OF ADHERENT BHK-CFTR-10xHIS CELLS TO SUSPENSION CULTURE DOES NOT AFFECT CFTR EXPRESSION.

Suspension cultures allowed for increased yield of cells and thus are optimal for protein purification. The stably transfected BHK-CFTR-10xHis cell line grows adherently, and so to transition these BHK cells to suspension culture, the cells must grow in clumps known as BHK pearls. It is imperative to confirm that the transition of the adherent BHK-CFTR-10xHis cell line to suspension culture does not affect CFTR expression. Western blot analysis of the expression profile of CFTR shows no change between adherent and suspension cultures (Figure 3.14).
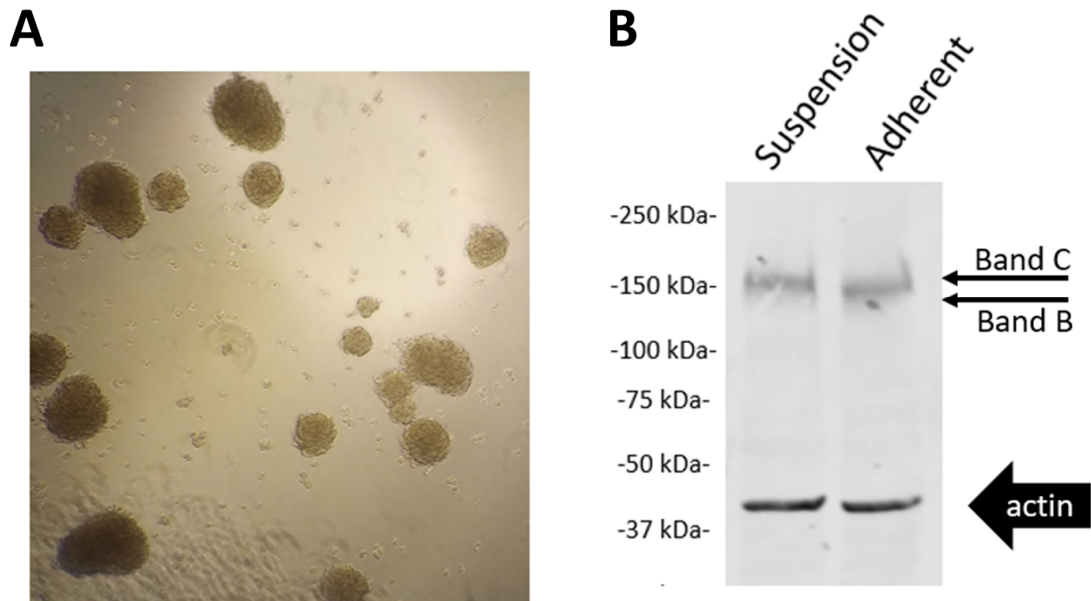
Figure 3.14: CFTR expression is unchanged under suspension cell culture conditions. CFTR expressed in the stably transfected BHK cell line. Cells were transitioned to suspension culture, growing as "pearls" for purification. (A) BHK-CFTR-10xHis pearls after a few days under suspension culture conditions. (B) Western blot comparing CFTR expression under suspension and adherent cell culture conditions. Immunoblotting for CFTR: Primary – mouse anti-CFTR 596 antibody, 1:1,500 and Secondary – IRDye® 680RD goat anti-mouse antibody, 1:10,000. Immunoblotting for Actin: Primary – mouse anti-actin antibody, 1:5,000 and Secondary – IRDye® 800CW goat anti-mouse antibody, 1:10,000.

3.3.2.3. IMPROVEMENTS TO DETERGENT-SOLUBILIZED CFTR PURIFICATION

INCREASED OVERALL YIELD.

A typical 2.4 L BHK-CFTR-10xHis suspension culture yielded a total of 4-6 g wet cell mass. Cell lysis via Dounce homogenizing showed that >90% of cells were lysed (Figure 3.15). A dramatic improvement in the CFTR yield was observed in changing the solubilization technique. Previously, CFTR was solubilized by the direct addition of 1% DDM followed by incubation over 30 minutes; however, by changing to the dropwise addition of 0.1% DDM/0.02% CHS over 30 minutes the yield of solubilized CFTR was dramatically improved (Figure 3.16). Overall, CFTR purity was dramatically improved by changing from Roche® cOmplete resin to Pierce HisPure™ Ni-NTA resin and by increasing the amount of imidazole in the wash steps (Figure 3.17). Phosphorylation of CFTR on the column during the first wash step also improved overall yield. The current
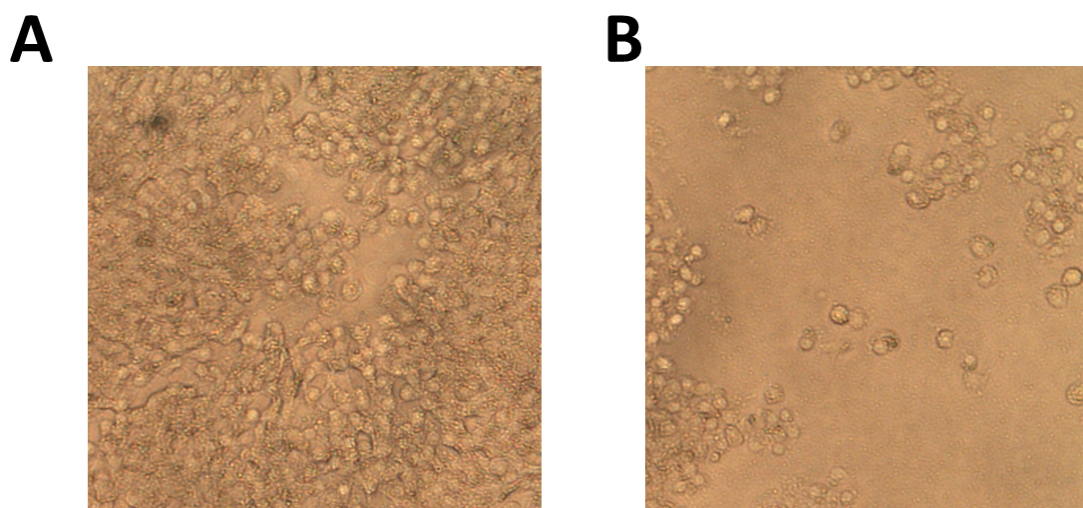
Figure 3.15: Microscopic confirmation of at least > 90% lysed cells. BHK cells are lysed using a Dounce Homogenizer. Cells imaged before (A) and after (B) lysis.

purification protocol yielded the mostly CFTR, albeit with one strong copurified protein (Figure 3.18). Even after size exclusion chromatography, this copurified protein remained present (Figure 3.19). The final yield of total protein concentration varies but was typically 50 - 200 µg with CFTR being approximately 20%-50% analyzed by densitometry.
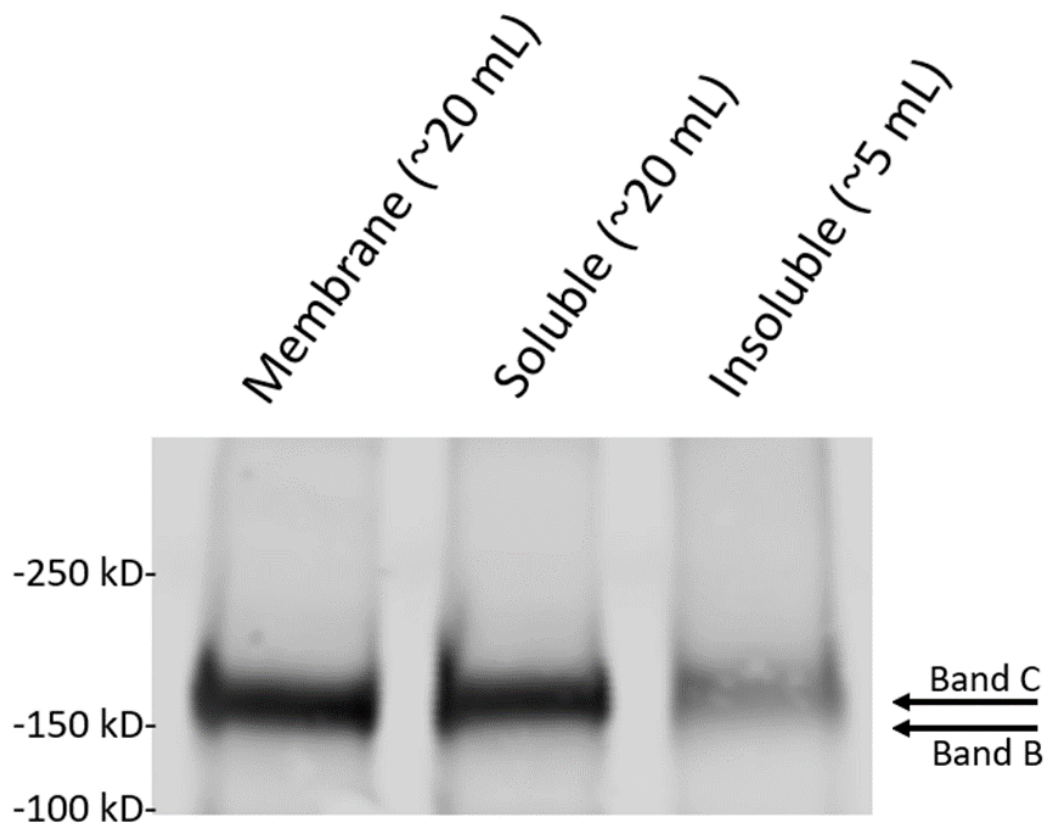
Figure 3.16: CFTR solubilization is improved by slow-dropwise addition of detergent. The method of solubilization for CFTR not only increases the amount of CFTR from the membrane fraction but also improves the overall yield. Immunoblotting for CFTR: Primary – 596 mouse anti-CFTR antibody, 1:1,500 and Secondary – LI-COR goat anti-mouse antibody, 1:10,000
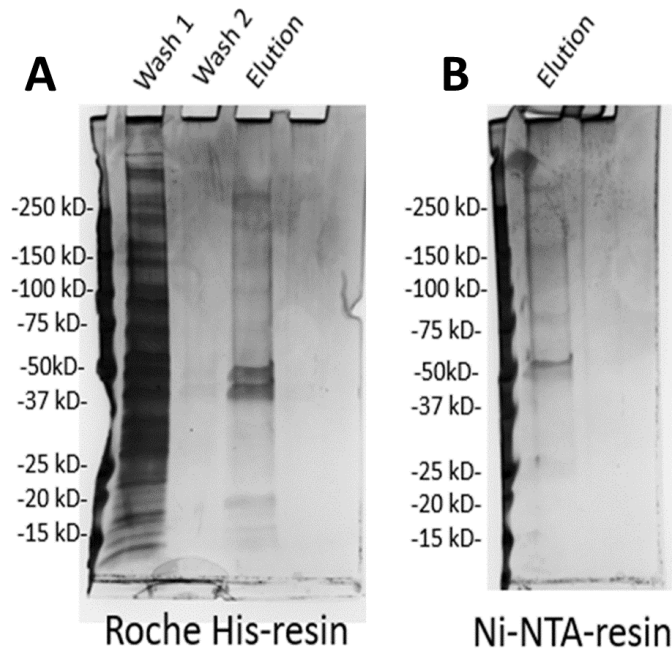
Figure 3.17: CFTR purity improved by changing the His-tag affinity resin used in purification. Silver stained Mini-PROTEAN® TGX™ pre-cast 4-15% acrylamide: bisacrylamide gradient SDS-PAGE gel showing the improvement in purity by changing the resin type. The elution fraction between the Roche® His-resin (A) and the HisPur™ Ni-NTA resin (B), shows a dramatic improvement to the number of protein bands in the elution lane in the HisPur™ Ni-NTA resin.
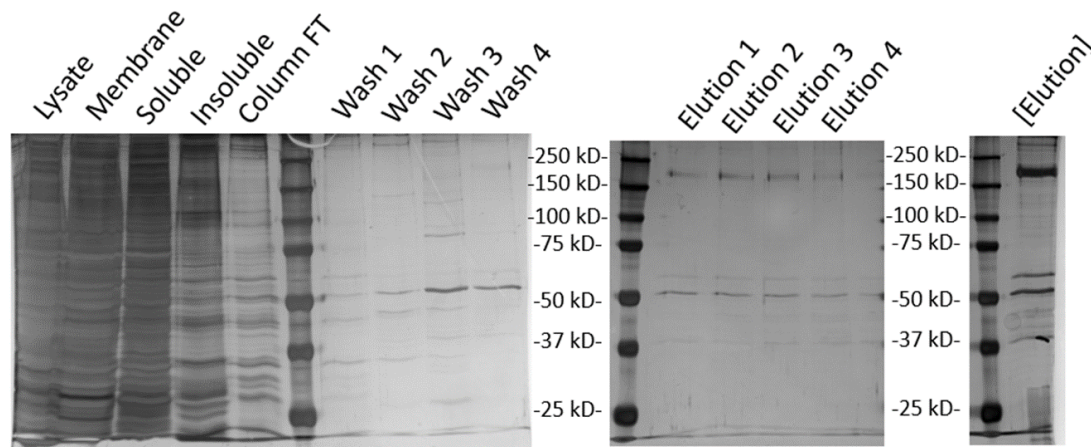
Figure 3.18: SDS-PAGE analysis of CFTR purification. Each lane, and lane label, represents the sample at each stage of the purification process described. Silver stain of 8% acrylamide: bisacrylamide hand-cast SDS-PAGE gel showing the overall purification, especially improving the purity of CFTR. An unknown copurified protein was mostly eluted in wash 3 and wash 4. However, this protein can still be seen in the final elution lane of CFTR ([Elution]).
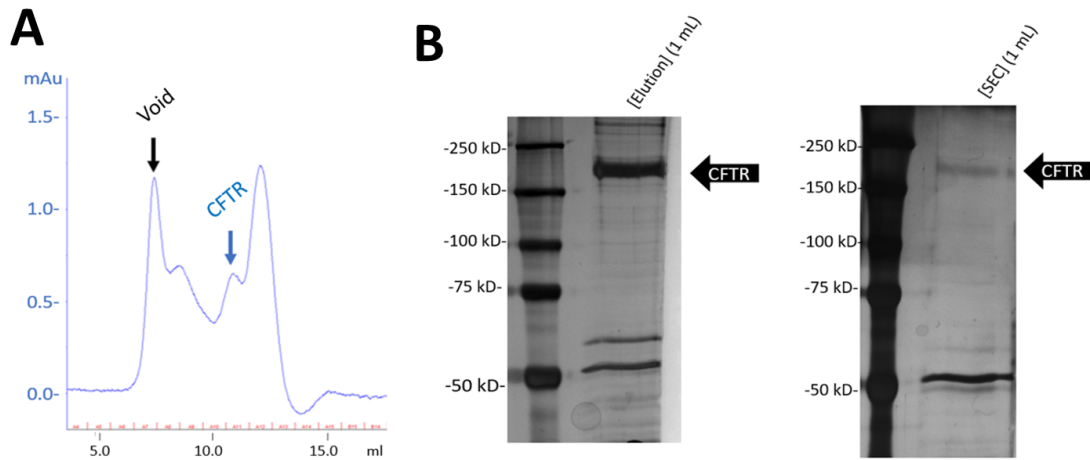
Figure 3.19: Size Exclusion Chromatography (SEC) of CFTR purified from BHK cells. (A) Full UV-spectra chromatogram from SEC with a Superdex™ 200 10/300 GL Column after injection with concentrated CFTR elution fractions. Void volume is marked by a black arrow and the monomeric CFTR peak is marked by a blue arrow. Several peaks present in the SEC chromatogram shows the presence of multiple proteins. (B) Silver stained 8% acrylamide: bisacrylamide hand-cast SDS-PAGE gel comparing the purity of CFTR from pooled elution fractions [Elution] to purity of CFTR after SEC fraction [SEC].

3.3.3. CHO-CFTR-3xFLAG expression system.

3.3.3.1. PRODUCTION OF A STABLY TRANSFECTED CHO-CFTR-3xFLAG CELL LINE.

The confirmed construct bearing CFTR-3xFLAG (ECL4) in pcDNA5/TO was transfected into the T-Rex™ CHO cell line with transfection monitored by the IRES-CFP system. Individual cells were sorted by flow cytometry allowing for the development of uniform cell colonies during the selection of stably transfected cell lines. From this method, 6 different cell lines were developed, with varying levels of CFTR expression and two, colony B2 and C1, are shown in Figure 3.7.

3.3.3.2. PURIFICATION OF DETERGENT-SOLUBILIZED CFTR FROM CHO-CFTR-3xFLAG CELL LINE.

Purification of CFTR from the CHO line showed a variety of dramatic improvements, including in purity (Figure 3.20), shortening the overall purification time, and shortening the amount of time CFTR is in detergent, while maintaining yield; however, the yield could be improved by the removal of some of the glycosylation signal.
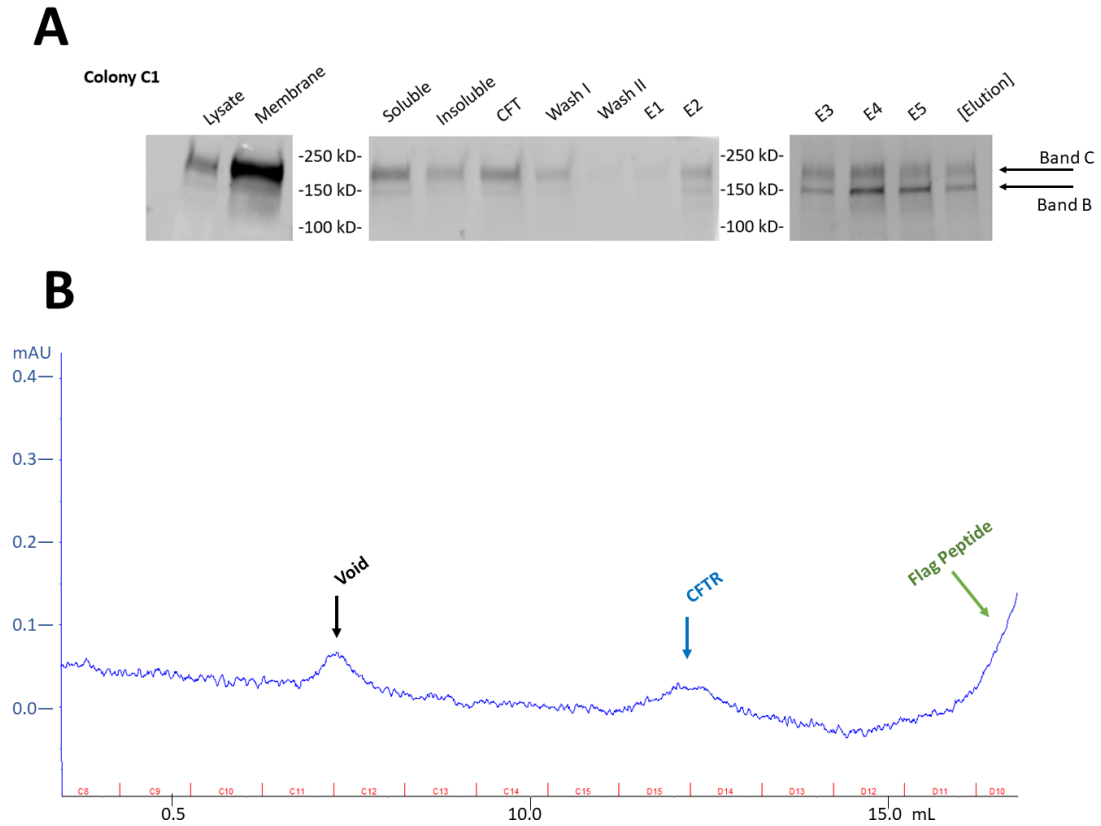
Figure 3.20: Analysis of purification of CFTR from CHO cells using Size Exclusion Chromatography (SEC) and Western blot. (A) Western blot analysis shows some CFTR binding to and eluting from resin, especially of Band B. Immunoblotting for CFTR: Primary – mouse anti-CFTR antibody 596, 1:1500, and Secondary – IRDye® 680RD goat anti-mouse antibody, 1:10,000. (B) Full UV-spectra chromatogram from SEC with a Superdex™ 200 10/300 GL column after injection with concentrated CFTR elution fractions. Void volume is marked by a black arrow, monomeric CFTR peak is marked by a blue arrow, and the FLAG® peptide is marked by a green arrow.

3.4. DISCUSSION.

The inaccessibility of the His-tag on CFTR produced in the Sf9 expression system renders the purification of CFTR from this expression system impossible. As to why the His-tag is inaccessible, it could be that CFTR was not fully translated in Sf9 cells. Since the tag is on the C-terminus of CFTR, the last portion of the protein to be translated, if CFTR was trapped in the ribosome towards the end of synthesis, then the tag may not have been synthesized. However, the protein band on the Western Blot is of correct reported size for CFTR expressed in Sf9 cells, and the antigen for the CFTR-specific antibody used is in a region (a.a. 1204 to 1211) in NBD2, the C-terminus-containing domain (132) (CFTR Antibodies Distribution Program, Cystic Fibrosis Foundation). Thus, for this to be the reason, only a small portion of CFTR is not translated. If this is the case, moving the His-tag to another section of the protein could improve the use of this cell expression system for CFTR purification. Modifications and improvements in the purification steps of CFTR from the BHK-CFTR-10xHis cell expression system improved the overall protein yield (from 20 µg to almost 100 µg) and can be used to inform CFTR purifications from any cell line. One of these modifications was in the detergent solubilization step of CFTR with the use of a cholesterol-derived detergent known as cholesteryl hemisuccinate (CHS). The use of this detergent has become popular in the purification of ABC transporters (262, 263), as well as shows improved thermal stability of other tricky membrane proteins (264, 265). It's possible that CHS has improved the thermal stability of CFTR in detergent, and thus provides a higher overall yield than CFTR purified without CHS. This hypothesis can be tested by a series of thermal melting curves of CFTR in different detergents, especially in the presence or

absence of CHS. The copurified proteins persistent with CFTR from the BHK-CFTR-10xHis system remained challenging to remove, even after increased resin washing steps and SEC. This is not uncommon for His-tag affinity chromatography systems, whereas FLAG-tag affinity chromatography systems are much improved in purity (266). Thus, to improve CFTR purity, a system using FLAG-tag affinity chromatography was developed. The CHO-CFTR-3xFLAG improved the purity of CFTR as shown by SEC. The use of this system, as opposed to the stably transfected BHK-CFTR-10His system, will allow for the quick, ~3 weeks, production of multiple individual stable cell lines for a single mutation or multiple mutations. The ability to generate stably transfected cell lines, without the need for viral titering, means disease-relevant or thermostabilizing mutations can be introduced with relative ease. The clear separation of Band B CFTR from Band C CFTR, unlike in the BHK cells, will also provide a way to track the production of Band C or Band B CFTR with the introduction of each new mutation. The ease of transition between adherent and suspension culture conditions means CFTR can be purified from this culture or recorded using a variety of electrophysiological techniques. This allows for more comparative studies of CFTR channel activity both pre- and post- purification.

CHAPTER IV

CFTR RECONSTITUTION AND FUNCTION

4.1.   INTRODUCTION.

Studying membrane proteins in a lipid bilayer provides a more physiologically relevant environment than detergent; however, the structures that lipid bilayer layers form have always made studying individual membrane proteins difficult. The recent development of individually packaged membrane proteins in lipid bilayers, meaning nanodiscs and native nanodiscs or SMALPS (or their derivatives), has revolutionized the study of membrane proteins (1, 181). In fact, structural and functional studies of even well-characterized membrane proteins have shown that the lipid environment of membrane proteins can dramatically alter the characteristics of the membrane protein—decreasing ATPase activity, but improved transport efficiency (267), rearrangement of transmembrane helices (268), identification of critical lipid binding positions (263), etc. These studies are supporting the hypothesis that lipids play a significant role in membrane protein function and structure. Recent structural studies of detergent-solubilized hCFTR have identified multiple electron-dense regions around the TMDs— possibly copurified lipids; however, the identities of these lipids are unknown (128). Other functional studies of CFTR demonstrate the importance of certain types of lipids in the ATPase activity of CFTR (133). This chapter will briefly discuss the expression and purification of Membrane Scaffold Protein (MSP) and the formation of nanodiscs using two different types of lipids. Also, this chapter will focus on the function of CFTR in detergent versus lipids, and between different lipid environments by both an ATPase

assay and planar lipid bilayer electrophysiology. Reconstitution of WT-hCFTR in nanodiscs demonstrates different ATPase activities dependent on the environment. The channel function of detergent purified CFTR reconstituted into proteoliposomes demonstrates comparable channel characteristics of CFTR as seen in cellular membranes; however, traditional inhibitors of CFTR show reduced efficacy which might be dependent on the type of lipid environment.

4.1.1. Individual Contributions.

I performed the reconstitution of CFTR in nanodiscs and proteoliposomes experiments and the ATPase activity assays. I designed and performed the MSP1D1 expression and purification experiments with the help of Ms. Isabela Povkov (a Georgia Tech undergraduate student). The planar lipid bilayer (PLB) experiments were conducted by Mrs. Kirsten Cottrill (an Emory graduate student). The first model was built with the help of Mr. Gorman Stock (a former student), which was later refined by Dr. Curtis Balusek, both of Dr. JC Gumbart's Lab.

4.1.2. Publications resulting from this chapter.

Parts of this chapter will be published as a chapter in *Methods in Molecular Biology* on the use of BioBeads^{TM} and the reconstitution of membrane proteins into nanodiscs and proteoliposomes. Other parts of this chapter will be published in downstream manuscripts.

4.2. METHODS.

4.2.1. Preparation of BioBeads^{TM}.

Bio-Beads™ (SM-2 Adsorbents cat#1523920) were weighed (~3 g) to fill 1% of the volume of a 50 mL conical tube. The BioBeads™ were washed by filling the 50 mL

conical tube with 100% methanol and rotated for at least 24 hours at RT. The beads were allowed to settle, so methanol could be removed and then washed in 50 mL double-distilled or milli-Q® (Millipore Sigma) water for 24 hours at RT, again with rotating. Water washes were repeated for at least four days before beads were stored in a new volume of water at 4°C. The BioBeads™ were tested for quality by forming empty nanodiscs under the most optimal conditions—with one of the three lipids known to form nanodiscs (See below) readily.

4.2.2. MSP1D1 expression and purification.

There are several commercially available MSP plasmids. Using a model of the 9.7 nm diameter nanodisc formed by the MSP1D1 protein and structures of CFTR, it was determined that CFTR could be incorporated into nanodiscs of this diameter with little hindrance. pMSP1D1 construct (plasmid #20061) was purchased from Addgene, originally gifted by Dr. Stephen Sligar, and shipped in DH5α *E. coli* cells (184) (Figure 4.1). The cells were streaked on LB-agar plates with 50 µg/mL kanamycin and incubated overnight at 37°C. Several bacterial colonies were selected and grown in 5 mL of LB-Miller (Difco™) broth with 50 µg/mL kanamycin. Bacteria were pelleted and the plasmid was purified using ZymoPURE™ Miniprep Kit. The purified plasmids were screened via restriction digestions (Figure 4.2). Briefly, 1 µg of pMSP1D1 was digested with 1 U of *PvuI* (New England BioLabs® (NEB)) in NEB buffer 3.1 for 1 hour at 37°C and double digested with 1 U of *HindIII* and *HincII* (New England BioLabs®(NEB)) in NEB buffer 2.1 for 1 hour at 37°C. Restriction digests were analyzed on a 1% agarose gel stained with 0.5 µg/mL Ethidium Bromide (EtBr) and imaged on a Bio-Rad ChemiDoc™ XRS+ system. Results of restriction digest informed the selection of a single bacterial colony
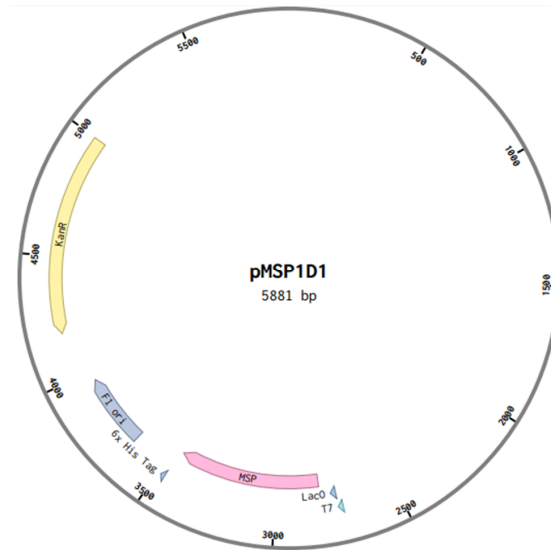
Figure 4.1: pMSP1D1 plasmid map. The pMSP1D1 construct is purified from DH5α *E. coli* and transformed into BL21 (DE3) *E. coli* for production of MSP1D1 protein, which can be purified using His-tag affinity chromatography and used in the formation of nanodiscs.
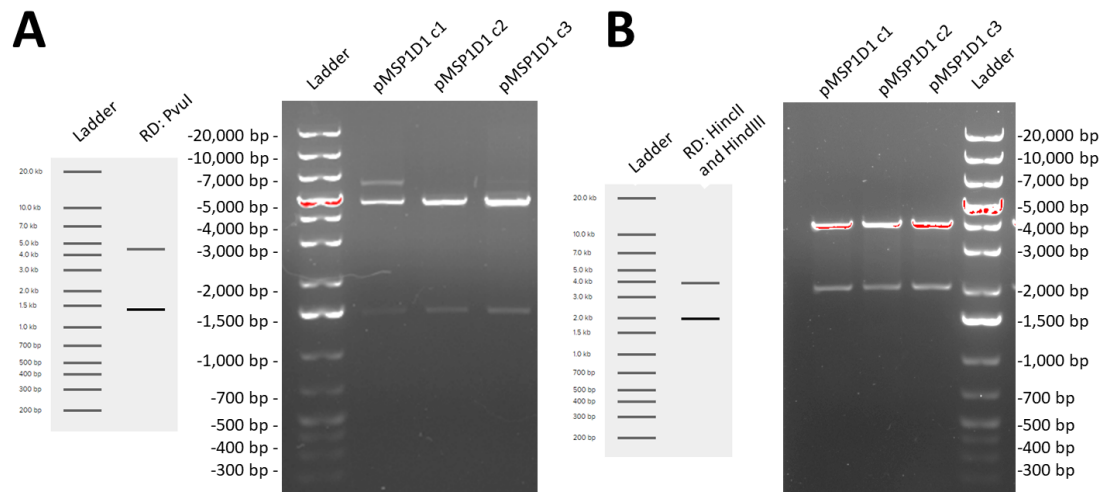
Figure 4.2: Restriction digestions of pMSP1D1. Results of restriction digestions, using *PvuI* (A) or *HincII* and *HindIII* (B), of pMSP1D1 purified from three different DH5α *E. coli* bacterial colonies (c1, c2, c3) on a 1% agarose gel stained with 0.5 µg/mL ethidium bromide. Theoretical gel for restriction digestion (left) was produced for ease of interpretation of experimental gel (right). Colony c3 was chosen as the source of pMSP1D1because the results of both restriction digestion experiments displayed anticipated banding patterns.

for large-scale amplification and plasmid purification using Maxiprep (ZymoPURE™). The final purified plasmid was confirmed by sequencing through GeneWiz©. For protein expression, pMSP1D1 was transformed into BL21 (DE3) *E. coli* cells in accordance with manufacturer's protocol. For the transformation of BL21 (DE3) *E. coli* cells, a range of pMSP1D1 concentrations was used (0.5 to 100 ng) and a large range of volumes of the transformed bacteria (10 to 250 µL) was plated on LB-agar plates with 50 µg/mL kanamycin. The best transformant was chosen for MSP1D1 expression and purification. Transformant starter culture, 5 mL of LB-broth and 50 µg/mL kanamycin, was grown at 37°C at 250 RPM for several hours until cloudy. A 1 mL volume of the starter culture was added to 150 mL of LB-broth with 50 µg/mL kanamycin and was grown at 37°C with shaking at 250 RPM until an OD_{600} of between 0.5 and 0.6 was reached. Protein production was induced with 0.1 mM IPTG overnight at 16°C with shaking at 250 RPM. Bacteria was pelleted at 4000 g for 20 minutes at 4°C and resuspended in 15 mL phosphate buffered saline (PBS) supplemented with protease inhibitor cocktail (PIC, Cell Signaling®). The bacterial cells were lysed over 10 minutes by sonication, by alternating 1 second sonication and 1 second resting period, at a 35% output and on ice. The insoluble material was separated from the soluble material by centrifugation at 11,000 g for 20 minutes at 4°C. The soluble fraction was incubated with 10 µL of equilibrated Roche® cOmplete His-Tag resin per each 1 mL of supernatant overnight at 4°C. The insoluble fraction was screened for MSP1D1 by resuspension in PBS and loading onto an SDS-PAGE. His-tag resin was packed in a gravity flow column and the flow-through was collected. The packed resin was washed sequentially in 30 resin volumes of Roche A buffer (50 mM NaH_2PO_4, pH 8.0 and 0.3M NaCl) at least five times. MSP1D1 was

eluted in 6 resin volumes of Roche B buffer (50 mM NaH_2PO_4, pH 8.0, 0.3M NaCl, and 250 mM imidazole) at least three times, and each elution fraction was collected in an individual tube. MSP1D1 for nanodiscs was further purified by SEC. The third elution fraction was injected into the ÄKTA™ Purifier with Superdex™ 200 10/300 GL column (GE Healthcare) using a flow rate of 0.5 mL/min in Roche A buffer (Figure 4.3). Protein purity and chromatography efficiency were determined by SDS-PAGE (Figure 4.3).
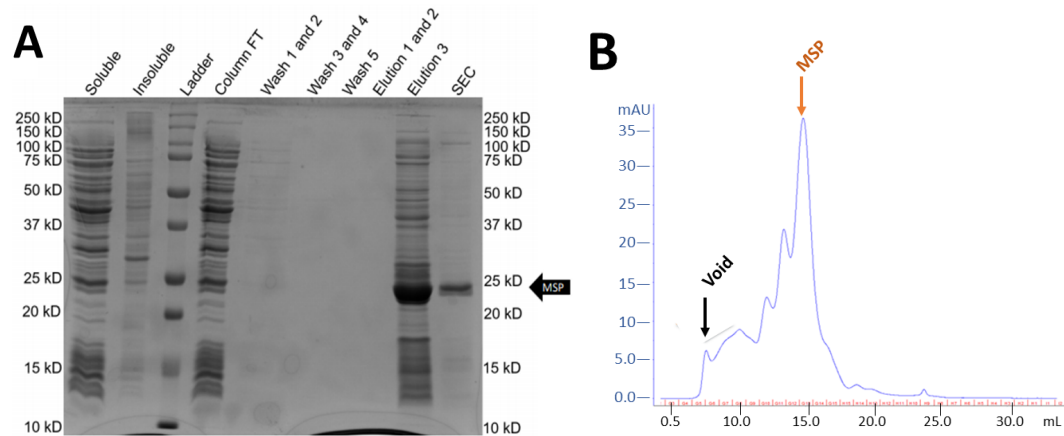
Figure 4.3: Purification of MSP1D1 from BL21 (DE3) *E. coli*. (A) Hand-cast 12% acrylamide: bisacrylamide SDS-PAGE stained with Coomassie to analyze MSP1D1 purity and efficiency of purification. Each lane represents a sample at each stage of the purification process. MSP1D1 begins eluting from the Roche® cOmplete His-Tag resin (resin packed in a gravity-flow column) at elution fraction E1 and continues until fraction E3. The most concentrated MSP1D1 fraction is E3, which was further purified using Size Exclusion Chromatography. (B) Full SEC UV-spectra chromatogram of affinity chromatography purified His-tagged MSP1D1 using a Superdex™ 200 10/300 GL column. Void volume is marked by a black arrow and MSP peak is marked by an orange arrow.

Briefly, each sample was mixed with 6x Laemmli loading dye (prepared in-house) to a final concentration of 1x and loaded in proportion into a hand-cast 12% acrylamide: bisacrylamide SDS-PAGE. The gel was run at 150 V for 1 hour and stained in 0.1 % Coomassie blue (R-250, in 10% acetic acid, 30% ethanol, and 60% water) for 1 hour with rocking and destained overnight in 10% acetic acid, 30% ethanol, and 60% water with rocking (Figure 4.3). Finally, the protein concentration was determined by Pierce™ BCA assay and MSP1D1 was stored at 4°C.

4.2.3. Formation of empty nanodisc controls.

To test the BioBeads™, the following control protocol for forming empty nanodiscs was used. Membrane Scaffold Protein (MSP1D1; 1 mg/mL; purified in-house or Sigma M7074-5MG) was thawed on ice and lipid stock, either DMPC or POPC (10 mg/mL in 3.5% NaDeoxycholate), was thawed at RT. MSP1D1 stock was gently mixed by flicking, and lipid stock was gently vortexed. MSP1D1 and the lipid of choice, DMPC or POPC, were added to nanodisc buffer (20 mM Tris pH 7.4, 0.1 M NaCl, 0.5 mM EDTA, 0.01% NaN_3) in a specific ratio of 80:1 or 65:1. Approximately 8-15 medium-sized Bio-Beads™ were added to the MSP-Lipid-Buffer volume and incubated for 2 hours at 24°C for DMPC or incubated for 4 hours at 4°C for POPC. Empty nanodiscs were screened by SEC on an ÄKTA™ Purifier using a Superdex™ 200 10/300 GL column, SDS-PAGE, and by transmission electron microscopy (TEM) (see below). To test for empty nanodisc formation under conditions used for forming CFTR-nanodiscs, the following protocol was used. BioBeads™ were weighed to a final wet mass of 0.35 g in a 2 mL microcentrifuge tube. MSP1D1 and lipid stocks were thawed as previously described. In a final volume of 1 mL, MSP1D1 was added to 0.7 mL Buffer G (50 mM Tris pH 7.5,

0.15 M NaCl, and 2.5 mM MgCl$_2$) and POPC was added to 0.3 mL of Buffer H.2 (50

mM Tris pH 7.5, 0.15 M NaCl, 2.5 mM MgCl$_2$, 10% glycerol, and 0.1% DDM/0.02%

cholesteryl hemisuccinate (CHS)) to result in a final MSP1D1:POPC ratio of 1:65. The

lipid-containing buffer was mixed with the MSP1D1-containing buffer by pipetting and

added to BioBeads™ in the 2 mL tube. MSP1D1-POPC-BioBead™ mixture was

incubated for 4 hours at 4°C. Empty nanodiscs were screened by SEC on an ÄKTA™

Purifier using a Superdex™ 200 10/300 GL column with a flow rate of 0.5 mL/min.

Empty nanodiscs also were screened using TEM on a JEM-1400 (JEOL) transmission

electron microscope at 120 kV. Empty nanodiscs were diluted 10 to 20-fold before

incubating 2 μL on carbon-coated copper grids for 60 seconds at RT. The sample was

blotted using Whatman® #4 filter paper at the side of the grid and then the sample was

stained in 2 μL of 2% uranyl acetate for 30 seconds at RT before being blotted. Empty

nanodiscs were screened at a magnification of 15,000x – 20,000x, before imaging at a

higher magnification (30,000x -50,000x). Electron micrographs were collected with

Gatan Ultrascan™ CCD camera and viewed with Digital Micrograph® software.

4.2.4. Reconstitution of CFTR into nanodiscs.

To form CFTR-containing nanodiscs, total protein concentration was determined by

Pierce™ BCA assay, in accordance with manufacturer's protocol. BioBeads™ were

weighed to a final wet mass of 0.35 g in a 2 mL microcentrifuge tube. MSP1D1 and lipid

stocks were thawed as previously described. In a final volume of 1 mL, POPC was added

to 0.3 mL of purified CFTR from BHK cells in Buffer H.2 (50 mM Tris pH 7.5, 0.15 M

NaCl, 2.5 mM MgCl$_2$, 10% glycerol, and 0.1% DDM/0.02% cholesteryl hemisuccinate

(CHS)) to make a final CFTR:Lipid ratio of 1:330 for POPC. The CFTR-POPC mixture

was incubated on ice for 10 minutes with gentle flicking. MSP1D1 was added to 0.7 mL Buffer G (50 mM Tris pH 7.5, 0.15 M NaCl, and 2.5 mM $MgCl_2$) and to the CFTR-POPC mixture to make a final CFTR:MSP1D1:POPC ratio of 1:11:330. The CFTR-POPC containing buffer was mixed with the MSP1D1-containing buffer by pipetting and was added to BioBeads in a 2 mL tube. The CFTR-MSP1D1-POPC-BioBead™ mixture was incubated at 4°C overnight. The formation of CFTR-nanodiscs was screened by FPLC on an ÄKTA™ Purifier using a Superdex™ 200 10/300 GL column with a flow rate of 0.25 mL/min. The SEC fraction containing CFTR-nanodiscs was concentrated using 2 mL Amicon® centrifuge filters with a MWCO of 100,000 by centrifugation at 1000 g for 10 minutes at 4°C until the final volume was $1/10^{th}$ of original.

4.2.5. ATPase Activity Assay.

CFTR in detergent or in nanodiscs was phosphorylated by the Promega® PKA α-catalytic subunit (100 U/mL) and 10 mM MgATP for 2 hours at 4°C. PKA, excess MgATP, and ADP were separated from CFTR-containing samples using SEC as previously described (Section 4.2.4). Confirmation of phosphorylation was achieved by SDS-PAGE and Pro-Q™ Diamond phosphorylation stain (Thermo Fischer Scientific) and phosphorylation immunostaining by Western blot analysis. Sample preparation and gel running conditions were previously described for SDS-PAGE and Western blots (Section 3.2.2.5). SDS-PAGE, hand-cast 8% acrylamide: bisacrylamide hand-cast, was stained with Pro-Q™ Diamond phosphorylation stain in accordance with the manufacturer's protocol. The SDS-PAGE gel was fixed in 50% methanol, 10% acetic acid two times for 30 minutes, and was washed in deionized water three times for 10 minutes. Then, the SDS-PAGE gel was stained in Pro-Q™ stain for 90 minutes, destained in 20% acetonitrile in 50 mM

sodium acetate pH 4 for 30 minutes three times, and washed in water for 5 minutes two times, all at RT. The SDS-PAGE gel was imaged on Bio-Rad ChemiDoc™ XRS+ system using UV transilluminator settings. Immunoblotting for phosphorylation on Western blots was performed as follows: blots were blocked in LI-COR Intercept® (PBS) buffer for 1 hour at RT before incubation in rabbit anti-phospho-(Ser/Thr) antibody (abcam17464) at 1:1000 in LI-COR Intercept® (PBS) blocking buffer and 0.1% Tween® 20 at 4°C overnight. Blots were washed for 15 minutes at RT in PBST three times before and after incubation in IRDye® 800CW goat anti-rabbit antibody, 1:10,000 in LI-COR Intercept blocking buffer and 0.1% Tween® 20. Blots were imaged on a LI-COR Odyssey® 9120 Infrared Imaging system (Figure 4.4). ATPase activity was measured using a Malachite Green ATPase assay kit from Sigma (MAK30) using a range of ATP concentrations from 10 mM to 0.1 pM in 100 μL reactions with CFTR in detergent or nanodiscs, for 1 hour at RT. Michaelis-Menten kinetics were determined by fitting ATPase assay data in IgorPro (Wavemetrics).

4.2.6. Reconstitution of CFTR into proteoliposomes.

The concentration of CFTR was determined by the Pierce™ BCA assay in accordance with the manufacturer's protocol. The dialysis tubing used was Spectra/Por™ 2 (Spectrum™) and had a MWCO of 12-14 kD with a flat width of 25 mm. A 2-inch strip was cut and prepared by washed with deionized water before incubation in Buffer H.2 (without detergent) for 10 minutes at RT. CFTR and POPC were mixed at 1:100 Protein:POPC molar ratio, placed into dialysis tubing and sealed with dialysis clips. The filled dialysis tubing was placed in 1 L of buffer H.2 (without detergent) with stirring at 4°C. Buffer H.2 without detergent was exchanged every 12 hours for 4 days.
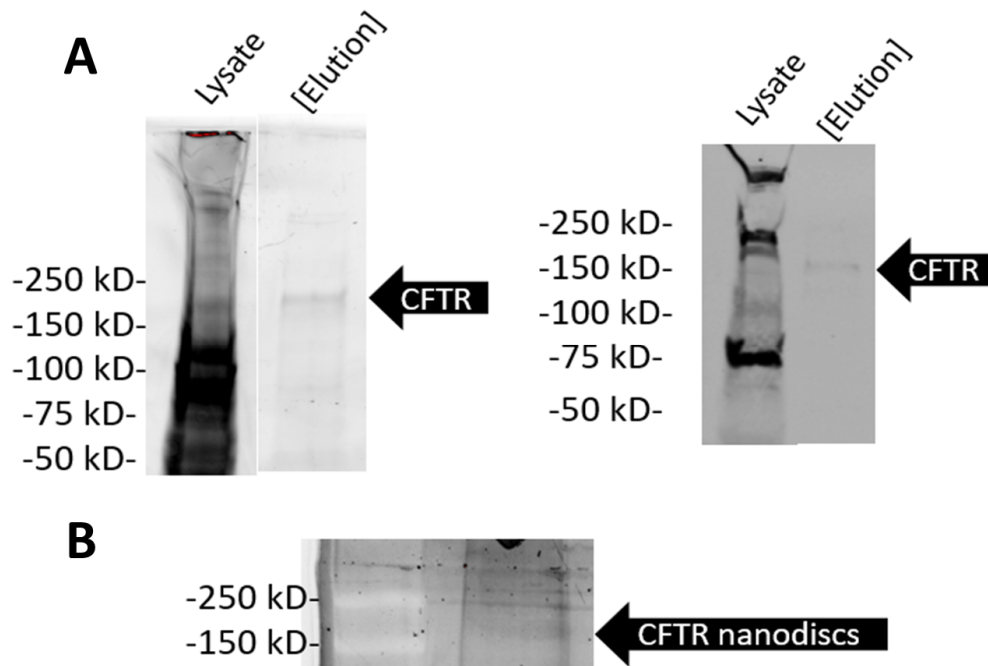
Figure 4.4: Phosphorylation of CFTR in detergent or in nanodiscs before ATPase activity measurements. CFTR in detergent and in nanodiscs was phosphorylated by Promega® PKA α-catalytic subunit at 100 U/mL in 1 mM ATP for 2 hours at 4°C. PKA, excess ATP, and ADP separated from CFTR in detergent or in nanodiscs using SEC. (A) Phosphorylation of CFTR in detergent confirmed by Western blot and hand-cast 8% acrylamide: bisacrylamide SDS-PAGE gel stained with Pro-Q™ Diamond phosphorylation stain. Immunoblotting for phosphorylation: Primary – rabbit anti-phospho-(Ser/Thr) antibody (abcam17464), 1:1000 and Secondary – IRDye® 800CW goat anti-rabbit antibody, 1:10,000. (B) Phosphorylation of CFTR in nanodiscs confirmed by hand-cast 8% acrylamide: bisacrylamide SDS-PAGE gel stained with Pro-Q™ Diamond phosphorylation stain.

Proteoliposomes were extracted from the dialysis bag and stored at 4°C until screening by TEM. Proteoliposomes, 2 µL, were incubated on a carbon-coated 400 mesh copper grid for 60 seconds at RT, and then were blotted away with Whatman® #4 filter paper. Samples were stained with 2 µL of 2% uranyl acetate for 30 seconds at RT before blotting. Proteoliposomes were screened on a JEM-1400 (JEOL) transmission electron microscope at an accelerating voltage of 120 kV.

4.2.7. Planar lipid bilayer measurement of CFTR channel activity.

Planar lipid bilayers were formed from a stock lipid solution of 7:3 POPE:POPS. For the preparation of the lipid stock, POPE and POPS in chloroform were mixed at a ratio of 7:3, and a final mass of 0.3 mg and the chloroform solvent was evaporated under a steady stream of nitrogen gas. The lipids were resuspended in 10 µL of decane and painted onto the aperture between the *cis* and *trans* wells which were filled with recording buffer (10 mM MOPS, pH 6.9, 1 mM $MgCI_2$, 2 mM $CaCl_2$, and 50 mM KCl). The formation of a stable bilayer was confirmed by the emergence of a square capacitive current wave under a voltage ramp protocol. Membrane proteins in BHK cellular membranes or CFTR proteoliposomes were phosphorylated by incubation of 20 µL of respective samples with 100 U/mL PKA (Promega® α-subunit) and 5 mM MgATP for 15 minutes at RT. Samples were stored on ice until use. BHK cellular membranes, 7 µL with a protein concentration of about 2 mg/mL, or CFTR proteoliposomes, 7 µL with a protein concentration of about 1 mg/mL, were added to the *cis* chamber containing recording buffer along with 0.5 mM MgATP and 50 U/mL PKA (Promega® α-subunit). A gradient across the *cis* and *trans* chambers was created by adding enough KCl to make a final concentration of 300 mM in the *cis* chamber while leaving an approximate 50 mM KCl in the trans chamber. Single

129

channel data were collected at 1 kHz and 0.1 kHz before digital filtering to 50 Hz and were recorded using Clampex 10.2^{TM} (Axon^{TM}). Single channel data were processed as follows in Clampfit 10.2^{TM} (Axon^{TM}):   when necessary, the baseline current was manually adjusted to 0, single channel properties were evaluated using single channel search, and histograms were generated and fitted.

4.2.8. Transmission Electron Microscopy (TEM) of CFTR-Nanodiscs.

A 2 µL volume of CFTR-nanodiscs was incubated on glow-discharged (15 seconds) carbon-coated copper grids for 60 seconds before blotting with Whatman$^{®}$ #4 filter paper. Samples were stained in 2% uranyl acetate for 30 seconds at RT and again blotted. Grids were screened at magnifications of 10,000x – 20,000x, before imaging at magnifications of 30,000x - 50,000x. Micrographs used for image processing were collected at 50,000x with a defocus range of 0.8 to 1.2 µm. Electron micrographs were taken on 2k by 2k Gatan Ultrascan™ charge-coupled detector (CCD) camera and were viewed with the Digital Micrograph$^{®}$ software before analysis with EMAN 2.3 (269). Particles were manually picked from 76 initial micrographs with a particle size of 125 and a box size of 192 and extracted. After contrast transfer function (CTF) correction, performed in EMAN by CTFFIND (270), 990 extracted particles were used in initial class averaging studies. Particles of poor quality were manually excluded resulting in about 500 particles for class averaging.

4.3.   RESULTS

4.3.1. The process of cleaning and storing BioBeads^{TM} affects the efficiency of nanodisc formation.

We found that the storage conditions of BioBeads™ greatly affected the ability of the resin to form nanodiscs. BioBeads™ stored on the benchtop at room temperature after a year developed a yellowish huge, clumped, and moisture within the storage bottle. This is different in appearance to new BioBeads ™ (Figure 4.5). However, BioBeads™ that have been washed well in methanol and stored in water at 4°C can be used a year after washing without a significant decrease in their ability to remove detergent. To improve the length of use, BioBeads™ are either stored washed or stored in the original bottle sealed with parafilm and stored in a desiccator at room temperature.

Figure 4.5: Comparison of old Bio-Beads™ to new Bio-Beads™. Old BioBeads™ (left), appeared to be clumped, yellowish in color, and had moisture along all walls of the bottle. New Bio-Beads™ moved freely, appeared white, and had no moisture in the bottle.

4.3.2.   Empty nanodiscs were formed using two different types of lipids.

Nanodiscs devoid of membrane protein, called empty nanodiscs, formed with the MSP1D1 protein of any single lipid composition, DMPC or POPC, were confirmed by SEC and SDS-PAGE. If empty nanodiscs have formed, there will be the emergence of a peak at 12 mL on Superdex™ 200 10/300 GL column and the presence of MSP in the 12 mL SEC fraction when analyzed on an SDS-PAGE. In Figure 4.6, empty nanodiscs were formed with both DMPC and POPC. Of note, even at the correct MSP:POPC ratio, POPC displayed a rather large void volume. When the void volume fraction was screened by TEM, there were small liposomes (Figure 4.7). Alteration of the MSP:POPC to prevent the presence of these liposomes, prevented the formation of the empty nanodiscs. Screening the 12 mL SEC fraction in which showed the presence of MSP on the SDS-PAGE (Figure 4.6) Empty nanodiscs formed under control conditions and empty formed under the same buffer conditions that would be used to form CFTR-nanodiscs were also screened by transmission electron microscopy (Figure 4.8). Empty nanodiscs formed under both conditions, the control buffer conditions and the buffer conditions for forming CFTR-nanodiscs, displayed the anticipated dimensions of 5 nm by 10 nm for empty nanodiscs formed with MSP1D1 when screened via negative stain TEM (Figure 4.8). Under our TEM studies, empty nanodiscs seemed to prefer a side orientation or an orientation in which the nanodiscs are sitting on edge (Figure 4.8).
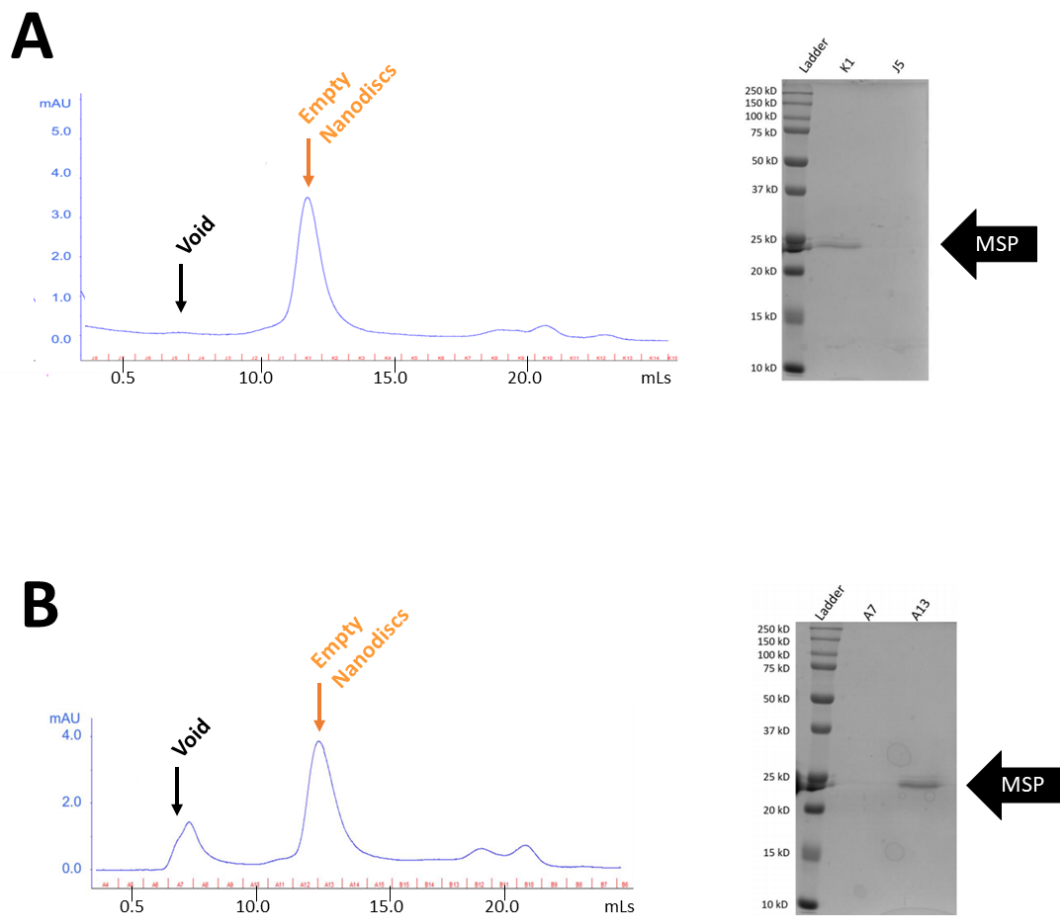
Figure 4.6: Confirmation of empty nanodiscs formed with two different lipids— DMPC and POPC. Empty nanodiscs formed under control buffer conditions with DMPC (A) and POPC (B) were evaluated using SEC and SDS-PAGE. Full UV-spectra chromatogram from SEC with a Superdex™ 200 10/300 GL Column after injection with empty nanodiscs on the left and key fractions analyzed for the presence of MSP on 12% acrylamide: bisacrylamide hand-cast SDS-PAGE gel stained by Coomassie on the right.
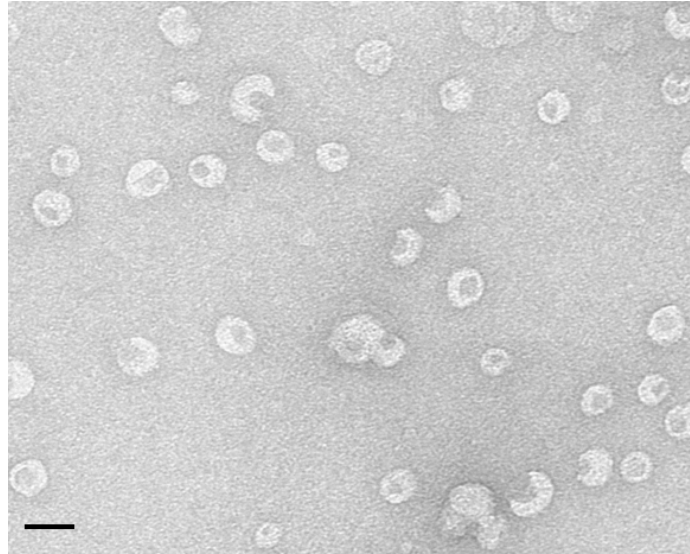
Figure 4.7: Transmission electron micrograph of liposomes present in the SEC void volume of POPC lipids. Even at the recommended Lipid-to-Protein (LPR) ratio for MSP and POPC, a void volume can be seen and contained what appears to be small liposomes. Samples were stained in 2% uranyl acetate. The scale bar corresponds to 50 nm.
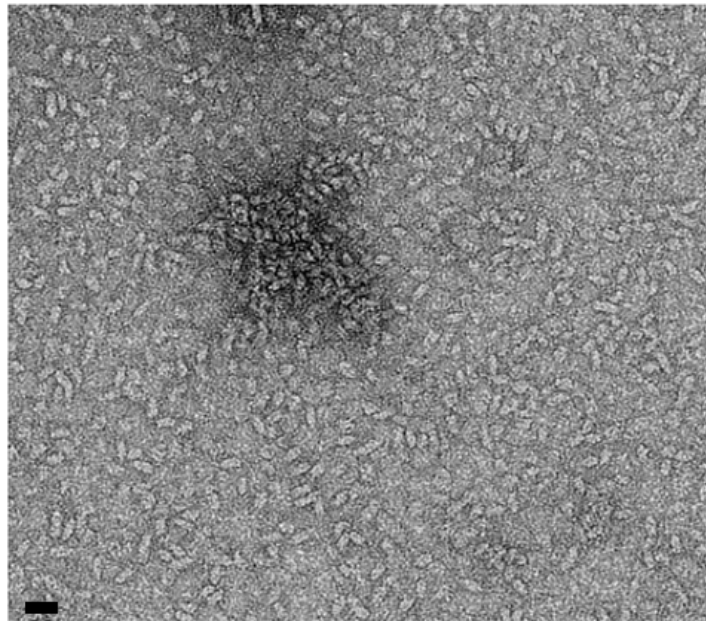
Figure 4.8: Micrograph of negatively stained (2% uranyl acetate) empty POPC Nanodiscs. The POPC nanodiscs show a preferred "side-view" orientation, providing critical information on successful formation of nanodiscs with a thickness and diameter of approximately 8 nm by 10 nm, respectively. These nanodiscs devoid of CFTR also provide an important control for reconstitution of CFTR into CFTR-nanodisc. The scale bar corresponds to 20 nm.

4.3.3. CFTR was incorporated into POPC-based nanodiscs.

Initial attempts to form CFTR-nanodiscs used DMPC as the lipid of choice due to its prevalence in membrane protein reconstitution. However, the formation of nanodiscs was inconsistent. By changing the choice of lipid to POPC, a lipid with a much lower phase transition temperature (DMPC is 24°C and POPC is 4°C) improved the consistency of nanodiscs formation. CFTR-nanodiscs were screened first by SEC, as CFTR-nanodiscs being of much larger molecular weight will elute earlier than both monomeric detergent-solubilized CFTR and empty nanodiscs. SEC results of CFTR-nanodiscs revealed the emergence of a peak shoulder at around 10 mL on Superdex™ 200 10/300 GL column, while monomeric detergent-solubilized CFTR alone eluted at 11 mL and empty nanodiscs eluted at 12 mL (Figure 4.9). Western blot analysis is one confirmation method of nanodiscs formation by the presence of CFTR and MSP in the same SEC elution fraction. We confirmed the presence of CFTR and MSP1D1 in the same SEC elution fraction using Western blot analysis (Figure 4.9). Another confirmation method of nanodisc formation and membrane protein confirmation is TEM. Before screening by TEM, a model of CFTR in a nanodisc was built for comparing particles seen in the proposed CFTR-nanodiscs SEC elution fraction to model. CFTR-nanodiscs are anticipated to be about 10 nm by 15 nm in size and demonstrate "mushroom" like features (described in more detail below). When the SEC elution fraction was screened by TEM, particles identified in micrographs displayed several characteristic features expected for CFTR in a nanodisc. The particles identified were 10 nm by 15 nm in size and demonstrated "mushroom" like features meaning an elongated "stalk" below a "cap", or the nanodisc as well as, several particles appear to have two separate densities at the base

of the "stalk," which could be separated NBDs (Figure 4.10).
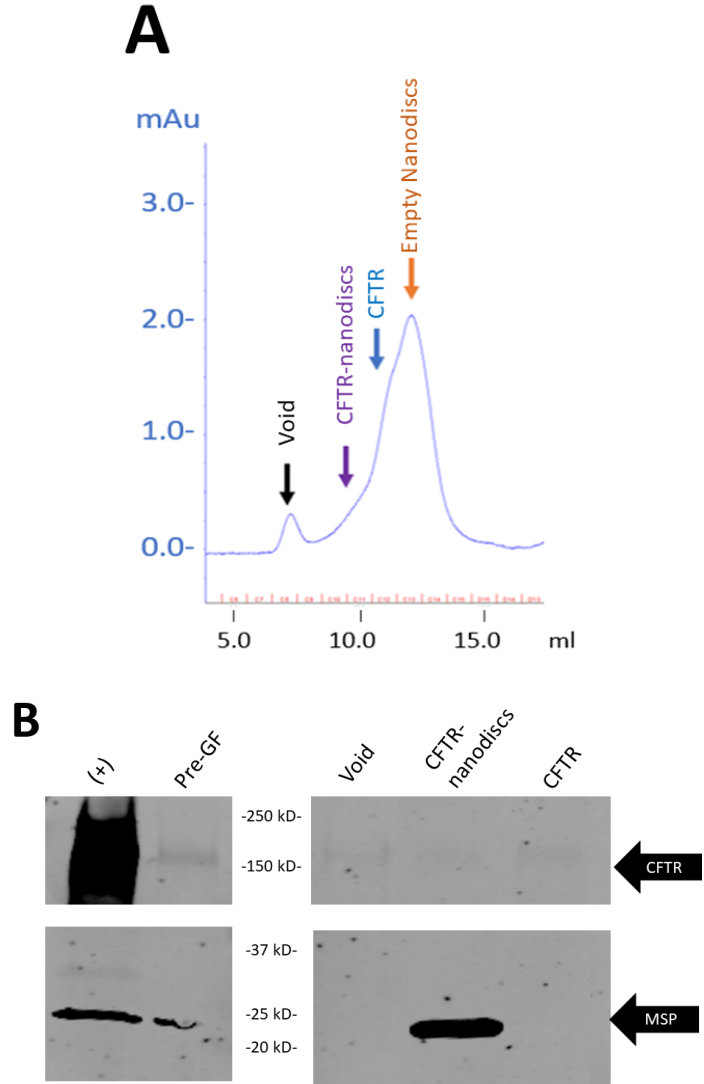
Figure 4.9: CFTR-nanodiscs generated from CFTR purified from BHK cells screened SEC and western blot. (A) UV-spectra chromatogram from SEC with a Superdex™ 200 10/300 GL Column after injection with CFTR-nanodiscs. Arrows indicate the following: void (black), CFTR-nanodiscs (purple), CFTR (blue), and empty nanodiscs (orange). (B) Western blot SEC fractions identifying CFTR (168 kDa) and MSP (24 kDa) in the same fractions. Immunoblotting for CFTR: Primary – mouse anti-CFTR 596 antibody, 1:1,500 and Secondary – IRDye® 680RD goat anti-mouse antibody, 1:10,000. Immunoblotting for MSP: Primary – rabbit anti-His-tag antibody, 1:1,000 and Secondary IRDye ® 800CW goat anti-rabbit antibody, 1:10,000.
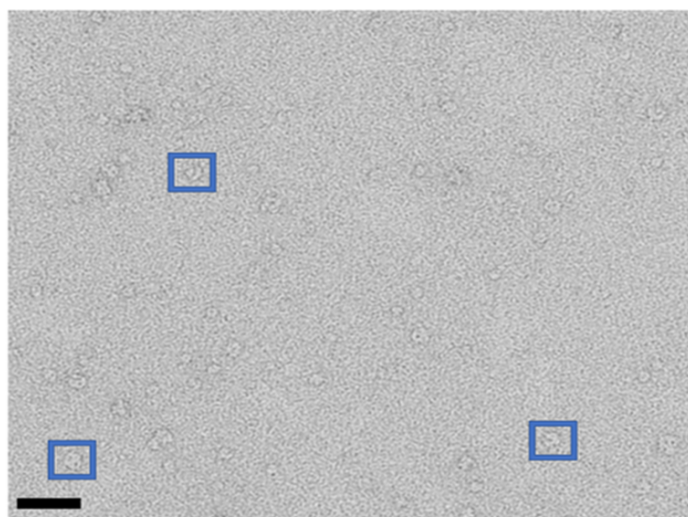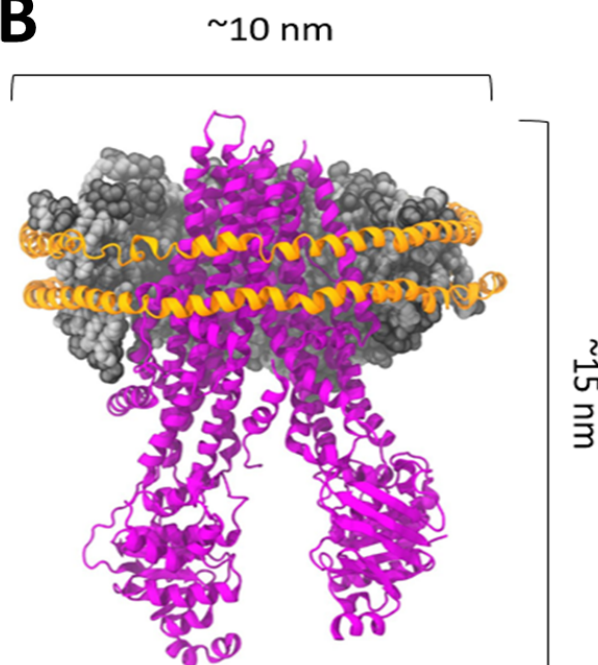
Figure 4.10: CFTR-nanodiscs generated from CFTR purified from BHK cells screened by TEM. (A) Micrograph of negatively stained CFTR-nanodiscs. A few examples of particles are boxed in blue. The micrograph shows a good distribution of particles and no aggregation. Scale bar represents 50 nm. (B) A CFTR-nanodiscs model was built of hCFTR (PDB ID: 5UAK) in a nanodisc (PDB ID: 4V6M), in Visual Molecular Dynamics (VMD). The lipids in front of CFTR in a nanodisc have been cut away to show TMDs.

4.3.4. ATPase activity of CFTR is improved in a lipid environment over a detergent environment.

CFTR phosphorylation, whether in nanodiscs or in detergent, was determined by SDS-PAGE and phosphorylation stain (Figure 4.4). CFTR concentration, whether in nanodiscs or detergent, was determined by densitometry (data not shown). The production of inorganic phosphate by the ATPase activity of CFTR was determined by the malachite green assay using an ATP concentration range 10 mM to 0.1 pM and each reaction was run in 100 µL volumes (Figure 4.11). ATPase kinetic data showed that CFTR in a single

CFTR-nanodiscs
$K_M = 0.172 \pm 0.117$ mM
$V_{max} = 63.5 \pm 9.75$ nmol/min/µg

CFTR detergent
$K_M = 0.00692 \pm 0.00176$ mM
$V_{max} = 7.9 \pm 0.36$ nmol/min/µg
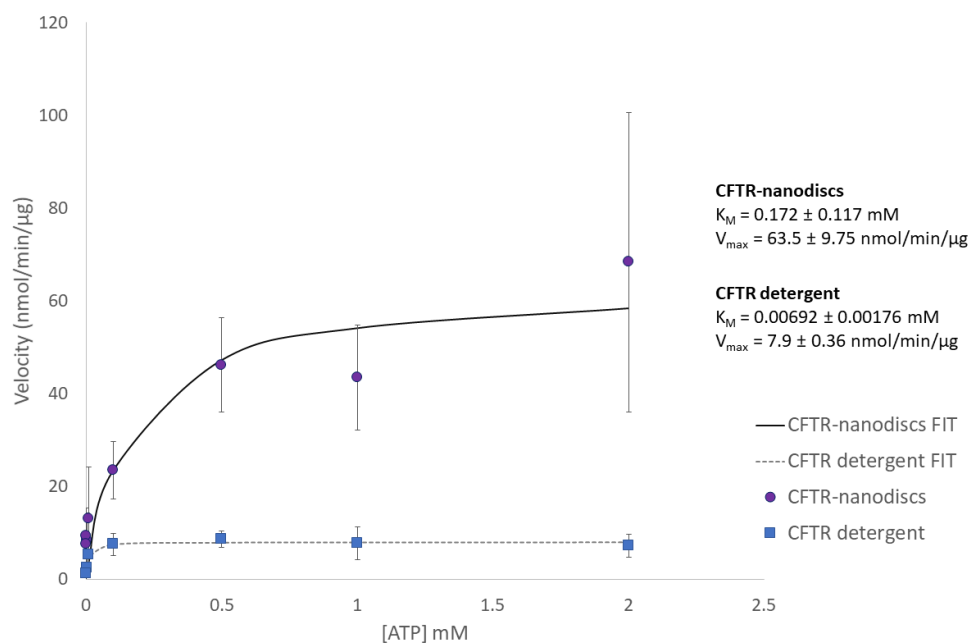
Figure 4.11: ATPase activity of CFTR-nanodiscs or CFTR in detergent (DDM) measured by Malachite Green Assay. After phosphorylation (Figure 4.4), PKA, excess ATP, and ADP were separated from phosphorylated CFTR using SEC. Inorganic phosphate produced by ATPase activity of CFTR was measured by Malachite green complexation for the following range of ATP concentrations in 100 µL volumes: 10 mM to 0.1 pM. Michaelis-Menten kinetics were determined in IgorPro and plotted as "fit". CFTR-nanodiscs exhibit a higher ATPase activity than CFTR in detergent. Error bars are SEM for three trials.

lipid, POPC, environment has an increased rate of ATPase activity rate of 63.5 ± 9.75 nmol/min/µg as compared CFTR in detergent with an ATPase activity rate of 7.9 ± 0.36 nmol/min/µg (Figure 4.11). There is also an increased Michaelis-Menten constant (K_M) of CFTR in a POPC lipid environment (0.172 ± 0.117 mM) compared to CFTR in detergent (0.00692 ± 0.00176 mM). An increased K_M usually signifies a reduction in the binding affinity of the substrate to the enzyme, but the increased V_{max} is proportional to the catalytic rate of the enzyme. These parameters indicate that ATP binding to CFTR in a lipid environment is reduced, but the enzymatic rate of ATP to ADP conversion has increased compared to that of CFTR in detergent.

4.3.5. Purified CFTR has the same channel function as CFTR in BHK cellular membranes.

CFTR was reconstituted into POPC-based proteoliposomes, and the membrane formation was screened by TEM (Figure 4.12). CFTR currents were recorded for CFTR from the BHK cellular membrane fraction, and from CFTR that was detergent-solubilized, purified, and reconstituted into proteoliposomes. Once fusion of either cellular membranes of proteoliposomes to planar lipid bilayer was observed, CFTR currents were recorded over several seconds. CFTR currents recorded from BHK cellular membrane fraction showed the expected -0.61 pA current (average for each channel) with an expected open probability, the percentage of time the channel was open divided by the entire recording time (P_o), of approximately 37% under a functional voltage of -90 mV (composed of an applied -45 mV and a Cl⁻ gradient voltage of -45 mV) (Figure 4.13). To confirm this channel is CFTR, the CFTR specific inhibitor INH172 was added to the *cis* chamber and showed a 94 % inhibition of the CFTR current from BHK cellular

membranes (Figure 4.13). Currents from CFTR proteoliposomes were measured to be -0.68 pA with an open probability of approximately 32% (and up to 50% in some recordings) (Figure 4.14). Again, to confirm this channel was CFTR, the use of INH172 was used. Incubation with CFTR inhibitor only showed approximately 25% inhibition (Figure 4.14). The difference in efficacy of INH172 on CFTR from proteoliposomes compared to CFTR from the cellular membranes could be due to two possibilities. The first could be the difference of lipid environment between the cellular membrane, which provides a multitude of lipid types. The second is that CFTR in POPC proteoliposomes was detergent-solubilized, purified and reconstituted. The detergent solubilization step could have introduced structural defects to the purified CFTR that are unable to be rescued by the reconstitution lipid environment.
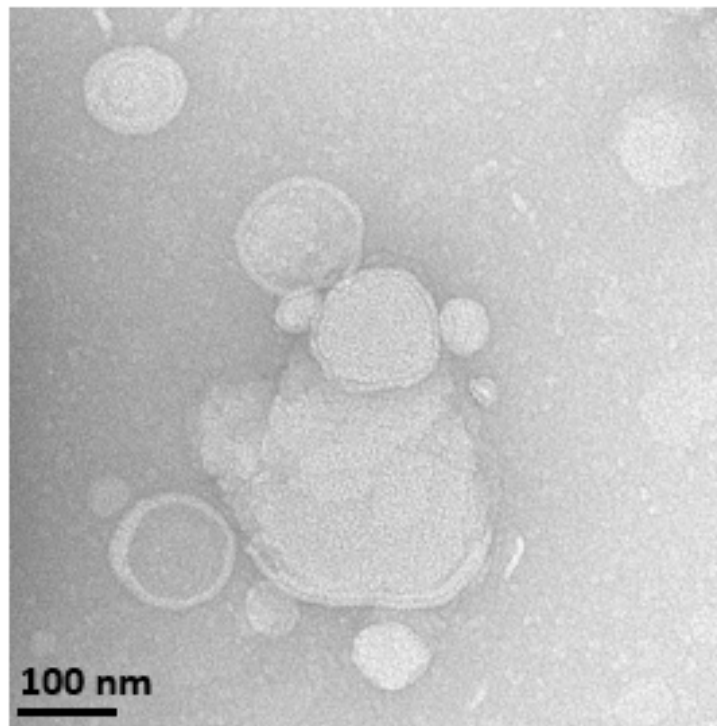
Figure 4.12: Micrograph of negatively stained (2% uranyl acetate) CFTR proteoliposomes. Purified detergent-solubilized CFTR was reconstituted into POPC-based proteoliposomes and screened by TEM. The scale bar corresponds to 100 nm.
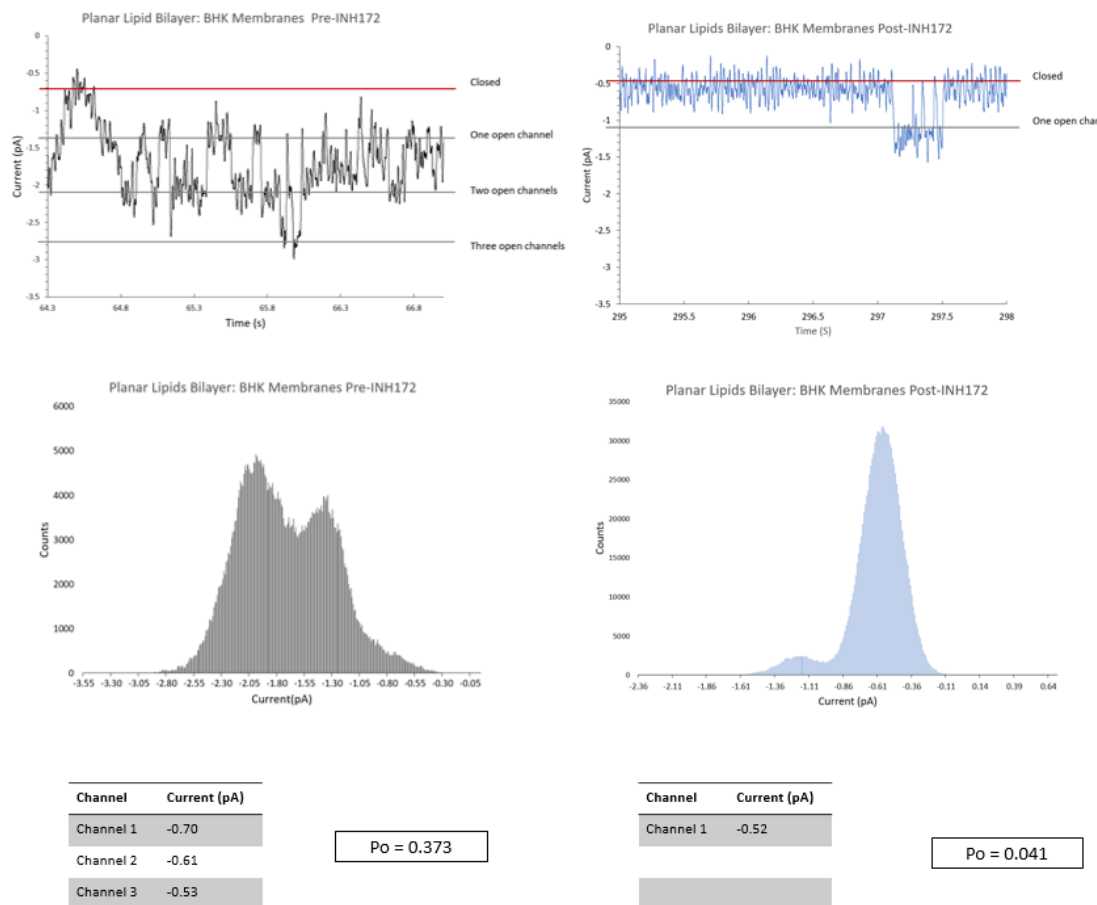
Figure 4.13: Planar lipid bilayer (7:3 POPE:POPS ratio) single-channel recordings of CFTR from BHK cellular membranes. Recordings of CFTR under an applied driving force of -90 mV for Cl⁻. PKA and ATP (50 U/mL and 0.5 mM final) were added to the cis chamber. Top graphs are of the planar lipid bilayer recordings pre-treatment with INH172 (A) and post-treatment with INH172 (B). A histogram for both pre-INH172 (A) and post-INH172 (B) treatments were plotted for each state—3 open channels, 2 open channels, 1 open channel or closed channels. Before the addition of INH172 (A), three CFTR channels can be seen in a single recording, each with a current amplitude of -0.70 pA, -0.61 pA, -0.53 pA and an average amplitude of -0.61 pA. The open probability for CFTR in this recording was 37%, as expected for CFTR. After the addition of INH172 (B), only a single CFTR channel can be seen in a single recording, a current amplitude of -0.52 pA. The open probability for CFTR in this recording was 4%. This represents 94% inhibition of CFTR by 10 µM INH172.
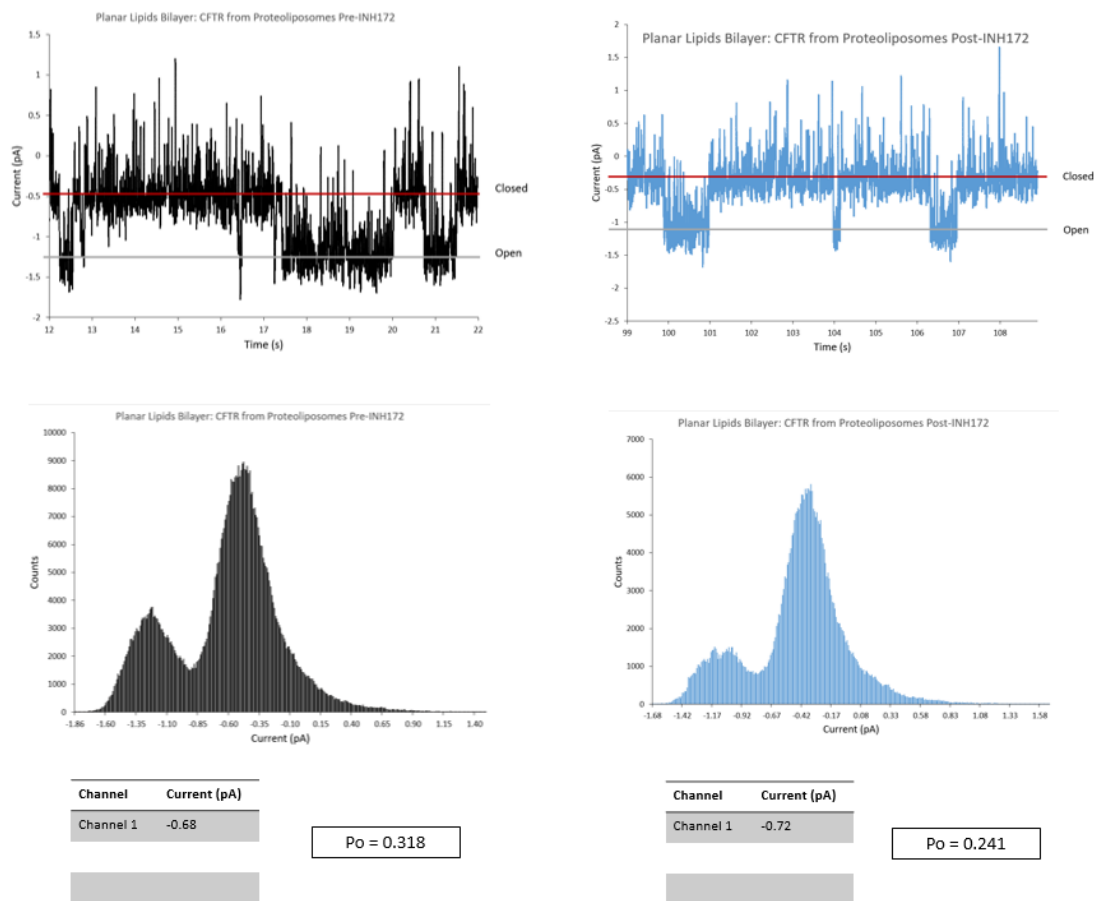
Figure 4.14: Planar lipid bilayer (7:3 POPE:POPS ratio) single-channel recordings of CFTR from proteoliposomes. Recordings of CFTR under an applied driving force of -90 mV for Cl⁻. PKA and ATP (50 U/mL and 0.5 mM final) were added to the cis chamber. Top graphs are of the planar lipid bilayer recordings pre-treatment with INH172 (A) and post-treatment with INH172 (B). A histogram for both pre-INH172 (A) and post-INH172 (B) treatments were plotted for each state—1 open channel or closed channels. Before the addition of INH172 (A), a single CFTR channel can be seen in a single recording displaying a current amplitude of -0.68 pA with an open probability of 32% for CFTR in this recording, as expected. After the addition of INH172 (B), a single CFTR channel can be seen in a single recording displaying a current amplitude of -0.72 pA and an open probability of 24% for CFTR in this recording. This represents 25% inhibition of CFTR by 10 µM INH172.

4.3.6. Preliminary class averages for CFTR-nanodiscs display expected characteristics of successful reconstitution of CFTR into nanodiscs.

Particles from images of negatively stained samples were manually picked using EMAN 2.3 (269). Initial class averages used standard EMAN 2.3 settings. Several classes contained particles of smaller sizes than expected for CFTR-nanodiscs, with dimensions of ~ 5nm by 10nm (thickness and diameters, respectively), closely corresponding to nanodiscs devoid of CFTR. Approximately 80% of particles had dimensions of ~ 15nm by 10nm corresponding to the expected dimensions of height and diameter for CFTR-nanodiscs. Following classification (Figure 4.15) of these larger particles, structural characteristics were observed that are consistent with the expected overall size and a density consistent with NBDs of CFTR protruding from an elongated density expected for a nanodisc in a "side view" orientation. Next, a 3D model will be calculated, which will be followed by cryo-EM studies. The large percentage of successfully reconstituted CFTR into nanodiscs, the homogeneity of the sample, and the good particle distribution without aggregation, are important steps towards cryo-EM as well as biochemical studies of CFTR.
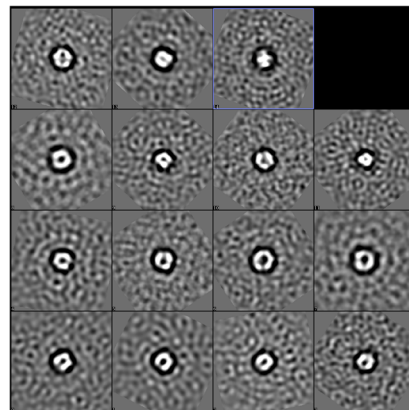
Figure 4.15: Preliminary class averages of CFTR-nanodiscs. Initial 2D class averages were generated with EMAN2.3 from a total of 918 particles.

4.4. DISCUSSION.

The nanodisc bilayer system has revolutionized the study of membrane proteins both structurally and functionally by providing a method for the individual packaging of membrane proteins in a variety of lipid environments, and this includes the studies presented here. In these studies, we report the emergence of a large void volume during SEC of empty nanodiscs formed using POPC, but not DMPC. And screening the void volume on a transmission electron microscope identified the presence of small lipid vesicles. The formation of these small vesicles is most likely a result of the lipid tails and can be confirmed by forming nanodiscs with other single lipid combinations with the same lipid tail, but different head groups, and TEM screening of the void volume. As for the studies on CFTR ATPase activity and the contributions of the lipid or detergent environment, these are the first studies in which both the orientation of CFTR is unrestricted to buffer conditions, unlike CFTR in proteoliposomes, and no detergent is present, unlike destabilized proteoliposomes. Other similar studies measuring the ATPase activity of CFTR in different lipids have utilized destabilized proteoliposomes, which still require the presence of detergent (133). The determined Michaelis-Menten constants of the ATPase activity for CFTR in detergent was a lower K_M, 0.00692 ± 0.00176 mM compared to CFTR-nanodiscs (0.172 ± 0.117 mM), and a lower V_{max}, 7.9 ± 0.36 nmol/min/µg compared to CFTR-nanodiscs (63.5 ± 9.75 nmol/min/µg). These results make for difficult interpretations. First, as K_M is an indicator of substrate binding, the lower the K_M the tighter the substrate binding to the enzyme. This suggests that ATP binds tighter to CFTR in detergent than CFTR in nanodiscs. In addition, the ATPase rate of CFTR is much higher for CFTR in nanodiscs than in detergent but can be expected

for the high K_M values of CFTR in nanodiscs. The increased ATPase rate for CFTR-nanodiscs does show a higher catalytic rate for CFTR, which could signify the ease of CFTR transitioning through the NDB-gating cycle. However, the variation in the values for the ATPase activity for CFTR-nanodiscs leaves room for improvement and optimization. Currently, only a single lipid nanodiscs system for CFTR has been tested. More complex lipid environments in the nanodiscs could result in dramatically improved the kinetic parameters for the ATPase activity of CFTR. The theory that a more complex, physiologically similar lipid environment affects the function of CFTR could be true for the differences in the efficacy of a specific CFTR inhibitor. For the first time, the difference in inhibition of CFTR by a common CFTR inhibitor (INH172) based on the lipid environment, or preparation state using a detergent for solubilization and purification, was observed. And while it is still unknown if the difference in INH172 efficacy is due to the detergent solubilization or the lipid environment, there are experiments that can elucidate the answer. The first of these experiments will be the incorporation of more complex lipids in the formation of the CFTR-proteoliposomes. The efficacy of inhibition by INH172 on CFTR from these complex lipid CFTR-proteoliposomes can then be screened again using planar lipid bilayer channel recordings. This work only further suggests the importance of the lipid environment on CFTR function—both as measured by ATPase activity and Cl⁻ channel activity.

CHAPTER V

DETERMINATION OF THE LIPID ENVIRONMENT OF CFTR

5.1.   INTRODUCTION.

Nanodisc technology, including SMALPs, has revealed that altering the lipid environment of a membrane protein can dramatically affect the function of and also the structure of the membrane protein (267, 271). Initial mass spectrometry (MS) of detergent-solubilized V-type ATPases revealed the identities of several copurified lipids (272). Native MS has additionally revealed that oligomeric states of membrane proteins are stabilized by the presence of specific endogenous lipids (273). This provides substantial evidence that lipids can play a critical role in the structure of membrane proteins, including CFTR. The most recent detergent-solubilized structures of CFTR reveal areas of electron density that could be several copurified lipids (128, 172); however, the only investigations into the identities of these lipids or the native lipid environment of CFTR are fluorescent microscopy studies. These studies show that CFTR localizes to cholesterol-enriched microdomains in the plasma membrane under certain conditions, but CFTR does exist outside of these microdomains (274). Determining the identity of the copurified lipids of detergent-solubilized CFTR by lipidomics MS can illuminate the importance of lipids structurally. Determination of the annular lipid environment by SMALP-purified CFTR will reveal the types of lipids critical for function and structure. Here, I show the first, critical steps towards SMALP-solubilization of CFTR. In addition, I discuss the lipidomics analysis of detergent-

solubilized CFTR and of SMALP-purified CFTR.

5.1.1. Individual contributions.

SMA preparation and purification of SMALP-CFTR was performed by myself. Lipidomics experiments and analyses were performed with the help of Georgia Institute of Technology's Parker Petit Institute for Bioengineering and Bioscience including the Systems Mass Spectrometry Core Facility, which has been supported by the CF@LANTA RDP Center with funding from the Cystic Fibrosis Foundation. Dr. Josh Chandler (Emory University) provided useful critiques and quality control parameters to the lipidomics data processing.

5.1.2. Publications resulting from this work.

Parts of this chapter will be published as a manuscript on determining the lipids critical for CFTR function.

5.2. METHODS

5.2.1. BHK-CFTR-10xHis expression system.

5.2.1.1. CFTR PURIFICATION FROM BHK-CFTR-10xHIS CELL LINE.

See the previous section (3.2.2.4).

5.2.1.2. SMALP-SOLUBILIZATION AND PURIFICATION OF CFTR.

BHK cells were pelleted in 50 mL conical tubes at 1000 g for 5 mins at 4°C, and the cell pellet mass was measured. All volumes listed are for 1 g cell pellet. The cell pellet was resuspended in 10 mL of 8 mM HEPES-Na, pH 7.2, 0.8 mM EDTA and 1 mM DTT. Cells were lysed using a Dounce Homogenizer for 20 strokes with the loose pestle followed by 20 strokes with the tight pestle. The cell lysate was then mixed with 1/7th volume of 2 M sucrose in 8 mM HEPES-Na, pH7.2, 0.8 mM EDTA and 1 mM DTT and

was incubated on ice for 10 minutes. Large cellular debris was pelleted twice at 1000 g for 10 minutes at 4°C. The supernatant was ultracentrifuged at 100,000 g for 1 hour at 4°C with slow braking. The pellet was washed in 5 mL of 50 mM Tris-HCl, pH 7.5, 0.5 M NaCl, and 10% glycerol by resuspension using a Dounce Homogenizer (3 strokes with the loose pestle and three strokes with the tight pestle). The resuspended pellet was ultracentrifuged again at 100,000 g for 1 hour at 4°C with slow braking. The membrane pellet was washed in 1 mL of 50 mM Tris-HCl, pH 8.0, and 0.2 M NaCl and resuspended using a Dounce Homogenizer. The resuspended membranes were transferred to a 5 mL tube. The total membrane mass (protein and lipid content) was measured by Pierce™ BCA assay in accordance with the manufacturer's protocol. To solubilize CFTR, enough 10% SMA was added to achieve a final concentration of 2.5% per 40 mg/mL lipid and protein mass. The SMA-membrane sample was incubated for 1 hour at RT. Solubilized CFTR was separated from insoluble material by ultracentrifugation at 100,000 g for 30 minutes at 4°C with slow braking. The supernatant was collected and incubated with equilibrated HisPur™ Ni-NTA resin (50 µL) for 1 hour at 4°C with rotation. The resin was packed in a gravity flow column and washed in increasing concentrations of imidazole (10 mM, 25 mM, and 75 mM) in 50 mM Tris-HCl, pH 7.5, and 0.15 M NaCl). The purity and confirmation of CFTR was analyzed by SDS-PAGE and Western blot (see section 3.2.2.5).

5.2.2. Untargeted Lipidomics.

5.2.2.1. PREPARATION OF DETERGENT-SOLUBILIZED SAMPLES FOR LIPIDOMICS MASS SPECTROMETRY.

The detergent-solubilized CFTR samples were vortexed with 0.6 mL of 2:1

chloroform:methanol (CHCl$_3$:MeOH) at 3000 RPM for 5 minutes (in pulse mode). An additional 0.4 mL of water was added, and the samples were vortexed again for 1 minute. The samples were centrifuged at 21,100 g for 5 minutes to enable phase separation. The organic layer was removed, and lipids were dried by vacuum. The lipids were further extracted by incubation of the aqueous layer with 0.4 mL 2:1 chloroform:methanol two additional times and dried as previously described. All dried extracts were resuspended in 0.4 mL isopropyl alcohol (IPA) containing deuterated lipids as standards and controls (3.3% v/v of the sample), sonicated for 5 minutes, vortexed for 5 minutes and centrifuged at 21,100 g for 5 minutes. The supernatant was extracted and stored at 4°C until injection into the mass spectrometer.

5.2.2.2. PREPARATION OF SMALP-CFTR SAMPLES FOR LIPIDOMICS MASS SPECTROMETRY.

The samples were vortexed in 1 mL IPA for 3 minutes at 3000 RPM. The samples were then sonicated in an ice bath for 3 minutes before 3 freeze-thaw cycles with liquid nitrogen. The samples were centrifuged at 21,200 g for 5 minutes, and the supernatant transferred and stored at 4°C until analysis.

5.2.2.3. ULTRA-PERFORMANCE LIQUID CHROMATOGRAPHY-MASS SPECTROMETRY (UPLC-MS).

Samples (2 µL) were injected into a Thermo Vanquish Ultra Performance Liquid Chromatography (UPLC) instrument equipped with an Accucore C$_{30}$ 2.6 µm, 150 x 2.1 mm column. The mobile phase A (40 % water / 60 % acetonitrile, 10 mM ammonium formate, 0.1 % formic acid) was exchanged to mobile phase B (90% IPA/ 10% acetonitrile, 10 mM ammonium formate, and 0.1 % formic acid) at a flow rate of 0.4

mL/minute using the following gradient protocol: 20 to 60% in 1 minute, 60% to 70% in 4 minutes, 70% to 85% in 0.5 minute, 85% to 90% in 0.5 minutes, 90% to 100% in 0.2 minutes, and ran at 100% B for 2.3 minutes before dropping to 20% in 0.2 minutes. The flow rate and temperature were held constant at 0.4 mL/minute and 50°C. The fractionated sample was then injected into a Thermo Orbitrap ID-X Mass Spectrometer using a scan range (*m/z*) of 150-2000 with a resolution of 240,000 FWHM. The data-dependent acquisition was collected under the following conditions using high-energy collisional dissociation (HCD) at collision energies of 15, 30, and 45 with an isolation window of 0.8 *m/z* and a resolution of 300,000.

5.2.2.4. DATA ANALYSIS FOR DETERGENT-SOLUBILIZED CFTR SAMPLES.

Lipidomics features were extracted from chromatograms (*m/z* and retention time) and identified through Compound Discoverer 2.X. using the following databases: mzVault, compound discover, mzCloud, and in-house mass list library (determined by theoretical masses of lipids of interest). For the detergent-solubilized samples, a total of 35,088 features were detected (28,482 features in positive mode and 6,607 features in negative mode). After the removal of background features and any features with a quality control score of greater than 30%, 1859 features were identified in positive mode and 267 features in negative mode. Each biological replicate sample was run in triplicate and normalized peak area was averaged. Features enriched in the three biological replicates as compared to the blank were determined by calculating the $\log_2$ (fold change) of the averaged peak areas for the sample blank to the same feature peak area in the sample. Only features enriched by more than one $\log_2$ (fold change) in the sample over the blank were analyzed further. The coefficient of variation (CV) was determined for each feature

across the biological triplicates, and features of less than 50% CV were analyzed. Confidence in the annotation of the final 383 lipid identities was determined based on the five confidence levels described by Schymanski *et al. (275),* listed in Table 5.1.

5.2.2.5. DATA ANALYSIS FOR SMALP-CFTR SAMPLES.

Lipidomics features were detected in an unbiased fashion, as described above. A total of 13,784 features were found across positive mode and negative mode acquisitions. Features that were enriched in the three biological replicates of the elution fraction containing CFTR were analyzed by $\log_2$ (fold change) as compared to the blanks and with a CV score of less than 50%, as reported above. A total of 1,520 lipids were identified at a confidence level of 4 or 5, in accordance with the Schymanski confidence levels (275).

Table 5.1: Schymanski level of confidence for MS identification.

Level	Confidence	Data Requirement
Level 1	Confirmed structure	MS, MS^2, retention time matching, and reference standard match
Level 2	Probable structure	MS, MS^2, library of MS^2 or experimental data.
Level 3	Tentative candidate	MS, MS^2
Level 4	Unequivocal molecular formula	MS isotope
Level 5	Exact mass	MS

5.3.   RESULTS.

5.3.1. SMALP-CFTR purification requires further optimization.

Both SDS-PAGE and Western blot analysis showed that CFTR can be solubilized by SMA but requires optimization to improve the solubility of CFTR. Another option to improve the overall solubility might be the use of one of the other available polymers (see section 1.4.3.2). There is CFTR present in the elution fractions, but the overall purification needs to be optimized as the majority of solubilized CFTR remains in the column FT fraction and is a result of weak binding of CFTR-SMALPs to the resin (Figure 5.1). There are many copurified proteins in the elution fraction, indicating the need for optimization (Figure 5.2).
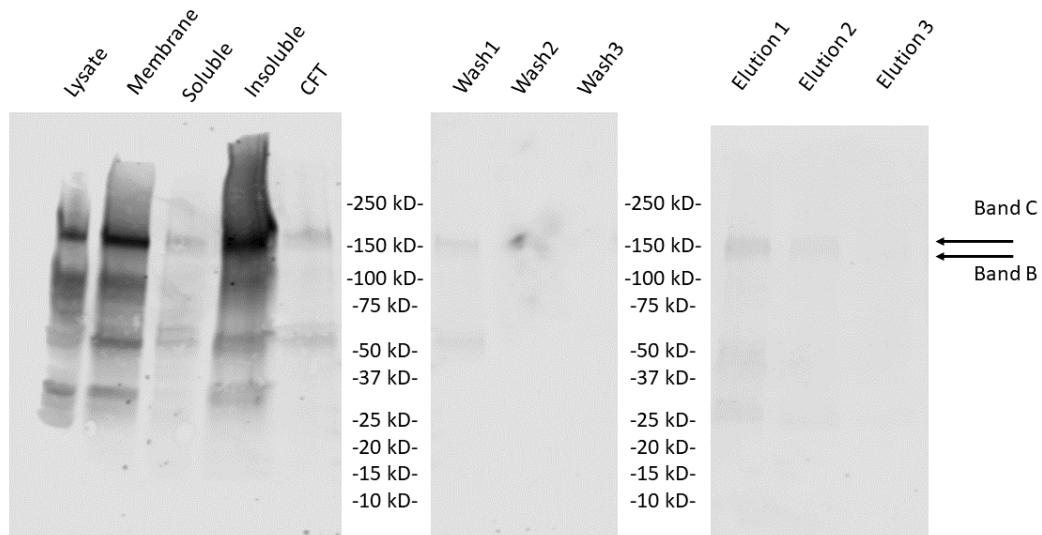
Figure 5.1: Western blot analysis of SMALP-CFTR. CFTR is present in the soluble fraction, but the majority of CFTR remains mostly in the insoluble fraction. CFTR-SMALPs also were present in the elution fraction, which indicates minimal binding of SMALP-CFTR to the resin. Immunoblotting for CFTR: Primary – mouse anti-CFTR 596 antibody, 1:1,500 and Secondary – IRDye® 680RD goat anti-mouse antibody, 1:10,000.
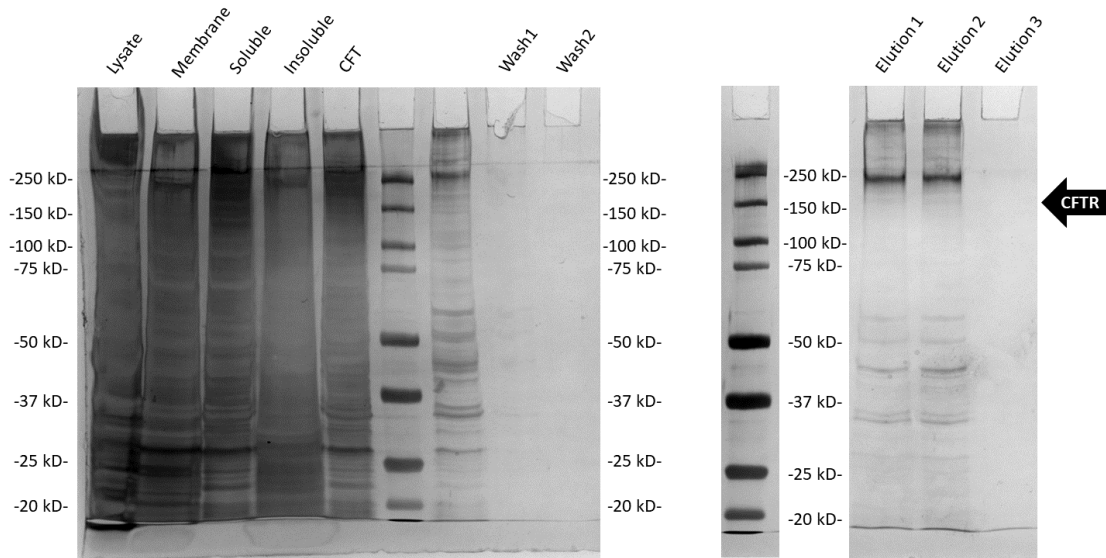
Figure 5.2: SDS-PAGE analysis of CFTR-SMALPs. Hand-cast 8% acrylamide: bisacrylamide SDS-PAGE gel, silver stained. CFTR-SMALPs can be seen in the elution fraction, along with several other copurified proteins.

5.3.2. Lipidomics Mass Spectrometry (MS) of detergent-solubilized CFTR.

Three biological replicates of detergent-solubilized CFTR samples were run in triplicate. A partial match in the mzCloud software, with a confidence level of 3, was 5α-cholesta-8,24-dien-3β-ol or zymosterol (276) (Table 5.2). Zymosterol is a precursor of cholesterol found in the plasma membrane and is structurally different from both cholesterol and cholesteryl hemisuccinate (a detergent used to solubilize CFTR) (Figure 5.3). This match along with the structural identification of cholesterol, or a cholesterol derivative, from a recently determined hCFTR detergent-solubilized structure, indicates the possible structural importance of cholesterol for CFTR (128). The cluster of other lipid identities falls under level 4 identity confidence. For 382 lipid features, these were

identified by their chemical formulas linked to a possible name through several databases. Of these compounds with possible identities, approximately half (15 of 25) are of odd chain lipids, which only compose a small portion of cellular membranes (277); however, these lipids were enriched in the detergent-solubilized CFTR samples (Table A.1). The other 277 features can only be identified by the chemical formula (Table A.2), and the last 80 features are at a confidence level of 5 and can only be identified by molecular weight (Table A.3).

Table 5.2: Lipidomics results of detergent-solubilized CFTR and analysis results.
The abbreviation FC is the fold change, and CV is the coefficient of variation.

Name	Formula	Molecular Weight	RT [min]	RSD QC Areas [%]	Average FC	Median FC	CV of FC
Zymosterol	$C_{27}H_{44}O$	384.33935	3.929	1	5.20	5.19	41.8

5.3.3. Lipidomics Mass Spectrometry of SMALP-CFTR.

Of the initial 2,097 lipid features identified, 1,520 lipids have linked chemical formulas, making for a level 4 confidence (Table A.4), and 577 lipids received a level 5 confidence with only a molecular weight determined (Table A.5). The copurified proteins taking up the majority of the SMALPs, however, complicates further interpretation of this data.
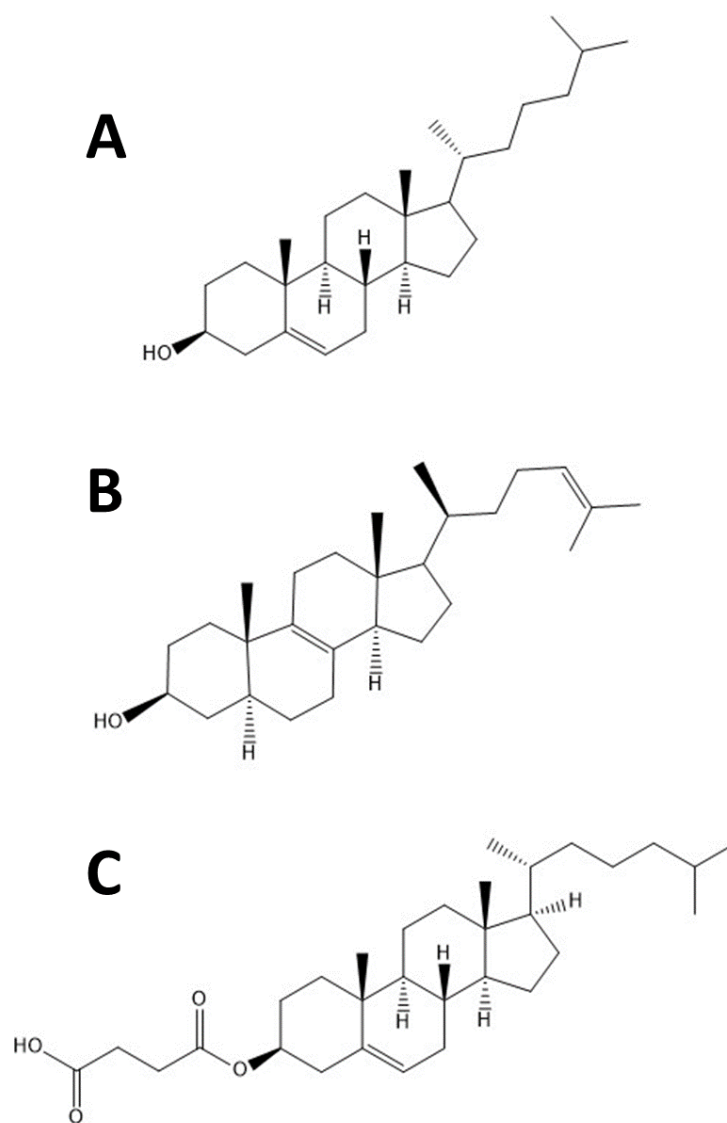
Figure 5.3: Structures of cholesterol, zymosterol, and cholesteryl hemisuccinate (CHS). There are apparent structural differences between the three sterol derivatives—cholesterol (A), zymosterol (B), and CHS (C). These structural differences include the double bond between C-5 and C-6 of the B ring in cholesterol and CHS, but only a single bond in zymosterol. Zymosterol has a double bond present between C-8 and C-9 of the B ring, which is a single bond in cholesterol and CHS. Zymosterol also includes another double bond present between C-24 and C-25, which is a single bond in both cholesterol and CHS.

5.4.   DISCUSSION.

The current work shows a preliminary search into the lipid identities of the annular lipid environment of CFTR; however, this data, in conjunction with the many copurified SMALPs, complicates the confidence for an interpretation. Also, as the majority of CFTR remained in an insoluble fraction, the lipid profile of the SMALP-CFTR in this fraction most likely represents the non-majority of CFTR. Work to investigate the annular lipid profile for the majority of CFTR might require a different strategy, including using one of the aforementioned polymers or the use of MSP (189). As for the copurified lipids in the detergent-solubilized CFTR, a precursor of cholesterol called zymosterol was identified, which is also supported by several other studies. The first and most crucial study shows electron density similar to cholesterol, or a cholesterol derivative, bound to detergent-solubilized hCFTR (128). Studies of other ABC transporters in nanodiscs show that cholesterol clusters around the TMDs (262). Further analysis and replicates with reference standards for the lipidomics data of the detergent-solubilized CFTR samples will increase the number of and confidence in the lipids identified.

CHAPTER VI

CONCLUSIONS

6.1. INTRODUCTION.

Nanodisc technology has revolutionized membrane protein research, leading to the ability to study individual membrane proteins in different lipid environments and to determine how the changes in these environments lead to functional or structural consequences. In order to utilize this technology in these types of studies, first, the membrane protein of interest must be purified in an active form.

6.2. REVIEW OF WORK.

6.2.1. CFTR homology models and understanding transition states.

In lieu of CFTR structures, homology models of CFTR were built to investigate the complex transitions of conformations in this protein (130, 160-165). This work compares a homology model by Rahman *et al.* (130), to two of the recently released structures of CFTR (126, 128) and investigates the optimization of a homology model by flexible fitting into electron density maps of the initial structures of CFTR (157). Through this work, the interaction of three residues (E543−K968−K1292) between the ICLs and NBDs that might play a role in translating the consequences of ATP binding at the NBDs to the conformation of the TMDs was experimentally investigated by molecular modeling and electrophysiology. Thus, this initial work shows this interaction is likely, but not without complications. These simulations do not include the R-domain, and thus details of its role or the role phosphorylation of the R-domain on this region was not explored; even though this region of CFTR does play an important role in both (278).

As more structures of CFTR orthologs are released, simulations of these structures can provide valuable insight into the mechanism of CFTR's conformational transitions as well as the interactions of CFTR with the lipid bilayer (167). As all of the structures of CFTR released in the last three years have been of detergent-solubilized CFTR, the use of molecular dynamics (MD) will replace the detergent micelle with the more physiologically relevant lipid bilayer environment; however, as these structures of CFTR were solved in detergent, the likelihood of detergent-induced artifacts is high. The strategies we employed for the improvement of the homology models could be employed to these newly released structures in detergent. The initial electron density maps of CFTR were solved by 2D crystallography, meaning CFTR was in the more physiologically relevant environment of a lipid bilayer, and not detergent. By allowing these new structures to relax within the constraints of a low-resolution map through the use of molecular dynamics flexible fitting (MDFF), it is possible that detergent-induced artifacts could be reduced. In fact, one study has explored this idea through the MDFF of two inward-facing structures of CFTR recently released (223) into these released 2D crystallography maps of CFTR. The states of all of these structures were closed, and so an open, fully conducting pore was not expected, nor was it seen (223). Thus, further MDFF studies of the outward-facing structures of CFTR, which is expected to be open within these maps of CFTR in a lipid bilayer, could reveal key interactions of the CFTR open state. Simulations of these modified structures could unveil the necessary interactions CFTR must undergo to transition from the variety of closed states to a conducting, fully open state for CFTR. The fact that none of the release structures or refined structures has displayed a fully conducting pore of CFTR begs the need for more

structures, especially structures of CFTR in a lipid bilayer.

6.2.2. CFTR expression and purification.

The complexity of CFTR biogenesis results in overexpression difficulties and places a high level of importance on the cell type, as is true for many other membrane proteins with complex biogenesis (279). We investigated three different cell types for the overexpression of WT-hCFTR and two different tagging systems for affinity chromatography to improve the yield of WT-hCFTR; importantly, we did not introduce solubilizing or stability mutations into our protein—a common strategy in the field. From these studies, we developed a reproducible protocol for the purification of decently pure and functional WT-hCFTR from BHK cells. Many of the optimizations methods learned in this system can be translated to other CFTR expressing cell lines, especially the optimization in the detergent solubilization step of the CFTR purification. The use of cholesteryl hemisuccinate (CHS) and dodecyl-maltoside (DDM) to solubilize CFTR improved the overall yield of CFTR from each purification. The use of this detergent, CHS, has shown to improve the thermal stability of other membrane proteins in detergent micelles (264, 265). Thus, the improvement in yield of monomeric CFTR could be contributed to the improved thermal stability of CFTR in a detergent micelle containing CHS. This hypothesis can be tested by measuring any shifts in the melting temperature of CFTR in different detergent micelles, including micelles containing CHS. And while many attempts to improve the purity of CFTR from a His-tag affinity chromatography system were somewhat successful, the complete removal of several co-purified proteins proved to be problematic. His-tag systems are notorious for having strict buffer incompatibilities, reduced selectivity for proteins from specific expression systems, and

high amounts of leached metal content in purified protein samples (280). The establishment of many other affinity chromatography systems, like the FLAG®-tag system, have dramatically improved the buffer compatibilities, purification of proteins from a variety of expression systems, and the overall purity (281). To improve the overall purity of CFTR, a modified T-Rex™ CHO cell line utilizing the FLAG®-tag affinity system was developed. This modified T-Rex™ CHO system utilized a CFP-reporting system and flow cytometry to single cell sort transfected cells for the generation of a homogeneous population of cells stably expressing CFTR. This newly developed system allows for the generation of new stably transfected cell lines in a few weeks, allowing for the production of many cell lines expressing different mutant versions of CFTR quickly. The purification of CFTR from this system still requires optimization, especially in the yield. One theory to the low yield could be occlusion of the tag by the glycosylation of CFTR, especially as the majority of solubilized CFTR remained in the column FT or unbound to the resin. There are a few options to improve the binding including: increasing the amount of resin, using deglycosylation enzymes to remove some of the glycosylation, or increasing the time of binding. If these strategies do not improve the overall yield, the FLAG-tag can be easily moved and several new cell lines development in a matter of weeks. The improvements and optimization of CFTR expression and purification allow a host of new questions to be answered, especially regarding the preferred lipid environment of CFTR.

6.2.3. CFTR reconstitution and functional studies.

The ability to purify CFTR has set the stage for the investigation into the functional consequences of changing the environment of CFTR. Previous work has begun to

investigate the consequences of the choice of detergent on ATPase activity and how the reconstitution of CFTR into the lipids of destabilized proteoliposomes, destabilized by detergent, may not be able to rescue the effects of detergent (133). The work presented here on CFTR-nanodiscs is the first study of CFTR ATPase activity in a lipid bilayer system without restricting access of the NBDs to ATP (i.e., proteoliposomes) or in the presence of detergent (i.e., destabilized proteoliposomes) and compares the activity to that measured in detergent. While only one lipid system (POPC) has been tested, the results clearly demonstrated differences in the ATPase activity of CFTR in POPC than in detergent alone. Additional single-lipid systems and complex lipid systems, including the presence of cholesterol, will provide further information on the importance of lipids and the critical type of lipids for the ATP function of CFTR. Pairing these ATPase functional studies of CFTR with the thermal stability studies of CFTR in different detergent micelles can correlate the changes to thermal stability with the changes to enzyme kinetic parameters measured by the ATPase assay. Not only in detergent micelles but these same studies, the thermal stability assays and kinetic enzyme assays, can be measured for CFTR in nanodiscs of varying lipid composition. While ATPase activity is commonly used to confirm functional purified protein, ATPase activity speaks indirectly to the channel activity of CFTR. Thus, we began investigating the effects of lipids on the channel function of CFTR, although the initial test was to confirm that our purified protein retained channel activity. Here we have shown that reconstitution of the purified protein into single lipid proteoliposomes, POPC only, and then measuring channel function by fusion of proteoliposomes into planar lipid bilayers confirms the channel function of purified CFTR. Not only does our purified protein retain channel activity, but

the effect of a common CFTR inhibitor, INH172, is reduced in studies of purified protein versus protein from cellular membranes. The cause of this difference, whether due to the presence of cholesterol or from detergent-induced structural changes unable to be rescued by lipids, has yet to be determined. Experiments to determine the cause of the reduced inhibition by INH172, first, would be to reconstitute the purified CFTR protein into increasingly more complex proteoliposomes and measure the efficacy of INH172 on CFTR from these different proteoliposomes. The next experiments would be to remove cholesterol from the cellular membrane fractions by treatment with methyl-β-cyclodextrin (MβCD) and recording the efficacy of INH172. The differences of efficacy for this specific CFTR inhibitor could ring true for other CFTR-specific inhibitors or even some of the approved modulators of CFTR. The mechanism of action for these modulator therapies is still being investigated, but the highly hydrophobic nature of these compounds hints towards possible binding to the TMDs. In fact, two recently released structures of CFTR show two bound modulators, one clinically approved and one not, in the TMDs (170). These results offer support for the importance of the lipid bilayer for the channel function of CFTR.

6.2.4. Determination of the lipid environment of CFTR.

The recent advances in the utilization of mass spectrometry to identify lipids and changes to the lipid environments of cells and membrane proteins have been fueled by the increased recognition that lipids are significant contributors to membrane protein structure and cellular function (282). This work utilizes the advancements of mass spectrometry lipidomics to investigate the annular lipid environment of CFTR by SMALPS and identify the copurified lipids of the detergent-solubilized CFTR. The lipids

identified from the SMALP-CFTR samples make for complex interpretations due to the many other copurified proteins in the samples. Currently, only one polymer, the commercially available SMA polymer, has been attempted in the solubilization and formation of native nanodiscs containing CFTR. As more polymers are released with various improvements, different polymers can be attempted, the first being polymers that have been shown to have similar capabilities of detergent (DDM) to solubilize membrane proteins. Moreover, the yield and purity of CFTR containing native nanodiscs can be improved by alteration of the affinity system used for purification. As previously discussed, His-tag affinity chromatography systems are not always the best choice due to buffer incompatibility, low purity, and challenges from a eukaryotic cell expression system. The development of the FLAG-tag affinity chromatography system in the CHO cells could provide increased purity of CFTR containing native nanodiscs. And while the purification of SMALP-CFTR and lipidomics of these SMALPs requires considerable improvement, the lipidomics results from the detergent-solubilized CFTR samples leads to two interesting conclusions. First, a cholesterol precursor known as zymosterol was identified at a level 3 confidence. This result, along with the identification of a cholesterol shaped electron density observed in one of the recently release CFTR structures (128), begs many questions about the importance of cholesterol for CFTR structure and function; this is an area of great interest to the McCarty lab as functional studies to investigate the importance of cholesterol has been much discussed in the previous sections. The second significant result is the large population of odd chain lipids present, which comprise a small portion of the lipid environment of cells. These results were both identified by untargeted lipidomics mass spectrometry with a relatively low confidence

level, level 3 and 4 respectively; however, confidence levels can be improved with the use of more targeted lipidomics studies. The introduction of reference standards with the detergent-solubilized CFTR samples can confirm the lipid identities currently hypothesized, at the lower confidence levels, to be bound to CFTR and will improve the overall confidence in the lipid identities. The lipids identified in the lipidomic results will inform our understanding of the structurally important lipids of CFTR and will inform our functional experiments of CFTR in a lipid environment.

6.3.   FINAL REMARKS.

This work highlights the importance of the cell expression system and affinity tagging method for producing pure and active WT-hCFTR. This work established the development and use of new techniques for studying the lipid environment of CFTR and the need for more investigations into the functional and structural consequences of the environment of CFTR, as well as the need for more structures of CFTR, especially in a lipid environment. This work also highlights the need for computational simulations, both structures already published and hopefully of more structures within the lipid bilayer, to investigate the complex transitions CFTR undergoes.

APPENDIX A

Table A.1: Lipidomics results of detergent-solubilized CFTR and analysis results.
The abbreviation FC is the fold change. The listed features were identified by the mass list developed by members of systems MS lipidomics core, giving a confidence level of 4.

Name	Formula	Molecular Weight	RT [min]	RSD QC Areas [%]	Ave. FC	Med. FC	CV of FC
Cer 37:1;1	C37 H73 N O2	563.56446	7.962	18	1.60	2.33	8.01
Cer 45:0;2	C45 H91 N O3	693.70045	9.397	16	1.54	2.43	12.65
Cer 45:0;1	C45 H91 N O2	677.70545	9.597	17	2.73	3.78	16.77
Tridemorph	C19 H39 N O	297.30327	2.766	12	2.31	3.23	17.54
LPA 25:0	C28 H57 O7 P	536.38452	5.895	18	3.44	3.41	18.10
N-Acetyl-D-sphingosine	C20 H39 N O3	341.29312	2.598	8	1.59	2.62	18.50
6-(alpha-D-Glucosaminyl)-1D-myo-inositol	C12 H23 N O10	341.1323	1.426	16	1.58	1.52	19.50
Cer 39:1;1	C39 H77 N O2	591.59601	8.396	24	1.65	2.7	19.60
Cer 45:0;1	C45 H91 N O2	677.70545	7.785	19	1.98	3.11	19.62
AcCa 18:0	C25 H49 N O4	427.3664	3.544	11	2.22	2.92	21.87
LPG 23:4	C29 H51 O9 P	574.32681	3.099	22	2.26	2.32	21.95
AcCa 24:5	C31 H51 N O4	501.3821	3.906	9	5.71	5.76	23.47
6-Hexanoyl-D-erythro-sphingosine	C24 H47 N O3	397.35575	3.37	22	1.15	1.76	23.48
PA 29:2	C32 H59 O8 P	602.39638	1.876	7	1.17	1.6	25.26
Cer 46:0;1	C46 H93 N O2	691.72116	6.44	26	1.20	1.62	26.10
Cer 47:0;2	C47 H95 N O3	721.73178	9.586	22	1.90	2.86	26.42
PC 29:1	C37 H72 N O8 P	689.50015	4.437	20	2.38	1.28	29.51
6-Hexanoyl-D-erythro-sphingosine	C24 H47 N O3	397.35574	3.493	8	1.58	2.63	30.27
Cer 42:1;2	C42 H83 N O3	649.63781	8.458	24	2.50	3.62	33.32
LPA 23:1	C26 H51 O7 P	506.33745	3.905	10	2.35	2.38	34.53
Cer 31:1;2	C31 H61 N O3	495.46547	5.971	11	1.01	1.56	37.94
[ST(2:0)]5alpha-cholesta-8_24-dien-3beta-ol	C27 H44 O	384.33935	3.929	1	5.20	5.19	41.82
Cer 43:1;1	C43 H85 N O2	647.65855	9.307	29	1.69	2.92	44.59
LPA 17:2	C20 H37 O7 P	420.22795	1.802	15	2.40	2.43	48.14
[ST(3:0)]cholest-5Z_7Z_24-trien-3beta-ol	C27 H42 O	382.32371	3.011	13	3.03	3.14	49.88

Table A.2: Lipidomics results of detergent-solubilized CFTR and analysis results.
The abbreviation FC is the fold change. As only a formula can be determined for these features, this gives a level 4 confidence.

Name	Formula	Molecular Weight	RT [min]	RSD QC Areas [%]	Ave. FC	Med. FC	CV of FC
	C57 H119 N9 P2 S2	1055.852	9.476	25	3.53	3.53	0.00
	C H3 N7 O3 P2	222.9776	4.523	13	3.39	3.39	0.17
	C26 H47 N8 O P	518.3617	3.009	25	4.29	4.29	0.36
	C23 H45 N O3	383.3401	3.219	7	2.46	2.45	0.47
	C55 H115 N3 O12	1009.847	9.187	12	3.81	3.81	0.79
	C67 H107 N5 O	997.8467	9.445	21	3.39	3.4	1.06
	C56 H104 O18 P2	1126.669	3.897	30	3.68	3.7	1.28
	C32 H44 N10 O17	840.2878	2.88	13	2.70	2.71	1.54
	C27 H53 N O3	439.4027	4.643	6	3.20	3.19	1.57
	C50 H112 N7 O4 P3	967.7996	8.486	10	4.38	4.35	1.94
	C80 H88 S	1080.659	10.005	18	2.19	2.21	1.99
	C44 H99 N9 O9	897.7581	10.006	4	2.65	2.62	2.08
	C64 H112 N9 O2 P	1069.868	9.475	24	3.26	3.29	2.15
	C49 H109 N9 O10	983.8312	9.546	25	3.56	3.59	2.34
	C31 H50 O6	518.3613	2.84	24	3.92	3.94	2.73
	C43 H49 O11 P	772.3004	2.88	11	2.84	2.81	3.13
	C90 H134 N8 O12	1519.012	3.907	10	4.60	4.68	3.20
	C68 H109 N5 O	1011.862	9.447	17	3.24	3.28	3.27
	C88 H144 N9 O7 P	1470.093	3.904	3	7.49	7.47	3.28
	C22 H41 N O7	431.2885	1.564	16	2.82	2.85	3.29
	C25 H56 N6 O18 P2	790.3112	2.835	18	3.12	3.16	3.39
	C18 H26	242.2035	10.006	16	2.67	2.68	3.40
	C23 H26 N2	330.2097	1.262	4	6.73	6.79	3.44
	C60 H121 N3 O5 P2	1025.878	9.448	18	3.98	3.9	3.48
	C63 H99 O4 P3	1012.675	3.906	7	3.16	3.15	3.49
	C2 H7 O10 P	221.978	4.515	11	2.95	2.97	3.63
	C25 H49 N O3	411.3714	3.876	9	3.88	3.87	3.74
	C23 H52 N10 O12 P2	722.3234	2.839	21	3.43	3.38	3.75
	C34 H47 N10 O P3	704.3127	2.876	14	2.84	2.82	3.76
	C62 H99 N O8	985.7375	3.906	4	6.42	6.42	3.82
	C30 H57 N O7	543.4138	1.784	25	2.07	2.1	3.83
	C27 H44	368.3445	10.008	4	2.55	2.52	3.86
	C27 H42	366.3288	3.905	1	5.25	5.23	3.92
	C61 H98 O5	910.7419	9.448	7	3.00	3	4.00
	C54 H103 N7 O P2	927.7686	9.459	7	2.98	2.94	4.01

	C66 H98 O P2	968.711	3.903	4	6.03	6.03	4.06
	C29 H55 N O6	513.4033	1.792	23	2.53	2.51	4.22
	C56 H111 N3 O4 P2	951.805	9.667	22	3.96	4.05	4.23
	C31 H50 O4	486.3712	4.516	25	3.79	3.8	4.24
	C49 H110 N7 O4 P3	953.7842	8.49	18	4.35	4.33	4.27
	C58 H94 O4	854.7156	10.008	5	2.82	2.75	4.30
	C16 H35 N O	257.272	1.666	4	3.14	3.15	4.31
	C22 H41 N O7	431.2885	1.687	4	2.11	2.06	4.37
	C22 H51 N10 O2 P	518.3935	1.562	5	3.57	3.55	4.37
	C89 H143 N4 O11 P	1475.048	3.903	10	5.98	5.9	4.43
	C52 H105 N2 O13 P3	1058.681	3.895	28	4.58	4.53	4.48
	C24 H51 N O8	481.3618	1.942	9	4.81	4.77	4.53
	C17 H33 N O3	299.246	2.087	8	3.25	3.21	4.60
	C67 H113 N S2	995.8313	9.187	17	3.11	3.04	4.65
	C16 H34 O4 S	322.2177	2.152	24	2.17	2.12	4.65
	C5 H12 N9 O P	245.09	1.688	15	2.88	2.94	4.66
	C20 H52 N10 O10 P2	654.3357	2.838	18	3.98	4.07	4.67
	C27 H42	366.3288	9.838	2	3.00	2.99	4.68
	C53 H99 N6 P3 S	944.6852	10.01	8	2.70	2.63	4.70
	C40 H60 N2 O3	616.4607	3.006	3	8.14	8.14	4.79
	C7 H10 N2 O2	154.0743	0.911	19	6.18	6.19	4.85
	C57 H93 N2 O P	852.7001	9.838	7	3.03	2.98	4.86
	C33 H63 O11 P	666.4097	2.03	9	4.05	3.95	4.93
	C42 H54 O2 S	622.3834	2.046	7	5.15	5.06	4.99
	C14 H31 N O	229.2407	1.25	5	2.71	2.66	5.03
	C32 H60 N9 P	601.471	3.011	12	3.27	3.18	5.03
	C61 H101 O4 P3	990.6928	3.905	7	4.73	4.7	5.11
	C52 H105 N3 O6 S	899.7735	10.008	8	2.45	2.44	5.11
	C21 H32	284.2505	3.907	7	3.64	3.54	5.15
	C33 H53 N2 O7 P3	682.3051	3.31	12	3.20	3.13	5.20
	C29 H51 N2 O11 P S	666.2947	1.951	12	2.66	2.62	5.22
	C39 H86 N9 O8 P	839.634	2.98	8	3.46	3.54	5.40
	C20 H47 N4 O7 P	486.3173	1.944	23	2.71	2.7	5.54
	C3 H8 N2 O7 S2	247.9775	4.514	12	5.78	5.84	5.68
	C18 H40 N5 O7 P	469.2654	1.486	11	4.19	4.24	5.70
	C63 H103 N O7	985.7741	9.477	10	3.04	3.05	5.94
	C32 H51 O3 P S	546.3303	3.315	10	4.27	4.31	6.14
	C23 H54 N10 O10 P2	692.3512	2.415	22	3.17	3.17	6.16
	C41 H52 O3 S	624.3637	2.408	24	3.44	3.43	6.26
	C27 H45 N5 O2 S	503.3304	1.816	6	5.29	5.19	6.27
	C27 H47 N	385.371	10.006	17	2.87	2.77	6.34

	C62 H103 N O4	925.7895	9.838	15	3.65	3.74	6.36
	C18 H39 N O	285.3033	2.075	2	2.31	2.34	6.62
	C39 H49 O2 P S	612.3203	2.173	9	1.90	1.97	6.84
	C35 H54 O8	602.3817	2.408	27	3.77	3.71	6.91
	C90 H153 O7 P	1377.134	7.145	20	5.13	5.2	6.94
	C56 H100 N2 O8 P2	990.6933	3.894	26	4.99	5.05	6.98
	C37 H76 N2 O3	596.5861	6.372	21	3.51	3.64	7.00
	C27 H42	366.3288	3.025	4	2.61	2.63	7.14
	C72 H144 N O11 P S	1262.019	10.007	3	3.74	3.83	7.29
	C41 H90 N9 O8 P	867.6653	3.399	24	3.25	3.2	7.35
	C14 H29 N	211.23	1.259	14	2.65	2.6	7.37
	C11 H25 N10 O P	344.1948	0.899	16	3.80	3.81	7.38
	C59 H88 N10 O2	968.7116	3.896	29	4.30	4.36	7.64
	C60 H99 N O5	913.7529	9.545	10	3.05	3.12	7.64
	C19 H38 O8	394.2566	1.566	20	2.60	2.53	7.65
	C16 H29 N O3	283.2149	1.59	19	2.76	2.84	7.67
	C34 H54 O2	494.4131	3.868	20	7.17	7.44	7.68
	C22 H48 N9 P	469.377	1.797	16	2.01	2.03	7.73
	C32 H64 N3 O4 P S2	649.4076	2.019	10	2.12	2.14	7.80
	C35 H53 N4 O2 P S	624.3643	2.404	6	3.77	3.7	7.85
	C27 H45 N6 O8 P	612.3018	2.88	21	2.16	2.13	7.95
	C46 H107 N10 O5 P3	972.7618	8.931	11	4.10	4.1	8.05
	C21 H44 N10 O6 P2	594.2913	3.43	27	3.09	3.1	8.08
	C19 H28	256.2192	10.007	3	3.45	3.33	8.12
	C64 H105 N5	943.8361	10.112	4	4.37	4.5	8.17
	C34 H57 N O5	559.424	4.249	8	3.17	3.31	8.20
	C35 H53 N O2	519.408	5.8	15	3.35	3.31	8.27
	C35 H57 N O8	619.4089	2.405	3	3.21	3.18	8.30
	C35 H70 N5 O7 P	703.503	2.403	8	3.12	3.03	8.38
	C35 H51 O5 P S	614.3177	3.314	11	3.74	3.79	8.50
	C61 H99 N O5	925.753	9.192	15	3.76	3.83	8.53
	C25 H54 N5 O6 P	551.3826	2.694	9	3.39	3.27	8.53
	C17 H44 N9 O2 P	437.3355	1.949	10	3.47	3.48	8.66
	C31 H53 N O5	519.3927	3.415	6	3.01	3.12	8.73
	C17 H41 N7 O S	391.3088	2.486	14	3.18	3.22	8.87
	C63 H105 N O4	939.805	9.838	10	3.33	3.49	9.20
	C74 H155 N9 O9 S2	1378.139	7.144	18	4.35	4.45	9.28
	C37 H82 N9 O7 P	795.6079	3.044	6	2.35	2.44	9.33
	C38 H47 O2 P S	598.3047	2.172	14	2.77	2.63	9.39
	C13 H28 O4 S	280.1712	1.552	14	2.94	2.95	9.54
	C28 H70 N9 O7 P3	737.4602	2.023	23	2.43	2.52	9.55

C4 H7 O5 P3	227.9507	4.497	18	2.03	1.98	9.62
C61 H93 N6 O2 P3	1034.657	3.925	15	2.77	2.82	9.69
C27 H66 Cl N9 O5 P2	693.4339	2.022	17	2.49	2.55	9.70
C57 H108 N5 P3 S	987.7534	8.061	27	3.41	3.54	9.71
C58 H92 O5	868.6952	8.708	19	3.52	3.66	9.72
C27 H42	366.3288	2.87	5	3.56	3.66	9.75
C62 H101 N O7	971.7583	8.94	13	4.22	4.3	9.76
C30 H62 N5 P3 S	617.3931	2.352	11	2.69	2.78	9.78
C31 H48 O5	500.3505	3.012	4	2.92	3.03	9.85
C25 H61 N7 P2 S	553.4193	2.233	8	2.99	3.05	9.85
C27 H53 N5 O7 S	591.3657	1.831	14	1.56	1.52	10.16
C65 H103 N5	953.8205	9.838	10	3.13	3.31	10.52
C38 H49 O4 P	600.3383	4.839	7	3.11	3.19	10.53
C33 H63 N O8	601.4558	1.774	13	2.41	2.48	10.63
C32 H47 O2 P S	526.3038	3.432	19	2.56	2.59	10.79
C35 H59 N5 S	581.4506	2.48	6	3.13	3.32	10.88
C26 H48 N9 P	517.377	3.01	4	2.86	2.97	10.96
C24 H42 O6	426.2984	1.79	10	2.26	2.36	11.02
C29 H57 N3 O13	655.3878	2.172	17	2.44	2.34	11.06
C64 H111 N O4	957.8519	10.112	2	3.82	4.06	11.18
C28 H47 N5 O3	501.3669	1.784	25	1.84	1.91	11.29
C26 H56 N9 O2 P	557.4295	1.785	15	2.12	2.13	11.31
C41 H55 N O S2	641.3722	2.174	2	2.50	2.4	11.34
C42 H99 N10 O11 P3	1012.672	10.01	9	2.23	2.33	11.44
C18 H28 N6 O2	360.2278	1.801	8	2.00	2.11	11.45
C26 H45 N4 O P S	492.3065	1.785	23	2.71	2.85	11.60
C25 H54 N5 P S2	519.3563	2.505	23	3.76	3.72	11.60
C21 H38 N2 O	334.2986	3.171	7	4.31	4.03	11.86
C62 H105 N O4	927.8052	10.008	6	2.65	2.74	12.02
C26 H46 O7	470.3246	1.784	6	2.18	2.28	12.14
C29 H49 N5 O	483.3927	1.796	8	2.13	2.21	12.18
C26 H49 N O7	487.3512	1.783	4	2.14	2.24	12.21
C19 H52 N9 O3 P3	547.3394	1.816	14	1.58	1.65	12.32
C28 H53 N O8	531.3774	1.775	3	2.09	2.17	12.41
C28 H50 O8	514.3509	1.775	4	2.11	2.19	12.58
C32 H67 N O10	625.4769	2.462	8	2.65	2.61	12.70
C38 H35 N10 P	662.2789	3.426	21	2.91	3.01	12.72
C75 H155 N9 O14	1406.169	7.317	23	3.74	3.85	12.80
C32 H47 N9 O3	605.3814	2.013	13	2.47	2.55	13.10
C37 H59 N O3	565.4498	4.394	11	5.86	6.01	13.14
C36 H54 O2 P2	580.3589	1.765	12	2.40	2.42	13.17

	C36 H52 N P S	561.355	2.004	26	2.46	2.54	14.35
	C24 H49 N4 O7 P	536.3328	1.776	15	2.59	2.65	14.43
	C56 H99 N4 O8 P	986.722	7.164	24	4.31	4.2	14.44
	C16 H22	214.1722	10.008	17	2.50	2.63	14.52
	C22 H38 O5	382.2721	1.795	7	2.21	2.33	14.64
	C63 H107 N O4	941.8205	10.007	5	2.57	2.71	14.65
	C34 H56 N10 S2	668.4115	1.75	12	2.15	2.17	14.70
	C23 H50 N9 O P	499.3876	1.792	17	2.17	2.17	14.75
	C23 H44 O2	352.3343	2.372	13	1.32	1.3	14.85
	C33 H51 N4 P3	596.3331	1.762	8	2.52	2.53	15.28
	C90 H154 N4 O13 S	1531.122	4.626	8	7.13	7.25	15.30
	C63 H103 N O4	937.7895	9.669	15	3.16	3.2	15.41
	C27 H49 Cl O9	552.3068	1.772	9	2.38	2.49	15.44
	C51 H100 N3 O4 P3	911.6917	3.322	10	3.73	4.03	15.51
	C65 H111 N S2	969.8156	8.705	12	3.72	3.89	15.53
	C23 H56 N9 O5 P	569.4145	1.921	7	4.11	4.09	15.58
	C31 H60 N3 P S	537.4244	2.501	22	2.54	2.57	15.58
	C31 H69 N3 O3 P2	593.4812	4.394	24	3.59	3.88	15.64
	C28 H55 N5 O2	493.4346	2.168	22	2.51	2.56	15.67
	C64 H109 N O4	955.8358	10.007	6	2.48	2.62	15.83
	C15 H42 N9 P	379.33	2.181	29	1.58	1.52	15.86
	C27 H54 N6 S	494.4131	2.994	18	3.13	3.24	15.98
	C63 H105 N O5	955.8	8.704	17	3.93	3.99	16.23
	C26 H57 N10 O7 P S	684.3856	1.749	17	2.34	2.32	16.45
	C28 H61 N10 O9 P	712.4378	1.742	12	2.22	2.32	16.52
	C18 H32 N4 O2	336.2526	0.918	29	3.29	3.22	16.67
	C22 H40 N4 O2	392.3153	0.917	4	3.39	3.41	16.69
	C90 H153 N6 O10 P	1509.14	4.622	7	6.06	6.21	16.98
	C31 H58 N6 O P2 S	624.3852	1.758	8	2.27	2.38	17.20
	C18 H34 N4 O2 S	370.2411	1.556	8	3.98	3.68	17.25
	C19 H34 N2 O	306.2672	2.711	7	2.97	2.73	17.44
	C21 H38 N4 O2	378.2996	0.917	3	3.35	3.36	17.89
	C7 H8 N2 O4	184.0484	0.866	13	5.24	5.36	18.05
	C15 H18 O5	278.1157	0.892	5	3.77	3.86	18.71
	C16 H40 N10 O6 P2 S	562.2335	1.962	14	3.04	3.15	18.72
	C29 H68 N9 O7 P	685.4981	2.197	8	3.47	3.09	18.97
	C27 H65 N7 O P2 S	597.4456	2.22	15	2.62	2.35	18.99
	C27 H51 N5 O4	509.393	2.243	26	2.18	2.38	19.03
	C30 H65 N10 O10 P	756.4641	1.734	14	2.05	1.9	19.36
	C37 H39 O P3	592.2231	2.172	6	2.12	2.05	19.78
	C38 H86 N9 O3 P S2	811.6028	2.682	11	2.96	3.26	19.86

C23 H42 N2	346.3349	2.202	12	3.54	3.61	19.87
C16 H25 N3 O2	291.1948	0.918	4	2.28	2.21	19.93
C25 H60 N8 O16	728.4119	1.74	5	2.34	2.35	20.06
C32 H57 O4 P	536.3981	4.622	15	4.15	4.45	20.35
C39 H86 N9 O9 P	855.6289	2.644	9	3.34	3.64	20.49
C35 H79 N7 O2 P2 S	723.5502	2.775	7	1.95	2.05	20.67
C35 H41 N O6	571.2939	2.173	14	2.41	2.33	20.73
C16 H32 N6 O2	340.2591	2.19	22	1.60	1.66	20.88
C45 H79 N5 O P2	767.5764	2.725	19	2.91	3.07	21.38
C31 H53 N O7	551.3826	2.419	21	3.09	2.85	21.47
C37 H65 N5 P2	641.472	2.205	16	3.04	2.83	21.57
C20 H51 N9 O12 S	641.3359	1.896	5	4.04	4.53	21.60
C20 H52 N9 P	449.4083	2.182	9	1.54	1.36	21.95
C63 H107 O8 P	1022.769	4.617	11	4.82	4.94	22.02
C22 H45 N O3	371.3401	2.712	22	1.45	1.3	22.23
C31 H72 N9 O7 P	713.5296	2.428	16	2.00	1.82	22.65
C48 H109 N10 O12 P3 S	1142.717	2.119	8	4.83	4.41	23.11
C65 H111 N O4	969.8516	10.007	6	2.82	3.05	23.15
C48 H106 N9 O12 P3 S	1125.69	2.118	4	4.75	4.35	23.58
C30 H63 N O11	613.4406	1.911	10	3.38	3.27	23.69
C27 H43 N6 P3 S	576.2492	2.173	2	2.02	1.81	24.01
C87 H142 N6 O11 P2 S	1540.994	3.934	22	5.10	4.86	24.27
C32 H46 N4 O2	518.361	2.726	17	2.46	2.33	24.43
C30 H48 N2	436.3819	4.621	11	4.42	4.56	24.73
C31 H73 N7 O2 P2 S	669.5033	2.446	8	2.34	2.26	24.77
C37 H50 P2	556.338	2.695	22	2.30	2.27	25.21
C34 H50 N2 O3	534.3824	3.946	11	5.08	5.13	25.31
C45 H90 N2 O2	690.7007	3.907	29	3.53	3.83	26.08
C20 H36 N4 O2	364.2838	0.925	6	3.29	3.55	26.82
C22 H47 N	325.3711	2.962	20	2.54	2.16	26.94
C17 H44 N8 O10	520.3168	2.707	14	2.43	2.27	27.14
C62 H117 N5 O	947.9247	9.608	15	1.47	1.47	27.49
C17 H46 N9 O P	423.3562	2.17	15	1.38	1.31	27.92
C48 H101 N7 O P2	853.7532	2.899	9	1.36	1.55	29.27
C45 H61 N2 O P	676.4511	2.211	19	1.26	1.31	30.25
C29 H66 N5 O6 P S	643.4454	1.213	26	3.05	3.32	30.43
C32 H66 N2 O	494.5178	4.347	16	2.04	2.03	31.82
C20 H40 N6 O4	428.3116	2.171	26	1.52	1.45	31.88
C36 H75 N O11	697.5345	2.745	21	2.20	1.96	32.09
C20 H42 O5	362.3034	2.226	22	1.45	1.27	32.51
C20 H44 N3 O14 P S	613.2269	1.43	29	2.55	2.56	33.29

	C5 H12 N6 O12 P2	409.9988	0.779	22	1.37	1.21	33.31
	C19 H27 N9 O2	413.2293	1.384	10	4.10	4.84	33.66
	C23 H51 O7 P3	532.2858	1.475	3	8.16	7.61	34.33
	C22 H52 N4 P2	434.3663	3.944	16	3.95	3.96	34.56
	C27 H64 N9 O7 P	657.4668	1.902	9	2.28	2.16	36.25
	C22 H43 N	321.3397	2.643	11	2.71	3.02	37.07
	C3 H4 N2 O6 P2	225.955	4.531	15	1.58	1.56	37.11
	C55 H99 N7 O6 S2	1017.711	2.863	14	3.25	3.63	37.40
	C44 H62 N9 O6 P	843.4564	1.98	29	2.14	2.53	37.47
	C34 H57 O18 P	784.3284	1.381	24	2.31	1.84	37.71
	C16 H33 N O3	287.2461	1.517	20	2.79	2.69	38.34
	C30 H59 N O P2	511.4087	2.147	7	1.32	1.03	39.03
	C41 H81 N O	603.6323	4.926	10	2.62	2.49	39.36
	C35 H70 N5 O4 P	655.5156	1.696	12	3.71	3.02	41.28
	C53 H103 N9 O18 S	1185.712	2.122	20	4.19	3.65	41.75
	C42 H83 N5 O10	817.6135	2.441	22	1.71	1.41	41.77
	C26 H36 N5 P	449.2697	2.106	13	2.36	2.64	42.89
	C54 H103 N	765.8098	7.542	17	2.07	2.51	42.90
	C38 H75 N5 O8	729.5608	2.471	8	1.44	1.12	43.07
	C32 H52 P2 S	530.3275	1.881	16	2.31	2.3	43.79
	C34 H80 N9 O8 P	773.5871	2.458	6	1.33	1.03	44.03
	C56 H100 N7 O9 P3	1107.68	2.2	21	3.43	2.6	44.46
	C30 H72 N9 O6 P	685.5345	2.487	9	1.36	1.19	44.77
	C19 H41 N	283.324	2.297	7	2.50	2.71	44.79
	C49 H111 N10 O12 P3 S	1156.733	2.117	5	3.81	3.32	45.10
	C23 H49 N	339.3866	2.948	8	2.12	2.25	45.68
	C26 H51 N O	393.3973	4.362	16	1.86	1.85	46.16
	C55 H104 N3 O13 P3	1107.68	2.194	7	3.21	2.52	46.27
	C61 H106 N O14 P S	1139.706	2.117	6	3.68	3.18	47.25
	C21 H45 N	311.3553	2.574	18	1.90	1.97	47.57
	C41 H90 N9 O9 P	883.66	2.889	25	2.97	3.16	47.63
	C44 H97 N8 O6 P3	926.6754	4.642	15	3.30	3.41	47.91
	C30 H72 N9 O7 P	701.5294	2.231	16	1.68	1.65	48.15
	C47 H97 N7 O P2	837.7216	3.905	20	3.73	4.56	48.33
	C33 H71 N8 O2 P S	674.5141	3.008	16	2.27	2.83	48.64
	C45 H92 N2 O2	692.7163	3.927	15	3.93	4.6	49.27
	C41 H86 N5 O4 P	743.6435	3.91	20	2.54	2.97	49.57
	C18 H32 O	264.2454	2.218	13	1.95	2.06	49.73

Table A.3: Lipidomics results of detergent-solubilized CFTR and analysis results.
The abbreviation FC is the fold change. For these listed features, only molecular weight and retention time (RT) can be determined, and thus determined at a level 5 confidence.

Name	Formula	Molecular Weight	RT [min]	RSD QC Areas [%]	Ave. FC	Med. FC	CV of FC
		1103.648	3.912	18	3.37	3.37	0.17
		169.9792	4.421	25	5.92	5.90	0.49
		913.7894	10.006	8	2.98	2.97	1.69
		1723.43	9.836	10	4.27	4.26	1.89
		1990.451	4.609	8	4.18	4.16	2.19
		1022.683	2.87	20	3.37	3.32	3.20
		457.3406	1.79	24	2.09	2.06	3.80
		1810.552	10.007	14	6.13	6.05	3.85
		1727.461	10.009	7	4.74	4.75	3.91
		258.2692	1.665	17	3.19	3.25	4.21
		1956.455	3.905	8	5.97	5.83	4.65
		1811.555	10.002	13	5.14	5.10	4.82
		1989.448	4.612	12	3.84	3.74	4.82
		1955.452	3.904	4	6.21	6.20	4.83
		645.4821	1.765	26	2.82	2.76	4.83
		969.7141	3.909	8	5.42	5.34	4.89
		279.2539	1.676	18	1.72	1.71	4.97
		1520.015	3.9	10	3.33	3.42	5.03
		220.9817	4.513	6	3.10	3.18	5.14
		1796.536	10.006	17	5.34	5.32	5.35
		1797.54	10.003	7	5.24	5.21	5.37
		1957.458	3.903	7	5.19	5.26	5.61
		1799.546	9.997	9	4.68	4.60	5.63
		1812.558	10.004	8	4.45	4.41	5.67
		485.372	1.791	19	2.07	2.09	6.13
		1090.67	2.881	26	3.82	3.92	6.19
		611.3179	2.126	10	1.82	1.87	6.24
		258.2349	10.005	7	2.54	2.50	7.40
		1228.635	3.309	8	3.70	3.73	7.61
		592.3357	3.019	16	2.44	2.48	7.75
		1148.647	10.009	18	2.78	2.79	8.29
		981.9459	7.329	16	1.86	1.90	8.49
		366.3288	8.542	18	2.56	2.58	8.80
		1982.389	3.903	13	4.07	3.95	9.34
		539.3592	2.7	8	1.47	1.46	9.88

		470.3804	1.811	1	2.03	2.08	10.03
		1022.683	2.875	28	3.45	3.53	10.46
		973.7648	8.93	15	3.77	3.63	10.83
		1960.404	3.899	28	3.62	3.82	12.55
		689.5083	1.759	6	3.12	3.24	12.63
		349.246	1.472	22	3.25	3.39	13.16
		516.3614	2.737	13	2.17	2.03	13.64
		366.3288	8.804	20	2.04	2.09	14.42
		1035.66	3.934	19	2.64	2.53	14.83
		271.2876	1.882	8	1.77	1.77	15.00
		1983.392	3.904	18	3.54	3.59	15.61
		990.7295	9.477	19	2.54	2.60	16.27
		1057.796	8.423	14	2.69	2.89	17.00
		955.7994	9.424	16	2.23	2.31	17.05
		614.3175	3.029	13	2.03	2.08	18.30
		1070.775	2.518	19	1.78	1.93	20.19
		435.2848	1.388	22	3.07	3.27	20.66
		1044.751	4.626	12	5.05	5.21	21.25
		3405.6	4.512	16	3.14	3.08	21.54
		228.1879	10.021	21	2.59	2.87	22.60
		1967.527	4.524	20	1.48	1.38	22.73
		1143.72	2.114	10	4.55	4.10	24.31
		188.1565	4.542	27	1.21	1.14	24.47
		653.5083	2.769	20	2.03	2.20	24.82
		1510.144	4.621	9	4.13	4.13	26.25
		386.3744	10.024	10	2.81	3.21	29.32
		481.3982	2.178	21	1.39	1.31	30.31
		997.8944	3.001	21	2.97	3.02	30.38
		383.3554	3.897	13	2.55	2.91	31.76
		423.4078	4.609	24	1.77	1.81	32.83
		582.6432	2.079	7	2.13	2.28	34.27
		1382.947	5.04	27	1.27	1.08	34.79
		562.325	2.717	21	2.73	3.08	34.96
		374.351	1.67	26	1.77	1.70	35.71
		371.3544	4.51	12	1.29	1.08	36.19
		551.592	3.825	27	1.56	1.46	36.32
		1018.713	2.863	11	2.49	2.75	37.77
		340.39	2.965	27	2.69	2.92	39.43
		316.2016	1.798	22	1.71	1.39	39.44
		455.2142	1.057	29	1.62	1.69	42.45
		237.2457	1.037	21	1.40	1.44	43.64

		1742.721	9.97	14	3.29	4.02	46.83
		639.3465	1.488	29	1.92	1.40	48.73
		386.3591	4.614	21	2.99	3.41	49.11
		517.3324	2.523	23	1.80	1.94	49.90

Table A.4: Lipidomics results of CFTR-SMALPs and analysis results. The abbreviation FC is the fold change. These features determined at a confidence level of 4 with the identification of the formulas only.

Name	Formula	Molecular Weight	RT [min]	RSD QC Areas [%]	Ave. E1	Ave. E2	Ave. E3	Med. E1	Med. E2	Med. E3	CV of FC E1	CV of FC E2	CV of FC E3
	C19 H36 N7 O16 P3 S2	775.0873	5.622	13	7.17	6.88	7.24	7.12	6.86	7.21	0.24	10.56	8.42
	C60 H124 N5 P	945.9598	12.377	9	2.58	2.60	2.37	2.51	2.53	2.47	0.37	26.40	12.68
	C38 H79 N O	565.6154	5.173	9	2.22	2.17	2.25	2.21	2.20	2.23	0.49	9.39	8.57
	C18 H38 N2 O2	314.2926	0.896	17	2.36	0.37	2.37	2.40	0.73	2.35	0.49	45.47	13.14
	C27 H44	368.3435	11.256	2	9.95	9.96	9.92	9.95	10.08	9.94	0.64	15.66	2.03
	C29 H53 O2 P S	496.3521	5.825	14	2.53	2.30	2.58	2.51	2.33	2.55	0.69	5.80	8.15
	C24 H56 N7 O9 P S	649.3624	2.296	22	2.26	1.40	2.29	2.31	1.51	2.30	0.76	38.50	3.51
	C27 H39 N O6	473.2771	2.062	15	9.93	8.66	10.04	9.89	8.77	9.90	0.76	25.95	20.94
	C23 H53 N7 O2	459.4258	3.884	19	2.33	2.48	2.44	2.47	2.43	2.49	0.77	9.33	7.32
	C28 H46	382.3592	11.365	15	2.99	3.12	3.19	3.06	3.54	3.15	0.78	43.68	9.30
	C46 H92 Cl N2 O2 P3	832.6068	5.129	3	4.14	4.10	4.11	4.17	4.29	4.14	0.79	24.37	13.49
	C46 H75 O8 P	786.5193	5.182	9	4.81	4.83	4.76	4.81	4.60	4.80	0.97	31.25	6.60
	C18 H43 N6 O5 P	454.3054	3.974	7	1.72	1.52	1.59	1.76	1.52	1.63	1.05	10.35	8.56
	C43 H73 O10 P	780.495	5.465	9	1.01	1.04	1.12	1.00	1.01	1.02	1.07	6.51	15.16
	C42 H83 N2 O8 P	774.5857	5.619	6	11.29	11.35	11.28	11.30	11.39	11.27	1.12	6.27	1.86
	C53 H110 N2 O6	870.8362	9.624	22	6.07	5.88	6.04	6.07	5.74	6.05	1.13	27.90	2.46
	C33 H62 O4	522.4639	9.627	3	6.00	5.85	5.95	5.97	5.76	5.92	1.14	11.53	3.67
	C42 H83 N O4	665.6313	6.574	8	2.08	1.92	2.15	2.11	2.06	2.55	1.23	31.79	46.87
	C23 H54 N5 P3	493.3609	2.314	5	5.03	4.18	5.02	4.99	4.27	4.99	1.23	36.16	5.79
	C47 H80 O7 S	788.5631	3.864	5	4.79	4.66	4.82	4.82	4.70	4.82	1.23	9.66	1.00

Formula	Mass											
C81 H166 N8 O12 P2	1505.21	5.615	4	10.45	10.42	10.49	10.46	10.62	10.47	1.29	22.88	1.79
C20 H47 N10 O3 P	506.3579	3.401	14	3.19	2.77	3.20	3.24	2.71	3.23	1.52	15.60	11.31
C35 H71 N O4	569.539	9.624	6	7.79	7.65	7.72	7.81	7.60	7.75	1.53	7.68	3.72
C30 H47 N O4	485.3519	2.666	18	2.96	2.93	3.06	2.93	2.91	3.04	1.64	5.94	8.39
C49 H73 N O6	771.5402	3.547	17	1.66	1.30	1.76	1.66	1.34	1.81	1.67	6.87	22.68
C54 H101 N3 O3 P2	901.7321	9.624	8	6.72	6.72	6.74	6.75	6.74	6.72	1.71	2.50	4.40
C20 H46 N5 O2 P	419.337	3.061	7	2.63	2.33	2.79	2.70	2.10	2.86	1.76	35.82	15.63
C48 H93 O8 P	828.6569	5.206	10	4.08	4.18	4.25	4.13	4.17	4.18	1.76	15.03	10.81
C29 H54 N O11 P S	655.3176	2.36	7	1.59	0.84	1.68	1.67	1.01	1.68	1.79	25.79	3.72
C34 H47 N O6	565.3413	3.471	19	2.37	1.90	2.53	2.41	1.98	2.58	1.80	14.82	23.54
C31 H70 N8	554.5731	7.628	6	5.63	5.57	5.64	5.65	5.59	5.64	1.87	6.07	1.37
C18 H35 N O4	329.2557	2.29	11	2.15	1.30	2.23	2.22	1.42	2.20	1.90	36.05	3.64
C28 H36 N6 O2 S	520.261	2.314	17	2.09	1.24	2.17	2.16	1.37	2.15	1.91	35.88	3.81
C25 H53 N	367.4171	3.458	3	2.61	2.58	2.67	2.62	2.65	2.68	1.94	9.84	7.59
C53 H104 N O8 P	913.7494	9.08	4	2.21	2.11	2.18	2.20	2.10	2.21	1.96	5.60	3.76
C27 H56 N6 S	496.4268	2.314	9	2.07	1.21	2.15	2.14	1.35	2.12	1.97	35.79	3.90
C50 H104 N2 O6	828.7895	9.623	5	13.79	13.61	13.76	13.79	13.58	13.76	2.01	7.70	0.43
C77 H159 N7 O16 P2	1500.132	5.203	22	2.86	2.70	3.04	2.96	2.55	3.03	2.02	20.74	15.30
C40 H86 N5 O12 P	859.6011	4.452	2	3.16	3.32	3.08	3.17	3.64	3.09	2.04	39.07	3.39
C42 H83 N5 O5	737.6393	4.611	4	4.95	4.94	4.96	4.94	4.95	4.96	2.05	1.93	0.96
C35 H71 N O4	569.539	5.208	3	7.74	7.69	7.73	7.77	7.75	7.78	2.05	6.50	6.09
C37 H74 N4 O13	782.5252	8.07	15	6.50	6.23	6.46	6.42	6.06	6.45	2.07	37.41	7.55
C47 H95 N4 P3	808.6767	4.669	3	2.77	2.60	2.69	2.79	2.61	2.70	2.08	4.80	1.90
C15 H33 N4 O14 P	524.1723	2.316	13	2.06	1.97	2.13	2.12	1.77	2.18	2.09	40.49	12.13
C63 H97 N O6	963.731	9.622	9	4.78	4.83	4.84	4.77	4.79	4.82	2.16	7.17	3.92
C20 H33 N7 O	387.2763	2.32	22	1.55	0.67	1.62	1.60	0.83	1.59	2.18	35.64	4.09

	C23 H40 N O7 P	473.2561	2.296	13	2.01	1.17	2.07	2.07	1.26	2.05	2.22	36.69	3.36
	C50 H75 N O6	785.5603	3.858	5	4.93	4.74	4.93	4.98	4.78	4.95	2.23	7.49	1.98
	C11 H19 N7	249.1702	3.137	12	4.46	4.25	4.54	4.50	4.28	4.51	2.23	12.48	9.71
	C42 H87 Cl N5 O2 P	759.6287	10.55	3	7.75	7.65	7.72	7.64	7.56	7.72	2.24	12.14	1.03
	C21 H36 N O7 P	445.2249	2.284	1	1.99	1.08	2.00	2.03	1.27	2.01	2.27	35.62	4.32
	C24 H55 N7 O S	489.4177	6.482	16	2.76	2.70	2.81	2.89	2.67	2.80	2.31	11.26	7.41
	C42 H80 N O8 P	757.5611	3.506	14	5.64	5.13	5.59	5.63	5.00	5.30	2.33	43.16	37.52
	C26 H53 N6 O3 P	528.3913	2.642	3	11.29	11.25	11.24	11.37	11.23	11.27	2.35	3.11	5.82
	C46 H79 O10 P	822.5421	5.227	13	6.65	6.66	6.57	6.66	6.85	6.52	2.41	24.38	7.63
	C44 H57 Cl N9 O P3 S2	919.3036	7.755	8	2.58	2.42	2.68	2.58	2.45	2.67	2.42	4.19	1.76
	C46 H90 N O2 P S2	783.616	4.775	12	1.52	1.25	1.66	1.55	1.05	1.62	2.45	31.26	5.68
	C27 H51 P3	468.3211	4.383	4	2.75	2.82	2.74	2.81	2.79	2.62	2.50	4.53	16.05
	C63 H133 N3 O2 P2	1025.987	11.249	2	8.95	8.94	8.96	8.95	8.98	9.01	2.50	6.46	5.73
	C39 H77 N2 O8 P	732.54	5.886	9	4.42	4.34	4.53	4.44	4.34	4.48	2.50	2.52	8.09
	C39 H81 N3 O2	623.6323	6.651	4	1.88	1.29	1.71	1.89	1.31	1.66	2.51	13.63	22.07
	C25 H54 N2 O P2 S	492.3422	3.928	11	2.91	2.65	2.91	2.93	2.66	2.91	2.53	0.81	2.24
	C49 H75 N O6	773.5563	3.532	12	1.50	1.24	1.62	1.50	1.26	1.72	2.65	3.21	19.32
	C43 H95 N9 O5 S	849.7182	9.629	14	8.13	8.07	8.20	8.10	8.03	8.16	2.67	10.60	9.07
	C26 H42 O4	418.3077	3.892	9	3.62	3.50	3.56	3.60	3.58	3.59	2.71	20.60	7.62
	C22 H49 N7 O8	539.3666	2.275	6	3.84	2.79	3.98	3.94	3.05	4.01	2.72	47.51	8.20
	C56 H116 N2 O6	912.8831	9.623	3	9.75	9.49	9.70	9.73	9.51	9.69	2.72	6.05	1.79
	C19 H39 N O4	345.2873	2.366	14	1.18	0.41	1.18	1.25	0.64	1.29	2.76	25.82	13.97
	C29 H28 O2	408.2082	2.301	12	2.07	1.24	2.11	2.12	1.31	2.10	2.78	36.86	3.15
	C28 H46 O4	446.339	4.384	4	2.32	2.32	2.29	2.37	2.34	2.25	2.79	3.33	6.95
	C27 H44 N O7 P	525.2851	2.317	8	1.82	0.91	1.87	1.85	1.09	1.85	2.80	35.44	4.45
	C27 H53 O12 P	600.3264	2.625	6	5.95	5.97	5.96	6.01	5.96	5.97	2.84	6.47	3.47

	C35 H77 N7 O7 P2	769.5364	5.594	23	7.24	7.12	7.09	7.34	7.18	7.02	2.88	16.18	20.15
	C36 H84 N10 O S5	832.5444	5.626	23	6.44	6.33	6.29	6.54	6.38	6.22	2.88	16.05	20.26
	C15 H44 N10 O P2	442.3186	2.706	2	8.33	8.35	8.34	8.40	8.33	8.35	2.92	3.46	3.07
	C21 H37 N O3	351.2768	2.31	18	2.22	1.39	2.28	2.47	1.45	2.31	2.92	36.96	4.83
	C39 H82 N9 O6 P	803.6118	3.557	15	0.99	0.68	0.98	1.01	0.70	1.03	2.93	5.71	14.77
	C33 H73 N10 O4 P	704.5542	5.896	6	2.04	2.03	2.08	2.11	2.09	2.10	2.96	10.49	2.77
	C17 H37 N O	271.2869	10.093	11	1.29	0.49	1.01	1.17	0.09	0.99	2.97	41.33	10.54
	C31 H68 N8 O	568.554	4.156	6	3.12	3.15	3.16	3.19	3.13	3.16	3.05	3.23	1.63
	C22 H48 N2 O4 S2	468.3061	2.37	17	1.71	0.96	1.88	1.78	1.18	1.84	3.10	29.17	9.61
	C42 H82 N O8 P	759.5815	5.206	3	8.16	8.11	8.20	8.19	8.12	8.17	3.10	4.22	6.96
	C25 H43 O6 P S	502.2501	2.312	22	2.08	1.25	2.12	2.13	1.31	2.10	3.12	37.10	3.06
	C36 H72 N2 O2	564.5588	7.352	3	1.03	0.59	1.05	1.06	0.59	1.06	3.12	8.10	10.31
	C49 H52 O8	768.3654	2.304	7	1.96	1.03	2.00	1.98	1.23	1.98	3.15	35.38	4.62
	C29 H64 N10 O6	648.499	2.669	17	2.78	2.59	2.95	2.90	2.59	2.94	3.21	20.14	17.79
	C42 H75 N3 O3 P2	731.5277	8.064	13	4.96	4.87	5.33	4.84	4.59	5.33	3.23	36.91	19.64
	C38 H75 N6 O4 P	710.5581	5.89	2	5.66	5.63	5.70	5.68	5.63	5.68	3.23	4.87	6.04
	C82 H97 N8 O18 P S4	1640.554	9.622	4	7.74	7.48	8.72	7.70	7.47	8.39	3.25	5.21	45.29
	C14 H27 O7 P	338.1499	2.321	5	1.92	0.98	1.96	1.94	1.19	1.94	3.29	35.36	4.69
	C11 H33 N10 O P	352.2584	3.076	4	7.23	6.61	7.33	7.27	6.45	7.42	3.33	27.31	13.38
	C23 H58 N9 O P	507.4499	3.992	5	2.05	2.03	2.14	2.12	2.00	2.10	3.36	3.63	7.62
	C41 H47 N10 O5 P	790.3481	2.288	10	2.19	1.36	2.22	2.24	1.41	2.21	3.37	37.26	3.00
	C19 H41 Br P2	410.1874	1.885	21	3.17	2.53	3.38	3.22	2.36	3.17	3.38	31.47	29.77
	C37 H80 N10 O9 S	840.5824	5.671	12	7.53	7.45	7.66	7.53	7.45	7.65	3.39	6.15	2.30
	C36 H75 N5 O11 S	785.5162	5.21	7	6.51	6.39	6.45	6.49	6.25	6.45	3.43	18.90	1.51
	C27 H55 N	393.4331	3.329	9	3.28	1.74	2.95	3.29	1.80	2.97	3.46	29.02	21.52
	C28 H25 N6 O18 P	764.0963	5.619	6	6.83	6.93	6.88	6.86	6.66	6.87	3.56	38.25	3.02

	C33 H38 S3	530.2154	2.311	19	2.00	1.17	2.03	2.05	1.22	2.02	3.57	37.41	2.96
	C28 H52 N O7 P	545.3499	2.316	15	2.26	1.31	2.29	2.27	1.53	2.27	3.59	35.34	4.83
	C24 H51 N O2	385.3914	2.827	12	1.64	0.14	1.34	1.56	0.17	1.21	3.60	37.64	29.81
	C53 H105 Cl N6 O3	908.7939	9.083	6	2.46	2.18	2.38	2.43	2.22	2.40	3.61	6.23	2.88
	C49 H82 N O8 P	843.5767	5.631	19	5.62	5.71	5.82	5.66	5.60	5.80	3.61	17.94	7.34
	C40 H78 N O10 P	763.5335	5.217	9	6.31	6.17	6.28	6.32	6.15	6.27	3.62	3.92	1.72
	C24 H42 N O9 P	519.2599	2.309	24	2.41	1.59	2.44	2.46	1.63	2.43	3.67	37.49	2.95
	C46 H92 N2 O2	704.7157	7.844	11	1.72	1.81	1.67	1.73	1.81	1.73	3.70	9.50	7.97
	C40 H82 N5 O P	679.6248	11.245	6	8.52	8.51	8.51	8.52	8.45	8.52	3.70	16.79	2.31
	C47 H79 O10 P	834.5422	5.62	25	4.44	4.23	4.26	4.45	4.23	4.39	3.80	1.53	15.93
	C19 H37 N O	295.2869	1.932	13	2.16	0.28	1.59	2.00	0.55	1.59	3.81	41.95	6.21
	C15 H41 N9 O P2	425.2921	2.706	6	6.27	6.17	6.25	6.32	6.19	6.26	3.84	6.31	4.96
	C22 H41 N4 O3 P	440.2897	3.866	6	3.84	3.79	3.80	3.84	3.88	3.81	3.87	31.57	8.05
	C47 H89 Cl2 N O P2	815.5798	5.124	6	4.51	4.55	4.49	4.58	4.61	4.53	3.87	8.01	10.80
	C39 H81 N7 O7	759.6197	5.177	4	8.35	8.51	8.26	8.39	8.67	8.23	3.88	23.95	3.97
	C30 H66 N10 O6	662.5149	2.676	20	2.63	2.60	2.70	2.68	2.58	2.76	3.90	12.93	11.75
	C32 H52 N6 S	552.3997	3.85	11	2.59	2.45	2.42	2.61	2.43	2.47	4.00	14.13	20.37
	C52 H83 N4 O2 P S	858.5977	4.382	9	3.39	3.46	3.37	3.35	3.50	3.34	4.01	13.73	7.49
	C24 H38 O4	390.2761	3.453	3	1.61	1.58	1.57	1.60	1.57	1.56	4.04	2.75	2.43
	C41 H78 N O7 P	727.5493	5.923	4	4.13	4.10	4.22	4.17	4.09	4.20	4.05	2.95	9.91
	C21 H33 O7 P	428.1977	1.884	16	3.06	2.48	3.26	3.13	2.29	3.03	4.06	34.68	30.18
	C25 H52 N6 S	468.3957	2.308	4	1.77	0.80	1.79	1.77	1.04	1.77	4.08	35.32	5.06
	C16 H41 N10 O P	420.3209	3.869	4	2.49	2.56	2.54	2.54	2.56	2.54	4.09	5.88	1.02
	C27 H50 N O7 P	531.3345	2.283	10	2.11	1.16	2.11	2.12	1.38	2.12	4.12	37.43	5.22
	C50 H101 N O6	811.7629	9.623	7	11.16	11.01	11.15	11.16	10.95	11.12	4.12	9.01	4.14
	C46 H84 Cl N7 O2 S	833.6099	5.129	4	3.34	3.29	3.35	3.47	3.44	3.41	4.14	22.04	11.61

C27 H55 N O8	521.3922	2.316	2	3.35	2.53	3.35	3.43	2.64	3.37	4.14	38.55	2.49
C16 H30 N O7 P	379.1764	2.321	11	1.89	0.91	1.90	1.88	1.15	1.89	4.15	35.32	5.09
C37 H75 N O	549.5846	5.515	2	1.10	0.45	0.73	1.07	0.19	0.81	4.16	43.08	12.38
C37 H71 N O5	609.532	7.314	5	8.32	8.40	8.30	8.36	8.46	8.30	4.18	16.07	0.96
C26 H54 N6 S	482.4113	2.323	4	1.98	1.01	1.99	1.98	1.24	1.98	4.18	35.33	5.11
C42 H78 N O8 P	755.5453	5.213	6	7.38	7.36	7.41	7.41	7.37	7.41	4.22	0.89	1.18
C16 H35 N9 S	385.2722	2.19	5	2.99	1.91	3.18	3.06	1.99	3.16	4.22	43.42	15.18
C37 H81 N9 O5 S	763.6088	5.131	12	5.59	5.60	5.57	5.64	5.62	5.57	4.24	5.24	2.44
C29 H65 N7 O2 S	575.4906	4.385	7	2.33	2.36	2.46	2.39	2.38	2.45	4.25	4.19	3.23
C31 H65 N3 O	495.5126	3.891	7	2.81	2.56	2.74	2.81	2.59	2.74	4.26	11.78	1.11
C42 H89 N2 O8 P	780.6356	5.135	12	6.74	6.75	6.71	6.79	6.77	6.71	4.29	5.59	2.13
C44 H87 N O4	693.6629	8.279	16	1.02	0.91	1.27	1.04	0.88	1.26	4.30	11.55	2.70
C33 H41 N O3	499.3082	2.281	10	2.10	1.15	2.15	2.13	1.40	2.13	4.31	35.53	5.37
C45 H75 N O7	741.5516	5.204	8	7.86	7.80	7.88	7.90	7.81	7.88	4.35	0.52	4.08
C34 H69 N O3	539.5268	5.598	9	2.60	2.58	2.57	2.62	2.66	2.56	4.36	10.63	3.38
C41 H87 N3 S2	685.6347	8.27	15	1.00	1.14	0.90	1.04	1.48	0.90	4.36	40.25	5.83
C53 H109 N2 O9 P	948.7875	6.662	13	3.41	3.35	3.63	3.38	3.21	3.70	4.36	17.50	12.03
C33 H63 N3 O	517.4966	3.889	7	2.03	1.78	1.96	2.04	1.80	1.96	4.39	11.22	1.15
C31 H46 N4	474.3703	5.813	6	2.72	2.30	2.93	2.74	2.34	2.93	4.45	10.22	31.87
C21 H40 N2	320.3186	2.825	8	1.38	0.18	1.13	1.25	0.40	1.08	4.47	28.35	10.56
C23 H44 O5	400.3179	2.792	29	3.38	2.48	3.50	3.60	2.29	3.53	4.52	33.10	22.39
C69 H86 O S	962.6402	8.343	8	2.57	2.50	2.48	2.60	2.46	2.55	4.52	7.08	7.83
C27 H53 N O5	471.3911	2.744	15	2.89	2.83	2.87	2.92	2.70	2.95	4.52	17.02	10.54
C26 H50 N O7 P	519.3323	2.36	15	1.78	1.53	1.96	1.84	1.44	1.90	4.53	30.75	9.97
C28 H43 N	393.339	4.778	8	1.77	1.28	1.86	1.78	1.37	1.89	4.53	28.52	4.23
C41 H74 N8 O5	758.5778	5.199	3	9.93	9.89	9.97	9.97	9.88	9.96	4.53	2.46	4.36

C43 H62 N O11 P	799.407	2.321	15	2.06	1.08	2.08	2.06	1.33	2.06	4.62	35.35	5.30
C39 H69 N O6	647.5118	5.472	8	3.09	3.29	3.02	3.08	3.28	3.06	4.63	11.71	5.37
C33 H73 N9	595.6009	6.65	8	2.56	2.27	2.49	2.65	2.25	2.55	4.63	18.93	14.69
C26 H41 N7 O2	483.3342	2.601	14	1.44	0.37	1.34	1.42	0.33	1.53	4.66	21.38	37.24
C33 H77 N9 O2 P2 S3	789.4866	8.11	19	3.84	3.67	3.82	3.88	3.67	3.67	4.66	6.41	21.32
C36 H74 N2	534.5844	5.561	19	2.61	1.21	2.21	2.61	1.31	2.19	4.66	39.03	13.38
C57 H115 N3 O4 P2 S	999.8091	7.314	16	4.13	4.31	4.09	4.20	4.25	4.12	4.67	9.88	5.00
C30 H50 N O7 P	567.3319	2.318	12	1.92	0.94	1.93	1.92	1.19	1.92	4.69	35.35	5.33
C15 H20	200.156	11.259	10	3.43	3.68	3.22	3.42	3.66	3.25	4.70	23.42	5.01
C20 H32 N9 O P	445.2454	1.341	20	6.88	6.44	7.02	7.00	6.59	6.98	4.73	35.36	49.26
C21 H40 N8 O3 S	484.2951	4.377	10	3.20	3.29	3.18	3.23	3.28	3.22	4.76	3.42	4.90
C26 H53 N O8	507.3766	2.315	3	3.75	2.77	3.71	3.81	2.95	3.71	4.78	37.63	2.28
C36 H72 N6 O	604.5766	7.314	4	7.38	7.44	7.35	7.46	7.44	7.34	4.78	7.70	3.09
C47 H71 N O6	745.5247	3.529	10	1.54	1.27	1.59	1.50	1.27	1.68	4.79	4.12	20.44
C34 H74 N3 O2 P	587.5502	7.315	3	6.68	6.75	6.66	6.73	6.79	6.65	4.80	13.39	1.92
C35 H52 O S	520.3737	4.508	5	2.96	2.79	2.92	3.02	2.97	2.91	4.82	21.50	6.28
C39 H82 Cl N3 O10	787.5701	4.023	12	3.11	3.12	3.05	3.12	3.12	3.06	4.83	5.64	3.08
C49 H83 N3 O S	761.6256	10.55	4	5.65	5.55	5.60	5.68	5.57	5.60	4.83	2.22	6.15
C60 H125 N6 P S	992.9427	2.69	28	0.11	0.58	0.08	1.28	0.73	0.08	4.83	44.18	22.97
C26 H49 N	375.3874	5.571	15	6.27	6.28	6.24	6.28	6.20	6.26	4.84	18.49	2.47
C27 H40 O2	396.3021	2.337	25	2.16	1.78	2.25	2.23	1.58	2.24	4.91	42.41	3.04
C19 H38 O4	330.2764	2.335	16	2.12	1.34	2.20	2.19	1.39	2.18	4.94	36.95	4.23
C87 H143 N9 O12	1506.086	5.205	21	2.39	2.34	2.32	2.32	2.32	2.28	4.95	3.99	20.16
C33 H59 N O2	501.4539	7.081	15	1.79	1.25	2.04	1.81	1.14	1.98	4.96	42.51	29.72
C53 H89 P	756.6699	10.55	7	5.78	5.51	5.82	5.77	5.41	5.84	4.96	19.15	4.48
C18 H41 N4 O4 P S2	472.2289	2.305	16	2.33	1.54	2.34	2.39	1.53	2.35	4.96	38.41	2.82

	C44 H77 O8 P	764.5369	5.249	4	5.94	5.94	5.94	5.97	6.17	5.97	4.97	25.95	3.30
	C25 H62 N9 O2 P	551.4758	3.935	6	2.03	1.95	2.03	2.10	1.96	2.05	4.97	5.46	6.69
	C57 H96 O15 P2 S	1114.595	3.512	9	5.81	3.03	5.69	5.80	3.22	5.78	4.98	40.86	43.52
	C37 H73 N O6	627.5424	5.4	22	2.21	1.49	2.40	2.52	1.39	2.66	5.03	43.36	28.40
	C65 H65 Cl2 N O13 S2	1201.327	8.025	6	1.22	1.07	1.25	1.16	0.90	1.31	5.07	42.31	14.12
	C85 H166 N3 O16 P	1516.201	5.625	14	4.77	4.78	4.81	4.84	4.61	4.80	5.08	22.63	4.34
	C19 H40 N2 O5 S	408.2654	2.7	10	2.18	1.86	2.02	2.20	1.80	2.06	5.08	9.38	10.96
	C29 H66 N10 O	570.5423	5.206	3	5.93	5.86	5.86	5.95	5.90	5.90	5.11	7.32	5.62
	C7 H15 Br3 Cl2 N5 O11 P3 S4	872.5798	1.481	17	1.59	0.81	1.32	1.70	0.85	1.41	5.14	23.28	11.97
	C63 H114 Cl P S	968.8067	9.187	16	1.55	1.40	1.54	1.43	1.35	1.54	5.14	7.69	5.84
	C18 H42 N9 O2 P	447.3192	2.429	25	5.29	5.11	5.30	5.34	5.11	5.23	5.17	34.48	13.06
	C13 H23 N O2	225.1725	3.133	22	1.61	1.25	1.49	1.46	1.28	1.49	5.20	2.93	8.09
	C54 H112 N O2 P S	869.815	9.622	8	4.21	4.11	4.31	4.29	4.05	4.30	5.21	23.20	2.50
	C45 H89 N3 O3 P2	781.6384	5.135	2	5.93	5.84	5.89	5.98	5.91	5.91	5.23	10.49	5.04
	C27 H56 N2 O	424.4386	3.832	9	2.14	0.59	1.64	2.09	0.83	1.68	5.25	28.92	17.68
	C41 H90 Br Cl N8 O	824.6109	10.472	22	5.43	5.21	5.37	5.44	5.25	5.43	5.26	13.57	7.30
	C13 H29 N8 O2 P	360.2141	2.431	11	4.16	4.14	4.18	4.26	4.15	4.12	5.28	2.73	7.86
	C52 H97 N2 P	780.7387	9.671	23	1.00	0.71	0.94	1.04	0.79	0.95	5.28	22.50	1.06
	C10 H31 N10 O8 P3 S	544.1255	3.079	13	0.92	0.54	0.84	1.08	0.41	0.77	5.29	18.41	10.24
	C23 H47 N6 O3 P	486.3446	2.662	2	8.70	8.78	8.80	8.67	8.79	8.81	5.32	2.33	2.28
	C46 H60 N P	657.4454	3.136	7	3.06	1.91	3.21	3.08	2.15	3.21	5.32	39.60	8.10
	C46 H75 N O7	753.5536	4.494	20	3.46	2.54	3.40	3.48	2.36	3.60	5.33	37.48	44.48
	C26 H41 N3 O8 P2	585.2392	2.353	15	1.87	1.24	1.99	1.98	1.22	1.96	5.34	27.47	6.54
	C18 H34 O3	298.2502	7.317	18	2.57	2.70	2.72	2.55	2.72	2.73	5.34	2.47	3.11
	C39 H84 N6 O14	860.6044	4.449	4	3.15	3.24	3.04	3.23	3.60	3.09	5.35	43.82	7.19

C27 H26 O3	398.1875	1.884	26	2.84	2.02	3.02	2.94	1.99	2.78	5.36	16.14	33.29
C30 H49 N O4	487.3675	2.749	15	3.68	3.65	3.58	3.81	3.59	3.67	5.42	11.21	14.65
C29 H43 N O	421.3337	3.918	10	1.72	1.70	1.81	1.82	1.71	1.75	5.42	5.27	8.74
C24 H53 N7 O6	535.4078	2.316	3	3.56	2.72	3.50	3.60	2.80	3.49	5.45	37.96	1.74
C34 H68 N2 O2	536.5276	6.648	3	2.43	1.86	2.32	2.42	1.91	2.38	5.47	10.90	9.08
C36 H73 N	519.5739	4.637	7	1.49	0.37	1.38	1.48	0.71	1.31	5.55	41.92	9.69
C22 H46 N O7 P	467.3006	1.856	6	3.20	2.97	3.38	3.17	3.21	3.21	5.63	30.59	29.15
C27 H62 N9 O5 P	623.4613	1.813	11	3.85	3.72	3.97	3.86	3.63	3.76	5.64	10.76	27.93
C42 H88 N2 O	636.6889	8.899	3	2.00	0.59	1.83	1.97	0.82	1.87	5.64	42.66	8.16
C36 H70 N O10 P	707.4724	3.552	20	1.11	0.88	1.18	1.16	0.79	1.21	5.67	13.57	10.28
C20 H36 N O7 P	433.2247	1.876	19	3.05	2.50	3.28	3.09	2.28	3.06	5.68	32.60	33.11
C20 H43 N9 O2 S	473.3278	1.949	12	2.47	1.74	2.59	2.49	1.65	2.46	5.73	18.28	29.09
C12 H37 N10 O P	368.2899	3.034	8	4.49	3.88	4.48	4.46	4.13	4.73	5.73	29.04	39.56
C12 H37 N10 O P	368.2899	3.097	8	4.29	3.69	4.28	4.26	3.93	4.54	5.73	28.95	39.56
C15 H12 O	208.0883	2.287	14	1.77	0.90	1.79	1.78	1.07	1.77	5.73	34.49	5.89
C35 H75 N2 P S	586.5407	7.34	4	3.85	3.36	3.89	3.92	3.39	3.90	5.74	8.95	9.79
C37 H32 N4	532.2609	2.344	11	2.07	1.11	2.06	2.04	1.32	2.06	5.79	34.31	3.24
C48 H77 O10 P	844.5242	5.24	13	4.38	4.61	4.40	4.36	4.49	4.24	5.81	30.88	26.11
C20 H27 N	281.2138	3.078	14	1.72	1.10	1.98	1.79	1.01	2.01	5.82	48.10	3.66
C22 H36 N4	356.2922	2.501	22	3.17	2.43	3.37	3.17	2.33	3.57	5.84	29.88	23.01
C38 H79 N3 O2	609.6163	5.525	10	1.05	0.79	1.14	1.18	0.79	1.13	5.85	18.92	11.95
C42 H79 O8 P	742.555	5.205	5	4.43	4.50	4.46	4.47	4.53	4.51	5.85	7.42	6.28
C46 H66 O8	746.4724	4.384	10	3.22	3.29	3.14	3.29	3.32	3.19	5.86	4.51	9.68
C29 H51 N O4	477.3813	3.414	10	2.16	2.34	2.20	2.21	2.33	2.20	5.91	2.76	5.44
C80 H102 Br N10 O8 P3 S5	1662.487	9.629	9	5.29	5.25	5.34	5.32	5.22	5.35	5.92	4.92	1.15

C44 H77 N9 O P2	809.5737	4.865	4	2.23	2.20	2.14	2.23	2.41	2.14	5.95	26.35	0.97
C26 H53 O4 P S	492.3404	2.314	4	4.58	3.82	4.59	4.57	3.89	4.59	6.02	35.98	1.02
C30 H60 N5 P	521.457	4.133	5	3.29	3.38	3.39	3.39	3.34	3.36	6.02	13.34	4.44
C86 H171 O5 P	1315.287	11.249	8	11.59	11.66	11.58	11.57	11.41	11.58	6.11	33.35	0.97
C37 H83 N7 S	657.6435	11.248	7	10.78	10.83	10.80	10.75	10.62	10.78	6.12	28.17	1.64
C27 H56 N8 O S	540.4287	3.212	11	5.24	5.33	5.31	5.22	5.31	5.35	6.13	4.78	5.10
C19 H37 N O7	391.2566	11.261	18	2.37	1.94	2.25	2.29	1.94	2.15	6.13	6.77	15.89
C25 H49 N4 P S3	532.2864	2.299	17	2.31	1.53	2.32	2.38	1.51	2.37	6.18	38.95	8.04
C63 H91 N O6	957.6845	8.334	19	4.48	4.28	4.54	4.52	4.27	4.54	6.18	12.88	4.17
C38 H75 N O4	609.5694	4.712	10	1.91	1.84	2.10	1.95	1.84	2.42	6.21	8.42	47.99
C16 H26	218.2029	11.257	12	3.47	3.65	3.40	3.46	3.69	3.39	6.21	22.98	3.77
C43 H85 N O6	711.637	8.037	20	2.58	0.93	2.43	2.68	0.72	2.66	6.24	28.01	37.52
C28 H57 N O	423.4434	6.363	5	1.62	0.41	1.47	1.60	0.61	1.39	6.24	34.29	18.89
C50 H99 N2 O6 P	854.7276	5.652	19	2.44	2.77	2.54	2.45	2.59	2.53	6.25	23.38	2.26
C26 H49 N O2	407.3757	5.5	5	2.98	1.35	2.49	3.02	1.49	2.57	6.26	30.76	22.05
C34 H71 N	493.558	5.511	3	1.98	0.45	1.75	1.99	0.64	1.73	6.27	43.01	16.26
C22 H47 N O2	357.3601	2.703	15	5.13	5.20	5.21	5.10	5.06	5.23	6.30	22.27	10.45
C42 H81 N O5	679.6114	8.074	5	1.87	1.53	2.03	1.89	1.54	2.03	6.31	11.30	6.04
C27 H62 N9 O4 P	607.4661	3.149	7	2.48	2.34	2.49	2.55	2.21	2.51	6.33	18.96	11.18
C29 H50 O2	430.3795	3.512	19	3.98	2.60	3.39	4.11	3.02	3.61	6.34	42.20	46.02
C11 H30 N10 O11	478.2111	2.291	18	2.06	1.35	2.10	2.17	1.30	2.12	6.34	39.96	2.90
C23 H37 O7 P	456.2295	2.282	8	2.00	1.14	2.07	2.05	1.27	2.07	6.39	38.15	1.84
C28 H58 N2 O6	518.4309	5.931	18	4.67	4.81	4.45	4.24	4.77	4.67	6.39	9.25	24.92
C12 H34 N10 O6	414.2651	3.411	8	2.73	3.02	2.93	2.78	3.02	2.82	6.39	14.69	22.32
C34 H80 N10 S3	724.5737	4.799	15	1.69	1.53	1.70	1.84	1.67	1.68	6.42	22.39	16.91
C37 H80 N5 O14 P	849.5429	1.543	17	3.77	3.40	3.73	3.90	3.14	3.68	6.43	48.06	14.42

	C28 H58 N O6 P	535.3994	3.53	14	1.59	1.32	1.46	1.48	1.29	1.58	6.43	9.97	15.51
	C22 H57 N10 O2 P3 S	618.3608	2.644	16	4.61	4.55	4.73	4.59	4.52	4.75	6.46	9.87	4.04
	C41 H82 N4 O3	678.6379	3.482	29	2.37	1.80	2.56	2.45	1.96	2.59	6.49	21.96	25.55
	C38 H67 N O6	633.4961	5.469	9	4.13	4.20	4.04	4.12	4.23	4.05	6.53	18.90	2.38
	C23 H47 N O8	465.3296	2.311	6	1.93	1.09	2.04	1.89	1.36	2.04	6.53	43.95	3.02
	C46 H80 N O7 P	789.5655	5.636	11	6.05	6.14	6.00	5.92	6.11	6.00	6.53	13.75	0.69
	C34 H71 N9 O8	733.5434	5.909	4	3.15	3.07	3.15	3.13	3.07	3.14	6.56	3.12	4.28
	C16 H34 O3	274.2502	2.801	11	2.64	2.04	2.49	2.45	2.02	2.46	6.56	22.34	6.81
	C39 H83 N3 O15 P2	895.5298	1.449	14	1.18	0.23	0.97	1.22	0.36	1.03	6.57	17.50	13.13
	C22 H51 N9 O16	697.3466	1.44	12	1.02	0.04	0.80	1.05	0.18	0.86	6.60	16.75	13.56
	C17 H35 O9 P	414.2032	1.34	23	2.64	2.03	2.62	2.68	1.92	2.47	6.63	45.25	48.65
	C29 H61 N6 O3 P	572.4542	2.749	7	5.12	5.30	5.00	5.38	5.26	5.07	6.63	13.67	12.09
	C20 H53 Cl N10 O2 P2	562.3526	2.243	4	4.43	4.35	4.50	4.46	4.36	4.47	6.64	16.54	13.21
	C44 H92 N2 O	664.7208	9.417	16	3.42	1.69	3.07	3.40	1.97	3.11	6.66	45.66	12.01
	C9 H21 N3 O4	235.1542	3.132	14	1.68	1.50	1.50	1.68	1.36	1.56	6.69	19.32	7.65
	C23 H52 N5 O2 P	461.3836	3.547	23	5.03	4.64	4.65	5.14	4.70	4.69	6.72	11.06	5.08
	C24 H54 N9 O P	515.4184	4.507	7	1.60	1.52	1.53	1.61	1.51	1.57	6.80	6.67	6.33
	C32 H70 N O12 P3	753.4092	2.3	21	2.20	1.46	2.21	2.28	1.40	2.23	6.80	39.86	2.94
	C53 H96 N O8 P	905.6882	8.099	14	1.04	0.71	1.22	1.07	0.49	1.18	6.82	33.98	18.63
	C15 H26 N2 O2 P2	328.1455	2.287	14	2.20	1.45	2.27	2.26	1.53	2.28	6.88	37.59	3.38
	C35 H71 N O	521.5532	8.467	12	3.85	2.51	3.71	3.87	2.75	3.67	6.88	34.98	9.23
	C21 H44 N6 O6 S	508.3021	1.462	12	1.32	0.43	1.13	1.39	0.56	1.18	6.89	16.63	13.40
	C41 H86 Cl N4 P S4	828.5168	4.873	17	3.02	2.86	2.85	3.06	3.22	2.81	6.94	37.25	18.44
	C28 H57 N O2	439.4384	6.553	2	1.18	0.11	0.89	1.22	0.11	0.95	7.01	39.70	13.25
	C31 H67 N9 O7	677.5193	7.315	16	3.80	3.66	3.82	3.79	3.49	3.82	7.02	32.37	3.55
	C29 H62 N8 O2 S	586.4702	3.278	14	2.32	2.29	2.23	2.42	2.24	2.25	7.03	6.93	6.15

C29 H64 N8 O17	796.4379	1.439	16	1.06	0.19	0.87	1.11	0.29	0.94	7.03	19.58	12.31
C25 H52 N8 O S	512.3972	2.707	9	4.95	5.02	4.91	5.07	4.95	4.83	7.03	9.53	9.65
C26 H57 N4 O5 P S	568.377	4.62	7	1.29	1.26	1.41	1.35	1.18	1.45	7.03	15.23	9.70
C39 H75 N7 O12	833.5474	5.615	13	4.99	5.01	5.01	5.07	4.97	4.99	7.05	8.01	8.74
C18 H26	242.2029	11.256	9	5.34	5.36	5.30	5.39	5.51	5.29	7.06	19.07	7.00
C22 H46 N6 O6 S	522.3182	1.958	10	2.05	1.43	2.19	2.12	1.30	2.10	7.15	23.57	29.62
C12 H16	160.1249	11.257	3	5.89	6.21	5.95	5.91	6.30	5.95	7.22	13.25	3.27
C24 H46 N2 O3	410.3502	2.678	18	2.95	2.91	2.72	3.06	2.80	2.73	7.23	25.28	7.38
C26 H49 N O3	423.3702	5.132	15	1.41	0.49	0.99	1.39	0.23	1.01	7.23	35.81	16.36
C26 H46 N2 O6	482.3363	5.339	9	4.04	3.93	3.92	4.06	3.94	3.92	7.25	4.17	5.43
C38 H58 O P2	592.399	2.423	14	2.00	0.06	1.60	1.90	0.43	1.41	7.26	46.44	28.23
C31 H59 N7 O	545.48	7.076	8	1.65	0.92	1.65	1.63	0.94	1.56	7.28	19.43	16.39
C22 H37 O7 P	444.2293	2.292	23	2.34	1.61	2.35	2.43	1.54	2.37	7.31	40.46	3.03
C69 H115 N6 O11 P	1234.836	5.181	22	5.33	5.13	5.34	5.49	5.34	5.26	7.32	43.35	11.44
C28 H51 N8 O P	546.3915	5.47	6	2.68	2.67	2.65	2.68	2.79	2.63	7.37	24.92	3.99
C32 H52 S	468.3789	4.065	6	2.88	2.88	2.87	2.85	2.93	2.88	7.38	5.55	3.30
C25 H50 N O7 P	507.3329	2.68	5	5.92	5.96	6.00	5.90	5.96	6.05	7.39	3.78	9.01
C27 H43 O9 P	542.267	1.986	21	2.33	1.59	2.51	2.43	1.54	2.37	7.41	10.44	35.92
C26 H55 N	381.4329	3.319	3	1.37	0.23	0.98	1.34	0.03	1.09	7.42	37.79	12.91
C36 H78 N5 O12 P	803.5382	3.43	10	2.01	2.46	1.90	1.93	2.40	1.90	7.42	9.01	17.78
C88 H158 N8 O7 P2	1501.173	5.196	18	3.73	3.75	3.71	3.76	3.46	3.72	7.44	41.26	5.25
C34 H80 N10 O3 P2	738.5886	5.21	8	4.92	4.80	4.85	5.01	4.99	4.88	7.46	22.45	4.62
C31 H69 N9	567.5698	6.656	11	2.37	1.93	2.31	2.32	1.96	2.33	7.47	20.93	5.26
C38 H81 N3 O3	627.6288	10.023	19	2.64	0.97	2.31	2.58	1.36	2.34	7.52	45.99	9.60
C26 H58 N8 O	498.4757	3.373	18	2.60	2.18	2.63	2.69	2.29	2.62	7.52	18.17	1.68
C34 H75 N9	609.6164	6.651	7	1.38	0.90	1.25	1.31	0.92	1.24	7.52	29.22	4.92

	C23 H55 Cl N6 O6 P2	608.3321	2.643	12	5.76	5.70	5.85	5.80	5.62	5.91	7.53	15.68	7.59
	C88 H166 N7 O17 P3	1686.154	2.976	23	1.24	1.24	1.77	1.44	1.23	1.87	7.56	3.53	34.19
	C15 H33 N3 O4	319.2479	2.249	17	0.97	1.01	0.97	1.05	0.74	1.04	7.58	36.20	10.15
	C28 H41 N3 O6	515.2978	2.753	11	5.57	5.32	5.66	5.59	5.32	5.64	7.59	10.15	6.46
	C25 H53 N3 O5	475.3997	3.892	22	2.17	2.01	2.23	2.39	2.05	2.17	7.62	12.28	12.09
	C32 H67 N	465.5271	4.676	2	1.47	0.14	1.20	1.46	0.07	1.26	7.65	42.88	11.89
	C54 H44 N8 O2	836.3594	1.902	29	3.08	2.40	3.29	3.27	2.30	3.04	7.66	17.86	34.41
	C8 H12 O3	156.0784	2.314	7	5.47	4.29	5.52	5.56	4.52	5.48	7.69	48.56	4.57
	C29 H54 N O7 P	559.3658	2.342	16	2.11	1.12	2.06	2.03	1.37	2.06	7.73	34.18	4.27
	C34 H71 N O	509.5529	10.2	4	1.81	0.44	1.52	1.78	0.49	1.55	7.75	39.88	10.67
	C22 H33 O9 P	472.1875	3.076	10	3.82	3.36	3.96	3.89	3.17	3.80	7.75	31.11	21.11
	C20 H40 N6 O	380.3261	4.199	12	1.62	1.69	1.59	1.69	1.68	1.69	7.75	4.85	19.39
	C31 H55 N O S	489.4025	2.83	1	1.36	0.38	1.52	1.38	0.61	1.49	7.77	45.18	7.45
	C22 H48 N8 O2 S	488.3602	2.758	8	3.59	3.55	3.61	3.67	3.59	3.66	7.78	5.42	8.48
	C83 H174 N5 O P S2	1352.29	11.287	15	2.51	2.53	2.49	2.52	2.67	2.46	7.81	31.64	15.03
	C27 H35 N2 O2 P S	482.2164	3.076	19	3.45	2.98	3.80	3.38	2.79	3.83	7.82	38.46	16.84
	C22 H41 N7	403.3427	3.289	13	1.77	0.54	1.55	1.99	0.64	1.55	7.83	13.58	32.86
	C43 H85 N O	631.6628	9.845	5	1.19	1.24	0.89	1.29	0.77	1.08	7.83	49.55	22.73
	C21 H34	286.2653	11.259	13	4.43	4.34	4.54	4.51	4.52	4.53	7.84	20.90	5.72
	C27 H45 N5 O2	471.3555	2.734	9	1.71	1.07	1.85	1.70	1.03	1.81	7.87	39.38	7.96
	C47 H75 O10 P	830.5134	4.869	4	1.62	1.66	1.36	1.55	1.79	1.33	7.87	36.07	18.88
	C39 H82 N5 O13 P	859.564	5.632	17	4.00	3.94	4.18	3.94	3.75	4.06	7.87	28.71	24.35
	C36 H74 N5 O16 P	863.4858	2.784	29	1.10	0.43	1.32	1.68	0.59	1.40	7.89	19.72	41.54
	C83 H141 N2 P	1197.083	7.314	19	5.05	5.06	5.02	5.11	5.08	4.98	7.91	21.67	4.88
	C24 H39 O7 P	470.2454	2.308	6	4.17	3.25	4.20	4.15	3.34	4.18	7.93	42.44	3.06
	C26 H59 N7 O8	597.4443	2.803	9	1.16	0.90	1.75	1.53	1.12	1.74	7.93	43.80	40.74

C23 H48 N6 S	440.3641	1.985	19	1.92	1.38	2.08	1.98	1.21	1.98	7.93	27.54	26.45
C87 H178 N P S2	1332.314	11.244	7	12.96	13.05	13.03	12.99	12.89	13.02	7.95	22.94	2.46
C12 H32 N8 O3 P2	398.2087	2.322	17	4.39	3.29	4.82	4.52	3.38	4.76	7.96	26.46	47.77
C40 H83 N3 O2	637.6479	6.651	17	2.00	1.27	1.83	2.02	1.30	1.91	7.97	12.14	9.86
C16 H33 N2 O P S3	396.15	1.845	8	3.18	2.98	3.45	3.21	3.04	3.22	8.01	12.83	34.30
C26 H55 N O2	413.4226	6.402	6	1.44	0.19	1.16	1.44	0.20	1.16	8.02	40.08	17.19
C32 H64 N2 O2	508.4961	5.543	8	2.41	1.94	2.58	2.53	1.99	2.53	8.02	10.12	11.25
C4 H4 O7 P2	225.9438	6.74	22	5.03	4.81	5.07	4.85	4.82	5.04	8.04	13.52	3.38
C77 H163 Br N7 O9 P S2	1504.087	5.211	3	2.88	2.88	2.92	2.97	2.85	2.95	8.06	4.88	3.08
C39 H79 N O	577.616	5.961	19	1.96	0.29	1.66	2.01	0.55	1.63	8.07	44.18	15.63
C26 H51 N O3	425.3863	3.382	6	2.33	1.95	2.36	2.45	1.98	2.32	8.08	6.23	10.86
C32 H53 O9 P	612.3438	2.657	19	4.15	4.11	4.08	4.16	4.12	4.11	8.09	7.23	8.85
C29 H65 N10 O3 P	632.4983	5.468	9	4.11	4.08	4.07	4.08	4.10	4.11	8.10	7.86	8.87
C19 H37 N O	295.287	3.346	16	1.67	0.37	1.41	1.77	0.45	1.36	8.11	21.48	14.94
C42 H93 N5 O10 P2 S2	953.5835	3.489	10	1.66	1.31	1.74	1.63	1.33	1.85	8.11	4.59	20.22
C10 H18 O2	170.1304	2.828	4	1.38	0.37	1.54	1.42	0.55	1.59	8.14	43.13	9.04
C24 H47 N O3	397.3552	3.014	10	2.35	2.18	2.26	2.31	2.12	2.26	8.14	9.11	4.66
C37 H73 N O5	611.5483	4.136	5	1.23	1.05	1.49	1.39	1.49	1.50	8.18	44.73	41.99
C36 H77 N7 O11	783.5693	3.442	10	4.55	4.98	4.30	4.58	5.04	4.20	8.18	13.37	31.56
C42 H75 N10 O5 P	830.5663	3.802	14	2.56	2.87	2.70	2.53	2.84	2.70	8.18	15.22	0.81
C36 H80 Br N9 O2	749.5632	10.758	10	3.66	3.41	3.30	3.60	3.46	3.42	8.19	22.31	17.42
C30 H44 N4	460.3547	5.321	10	2.95	2.85	2.80	2.95	2.91	2.81	8.22	10.02	3.88
C38 H76 N3 O3 P S	685.5342	3.126	13	1.72	1.78	2.00	1.94	1.75	2.03	8.23	9.02	15.76
C62 H93 O12 P S	1092.612	3.517	6	5.28	2.99	5.13	5.34	3.02	5.28	8.24	23.68	36.21
C24 H47 O12 P	558.2792	2.643	20	2.33	2.47	2.62	2.46	2.36	2.64	8.24	21.31	15.60
C30 H39 N5	469.3192	2.593	19	3.28	1.86	3.45	3.30	2.03	3.57	8.25	20.10	45.41

C18 H38 O3	302.2816	3.12	11	3.77	3.52	3.90	3.78	3.55	3.87	8.27	5.91	4.89
C19 H41 N3 O5	391.3055	2.753	15	3.03	2.59	2.95	3.07	2.51	3.06	8.27	29.56	19.41
C30 H34 O4	458.2449	2.333	24	2.36	1.65	2.36	2.44	1.54	2.38	8.27	41.42	4.05
C26 H51 N5 O3	481.3974	2.829	12	2.73	1.85	2.91	2.73	1.80	3.13	8.33	27.27	34.08
C15 H43 N10 P	394.3425	4.769	13	3.09	2.80	3.33	3.20	2.76	3.36	8.35	29.47	6.30
C19 H38 O4	330.2765	3.075	10	5.83	5.05	5.91	5.86	4.84	6.03	8.36	28.19	17.81
C36 H66 N2 O2	558.5096	6.661	4	2.64	2.10	2.58	2.64	2.14	2.63	8.40	12.43	8.43
C39 H84 Cl N9 P2	775.6023	10.553	8	4.35	4.21	4.33	4.33	4.14	4.29	8.40	23.45	5.02
C37 H75 N O	549.5846	5.02	3	1.94	0.53	1.67	1.93	0.73	1.72	8.44	42.58	8.99
C13 H27 N O	213.2089	2.178	12	1.37	0.83	0.88	1.48	0.61	0.83	8.44	33.65	17.40
C50 H106 N10 O2 P2	940.797	8.077	20	1.33	0.97	1.52	1.37	1.32	1.50	8.46	43.32	11.69
C59 H103 N2 O5 P S2	1014.705	3.465	19	5.45	2.15	5.37	5.29	2.59	5.33	8.47	48.68	25.32
C20 H43 N O3	345.3254	7.317	16	2.35	2.42	2.27	2.35	2.49	2.22	8.50	9.40	9.82
C39 H76 O2 S2	640.5312	3.831	7	2.76	2.67	2.75	2.84	2.72	2.76	8.52	12.43	4.58
C52 H95 O13 P	958.6504	5.471	5	2.78	2.74	2.76	2.86	2.99	2.77	8.53	40.26	7.47
C42 H87 N O6	701.6526	8.063	15	1.04	0.83	1.16	1.11	1.03	1.24	8.56	24.65	14.02
C37 H82 N6 O7 P2	784.5717	3.442	9	3.92	4.51	3.77	4.05	4.56	3.62	8.57	10.01	47.75
C35 H71 N O4	569.5387	7.315	7	5.54	5.62	5.50	5.58	5.59	5.53	8.58	5.65	4.20
C23 H48 N O7 P	481.3161	3.852	8	1.72	1.65	1.81	1.73	1.48	1.67	8.58	32.64	20.89
C27 H66 N9 O4 P	611.4966	3.362	7	3.12	3.16	3.37	3.24	3.24	3.37	8.58	12.23	21.94
C31 H51 N4 P3 S	604.3074	4.836	15	1.15	0.22	1.60	1.09	0.17	1.38	8.59	27.21	48.48
C82 H175 N10 O16 P3 S2	1713.183	3.271	7	3.56	3.75	4.10	3.87	3.72	4.06	8.59	3.62	8.42
C40 H86 N5 O2 P	699.6509	8.457	4	1.86	2.16	1.96	1.95	2.24	1.95	8.60	22.43	6.89
C40 H79 N O6	669.59	8.091	15	4.48	3.17	4.32	4.38	3.35	4.61	8.61	23.63	40.56
C57 H89 N O13 S	1027.605	3.466	9	5.47	4.86	5.96	5.52	4.83	5.91	8.64	17.96	43.20

	C14 H24 O5	272.1618	2.312	5	3.90	2.98	4.18	3.91	3.16	4.20	8.64	47.16	3.17
	C35 H73 N	507.5733	6.2	17	3.88	1.59	3.71	3.81	1.97	3.49	8.67	45.30	29.37
	C85 H172 N2 O3 P2 S2	1395.228	11.251	12	5.51	5.58	5.51	5.60	5.27	5.55	8.71	40.09	11.67
	C16 H35 N O	257.2715	2.341	5	3.09	2.94	3.21	3.40	2.86	3.70	8.72	9.60	49.35
	C63 H103 N O6	969.776	8.079	18	1.25	0.76	1.37	1.30	0.65	1.44	8.73	34.00	13.98
	C37 H77 N O	551.5998	5.436	3	1.13	0.17	0.81	1.17	0.13	0.84	8.73	42.26	6.44
	C31 H55 N O4	505.4128	4.387	11	2.27	2.35	2.32	2.35	2.37	2.35	8.76	11.12	7.28
	C22 H46 N8 O S	470.3502	3.214	8	3.78	3.76	3.90	3.77	3.76	3.83	8.76	4.04	12.88
	C19 H35 N3	305.2825	1.831	10	8.08	8.01	8.16	8.07	8.03	8.22	8.78	2.41	11.86
	C37 H73 N2 O8 P	704.5089	8.057	28	8.06	7.34	7.70	8.10	7.30	7.89	8.80	9.15	22.61
	C27 H55 N O	409.4277	5.924	6	2.05	0.60	1.76	1.97	0.88	1.74	8.82	37.21	18.97
	C44 H88 N9 O13 P S	1013.596	3.529	6	6.99	6.79	7.23	7.14	6.81	7.25	8.83	44.82	39.08
	C51 H108 N5 O3 P	869.8188	5.047	15	3.82	2.48	3.35	3.78	2.36	3.41	8.88	45.80	18.00
	C13 H25 O7 P	324.1342	1.969	7	1.92	1.43	2.10	2.03	1.24	1.99	8.89	25.31	29.53
	C87 H150 N9 O5 P S3	1528.068	5.215	21	2.30	2.36	2.41	2.34	2.32	2.37	8.90	9.84	8.76
	C30 H73 N9 O2 P2	653.5389	7.313	8	2.18	2.47	2.18	2.28	2.29	2.16	8.90	22.18	15.01
	C27 H53 N O2	423.4069	7.321	4	1.91	0.37	1.62	1.88	0.58	1.66	8.97	39.90	15.92
	C25 H52 N O7 P	509.3479	4.379	7	2.93	3.02	2.90	2.87	3.01	2.90	8.98	3.38	1.52
	C22 H47 N O2	357.36	4.886	6	2.55	1.37	2.10	2.66	1.46	2.27	9.01	19.17	19.65
	C32 H41 N P2	501.2717	1.696	13	8.45	8.55	8.73	8.45	8.57	8.72	9.04	24.22	13.86
	C37 H87 N8 O5 P3	816.6025	3.59	14	1.95	2.06	2.25	2.08	2.08	2.24	9.05	9.55	11.51
	C39 H76 N6 O2	660.6048	8.064	12	1.11	0.92	1.22	1.17	0.85	1.28	9.07	9.17	13.96
	C40 H84 N2 O2	624.6521	5.978	16	1.75	0.28	1.76	1.77	0.29	1.45	9.12	44.14	41.12
	C23 H42 N O7 P	475.2719	2.323	27	2.50	1.81	2.51	2.60	1.68	2.53	9.14	41.94	3.48
	C48 H80 N O8 P	829.566	10.474	3	4.34	4.28	4.40	4.38	4.27	4.39	9.14	11.05	7.17
	C32 H66 N6 O	550.5318	11.252	23	1.14	0.82	1.16	1.14	1.15	1.14	9.15	35.41	7.34

C31 H51 N3 S	497.3815	3.878	17	3.80	3.85	3.93	3.77	3.88	3.92	9.18	14.60	4.65
C27 H55 N O	409.4277	7.678	7	1.40	0.08	1.07	1.38	0.01	1.13	9.22	33.64	29.20
C35 H53 Cl N6 O	608.3945	2.622	10	3.89	3.75	3.76	3.94	3.74	3.81	9.23	7.61	14.56
C13 H20 O2	208.146	3.129	18	1.83	1.41	1.65	1.67	1.42	1.61	9.24	7.82	12.45
C38 H79 N O	565.6156	4.917	7	4.38	4.62	4.37	4.34	4.61	4.45	9.24	11.78	11.46
C20 H32 N2 O2	332.2458	2.186	2	2.13	0.83	1.77	2.05	0.77	1.80	9.25	44.76	8.07
C27 H53 N O	407.4121	5.5	5	2.64	1.48	2.46	2.61	1.55	2.38	9.26	41.64	18.88
C40 H30 N9 O2 P	699.226	4.73	8	2.11	2.12	2.17	2.04	2.15	2.17	9.29	12.16	3.13
C58 H115 N O6	921.8715	11.632	4	2.30	1.41	2.25	2.31	1.67	2.43	9.30	36.82	35.93
C65 H129 N O6	1019.982	11.757	7	2.70	1.79	2.85	2.67	2.18	3.10	9.33	47.34	38.61
C21 H32 Br3 Cl4 N6 O3 P3 S2	949.7501	8.078	14	1.13	0.95	1.23	1.14	1.30	1.28	9.34	49.32	13.97
C25 H51 N O2	397.3914	6.959	16	1.84	0.67	1.69	1.92	0.66	1.63	9.34	34.73	12.24
C39 H73 N O13	763.5063	1.961	11	2.07	1.69	2.24	2.14	1.83	2.15	9.35	20.68	25.44
C51 H97 N10 P	880.7636	8.185	16	2.12	2.25	2.28	2.37	2.27	2.29	9.35	6.24	10.60
C86 H163 N O18	1498.189	8.073	12	0.99	0.84	1.28	1.05	0.90	1.16	9.39	15.56	16.97
C24 H47 N O7	461.3344	2.427	12	1.81	1.81	1.89	1.81	1.72	1.88	9.40	16.08	15.76
C38 H77 N O	563.6002	4.248	22	1.28	1.70	1.39	1.19	1.56	1.36	9.45	30.27	10.20
C37 H73 N5 O8	715.5437	2.909	10	5.09	4.17	5.26	5.15	4.12	5.39	9.47	14.90	43.22
C17 H45 N9 O P2	453.3232	3.236	9	3.68	3.63	3.73	3.59	3.65	3.65	9.49	2.54	14.19
C12 H20 O6	260.1254	2.314	25	5.16	3.62	5.51	5.26	3.80	5.50	9.54	29.60	5.82
C26 H51 N O2	409.3913	7.036	4	1.11	0.51	0.63	1.13	0.22	0.78	9.55	34.40	19.31
C36 H35 N4 O6 P S	682.202	2.659	11	3.48	3.54	3.46	3.73	3.54	3.43	9.58	2.37	8.36
C35 H73 N O	523.5687	4.875	5	1.10	0.21	0.92	1.22	0.21	0.96	9.60	40.54	16.70
C36 H76 N2 O	552.5951	7.319	7	1.26	0.21	0.98	1.19	0.08	0.99	9.63	35.49	9.75
C16 H31 N O4	301.2247	1.961	21	2.45	1.98	2.62	2.55	1.78	2.55	9.63	30.73	27.68

	C35 H71 N	505.558	5.307	9	1.90	0.70	1.77	1.85	0.65	1.70	9.63	41.44	17.33
	C21 H48 N5 O2 P	433.3524	3.12	13	2.78	2.35	3.13	2.96	2.38	3.15	9.67	16.58	3.75
	C59 H61 Cl2 N7 O4 P2 S2	1127.308	7.909	10	3.77	3.78	3.70	3.71	3.69	3.76	9.68	17.42	13.31
	C27 H50 N4 O2	462.3926	2.306	13	1.65	0.24	1.17	1.55	0.56	1.13	9.68	34.86	18.43
	C19 H33 O9 P	436.1853	3.397	12	2.98	1.97	2.83	3.08	1.90	2.95	9.72	14.82	29.95
	C28 H59 N2 O4 P	518.4192	2.327	19	2.18	0.97	1.12	2.14	0.93	1.19	9.72	9.75	15.11
	C15 H35 N7 S2	377.2414	2.418	17	4.84	4.81	4.84	5.05	4.90	4.83	9.74	11.22	2.97
	C57 H126 N8 O6 P2 S	1112.9	9.659	21	5.50	5.58	5.63	5.55	5.44	5.62	9.79	23.82	10.58
	C15 H36 N5 O P S	365.2384	2.927	14	2.19	1.29	2.43	2.36	1.41	2.42	9.79	45.69	9.74
	C27 H58 N8 O2 S	558.4387	2.746	4	6.32	6.17	6.11	6.47	6.16	6.14	9.82	11.87	6.99
	C21 H44 N O7 P	453.2848	3.418	16	1.31	1.70	1.41	1.34	1.72	1.35	9.85	3.81	11.18
	C30 H61 N O	451.4749	7.948	18	1.55	0.16	1.31	1.50	0.24	1.44	9.87	37.15	24.95
	C16 H23 N3 O4	321.1682	1.806	20	2.86	1.87	2.53	2.71	2.08	2.57	9.92	23.94	7.78
	C26 H47 N O2	405.3603	4.304	4	2.47	0.82	1.83	2.38	0.99	1.97	10.01	39.03	19.79
	C15 H35 N10 O2 P	418.2671	11.257	8	3.99	3.76	3.73	3.91	3.89	3.82	10.04	28.10	11.25
	C24 H49 N7 O	451.4016	3.497	17	3.12	3.04	2.94	3.12	3.09	2.99	10.05	8.17	12.91
	C56 H104 O12 P2	1030.7	2.79	25	3.88	1.94	3.48	3.79	2.00	3.46	10.05	33.22	33.81
	C63 H93 N O6	959.7003	8.579	16	2.49	2.35	2.43	2.61	2.24	2.40	10.06	19.28	6.94
	C25 H56 N5 P	457.4277	6.832	7	1.43	0.64	1.37	1.48	0.51	1.28	10.06	44.63	14.41
	C18 H43 N6 O14 P	598.2548	1.444	26	0.93	0.21	0.84	1.11	0.15	0.88	10.08	17.56	16.63
	C31 H70 N10 O	598.5726	8.028	13	0.94	0.63	1.05	1.01	0.42	1.12	10.11	40.42	16.94
	C56 H74 N2 O2	806.5745	3.926	19	1.09	1.26	1.10	1.26	1.14	1.12	10.12	26.00	2.16
	C43 H87 N O4	681.663	8.089	22	1.60	1.18	1.25	1.53	1.15	1.25	10.13	18.04	1.69
	C28 H46 O4	446.3401	3.223	6	2.63	2.11	2.63	2.79	2.18	2.53	10.15	8.88	33.03
	C37 H37 N3 O4 S3	683.1949	6.401	9	2.79	2.63	2.78	2.70	2.66	2.78	10.15	9.37	1.78

C35 H77 N4 O2 P	616.5784	8.071	9	1.14	0.96	1.23	1.15	1.33	1.27	10.15	49.72	14.03
C29 H45 N O4	471.3339	2.748	2	6.54	6.52	6.62	6.53	6.51	6.62	10.19	1.57	5.18
C31 H65 N O	467.5061	9.652	4	2.97	1.54	2.71	2.98	1.69	2.71	10.21	40.66	11.96
C25 H53 N O	383.412	8.187	5	1.88	0.38	1.58	1.87	0.56	1.68	10.23	38.70	18.86
C59 H99 N S	853.7484	9.631	18	4.51	4.48	4.54	4.68	4.78	4.48	10.28	33.81	14.98
C41 H58 Cl N7 P2 S5	905.2513	7.547	8	2.55	2.44	2.46	2.50	2.41	2.54	10.30	22.45	9.91
C40 H84 N2 O	608.6574	8.466	5	1.40	0.15	1.21	1.33	0.10	1.28	10.30	47.73	12.55
C20 H45 N3 O5 S	439.3056	2.752	9	3.15	3.23	3.30	3.30	3.32	3.34	10.33	11.70	6.76
C21 H17 N5 O16 P2 S	688.9863	3.052	15	3.48	3.56	4.04	3.94	3.55	4.13	10.37	9.79	21.87
C28 H45 N O4	459.3349	2.283	6	4.81	4.78	4.85	4.85	4.73	4.82	10.42	6.49	6.97
C16 H28 O6	316.1881	2.314	2	2.07	1.11	2.13	2.07	1.25	2.16	10.45	45.85	4.63
C37 H80 N4 O10 P2	802.5357	3.338	6	3.41	3.72	3.29	3.32	3.72	3.24	10.48	9.66	15.22
C54 H74 O3 S	802.5349	3.421	6	1.79	2.10	1.67	1.70	2.10	1.62	10.48	9.66	15.22
C39 H77 N O5	639.5798	4.781	7	2.30	2.34	2.42	2.54	2.71	2.64	10.51	39.18	32.85
C50 H104 N4 O3 S2	872.7552	3.385	27	5.75	5.12	5.96	6.03	5.13	5.81	10.51	12.35	20.35
C24 H54 N5 O P	459.407	6.628	7	1.58	0.29	1.32	1.61	0.33	1.32	10.52	38.49	12.26
C21 H35 N	301.2763	4.185	8	1.17	0.24	0.98	1.12	0.19	1.00	10.52	38.49	6.18
C21 H38 N O7 P	447.2403	1.919	17	2.50	1.94	2.68	2.59	1.74	2.50	10.54	32.94	28.21
C28 H60 N2 O	440.4702	4.11	7	2.52	0.40	1.85	2.39	0.75	1.92	10.54	40.13	20.53
C24 H49 N O	367.3813	2.616	14	1.59	0.41	1.47	1.54	0.47	1.47	10.55	42.69	15.46
C5 H14 N O4 P	183.0657	5.62	16	3.24	3.17	3.23	3.29	3.35	3.21	10.56	21.46	3.05
C37 H67 O10 P	702.4458	4.867	19	6.35	5.42	6.39	6.25	5.23	6.47	10.58	38.52	24.37
C82 H164 N10 O9 P2 S	1527.188	5.617	7	7.84	7.82	7.87	7.99	7.89	7.92	10.60	14.90	10.70
C16 H45 N10 O4 P	472.3372	2.751	4	5.83	5.53	5.82	5.70	5.53	5.83	10.61	2.12	12.47
C21 H33 N3 O4	391.2466	2.08	8	1.19	0.43	0.55	1.19	0.58	0.58	10.69	44.64	26.56
C31 H63 N O3	497.4799	3.497	13	1.97	1.63	2.03	1.91	1.66	2.15	10.69	7.35	19.45

C44 H25 O9 P3	790.0713	5.652	17	2.32	2.22	2.33	2.36	1.95	2.35	10.70	46.60	1.78
C19 H31 N O4	337.2244	1.883	22	2.85	2.33	2.98	3.30	2.11	2.80	10.71	37.70	27.98
C60 H120 N2 O15 S	1140.841	3.499	16	3.07	3.07	3.30	3.31	3.16	3.30	10.71	13.38	20.76
C27 H55 N O2	425.4227	6.492	2	1.03	0.09	0.76	1.01	0.03	0.81	10.74	30.81	13.40
C23 H58 N10 O6	570.4528	2.717	3	3.20	2.42	3.36	3.22	2.44	3.45	10.74	9.85	36.70
C21 H39 N O	321.3025	5.033	15	1.81	0.56	1.57	1.82	0.69	1.51	10.76	17.62	10.94
C19 H34 O4	326.2451	2.33	15	5.33	4.07	5.21	5.61	4.16	5.47	10.78	15.11	32.71
C25 H45 N3 O2	419.3508	2.186	3	1.42	0.16	0.96	1.33	0.04	0.90	10.80	40.47	10.14
C13 H18	174.1405	11.257	7	5.04	5.22	5.17	5.06	5.28	5.16	10.81	8.15	9.88
C38 H76 N2 O2	592.5902	7.658	4	1.20	0.45	1.43	1.38	0.56	1.33	10.82	22.11	24.33
C20 H46 N10	426.3897	4.814	23	1.66	1.32	1.43	1.67	1.37	1.47	10.82	10.10	8.05
C37 H75 N O	549.5847	8.894	6	3.05	1.54	2.76	2.99	1.80	2.78	10.83	37.66	10.10
C21 H33 N3 O3	375.2511	1.54	9	2.28	1.26	2.06	2.34	1.35	2.09	10.87	16.57	5.38
C15 H22	202.1717	11.258	22	4.10	4.36	4.29	4.18	4.33	4.28	10.94	20.23	8.61
C23 H31 O7 P	450.1806	2.28	6	1.96	1.05	2.00	1.92	1.24	2.01	10.96	37.58	1.24
C23 H48 N O7 P	481.3164	2.291	6	5.92	5.90	5.97	5.96	5.86	5.93	10.96	5.56	7.57
C30 H61 O4 P	516.4294	3.085	6	3.18	1.91	3.37	3.19	2.32	3.40	10.98	45.34	7.06
C21 H49 N10 O6 P	568.357	3.557	22	4.82	4.63	4.55	4.75	4.66	4.58	10.99	9.17	6.07
C21 H49 N10 O6 P	568.3569	3.54	22	4.90	4.88	4.76	4.83	4.89	4.73	10.99	12.07	9.68
C27 H53 N O	407.4121	5.892	4	1.91	0.59	1.49	1.87	0.76	1.45	11.00	31.92	8.16
C23 H43 N O2	365.329	3.752	19	1.08	0.83	0.67	1.11	0.53	0.69	11.02	43.06	15.08
C29 H59 N O6	517.4341	3.113	7	3.04	1.76	3.23	3.05	2.18	3.25	11.06	45.39	7.18
C58 H63 N8 O18 P3 S2	1316.291	11.245	5	7.12	7.16	7.26	7.14	7.09	7.25	11.06	19.54	2.04
C22 H48 N9 O2 P	501.3661	2.618	4	3.61	3.17	3.80	3.78	3.08	3.82	11.10	10.98	20.55
C25 H52 N6 S	468.3958	2.357	4	1.45	0.68	1.58	1.51	0.98	1.66	11.10	36.87	12.32
C31 H60 N3 O P3	583.3929	2.261	8	4.16	2.80	4.38	4.01	3.17	4.41	11.14	42.63	5.52

C54 H98 Cl N3 O S2	903.6839	9.187	13	3.82	3.92	4.02	3.76	3.89	4.12	11.14	11.27	12.08
C23 H54 N9 O P	503.4181	2.831	3	1.63	0.38	1.68	1.52	0.72	1.68	11.15	38.49	7.16
C12 H27 N9 O4	361.2172	11.25	8	4.02	4.31	4.36	4.11	4.20	4.37	11.17	17.95	9.71
C72 H144 N5 O2 P3	1204.053	9.629	13	4.37	4.48	4.57	4.38	4.52	4.51	11.17	10.27	9.29
C18 H46 N8 O6 S	502.3247	2.312	17	3.37	2.69	3.36	3.37	2.84	3.30	11.20	38.22	8.43
C27 H44 O3	416.3283	3.472	23	2.37	2.05	2.42	2.31	2.06	2.58	11.22	8.90	17.31
C25 H58 N9 O P S	563.4217	4.621	12	1.51	1.46	1.66	1.62	1.47	1.69	11.23	5.24	11.62
C30 H69 N10 O7 P	712.5096	4.882	16	3.48	2.69	3.59	3.62	2.79	3.94	11.24	24.19	46.59
C18 H48 N9 P3	483.3251	3.081	7	3.52	2.00	3.66	3.47	1.98	3.75	11.25	18.87	41.67
C8 H19 N8 P	258.1462	8.042	13	4.02	2.94	3.70	3.86	3.07	3.79	11.26	49.11	31.98
C49 H98 Cl N3 O8	891.7034	9.625	20	6.09	6.06	6.13	6.29	6.34	6.08	11.26	31.98	15.48
C23 H47 N3 O2	397.3661	1.889	11	2.49	1.98	2.62	2.53	1.95	2.44	11.28	13.88	27.67
C25 H58 N9 O3 P	563.4391	2.314	3	3.49	2.56	3.39	3.48	2.62	3.40	11.28	42.50	1.53
C20 H46 N7 O P	431.3507	2.048	23	1.63	0.40	1.30	1.48	0.01	1.36	11.30	48.94	10.69
C23 H49 N	339.3858	2.812	9	1.16	0.21	1.06	1.15	0.08	1.10	11.31	38.38	10.72
C68 H75 Cl N O14 P S3	1291.378	7.748	18	2.80	2.33	2.89	2.75	2.45	2.90	11.35	17.17	9.78
C80 H173 N10 O18 P3 S	1687.186	3.288	13	1.91	1.68	2.04	2.16	1.53	2.10	11.36	18.41	16.53
C26 H45 N O	387.3494	4.729	5	1.29	0.54	1.01	1.39	0.10	0.99	11.38	44.74	22.14
C39 H61 N9 O P2 S2	797.3912	2.321	30	2.54	1.91	2.58	2.66	1.72	2.58	11.39	44.10	4.27
C37 H77 N O	551.6002	5.055	5	1.60	0.08	1.18	1.50	0.13	1.16	11.43	47.85	17.51
C12 H27 N9 O4	361.2173	7.747	8	1.56	1.03	1.96	1.48	0.89	1.93	11.46	25.72	37.22
C33 H51 N O13	669.3334	2.363	27	2.11	1.63	2.11	2.13	1.34	2.15	11.48	45.93	7.68
C39 H59 N5 O3 P2	707.4062	3.458	1	4.65	4.16	4.93	4.76	4.06	5.03	11.52	27.98	42.55
C23 H51 N7 O	441.4178	4.574	11	1.46	0.03	0.91	1.40	0.02	0.97	11.53	41.40	14.10
C28 H59 N	409.4643	3.632	4	2.12	0.46	1.63	2.04	0.68	1.76	11.55	33.68	17.56
C35 H44 O23	832.231	7.39	16	2.94	2.65	3.01	2.74	2.63	2.94	11.59	12.80	10.52

C28 H57 N	407.4485	3.408	10	1.33	0.19	0.60	1.30	0.09	0.67	11.60	41.70	15.54
C51 H92 N O8 P	877.6574	8.028	29	1.03	0.28	0.97	1.06	0.27	1.10	11.61	20.00	15.23
C38 H77 N O	563.5998	5.977	17	2.67	2.96	2.72	2.66	2.82	2.75	11.63	17.48	3.59
C42 H86 N2 O4	682.6582	3.074	12	3.44	1.75	3.07	3.49	2.07	2.77	11.65	38.90	47.82
C43 H81 O7 P	740.5695	6.532	14	3.38	3.60	3.57	3.35	3.49	3.48	11.69	26.75	17.27
C20 H45 O P3	394.2693	2.49	10	8.98	7.97	8.80	9.07	7.70	8.88	11.77	47.89	16.38
C31 H36 O8 S	568.2129	2.358	13	1.73	1.05	1.85	1.80	1.17	1.85	11.80	37.57	2.92
C25 H43 N3 O2	417.3347	2.047	4	1.31	0.77	0.90	1.20	0.44	0.95	11.91	49.52	6.93
C47 H39 Cl N7 O2 P S	831.2317	7.396	5	2.93	2.67	2.86	2.77	2.66	2.82	11.92	15.61	5.57
C23 H51 N7 O2	457.4123	5.812	18	2.13	1.01	2.57	2.22	1.29	2.48	11.92	43.38	42.11
C14 H33 N4 O3 P S2	400.1734	1.902	15	2.56	2.13	2.71	2.66	1.86	2.55	11.93	41.16	25.94
C82 H158 N8 O14	1479.191	5.194	16	3.54	3.62	3.66	3.66	3.46	3.62	11.93	21.51	7.18
C26 H50 N4	418.4051	2.542	23	0.87	0.77	0.58	1.08	0.71	0.47	11.95	27.46	14.57
C21 H43 N O	325.3338	2.809	3	2.40	1.93	2.43	2.44	1.80	2.57	11.96	18.81	19.92
C75 H137 N9 O S	1212.066	6.075	5	1.21	0.94	0.97	1.09	0.95	0.99	11.97	30.51	7.17
C27 H46 O10	530.3085	2.668	7	5.44	5.52	5.71	5.44	5.50	5.62	11.98	3.67	17.08
C31 H63 N O3	497.4801	6.799	3	1.32	0.25	1.09	1.28	0.18	1.05	11.99	41.75	13.53
C18 H44 N6 O S	392.3283	8.069	8	1.06	0.64	1.14	1.02	0.42	1.15	12.00	45.95	14.24
C90 H175 P S2	1351.285	11.277	26	3.39	3.55	3.29	3.42	3.46	3.32	12.04	19.41	15.73
C35 H78 N9 O2 P	687.6005	7.494	5	4.60	3.63	4.45	4.51	3.38	4.53	12.05	46.67	14.03
C28 H57 N O2	439.4384	7.06	5	1.61	0.40	1.30	1.57	0.45	1.33	12.06	32.01	12.04
C17 H44 N9 O4 P	469.3244	4.899	12	1.98	2.21	2.50	2.05	2.23	2.29	12.15	12.21	34.15
C19 H45 N9 O4	463.3597	1.955	7	1.96	1.01	1.42	1.82	0.72	1.29	12.20	48.65	36.05
C22 H45 N O4	387.3342	2.711	7	2.92	2.66	2.81	3.05	2.79	2.82	12.21	15.29	7.63
C13 H34 N10 O7	442.2598	3.498	10	3.79	3.52	3.79	3.85	3.33	3.79	12.21	38.78	3.22
C38 H54 N2 O3	586.4166	2.848	18	1.74	1.97	1.73	1.94	2.00	1.63	12.23	8.04	49.01

Formula												
C16 H24 O4	280.1671	2.291	17	2.12	2.04	2.14	2.26	2.31	2.17	12.24	38.51	9.66
C28 H51 N9 O S	561.3943	2.667	9	2.09	1.93	2.30	2.15	2.00	2.22	12.24	18.84	10.58
C48 H73 N O6	759.5454	5.793	9	1.43	0.19	1.05	1.39	0.09	0.98	12.26	45.45	12.49
C87 H174 N5 O17 P3 S	1686.184	3.28	19	2.20	1.77	2.16	2.06	1.75	2.28	12.27	4.77	14.56
C22 H47 N O2	357.3601	2.81	3	2.42	1.95	2.44	2.45	1.81	2.59	12.28	19.63	20.14
C22 H38 N4 O3	406.2935	1.498	11	2.91	2.49	2.75	2.67	2.42	2.75	12.29	18.28	2.95
C12 H22 O4	230.1512	3.498	4	2.02	2.14	2.10	2.01	2.05	2.10	12.33	12.80	0.72
C57 H75 N9 O2	917.6047	3.466	17	3.71	1.72	4.15	3.32	1.74	3.96	12.35	2.62	25.23
C41 H80 Cl N6 O4 P	786.5659	4.943	9	2.96	2.88	2.84	2.82	2.88	2.80	12.36	2.36	9.39
C16 H24 Cl N3 O2	325.1551	1.296	4	2.00	0.78	1.71	1.86	0.92	1.63	12.37	28.28	11.52
C29 H61 N	423.4798	3.835	2	1.19	0.28	0.84	1.11	0.04	0.92	12.42	33.73	11.52
C20 H39 N	293.3077	2.6	19	1.28	0.94	0.89	1.22	0.44	0.81	12.42	48.59	15.89
C21 H50 N5 O P	419.3757	3.751	7	2.31	0.88	1.99	2.34	1.19	2.06	12.43	38.40	15.32
C23 H43 P3	412.2583	3.421	11	1.53	1.56	1.36	1.41	1.60	1.27	12.45	7.56	13.54
C41 H80 Cl N6 O4 P	786.5664	3.862	14	7.01	6.92	7.06	7.00	6.98	7.00	12.47	7.91	13.12
C19 H28	256.2184	11.257	10	4.82	4.74	4.84	4.76	4.85	4.79	12.48	13.43	10.56
C41 H65 N2 O8 P3 S	838.3668	1.876	17	2.72	2.25	2.85	2.76	2.00	2.65	12.51	41.19	25.44
C7 H17 N O5	195.1102	1.932	22	2.33	1.82	2.52	2.46	1.63	2.38	12.53	30.23	27.32
C58 H113 N O7	935.8509	9.699	21	1.10	0.84	0.99	1.01	0.94	0.99	12.55	17.74	3.03
C38 H79 N O	565.6155	4.432	13	1.72	1.58	1.52	1.62	1.62	1.54	12.55	27.68	3.19
C25 H51 N O2	397.3912	5.287	9	2.04	0.89	1.69	2.01	0.83	1.76	12.57	36.37	12.81
C60 H119 N O6	949.9026	11.232	6	3.64	2.36	3.77	3.63	2.53	3.99	12.59	21.38	47.77
C32 H63 N O3	509.4805	3.604	9	1.84	1.99	2.03	2.01	1.96	2.10	12.62	5.64	12.02
C48 H100 N O14 P3	1007.636	3.475	10	8.90	8.11	9.16	8.95	8.18	9.18	12.62	12.19	37.21
C18 H38 N2 O	298.2977	3.285	12	1.36	0.19	1.07	1.20	0.12	0.99	12.65	45.12	11.59
C42 H89 N2 O8 P	780.6361	6.748	7	2.70	2.73	2.80	2.69	2.75	2.73	12.66	10.65	12.03

C45 H79 N O7	745.5865	3.501	8	9.71	9.35	9.62	9.69	9.37	9.69	12.67	10.55	9.32
C21 H39 N7	389.3263	3.91	10	4.33	2.65	4.03	4.25	2.95	4.00	12.71	37.76	15.27
C37 H69 N	527.5426	4.444	4	1.52	0.35	1.22	1.50	0.45	1.28	12.81	39.30	25.70
C20 H43 N O3	345.3255	2.751	4	6.94	6.89	6.98	7.04	6.90	6.98	12.82	3.54	14.75
C34 H43 N O7	577.3035	2.279	26	2.16	1.45	2.24	2.34	1.52	2.26	12.84	36.76	6.39
C23 H48 N O7 P	481.3163	2.114	19	1.96	1.07	1.05	1.72	1.20	1.17	12.89	24.58	28.73
C24 H54 N5 O2 P	475.3998	7.308	12	1.50	1.64	1.14	1.43	1.64	1.14	12.90	37.46	19.62
C39 H77 N2 O7 P	716.5464	2.894	18	3.60	2.71	3.87	3.65	2.59	3.94	12.90	28.01	41.43
C22 H49 N5 O3	431.383	3.389	18	1.45	0.65	1.12	1.32	0.19	1.11	12.92	48.44	32.09
C42 H75 O8 P	738.517	4.884	18	6.55	5.96	6.65	6.86	5.95	6.58	12.93	7.01	12.45
C36 H72 N4	560.5771	2.623	29	0.60	0.13	0.68	1.27	0.32	0.69	12.94	28.22	5.85
C28 H57 O9 P	568.3733	5.48	5	5.01	5.00	4.97	5.00	5.12	4.92	12.97	35.33	6.15
C35 H70 N9 O P S	695.5181	3.105	13	2.45	2.04	2.64	2.63	2.11	2.62	12.97	15.49	8.82
C19 H36 O3	312.2659	2.963	15	1.85	1.44	1.33	1.90	1.33	1.52	12.98	33.37	43.94
C25 H53 N O S2	447.3557	3.108	5	2.89	1.49	2.99	2.83	1.77	2.99	13.03	45.32	5.50
C32 H66 N2 O	494.5169	5.502	4	1.74	0.86	1.76	1.73	0.96	1.74	13.04	40.20	9.24
C23 H44 N2 O	364.3451	3.203	4	1.21	0.19	0.67	1.21	0.04	0.81	13.06	31.94	17.37
C17 H46 N10 O8 P2 S	612.2713	1.946	20	2.43	1.78	2.64	2.57	1.67	2.49	13.08	25.60	27.50
C22 H56 N9 O2 P	509.4291	3.231	8	3.25	2.99	3.59	3.26	2.97	3.53	13.08	6.06	24.36
C46 H90 Cl N4 P3	826.6072	10.469	7	3.10	3.09	3.06	3.06	3.01	3.03	13.09	16.16	6.94
C28 H70 N10 O3 P2 S	688.4848	3.051	19	2.65	2.03	3.04	2.88	2.10	3.16	13.11	23.00	24.15
C13 H22 O2	210.1617	3.117	11	1.70	1.79	1.99	1.78	1.92	1.99	13.12	16.70	3.14
C35 H48 N3 O7 P	653.3241	2.713	13	5.01	4.37	5.24	5.00	4.44	5.45	13.13	35.42	45.23
C13 H25 N O2	227.1883	3.111	12	1.44	1.54	1.75	1.53	1.67	1.76	13.14	16.93	2.86
C28 H35 N5 O2	473.2769	1.666	17	9.41	9.18	9.45	9.32	9.07	9.25	13.14	17.12	38.59
C41 H81 N O2	619.6262	10.058	15	1.38	0.48	1.21	1.22	0.15	1.17	13.15	45.42	17.30

Formula	Mass	RT	N	V1	V2	V3	V4	V5	V6	V7	V8	V9
C11 H30 N9 O6 P	415.2067	1.745	15	11.16	10.82	11.30	11.36	10.87	11.18	13.18	19.45	25.45
C29 H62 N O P S	503.4308	4.532	25	2.84	2.84	2.77	2.91	2.94	2.81	13.20	16.06	14.11
C20 H47 N7	385.3911	5.236	5	1.17	0.42	0.71	1.09	0.23	0.80	13.20	36.56	14.95
C11 H19 N7	249.17	1.142	14	2.23	2.63	0.96	2.00	2.26	0.61	13.21	46.91	49.18
C21 H43 N O2	341.329	4.684	8	1.52	0.07	0.99	1.55	0.08	1.08	13.24	36.28	13.38
C24 H52 N9 O3 P	545.3927	2.611	4	3.85	3.40	4.06	3.95	3.45	3.99	13.25	7.27	17.96
C75 H151 N10 O17 P S	1527.072	5.202	19	3.38	3.53	3.47	3.38	3.32	3.45	13.27	31.52	7.41
C26 H56 N9 O14 P S3	845.2848	7.622	10	2.46	2.24	2.37	2.36	2.22	2.34	13.28	3.35	5.71
C19 H43 N8 O P	430.329	3.111	5	3.57	2.29	3.71	3.52	2.51	3.75	13.30	45.31	6.50
C27 H55 N O	409.4276	5.256	14	1.56	0.22	1.35	1.66	0.32	1.44	13.32	42.19	11.00
C12 H26 O3	218.1879	2.179	4	6.72	6.34	6.00	6.71	6.16	6.01	13.36	28.48	2.96
C28 H41 Br N6 O7 S	684.1941	6.404	17	3.48	3.30	3.29	3.38	3.23	3.34	13.37	11.38	7.49
C27 H48 N O7 P	529.3164	2.688	8	5.86	5.93	6.16	5.83	5.93	6.09	13.39	0.82	9.44
C48 H65 N6 O P	772.4965	8.097	12	5.03	5.14	5.43	5.07	5.19	5.44	13.39	9.35	7.72
C55 H81 N8 O8 P	1012.592	3.451	16	10.82	10.81	11.27	11.08	10.92	11.26	13.40	47.77	39.05
C14 H35 N10 O2 P	406.2685	2.755	19	1.29	1.58	1.34	1.14	1.52	1.35	13.42	23.08	4.54
C16 H41 N8 P	376.3185	2.867	7	2.75	2.00	3.01	2.72	2.05	3.01	13.43	15.05	41.35
C9 H14 O3	170.0939	3.5	8	2.12	2.10	2.18	1.96	2.08	2.18	13.43	7.11	2.07
C21 H44 N O7 P	453.2846	5.467	20	3.48	3.37	3.38	3.53	3.54	3.42	13.46	18.72	7.71
C42 H76 N O7 P	737.5325	4.873	13	5.12	4.23	5.23	5.12	4.20	5.44	13.49	43.80	46.24
C44 H88 N5 P3	779.6261	5.926	13	1.30	1.55	1.52	1.31	1.60	1.50	13.50	7.51	3.52
C29 H70 N9 O4 P	639.528	3.838	13	2.37	2.14	2.42	2.45	2.22	2.36	13.52	12.56	8.39
C23 H47 N O2	369.3601	4.37	2	1.27	0.11	0.85	1.20	0.02	0.94	13.54	30.85	13.09
C25 H49 N O	379.3809	4.575	5	1.16	0.03	0.92	1.12	0.17	0.93	13.56	30.44	10.96
C38 H77 N O12	739.5441	3.085	7	3.48	3.07	3.56	3.56	3.10	3.59	13.62	9.75	10.18
C25 H52 O7	464.3708	2.834	8	2.54	1.77	2.68	2.50	1.65	2.92	13.64	21.86	32.47

C43 H87 N O5	697.6581	8.071	17	2.23	2.37	1.94	2.07	2.38	2.03	13.66	3.12	20.34
C56 H102 N O6 P3 S5	1137.552	2.032	16	1.55	1.14	1.73	1.64	0.95	1.63	13.69	29.58	31.45
C24 H51 N O	369.3965	7.858	2	1.33	0.13	0.99	1.26	0.08	1.06	13.70	31.47	14.66
C28 H50 N O7 P	543.3339	2.348	25	1.72	0.88	1.85	1.68	1.20	1.80	13.74	36.17	13.69
C43 H69 N O7	711.5062	4.878	18	5.27	4.77	5.43	5.42	4.68	5.66	13.74	18.23	49.10
C12 H20 O	180.1511	3.207	6	1.75	1.77	1.90	1.79	1.72	1.87	13.74	11.60	6.25
C13 H36 N9 O4 P	413.2616	3.41	9	3.54	3.61	3.44	3.46	3.68	3.41	13.76	9.12	17.06
C27 H57 N	395.4483	3.454	2	1.01	0.02	0.67	1.05	0.18	0.69	13.77	32.89	30.43
C28 H55 N O2	437.4228	7.545	2	1.24	0.33	0.83	1.14	0.14	0.92	13.78	39.62	14.14
C23 H49 N O	355.3809	2.909	3	1.38	0.21	0.91	1.28	0.04	0.98	13.78	32.96	12.23
C34 H46 N4 O4 P2	636.2969	2.789	11	5.15	4.52	5.40	5.18	4.59	5.62	13.79	34.98	45.32
C33 H70 N3 O7 P	651.4922	3.127	4	1.66	1.07	1.64	1.53	1.18	1.57	13.80	16.43	13.21
C18 H38 N2 O	298.2978	1.894	10	2.72	2.34	2.88	2.78	2.48	2.71	13.83	20.90	26.33
C27 H46	370.3587	11.258	12	3.33	3.23	3.42	3.38	3.28	3.36	13.86	10.73	9.06
C46 H38 O	606.2935	1.915	24	2.82	2.23	3.07	2.99	2.26	2.93	13.87	9.80	27.07
C18 H36 N2	280.2873	2.473	10	2.14	1.45	1.74	2.11	1.53	2.04	13.92	29.26	33.73
C8 H28 N9 O2 P S	345.182	1.292	6	1.12	0.01	0.95	1.07	0.11	0.85	13.93	36.11	14.77
C36 H82 N9 O3 P	719.6284	6.356	5	3.97	4.07	4.11	3.99	4.20	4.13	13.95	15.40	8.17
C27 H57 N	395.4483	3.869	13	1.15	0.01	0.75	1.07	0.04	0.80	13.97	30.31	10.02
C8 H12 O4	172.0733	2.314	4	4.69	3.65	4.78	4.63	3.82	4.81	13.98	45.47	3.12
C30 H59 N O3	481.4489	6.44	9	1.35	0.01	0.64	1.48	0.20	0.91	13.98	24.71	35.91
C30 H61 N	435.4799	3.848	7	2.75	1.09	2.35	2.57	1.39	2.37	14.01	37.19	8.25
C18 H12 N6	312.1118	2.368	11	1.34	0.49	1.47	1.26	0.60	1.55	14.06	42.08	11.71
C36 H71 N O P2	595.5017	3.882	15	2.07	2.04	2.08	2.14	2.02	2.12	14.15	9.53	6.99
C24 H47 N O	365.3654	4.199	3	1.70	0.62	1.83	1.66	0.58	1.93	14.18	5.96	33.09
C37 H67 O10 P	702.4466	4.608	6	4.64	3.87	4.63	4.69	3.74	4.92	14.18	41.87	46.92

C24 H49 N O9	495.3402	2.289	3	3.93	2.86	3.94	3.88	3.03	3.99	14.18	46.44	6.11
C62 H119 O5 P3	1036.828	8.091	10	5.99	6.49	6.01	6.08	6.48	6.08	14.20	16.61	12.41
C43 H83 N7 O2	729.6626	3.411	12	2.78	0.95	2.21	2.62	1.26	1.99	14.22	33.68	28.80
C14 H17 O P	232.1029	2.044	19	0.77	0.06	0.99	1.87	0.00	1.01	14.23	7.18	38.68
C24 H47 N O2	381.36	5.724	4	2.19	0.73	1.85	2.16	0.86	1.90	14.24	35.43	11.42
C33 H58 Cl N6 P	604.4155	2.492	20	1.30	1.63	0.45	1.04	1.16	0.46	14.25	46.79	22.94
C41 H90 N5 O2 P	715.6838	3.249	16	0.99	0.12	1.05	1.19	0.07	1.03	14.28	39.13	11.71
C38 H68 N8 O17	908.4714	8.094	26	2.98	2.82	2.60	3.07	2.75	2.68	14.28	37.07	11.24
C38 H77 N O	563.6002	4.978	21	2.02	1.90	1.98	1.94	1.94	1.99	14.32	14.53	2.02
C37 H63 N O2 P2 S2	679.3752	3.456	12	7.52	7.07	7.85	7.55	7.00	7.85	14.33	15.32	49.95
C27 H42 S	398.3004	2.857	9	5.05	4.04	5.51	5.16	4.21	5.38	14.38	19.03	47.88
C29 H61 N O S	471.4479	2.734	10	1.70	1.67	1.70	1.83	1.68	1.68	14.39	3.05	2.95
C23 H49 N O	355.3808	11.268	3	2.14	0.54	1.68	2.04	0.63	1.75	14.40	40.70	8.87
C45 H73 N O7	739.5377	4.883	9	5.12	4.16	5.16	5.13	4.26	5.42	14.43	28.90	45.23
C19 H35 N O	293.2713	2.988	11	1.60	1.26	1.37	1.48	1.05	1.42	14.44	28.19	18.28
C55 H109 N O6	879.8243	11.226	1	4.83	3.59	4.92	4.78	3.73	5.13	14.51	19.19	44.72
C25 H52 N2 O4	444.3924	3.15	20	2.85	3.04	2.82	2.84	2.77	2.81	14.52	43.04	8.04
C22 H42 O5	386.3026	2.964	8	3.69	2.67	3.51	3.66	2.49	3.67	14.52	31.26	32.98
C59 H127 N10 O9 P3	1212.9	2.759	13	2.24	2.16	2.45	2.68	2.26	2.34	14.54	16.29	14.65
C25 H53 N2 O5 P	492.3674	2.087	8	1.16	0.27	0.68	1.12	0.45	0.73	14.55	43.15	26.09
C27 H62 N10 O S	574.4811	1.503	10	3.03	2.24	2.75	3.18	2.14	2.92	14.56	49.64	21.92
C13 H18 O	190.1354	3.124	16	2.25	2.17	1.92	2.04	2.19	1.98	14.62	10.13	8.58
C36 H71 N O7	629.5222	2.629	4	2.83	1.23	2.51	2.96	1.47	2.39	14.64	27.59	33.36
C41 H82 N3 O3 P S	727.58	3.752	5	3.30	2.96	3.33	3.43	2.98	3.31	14.67	4.28	13.71
C86 H183 N10 O18 P3 S2	1801.236	3.248	19	3.07	2.53	3.01	3.02	2.49	3.09	14.68	7.78	20.24

C33 H68 N2 O	508.5326	5.501	9	1.32	0.05	1.09	1.33	0.36	1.20	14.69	34.35	12.90
C64 H108 O11	1052.789	3.55	7	3.10	2.96	3.14	3.27	2.92	3.09	14.72	6.30	15.57
C46 H92 N2 O2	704.7158	8.01	12	1.93	1.35	1.61	1.69	1.47	1.56	14.73	39.06	9.82
C46 H87 N6 P	754.6733	10.549	13	5.63	5.39	5.96	5.72	5.36	5.96	14.73	13.42	2.90
C32 H68 N2 O	496.5324	5.248	18	1.42	0.26	1.20	1.33	0.12	1.24	14.76	42.80	15.14
C26 H54 N5 P3	529.3581	1.936	7	2.23	1.69	2.46	2.40	1.59	2.33	14.78	23.63	26.04
C13 H34 N9 O P	363.2615	2.352	10	2.62	1.26	2.37	2.53	1.58	2.38	14.79	37.21	6.50
C41 H81 N O	603.6309	9.268	27	1.45	0.36	1.54	1.90	0.43	1.54	14.83	16.62	23.16
C44 H89 N O6	727.6682	8.043	20	1.16	0.86	1.19	1.02	0.70	1.17	14.86	31.81	15.22
C70 H95 O P	982.7117	2.701	9	2.87	2.54	2.87	3.04	2.57	2.92	14.89	10.47	12.14
C21 H42 N2 O2	354.3242	2.009	9	1.61	0.98	1.86	1.82	1.28	1.81	14.89	34.67	33.51
C26 H53 N O2	411.407	5.759	4	2.82	1.42	2.60	2.74	1.42	2.57	14.89	34.45	5.88
C27 H53 N5 O4	511.4082	2.704	3	7.19	6.14	7.51	7.18	6.25	7.50	14.92	14.47	49.93
C28 H55 N5 O4	525.4235	2.817	8	2.31	1.53	2.78	2.27	1.52	2.71	14.95	8.07	42.96
C19 H39 N	281.3078	4.838	4	1.78	0.05	1.15	1.64	0.23	1.29	14.97	33.09	17.61
C35 H71 N O5	585.5326	7.471	4	3.24	2.55	3.23	3.17	2.70	3.38	14.97	37.95	31.61
C16 H31 N	237.2451	2.008	12	2.73	1.31	2.12	2.56	1.44	2.02	14.98	18.70	19.62
C21 H50 N9 O P	475.3869	2.831	7	2.54	1.83	2.77	2.68	1.87	2.67	15.01	39.62	13.50
C22 H38 O2	334.2866	2.788	12	1.02	0.98	1.24	1.16	0.93	1.17	15.04	17.58	34.97
C24 H45 N4 P S	452.3109	3.118	13	4.22	3.25	4.63	4.20	3.38	4.59	15.16	43.72	12.73
C22 H35 N O4	377.2579	1.48	3	2.31	1.54	2.00	2.26	1.57	2.06	15.17	17.64	18.50
C29 H67 N7 O8	641.508	3.147	12	2.08	2.15	2.55	2.36	2.10	2.54	15.19	12.87	27.22
C22 H46 N6 O5 P2	536.299	2.714	17	1.34	1.23	1.29	1.48	1.34	1.64	15.24	33.11	37.09
C40 H85 N2 O8 P	752.6044	5.616	18	12.56	12.02	12.55	12.55	12.40	12.49	15.27	40.46	22.45
C32 H73 N10 O4 P	692.556	7.499	8	4.73	4.02	4.66	4.61	3.81	4.82	15.28	30.96	26.21
C21 H39 N O4	369.2873	2.64	12	0.83	0.48	1.22	1.15	0.46	1.24	15.30	10.81	26.28

	C22 H51 N7 O2	445.4121	5.194	20	2.99	1.67	3.11	3.00	1.83	3.13	15.34	46.73	15.27
	C62 H123 N O6	977.9341	11.49	6	6.57	5.27	6.55	6.49	5.22	6.82	15.36	9.15	37.14
	C33 H65 N5 O7	643.4866	2.675	2	6.14	5.19	6.39	6.17	5.04	6.48	15.38	18.05	48.96
	C17 H35 N	253.2766	2.2	6	2.74	0.35	2.20	2.60	0.65	2.11	15.43	43.77	21.12
	C39 H84 N9 O2 P3	803.5961	2.895	14	3.29	2.40	3.60	3.38	2.50	3.66	15.48	16.09	46.50
	C29 H61 O2 P S	504.4147	5.504	28	3.21	3.17	3.30	3.27	3.15	3.35	15.52	18.62	8.83
	C40 H61 N5 O3 P2	721.4219	3.456	2	4.53	4.02	4.89	4.66	3.96	4.97	15.53	27.71	45.80
	C44 H85 N8 O9 P	900.6177	3.244	8	2.43	1.99	2.26	2.47	2.01	2.47	15.54	4.68	23.93
	C40 H77 N O9 S	747.5344	2.412	10	1.51	0.68	1.51	1.47	0.65	1.39	15.57	7.88	35.58
	C19 H33 O9 P	436.1856	3.919	7	3.28	2.82	3.28	3.08	2.87	3.22	15.58	8.36	24.38
	C18 H45 N8 O P	420.3447	2.852	6	2.47	1.78	2.63	2.44	1.70	2.90	15.58	12.05	35.36
	C23 H45 N O	351.3496	4.101	4	1.92	0.06	1.24	1.88	0.34	1.35	15.61	45.57	18.29
	C5 H13 N8 P	216.0994	2.313	5	3.70	2.71	3.71	3.51	2.78	3.70	15.61	48.58	8.53
	C17 H42 N9 P	403.3295	2.501	13	5.20	4.08	5.44	5.50	4.01	5.42	15.62	41.33	36.04
	C46 H89 N O4	719.6781	8.064	9	1.60	1.80	2.23	1.65	1.62	2.10	15.62	46.37	32.95
	C31 H65 P S	500.4544	3.547	23	1.21	0.75	1.11	1.14	0.74	1.13	15.63	9.22	17.47
	C29 H52 N O7 P	557.3501	2.275	14	1.90	0.98	1.93	1.82	1.22	1.91	15.66	35.38	6.17
	C28 H49 N O2 S	463.3503	2.781	10	1.38	0.70	1.40	1.33	0.79	1.63	15.67	15.19	32.33
	C51 H92 N5 O5 P S2	949.6277	3.334	19	1.99	1.22	2.40	2.10	1.28	2.42	15.68	7.53	43.10
	C55 H114 N9 O10 P S	1123.815	3.493	12	3.36	3.37	3.62	3.59	3.41	3.56	15.69	9.41	22.53
	C16 H37 N8 P	372.2874	2.501	13	7.68	6.61	7.53	7.69	6.44	7.71	15.71	40.14	20.83
	C19 H34 N4 O4 S	414.2288	3.075	6	4.29	3.55	4.27	4.22	3.40	4.31	15.71	29.96	11.86
	C20 H41 N O	311.3184	2.578	6	1.99	0.82	1.51	1.87	0.95	1.56	15.72	23.74	14.22
	C45 H89 O10 P	820.619	3.396	22	5.32	5.30	5.33	5.17	5.29	5.37	15.75	4.59	5.19
	C63 H89 N O6	955.6683	7.956	20	3.17	2.74	3.06	3.08	2.79	3.06	15.77	14.81	10.10
	C8 H17 N4 O P	216.1145	1.5	20	1.31	0.65	0.76	1.25	0.63	0.81	15.81	24.56	27.17

C25 H59 N6 P	474.4546	4.727	5	1.86	0.15	1.48	1.81	0.45	1.47	15.83	40.87	18.94
C17 H28	232.2185	11.257	12	3.33	3.62	3.51	3.46	3.72	3.47	15.84	11.94	11.71
C27 H56 N2 O3	456.4287	2.715	8	2.11	2.80	2.29	2.24	2.59	2.32	15.84	26.08	23.59
C24 H51 N7 O5	517.3974	3.26	23	2.02	2.04	1.78	2.32	2.24	1.79	15.85	24.36	4.93
C8 H23 N4 O3 P	254.1513	2.314	11	3.14	2.16	3.37	3.11	2.48	3.40	15.93	45.11	7.37
C27 H54 S	410.3946	6.516	11	1.42	0.25	1.16	1.27	0.28	1.13	15.94	28.63	19.00
C33 H65 N O2 P2	569.4496	2.806	8	2.63	1.58	2.73	2.62	1.62	2.82	15.95	16.35	44.84
C39 H74 N O10 P	747.5039	4.836	12	2.33	1.85	2.36	2.50	2.09	2.56	16.00	35.84	38.47
C21 H47 N4 O6 P	482.3217	3.077	8	6.05	4.64	6.40	6.17	4.75	6.32	16.00	22.47	36.82
C32 H63 N5 O6	613.4756	2.794	11	2.66	1.54	2.84	2.72	1.70	2.95	16.03	19.12	43.27
C27 H58 N9 O4 P	603.4341	2.684	11	3.47	3.35	3.36	3.44	3.38	3.44	16.03	5.03	9.71
C23 H50 N8	438.4179	2.797	10	0.93	1.09	0.99	1.02	1.14	1.11	16.06	18.55	16.62
C45 H87 N O6	737.6528	8.403	21	1.18	1.16	1.41	1.33	1.23	1.37	16.06	47.22	18.24
C24 H47 O9 P	510.2981	1.505	20	2.71	1.75	2.37	2.85	1.81	2.49	16.06	48.51	15.15
C12 H28 N2 O9	344.1787	1.297	4	1.78	0.54	1.51	1.63	0.66	1.42	16.11	28.31	14.70
C25 H54 N9 O3 P	559.4079	2.694	19	1.13	1.05	1.30	1.17	0.81	1.30	16.13	37.73	21.61
C21 H49 N8 O6 P S	572.3213	1.488	18	1.82	0.70	1.50	1.98	0.89	1.59	16.15	36.50	17.14
C18 H35 N O	281.2712	6.652	5	2.03	1.47	1.92	1.85	1.40	1.91	16.18	49.60	12.35
C37 H65 N7 O5 P2	749.4533	3.457	4	7.48	7.07	7.85	7.64	6.96	7.95	16.19	34.05	44.35
C24 H49 O7 P	480.3214	3.078	8	5.62	4.30	5.97	5.64	4.25	5.94	16.19	17.44	47.59
C25 H44 O6	440.3132	2.622	3	3.56	3.02	3.68	3.59	2.96	3.72	16.21	15.24	18.41
C27 H51 N O2 S	453.3661	2.601	7	3.15	2.43	3.06	3.21	2.33	3.28	16.25	27.11	25.08
C25 H49 N O3	411.3707	3.122	20	1.49	1.58	1.71	1.48	1.60	1.70	16.25	4.50	4.54
C26 H56 N9 O4 P	589.4189	2.603	6	3.66	3.03	3.77	3.67	3.05	3.71	16.26	10.35	12.95
C14 H36 N10 O2 S	408.2731	2.067	10	1.87	0.84	1.41	2.20	0.65	1.53	16.26	40.59	26.02
C27 H47 N O	401.3654	4.644	4	1.60	0.29	1.21	1.56	0.39	1.33	16.28	33.61	18.54

C23 H43 N O	349.3339	3.924	19	1.56	1.41	1.35	1.52	1.66	1.34	16.29	28.37	3.35
C25 H47 N O6	457.3398	2.627	4	3.77	3.22	3.89	3.79	3.16	3.92	16.30	15.32	17.38
C22 H46 O5	390.3342	3.067	12	5.50	4.34	5.81	5.49	4.45	5.82	16.30	21.29	47.68
C36 H67 N O3	561.5113	4.855	5	1.44	1.04	1.30	1.33	1.03	1.26	16.40	8.97	16.82
C35 H74 N9 P S	683.5541	3.789	6	2.15	1.94	2.18	2.19	1.90	2.12	16.41	7.22	11.69
C31 H49 N O4	499.3655	3.268	19	1.79	1.40	1.63	1.78	1.50	1.55	16.43	14.81	25.45
C54 H100 N O8 P	921.7142	3.624	14	3.06	3.01	3.24	3.46	3.02	3.28	16.44	4.98	14.84
C17 H46 N9 P	407.3608	3.03	16	3.45	2.27	3.77	3.42	2.36	3.78	16.53	22.03	47.64
C29 H63 O12 P3	696.3545	2.789	4	7.30	6.70	7.54	7.28	6.69	7.79	16.55	31.05	46.78
C36 H53 N3 O3	575.4099	2.668	15	1.49	1.00	1.38	1.46	0.94	1.35	16.57	30.97	23.04
C43 H88 N4 O P2	738.6427	4.612	6	3.34	3.32	3.33	3.36	3.38	3.38	16.58	8.42	5.87
C45 H78 N O10 P	823.5331	5.236	21	1.71	1.98	1.66	1.89	1.96	1.64	16.61	17.57	6.21
C23 H38 N9 O2 P	503.2879	2.162	11	2.77	1.67	2.22	2.86	1.69	2.26	16.61	32.24	9.72
C16 H33 N	239.2608	2.477	9	1.89	0.95	1.57	1.65	1.18	1.59	16.62	36.93	31.82
C14 H31 O12 P	422.1555	1.917	15	2.21	1.93	2.45	2.39	1.63	2.34	16.64	40.93	24.17
C29 H57 N5 O2	507.4497	2.852	17	2.90	1.77	3.05	2.84	2.01	3.15	16.70	37.00	45.51
C57 H104 O6	884.7797	11.225	8	6.58	5.43	6.71	6.58	5.51	6.92	16.70	17.04	46.26
C21 H46 N P S	375.3105	3.77	16	2.20	2.12	2.09	2.16	2.04	2.11	16.71	12.28	9.25
C41 H76 N7 P S	729.5602	3.107	5	2.54	2.37	2.60	2.75	2.32	2.79	16.73	15.88	22.25
C34 H79 N7 O6 P2	743.558	5.214	15	2.51	2.63	2.63	2.67	2.67	2.64	16.78	12.80	2.44
C20 H45 N4 O4 P	436.316	3.719	14	4.29	3.04	4.59	4.25	2.99	4.55	16.81	13.92	38.92
C19 H44 N10 O	428.3692	2.394	6	1.61	0.45	0.45	1.72	0.49	0.44	16.82	33.07	18.61
C16 H24 N8 S	360.1844	3.531	14	1.48	0.18	1.33	1.42	0.12	1.12	16.82	38.49	37.98
C20 H37 N7 O2	407.3009	3.108	13	3.57	3.60	3.74	3.60	3.52	3.72	16.87	14.44	6.87
C30 H59 N O3	481.449	2.775	18	1.07	0.34	1.33	1.31	0.12	0.98	16.89	47.91	47.70
C39 H77 N5 O10	775.5651	2.649	2	6.17	5.21	6.45	6.22	5.29	6.50	16.90	16.49	42.35

	C22 H53 N10 O P	504.4144	5.557	28	1.99	2.37	2.79	2.45	2.24	2.85	17.02	27.22	8.24
	C41 H81 N O6	683.6056	7.75	5	5.08	4.20	5.07	4.94	4.05	5.21	17.03	22.58	29.92
	C56 H111 N O11 P2	1035.763	3.541	7	3.38	3.14	3.39	3.49	3.13	3.36	17.03	1.70	17.87
	C36 H72 N2 O8	660.5299	6.821	14	6.27	5.67	7.04	6.56	5.88	6.87	17.04	24.06	33.36
	C50 H99 N3 O2	773.7738	8.444	19	1.95	1.97	2.11	1.95	2.00	2.10	17.04	16.11	9.46
	C29 H51 Cl P2	496.3174	1.946	15	0.91	0.88	0.36	1.03	0.68	0.14	17.05	39.18	28.11
	C39 H68 N10 O4	740.5405	4.879	7	3.60	2.67	3.60	3.53	2.67	3.85	17.07	30.01	45.12
	C24 H51 N O	369.3967	2.599	11	1.79	0.04	1.35	1.70	0.44	1.30	17.07	40.51	22.08
	C58 H115 N O6	921.8716	11.494	20	2.15	1.19	2.23	2.03	1.14	2.39	17.15	14.09	34.51
	C20 H45 O P3	394.2694	2.575	6	7.78	6.86	7.76	7.84	6.73	7.82	17.15	40.35	16.64
	C26 H53 N O3	427.4022	5.129	21	2.09	0.70	1.82	1.97	0.84	1.91	17.18	17.14	16.73
	C37 H85 N10 O8 P	828.6291	2.001	8	1.82	1.34	2.00	1.94	1.41	1.93	17.22	11.87	33.15
	C23 H43 N O5	413.3135	2.634	18	3.67	2.71	3.80	3.53	2.74	3.79	17.23	5.24	25.04
	C27 H63 N7 O7	597.482	3.17	6	3.30	3.21	3.37	3.51	3.26	3.49	17.23	10.45	14.54
	C47 H80 N2 O3 P2	782.5651	3.442	23	4.68	5.37	4.64	4.62	5.34	4.38	17.24	21.35	43.37
	C42 H81 N O4	663.6158	8.025	2	3.35	2.83	3.64	3.36	3.14	3.59	17.25	37.80	30.62
	C61 H121 N O6	963.9183	11.225	7	3.28	1.98	3.32	3.20	2.07	3.53	17.25	19.36	47.10
	C17 H37 N O	271.287	2.285	9	1.66	1.01	0.58	1.25	0.87	0.61	17.30	33.43	9.19
	C18 H42 N9 O2 P	447.3188	7.067	15	4.45	4.48	4.50	4.31	4.69	4.58	17.31	28.23	19.32
	C16 H29 N O3	283.2144	2.005	7	1.85	1.35	2.10	2.09	1.28	2.05	17.34	14.19	33.65
	C22 H33 N O4	375.2407	2.429	11	2.60	2.59	2.64	2.74	2.63	2.73	17.35	4.97	16.26
	C38 H75 P3	624.5112	7.32	6	2.12	1.82	1.98	1.95	2.11	1.96	17.36	42.15	4.17
	C29 H69 Cl N9 O P	625.5059	7.316	14	3.25	3.32	3.19	3.08	3.41	3.19	17.37	17.22	2.06
	C21 H45 N O	327.3496	2.638	4	1.70	0.07	1.25	1.57	0.10	1.28	17.39	26.60	9.97
	C19 H36 N6 O2	380.2895	3.506	10	9.19	8.61	9.03	9.20	8.32	9.07	17.39	45.33	11.79
	C40 H79 N O2	605.6108	10.494	8	2.53	0.23	1.93	2.38	0.64	1.68	17.41	43.69	39.87

Formula												
C44 H86 Cl4 N2 O2	814.5452	10.68	14	4.03	3.32	3.84	3.83	3.38	3.97	17.43	17.98	17.43
C29 H51 N O S	461.3709	2.828	8	2.31	1.04	2.19	2.24	1.38	2.35	17.44	35.75	20.21
C13 H20 O	192.1511	3.12	7	1.95	1.78	2.02	1.87	1.79	2.00	17.46	7.49	10.67
C32 H73 N7 O11	731.5389	2.657	3	5.11	4.18	5.41	5.21	4.16	5.45	17.48	19.74	47.14
C42 H65 N O6	679.4795	3.073	8	2.45	1.00	2.72	2.30	1.00	2.91	17.51	40.79	26.46
C30 H64 N9 O6 P	677.4714	2.589	4	3.31	2.80	3.29	3.35	2.82	3.41	17.54	11.95	17.61
C35 H69 N O6	599.5117	7.75	22	0.73	0.16	1.38	1.09	0.24	1.46	17.57	14.32	37.20
C62 H123 N O6	977.9347	12.139	21	2.85	2.40	3.22	2.90	2.67	3.26	17.58	36.51	37.28
C79 H151 N4 O8 P	1315.127	8.039	12	5.20	4.67	5.65	5.36	4.34	5.57	17.59	47.60	39.59
C28 H58 N8	506.4803	5.182	20	2.08	2.26	1.92	2.13	2.20	1.89	17.60	26.01	9.94
C15 H26 N7 P	335.1991	2.276	18	1.46	0.48	1.50	1.34	0.78	1.46	17.62	36.87	6.67
C49 H86 Cl O2 P S	804.5773	3.934	7	3.81	3.88	4.05	3.84	3.89	4.03	17.62	11.26	7.16
C63 H126 O4 S	978.9375	12.141	8	1.68	0.68	2.35	1.94	0.97	2.35	17.63	42.83	13.54
C27 H53 N O3	439.4022	4.966	9	1.44	0.23	1.14	1.49	0.02	1.13	17.67	38.67	13.83
C25 H49 N O	379.3808	5.204	12	2.26	0.92	2.00	2.20	1.15	2.05	17.71	37.60	6.74
C30 H55 N2 P S	506.3828	2.74	15	1.23	0.89	1.42	1.44	0.82	1.39	17.88	9.33	7.07
C23 H47 N O	353.3652	5.887	5	2.13	0.54	1.72	2.03	0.71	1.76	17.89	36.06	9.73
C23 H49 N	339.3859	3.044	14	3.40	2.94	3.26	3.26	2.85	3.29	18.01	16.03	5.91
C22 H47 P S	374.3152	2.981	13	2.10	0.41	1.93	2.20	0.70	2.03	18.01	31.26	21.41
C55 H105 N O6	875.7922	11.225	7	6.22	5.05	6.30	6.17	5.23	6.51	18.02	23.82	45.11
C40 H61 N4 P3	690.4105	3.413	26	2.80	3.56	2.29	2.40	3.24	2.65	18.05	43.40	43.19
C32 H43 N4 O8 P	642.2833	3.484	2	11.03	9.95	11.26	11.05	9.90	11.43	18.05	13.61	42.71
C21 H54 N9 P	463.4235	2.866	6	3.89	3.08	4.20	3.93	3.09	4.23	18.06	22.78	36.24
C16 H43 N10 O6 P	502.3112	1.961	9	7.72	6.75	7.85	7.92	6.50	7.60	18.06	42.16	49.39
C46 H85 N5 O3 P2	817.6122	3.066	16	1.86	1.63	1.99	2.15	1.63	2.06	18.11	0.61	45.12
C34 H67 N5 O7	657.5015	2.781	7	2.74	1.57	2.88	2.75	1.70	2.97	18.11	18.30	48.44

C23 H45 N7	419.3757	4.688	7	1.41	0.44	1.07	1.39	0.13	1.08	18.11	43.49	12.95
C17 H41 N8 O P	404.3133	2.968	5	4.15	3.46	4.33	4.45	3.23	4.38	18.12	39.44	29.63
C63 H125 N O6	991.9498	11.49	5	6.07	4.80	6.02	5.97	4.77	6.34	18.14	8.97	37.64
C48 H99 N6 O3 P	838.7515	4.688	7	1.35	0.50	1.01	1.33	0.18	1.02	18.14	43.49	12.92
C31 H61 N5 O6	599.4605	2.685	3	5.32	4.43	5.57	5.38	4.34	5.66	18.14	16.77	47.22
C25 H53 N O2	399.407	7.102	3	1.24	0.39	1.04	1.27	0.05	1.04	18.16	36.98	13.64
C28 H58 N8	506.4807	3.753	6	1.51	0.19	1.16	1.41	0.38	1.12	18.17	31.54	8.46
C23 H47 N O	353.3653	4.798	3	1.56	0.50	1.54	1.44	0.62	1.38	18.19	24.94	20.98
C29 H62 N O13 P S	695.3704	2.789	6	5.83	5.13	6.26	6.12	5.29	6.38	18.21	35.60	49.76
C36 H71 N5 O8	701.5279	2.771	2	4.39	3.46	4.49	4.43	3.47	4.64	18.22	11.11	44.34
C17 H44 N9 O P	421.3398	2.963	5	3.72	3.17	3.67	3.84	2.88	3.88	18.23	44.73	24.11
C34 H70 Br N S	603.4409	3.926	9	1.88	1.69	1.91	1.98	1.89	1.98	18.25	23.13	16.49
C36 H65 N9 O4	687.5128	2.666	3	5.96	4.94	6.18	5.98	4.90	6.25	18.26	14.20	47.52
C35 H73 N4 O5 P	660.5298	6.472	10	7.22	6.67	7.67	7.29	6.74	7.56	18.27	19.31	30.52
C38 H75 N O2	577.5795	9.761	11	1.20	0.40	0.93	1.05	0.15	0.95	18.35	29.96	23.16
C25 H43 N O4	421.3185	3.417	20	2.94	3.16	3.13	2.98	3.25	3.01	18.36	19.61	16.18
C33 H65 N5 O6	627.4915	2.932	4	5.26	4.21	5.38	5.33	4.22	5.54	18.38	20.71	47.72
C26 H59 N7 O5 P2 S5	771.2658	7.471	22	2.62	2.50	2.50	2.50	2.49	2.49	18.38	4.26	3.52
C29 H51 N O2 S	477.3662	3.073	13	3.46	1.25	3.52	3.47	1.54	3.78	18.42	46.21	40.84
C76 H131 N4 O12 P3	1384.897	3.485	8	8.09	6.98	8.19	8.01	7.10	8.27	18.44	17.91	31.42
C18 H30	246.2341	11.258	15	3.34	3.43	3.18	3.24	3.25	3.23	18.48	32.15	10.10
C44 H94 N9 O5 P3	921.6601	2.717	15	2.69	2.77	3.02	2.84	2.66	3.17	18.52	15.21	17.94
C25 H48 N2	376.381	3.58	11	1.43	0.21	0.72	1.33	0.00	0.94	18.54	36.67	31.87
C30 H59 N O	449.4593	3.883	17	0.99	0.63	1.39	1.14	0.53	1.44	18.55	13.33	29.14
C35 H71 N O4	569.5392	5.891	13	1.32	1.15	1.43	1.29	1.17	1.38	18.57	5.67	6.74
C23 H47 N O	353.3653	5.001	7	2.38	0.87	2.04	2.28	1.06	2.18	18.58	37.18	17.10

C33 H60 N9 O3 P3	723.4015	3.032	21	6.04	5.10	6.14	6.00	5.19	6.51	18.61	11.07	44.46
C54 H83 N O6	841.6208	2.783	4	5.43	4.73	5.57	5.61	4.62	5.60	18.62	14.31	39.66
C23 H58 N9 O2 P	523.4441	3.428	19	1.67	1.92	1.89	1.72	2.04	1.93	18.63	21.50	7.79
C27 H60 N8 O	512.4913	3.857	15	1.41	1.40	1.64	1.64	1.47	1.64	18.65	19.81	13.07
C34 H76 N9 P3 S	735.5125	2.66	10	3.52	3.11	3.47	3.56	3.07	3.47	18.66	5.87	3.07
C26 H53 N O	395.4119	5.59	10	2.84	1.37	2.74	2.80	1.65	2.54	18.69	35.77	28.93
C27 H58 N6 O5 S	578.4196	3.116	3	2.77	2.46	2.80	2.89	2.44	2.81	18.71	3.88	24.59
C41 H81 N5 O5	723.6231	4.823	6	1.51	1.34	1.40	1.35	1.69	1.41	18.75	37.55	1.49
C57 H113 N O6	907.8557	11.489	2	7.30	6.02	7.19	7.15	6.02	7.54	18.76	6.73	39.91
C23 H49 N3 O	383.3869	1.952	16	1.87	1.66	2.11	2.05	1.77	2.01	18.78	21.24	23.17
C20 H41 N O	311.3183	3.765	5	1.67	0.47	1.32	1.52	0.65	1.24	18.78	23.05	13.71
C43 H72 N7 O2 P	749.5491	6.047	3	1.74	0.85	1.39	1.55	1.04	1.44	18.82	26.14	8.62
C10 H29 N10 P	320.232	2.691	8	2.43	1.89	2.59	2.83	1.96	2.56	18.83	7.42	21.49
C20 H22 O4	326.1515	2.252	8	3.15	1.75	2.65	3.05	1.75	2.65	18.84	41.49	10.01
C36 H69 N O7 S	659.4821	2.427	8	1.97	1.40	2.14	2.15	1.37	2.19	18.89	11.77	26.73
C21 H47 O P3	408.2845	3.355	5	3.79	2.23	4.01	4.01	2.39	4.04	18.89	29.84	49.05
C21 H56 N10 O P2	526.4124	2.705	10	3.78	3.67	3.65	3.94	3.65	3.63	18.96	3.93	9.41
C20 H43 N2 O3 P	390.3018	3.445	10	3.61	2.68	2.65	3.24	2.61	2.70	18.97	22.30	18.94
C9 H26 N4 O7 P2	364.1284	2.335	16	4.08	4.36	4.24	3.98	4.06	4.32	18.99	45.64	9.84
C49 H74 O P2	740.5218	4.908	8	2.15	1.60	2.22	2.30	1.67	2.31	18.99	13.11	29.49
C27 H56 N2 O4	472.4241	3.148	12	2.16	2.00	2.02	2.01	2.04	1.99	19.00	5.39	9.53
C18 H34 O3	298.2504	2.672	16	1.35	1.31	2.15	1.61	1.30	2.12	19.01	43.19	4.73
C17 H24	228.1872	11.256	13	3.79	4.12	3.83	3.58	4.06	3.81	19.03	15.40	6.54
C37 H67 N7 O P2 S2	751.4331	2.79	3	5.55	4.99	5.82	5.54	4.98	6.02	19.07	35.91	43.72
C35 H69 O10 P	680.4638	4.878	2	8.43	7.65	8.47	8.41	7.57	8.70	19.09	35.57	43.29
C28 H49 N O4	463.3657	3.413	18	1.77	2.10	1.90	1.67	2.04	1.92	19.16	23.02	15.52

C17 H42 N8 O4 S	454.3055	4.508	14	2.79	2.72	2.84	2.89	2.82	2.81	19.16	12.57	3.37
C31 H66 N9 O6 P	691.4865	2.663	13	3.07	2.63	3.20	3.26	2.70	3.04	19.20	18.19	21.32
C29 H60 N8	520.4964	3.753	17	1.71	0.54	1.70	1.95	0.51	1.60	19.22	38.85	17.81
C66 H128 N8 O16 P2	1350.892	3.448	22	1.61	1.38	1.71	1.54	1.35	1.89	19.23	7.51	25.53
C41 H81 N O5	667.6095	5.605	23	3.53	3.83	4.17	4.10	4.32	4.04	19.25	47.47	20.27
C20 H32	272.2496	11.259	17	3.62	3.58	3.62	3.65	3.59	3.52	19.28	7.70	12.16
C19 H38 O S2	346.2349	2.356	9	4.01	2.47	3.85	3.92	2.80	3.81	19.32	46.16	5.92
C22 H45 N O	339.3496	5.345	5	1.56	0.23	1.06	1.43	0.22	1.11	19.35	27.66	13.98
C31 H74 N9 O6 P	699.5493	3.303	5	3.21	2.90	3.28	3.28	2.97	3.30	19.37	16.51	14.17
C24 H52 N8 O2	484.4234	4.4	18	2.92	2.62	2.93	2.75	2.48	2.92	19.41	49.88	6.01
C40 H67 N O7 P2	735.4377	3.46	2	6.22	5.62	6.64	6.40	5.48	6.78	19.44	27.20	49.99
C44 H50 N10 O3 P2	828.3525	9.627	20	3.13	2.82	2.63	2.88	2.46	2.64	19.46	47.56	8.08
C22 H51 N10 O3 P	534.3894	3.891	19	1.74	1.47	2.38	1.77	1.91	2.36	19.50	44.54	8.87
C29 H61 N5 O2 P2	573.4301	3.697	3	5.58	4.24	5.22	5.48	4.37	5.26	19.51	39.40	5.58
C23 H40 O5	396.287	2.63	14	2.75	1.71	2.90	2.60	1.71	2.82	19.52	0.32	33.78
C31 H67 N4 O4 P	590.488	7.472	3	5.72	5.05	5.78	5.59	5.01	5.84	19.52	21.60	30.09
C43 H77 O10 P	784.5217	6.037	24	1.22	0.36	0.46	1.72	0.40	0.58	19.57	35.88	16.63
C20 H24 N8 O4 S	472.1626	2.279	8	1.92	0.82	1.89	1.73	1.07	1.84	19.62	45.69	7.03
C20 H39 N O2	325.298	3.22	11	3.62	2.55	3.84	3.51	2.49	3.82	19.64	25.61	34.13
C23 H55 N6 O5 P	526.3951	3.556	4	2.77	2.77	2.94	3.06	2.80	2.91	19.64	4.00	17.41
C30 H66 N6 O4 P2	636.4601	3.431	15	3.20	2.99	3.10	3.36	3.06	3.20	19.71	9.07	21.74
C49 H95 O8 P	842.6725	5.208	21	2.71	2.99	2.83	2.73	2.94	2.90	19.73	13.27	10.59
C24 H48 O6	432.3446	3.357	2	7.82	6.96	8.11	8.13	6.70	8.15	19.75	36.20	31.83
C38 H77 N O3	595.5897	9.761	11	1.39	0.22	1.12	1.24	0.04	1.14	19.76	29.50	22.05
C24 H56 N5 P	445.4276	3.563	17	1.84	0.27	0.86	1.65	0.44	1.05	19.77	20.19	31.80
C84 H123 N2 O11 P	1366.887	3.486	4	8.06	6.80	8.10	7.90	6.85	8.18	19.79	17.98	30.18

C44 H89 N O15	871.6235	3.037	9	1.51	1.06	1.74	1.73	1.25	1.60	19.81	26.73	21.46
C25 H62 N9 O3 P	567.4705	3.394	7	2.60	2.48	2.79	2.44	2.60	2.92	19.82	36.54	19.75
C51 H74 O2	718.5714	7.974	12	1.68	0.62	1.34	1.71	0.39	1.72	19.86	46.98	38.45
C16 H25 N3 O3	307.189	2.073	12	1.91	0.26	1.23	1.92	0.26	1.31	19.91	34.61	13.85
C20 H45 N6 O3 P	448.3291	11.259	17	3.33	3.79	3.48	3.45	3.91	3.45	19.92	13.94	3.84
C29 H59 N O S2	501.4024	3.399	22	2.46	2.14	2.22	2.54	2.16	2.18	19.93	8.34	28.23
C34 H75 N10 O6 P	750.5601	4.159	7	6.23	5.48	6.26	6.23	5.49	6.53	19.94	26.46	45.77
C41 H81 N O2	619.6263	10.23	12	1.71	0.48	1.29	1.83	0.05	1.23	19.95	48.07	12.56
C15 H29 N O4	287.2089	1.926	7	5.23	3.72	5.09	4.93	4.14	5.18	19.96	43.92	12.29
C19 H51 N10 O5 P	530.3789	2.813	15	3.75	3.01	4.09	3.76	2.92	4.18	19.96	36.21	46.96
C17 H33 N O3	299.2455	1.881	13	1.02	0.19	0.12	1.45	0.20	0.01	19.99	7.52	17.26
C25 H49 N O5	443.3603	3.568	19	1.28	0.73	1.17	1.14	0.75	1.26	20.02	9.98	10.64
C41 H81 N O6	683.6055	7.264	16	3.41	2.38	3.63	3.43	2.51	3.60	20.03	32.50	23.53
C16 H40 N10 O	388.3386	2.958	6	3.69	2.95	3.88	4.01	2.77	3.88	20.03	30.92	30.35
C25 H53 N	367.4172	3.038	2	2.31	0.54	1.93	2.25	0.85	2.06	20.04	40.13	16.45
C38 H49 N O6	615.3554	2.772	22	3.20	2.58	3.48	3.40	2.55	3.31	20.07	15.63	34.58
C34 H63 N	485.4957	3.853	18	1.55	0.02	1.14	1.70	0.06	1.15	20.09	17.57	19.01
C20 H38 N6 O4	426.2951	2.97	7	5.63	4.90	5.85	5.97	4.71	5.84	20.09	35.24	31.85
C16 H35 N	241.2766	2.291	4	2.21	0.70	1.78	2.06	0.85	1.77	20.10	32.13	11.58
C41 H65 N O7	683.4757	4.163	18	4.23	3.03	4.21	4.11	3.00	4.44	20.14	38.83	44.97
C33 H67 N7 O10	721.4977	2.582	5	2.87	2.58	2.85	3.09	2.54	2.93	20.21	5.65	12.21
C38 H77 N O	563.5997	7.275	10	2.75	2.68	2.98	2.90	2.94	2.84	20.22	32.27	18.40
C8 H6 O4	166.0263	2.447	6	2.20	2.21	2.25	2.12	2.32	2.37	20.22	25.29	22.37
C43 H83 N O5	693.6264	8.025	3	3.70	3.10	3.76	3.52	3.15	3.70	20.27	8.81	20.24
C29 H52 N4 O3	504.4029	1.476	15	1.67	0.55	0.65	1.50	0.42	0.90	20.33	37.91	29.31
C51 H62 Cl2 N O4 P3 S2	979.2704	7.677	12	2.59	2.46	2.50	2.43	2.45	2.41	20.33	17.78	11.35

C18 H37 N O4	331.2719	2.019	26	2.09	1.08	2.12	2.21	1.11	2.10	20.33	12.26	45.05
C54 H77 Cl N9 O17 P S4	1317.375	8.128	28	2.60	2.29	3.02	2.70	2.15	2.82	20.35	26.87	37.01
C34 H74 N6 O4 P2	692.5228	3.257	2	2.11	1.91	1.98	2.01	1.91	2.01	20.35	3.07	5.45
C19 H33 N	275.2608	2.614	12	1.05	0.27	0.76	1.22	0.30	0.65	20.39	38.91	14.74
C46 H89 N O3	703.684	8.273	10	1.55	1.58	1.51	1.47	1.52	1.47	20.45	8.26	16.36
C41 H83 N O3	637.6362	8.072	7	1.22	1.44	0.98	1.48	1.40	1.17	20.46	5.76	32.90
C28 H58 N8 O S	554.4442	3.214	21	4.45	4.38	4.43	4.18	4.37	4.43	20.47	6.90	3.39
C14 H20	188.156	11.258	11	3.17	3.33	3.00	3.26	3.61	3.08	20.47	35.23	18.17
C21 H40 O3	340.297	3.362	11	4.58	3.51	4.60	4.67	3.36	4.75	20.48	21.31	26.99
C45 H70 N P	655.5232	3.332	7	3.52	3.22	3.51	3.56	3.26	3.60	20.49	13.56	17.38
C30 H65 N9 O7	663.5024	3.211	5	2.26	2.04	2.22	2.20	2.09	2.20	20.49	6.83	3.18
C22 H49 O P3	422.3002	3.347	3	8.39	7.54	8.69	8.73	7.26	8.73	20.50	35.72	30.46
C31 H66 N10 O8	706.5059	8.054	18	5.96	5.70	5.78	5.67	5.44	5.77	20.50	35.59	0.62
C30 H69 N7 O11	703.508	2.423	10	1.04	0.59	1.42	1.25	0.35	1.39	20.55	39.49	18.50
C26 H58 N O10 P3	637.3281	3.62	25	5.54	5.05	6.10	5.68	4.94	5.95	20.56	28.37	44.21
C29 H59 N9 O6	629.4567	3.273	6	1.37	0.25	0.74	1.18	0.02	0.73	20.60	41.06	10.58
C43 H75 O8 P	750.517	4.884	12	3.54	3.00	3.67	3.77	3.20	3.84	20.60	38.52	37.63
C47 H77 N O7	767.5685	4.883	5	8.84	8.08	8.88	8.86	8.12	9.13	20.63	23.72	43.72
C25 H45 N5 O	431.3613	2.573	20	2.96	2.10	2.38	2.98	2.17	2.16	20.67	27.66	29.48
C43 H87 N O	633.6784	10.759	18	1.65	0.34	1.01	1.42	0.02	1.17	20.67	43.02	21.52
C42 H71 O14 P	830.4554	8.105	24	4.15	4.15	4.22	4.03	4.27	4.11	20.71	17.52	21.60
C29 H71 N10 O P	606.5579	11.489	4	5.02	3.62	4.88	4.87	3.58	5.31	20.72	6.41	43.39
C35 H78 N9 O P3 S	765.5241	2.576	5	3.04	2.59	2.95	3.12	2.61	3.04	20.74	3.22	10.90
C34 H75 N9 O3 P2 S	751.5207	4.896	12	1.84	1.32	1.92	2.10	1.47	2.10	20.75	40.75	40.69
C74 H144 N5 O17 P	1406.028	6.043	24	0.94	0.65	0.89	1.06	0.51	0.83	20.77	34.45	12.73
C20 H44 N2 O9	456.3037	1.312	8	2.39	0.54	1.38	2.62	0.69	1.55	20.79	37.43	28.95

C48 H89 N O3 P2 S2	853.5768	2.566	4	2.51	2.11	2.33	2.60	2.14	2.46	20.79	4.35	15.11
C38 H63 N O8 P2	723.4017	2.791	3	6.25	5.51	6.36	6.20	5.62	6.67	20.79	32.24	43.63
C23 H45 N O2	367.3444	2.877	23	1.61	1.94	2.16	1.84	1.96	2.41	20.80	4.79	48.09
C27 H52 N2 O	420.4072	4.384	7	1.37	0.01	0.85	1.10	0.04	0.87	20.81	41.63	10.32
C65 H141 N10 O10 P3 S2	1378.947	2.614	21	5.14	4.73	4.74	5.43	4.82	4.87	20.88	27.43	18.08
C35 H56 N O10 P	681.3625	3.474	4	9.31	8.15	9.52	9.29	8.16	9.71	20.88	13.91	49.92
C82 H165 N7 O14 P2 S2	1598.132	3.313	18	4.29	3.98	4.22	4.21	4.01	4.36	20.89	4.71	19.61
C41 H72 N4 O2	652.5634	7.492	16	1.76	0.96	1.88	1.58	0.66	1.86	20.92	44.45	17.64
C25 H45 N7	443.3722	3.119	13	4.84	4.31	4.67	4.72	4.48	4.66	20.94	20.57	2.22
C19 H30	258.2341	11.256	6	4.43	4.36	4.36	4.21	4.33	4.25	20.96	18.29	14.41
C40 H61 N5 O4 P2	737.4173	2.79	2	6.56	5.78	6.72	6.50	5.91	6.97	20.97	30.31	42.89
C31 H64 N6 O3	568.506	7.473	2	4.02	3.32	4.08	3.88	3.28	4.14	20.99	24.24	31.52
C50 H107 N10 O10 P S	1070.764	2.658	13	4.13	4.06	4.11	4.39	4.05	4.12	21.01	5.71	20.44
C19 H46 N9 O P S	479.3273	2.56	4	2.37	2.16	2.11	2.54	2.19	2.29	21.03	4.97	23.47
C35 H68 N6 O2	604.5422	7.757	9	1.89	0.56	1.94	1.91	0.83	2.04	21.08	35.48	22.76
C10 H25 N4 O P	248.1771	3.231	6	2.93	2.57	2.61	2.83	2.55	2.50	21.25	9.37	14.61
C42 H89 N3 P2	697.6536	3.912	20	4.09	4.47	4.15	4.05	4.40	4.06	21.29	23.08	13.67
C40 H38 N4 O16	830.2304	9.624	19	3.76	3.61	3.46	3.84	3.56	3.50	21.30	5.74	14.38
C27 H56 N2 O3	456.4287	3.378	28	3.49	3.38	3.55	3.63	3.46	3.46	21.31	33.43	24.40
C18 H41 O P3	366.2377	2.334	18	5.82	4.43	5.63	6.14	4.56	5.61	21.32	16.77	29.90
C30 H61 N7 O8	647.4603	2.674	9	3.70	3.12	3.70	3.70	3.28	3.63	21.38	23.46	23.05
C60 H119 N O6	949.9026	11.491	7	3.56	2.16	3.70	3.48	2.27	3.90	21.43	14.96	43.65
C29 H59 N	421.4641	3.919	14	1.24	0.10	1.10	1.27	0.10	1.06	21.44	31.60	17.11
C29 H54 N2 O2	462.4176	5.718	11	1.61	0.13	1.03	1.44	0.09	0.96	21.44	40.65	23.03
C37 H78 N6 O10 S	798.5504	3.004	13	4.17	3.73	4.30	4.39	3.75	4.41	21.55	7.70	19.39

	C32 H63 N5 O7	629.4714	2.573	7	3.27	2.53	3.46	3.49	2.49	3.54	21.63	15.98	40.33
	C42 H83 N O6	697.6221	8.469	9	3.23	1.94	3.39	3.15	1.82	3.54	21.64	20.52	48.76
	C59 H118 O4 S	922.875	11.493	19	2.22	1.01	2.17	1.99	1.00	2.37	21.66	4.75	32.68
	C44 H79 N3 O8	777.5868	4.886	3	8.72	7.92	8.69	8.67	7.94	8.95	21.68	26.76	43.32
	C48 H79 N O7	781.5839	4.882	4	7.03	6.26	7.07	7.02	6.26	7.34	21.68	28.61	43.08
	C28 H60 N9 O5 P	633.4451	2.596	8	3.85	3.22	3.83	3.83	3.29	3.83	21.70	22.06	11.40
	C22 H43 N O2	353.3293	3.678	20	2.82	1.96	3.10	3.32	2.16	3.10	21.72	40.16	19.50
	C33 H65 O10 P	652.4333	4.161	1	6.65	5.80	6.64	6.59	5.76	6.91	21.74	39.38	44.68
	C37 H80 N6 O5 P2	750.565	3.363	7	2.41	2.45	2.42	2.26	2.44	2.40	21.76	3.27	6.73
	C28 H57 N3 S	467.427	3.39	17	1.65	1.85	1.94	1.93	1.70	1.93	21.76	19.98	6.96
	C31 H50 O2 S	486.3527	2.829	6	3.99	3.41	4.27	4.07	3.83	4.42	21.88	45.62	47.07
	C88 H179 N10 O12 P3 S3	1757.209	3.258	15	2.58	2.25	2.69	2.71	2.32	2.79	21.91	9.10	14.87
	C48 H79 N O7	781.584	4.602	6	4.80	4.05	4.79	4.80	3.94	5.09	21.92	45.10	45.54
	C73 H157 N10 O7 P3 S2	1443.089	3.308	5	1.43	1.28	1.27	1.32	1.25	1.30	21.93	4.14	4.32
	C36 H79 N6 P S2	690.5571	8.04	18	4.67	4.38	4.78	4.79	4.35	4.69	21.94	41.62	14.11
	C76 H165 N10 O16 P3 S	1599.134	3.308	12	2.67	2.29	2.69	2.76	2.26	2.61	21.94	11.57	22.32
	C20 H46 N5 O2 P	419.3371	2.974	7	2.76	2.69	3.23	2.92	2.69	3.18	21.95	14.72	20.49
	C49 H81 N O7	795.5991	4.886	3	7.77	7.03	7.82	7.78	7.07	8.09	21.95	25.94	43.17
	C18 H35 N	265.2767	2.558	3	2.25	0.40	1.80	2.07	0.59	1.74	21.95	34.58	17.35
	C30 H53 N P2	489.3658	3.187	13	2.18	2.10	2.47	2.40	2.09	2.50	21.97	17.72	18.47
	C23 H40 N3 O2 P	421.2865	3.914	11	2.66	2.73	2.83	2.75	2.79	2.79	22.03	13.33	7.29
	C61 H131 N10 O10 P S3	1290.895	2.627	8	2.18	1.70	2.09	2.49	1.84	2.11	22.04	28.30	18.77
	C37 H67 N O15	765.4487	2.792	3	3.74	3.03	3.82	3.67	3.10	4.23	22.10	42.64	46.77
	C86 H161 N8 O15 P S2	1641.127	2.978	20	2.86	2.69	3.13	3.25	2.60	3.36	22.15	11.92	27.14
	C27 H56 N6 O2	496.4483	5.942	19	3.02	3.51	2.65	3.11	3.36	2.95	22.16	25.72	34.87

C38 H66 N4	578.5266	11.228	5	3.98	2.74	4.07	4.04	2.69	4.47	22.17	26.46	42.62
C35 H69 O10 P	680.4639	4.6	4	6.50	5.77	6.52	6.53	5.61	6.80	22.17	49.69	44.10
C40 H80 N O8 P	733.561	3.478	16	2.03	1.59	2.40	1.83	1.60	2.31	22.25	10.43	23.86
C19 H17 N3 O7	399.1069	1.933	20	2.06	1.47	2.08	2.20	1.21	1.94	22.26	40.48	27.78
C22 H43 N O	337.3339	3.907	7	1.78	1.52	1.73	1.79	1.81	1.73	22.28	31.85	4.32
C33 H73 N9	595.6008	7.352	9	2.14	1.86	2.15	2.01	1.88	2.10	22.31	22.20	6.84
C22 H45 N O	339.3496	5.483	3	2.26	0.70	1.82	2.12	0.86	1.87	22.35	33.82	16.40
C29 H41 Cl2 N	473.26	1.658	14	8.02	8.24	7.95	7.83	8.00	7.74	22.37	32.94	31.85
C37 H73 N O2	563.5633	7.488	3	3.36	3.11	3.69	3.23	3.00	3.50	22.40	22.45	30.89
C28 H58 N2 O4	486.4398	3.153	29	2.40	2.07	2.14	2.35	2.24	2.15	22.44	27.58	11.09
C40 H87 Cl N4 O2 P2 S2	816.5424	10.678	18	3.76	3.05	3.80	3.70	3.21	3.80	22.44	19.06	8.35
C45 H60 N P	645.4477	2.629	12	2.12	2.03	2.01	2.51	1.89	1.99	22.48	34.66	11.64
C60 H112 N3 O2 P	937.8477	3.074	28	2.71	0.25	2.64	3.11	0.00	2.65	22.48	43.52	2.27
C45 H73 N O7	739.5381	4.16	11	8.68	7.85	8.74	8.67	7.80	8.95	22.49	36.24	46.93
C42 H79 N O4	661.5999	5.379	3	4.52	4.50	4.53	4.38	4.41	4.36	22.52	40.96	24.84
C24 H54 N6 O P2	504.3815	3.567	4	3.11	3.08	3.24	3.45	3.09	3.18	22.55	3.45	24.54
C38 H61 N4 O2 P S2	700.4005	6.06	10	1.94	1.44	1.43	1.95	1.41	1.26	22.57	20.98	34.63
C42 H85 N O3	651.6519	11.059	18	2.80	1.35	2.49	2.75	1.53	2.65	22.64	49.50	18.00
C28 H50 N O7 P	543.3345	2.268	9	1.33	0.31	1.27	1.08	0.61	1.23	22.68	40.49	8.11
C50 H83 N O7	809.6157	4.882	4	4.40	3.70	4.51	4.39	3.71	4.68	22.77	29.38	43.17
C43 H64 N P	625.4766	3.09	17	1.63	1.50	1.78	1.49	1.55	1.80	22.79	9.76	18.14
C18 H37 N O	283.2869	3.767	10	2.65	1.17	2.11	2.57	1.35	2.11	22.79	22.15	19.82
C14 H17 N	199.1356	1.659	21	4.90	5.20	4.80	4.76	5.20	4.92	22.80	34.39	17.03
C22 H43 N O2	353.329	2.685	3	1.85	1.74	1.61	1.85	1.59	1.74	22.80	35.16	15.04
C27 H56 N6 O4 S	560.4108	3.123	8	1.79	0.48	1.32	1.51	0.70	1.35	22.83	38.28	6.14
C50 H83 N O7	809.6166	4.95	4	7.70	7.00	7.81	7.69	7.00	7.98	22.83	29.49	43.22

C39 H84 N9 O P3	787.6009	2.784	17	1.52	1.17	1.38	1.36	1.00	1.40	22.84	45.76	9.34
C24 H49 N O2	383.3759	3.051	4	3.22	1.56	3.10	3.03	1.57	3.27	22.85	12.10	35.52
C30 H56 N6 O2	532.4465	6.38	13	7.09	7.38	7.23	7.19	7.08	7.20	22.86	39.45	12.74
C19 H44 N5 O2 P	405.3216	3.128	14	2.55	2.59	2.71	2.46	2.58	2.67	22.89	11.68	5.57
C35 H78 N8 O4 P2 S	768.5323	1.546	4	4.04	2.37	3.24	4.26	2.41	3.52	22.89	43.63	31.46
C22 H37 N6 O2 P S	480.2458	3.379	27	3.11	2.19	3.09	3.42	2.18	3.15	22.89	12.50	8.37
C45 H81 N5 O6 S	819.5912	2.643	8	5.36	4.41	5.58	5.40	4.46	5.64	22.92	19.14	43.69
C64 H132 N2 O12 P2 S2	1246.869	2.633	5	4.79	4.52	4.79	5.23	4.62	4.87	22.92	21.43	15.84
C42 H83 N O2	633.6415	11.062	18	3.01	1.58	2.71	2.97	1.76	2.86	22.93	49.16	18.20
C38 H77 N O3	595.5897	7.486	3	3.42	3.15	3.76	3.29	3.05	3.57	22.94	22.96	31.98
C75 H141 N8 O3 P3 S	1327.005	3.216	4	2.03	1.76	1.98	1.92	1.85	1.96	22.96	10.30	3.51
C34 H74 N9 O3 P	687.564	7.288	22	3.19	2.41	3.88	3.41	2.46	3.81	22.96	42.14	25.50
C20 H45 N4 O4 P	436.316	3.842	12	5.85	4.54	6.24	6.09	4.73	6.33	23.01	26.87	46.38
C24 H49 N7 O5	515.3815	2.703	11	2.34	2.16	2.46	2.33	2.17	2.49	23.03	18.05	11.69
C85 H170 N5 O16 P3 S	1642.158	3.297	14	3.59	3.39	3.77	3.90	3.42	3.61	23.04	9.20	36.27
C75 H147 N4 O11 P3 S	1405	3.375	2	2.87	2.75	3.05	3.15	2.79	3.09	23.10	5.28	19.55
C77 H153 N7 O17 P2	1510.078	3.339	13	2.72	2.72	3.07	3.28	2.67	2.97	23.11	12.47	28.98
C42 H83 N4 O2 P	706.6256	8.087	16	2.83	2.55	2.85	2.54	2.77	2.70	23.21	34.97	27.55
C87 H142 N4 O5 P2	1385.046	3.26	3	2.35	2.02	2.13	2.23	2.11	2.14	23.22	11.68	6.66
C11 H26 N6 O2 S	306.1824	4.385	16	2.29	2.28	2.09	2.10	2.19	2.09	23.23	18.18	1.06
C25 H58 N9 O3 P	563.44	3.176	8	1.48	1.12	1.46	1.42	1.13	1.47	23.24	18.96	4.15
C81 H148 N7 O7 P S2	1426.062	3.306	4	1.40	1.24	1.26	1.27	1.21	1.25	23.26	3.90	4.11
C23 H55 N7 O7	541.419	2.586	12	2.46	1.57	2.32	2.41	1.47	2.46	23.29	12.94	22.45
C20 H45 N6 O P	416.3373	3.771	18	2.24	2.18	2.22	2.16	2.07	2.17	23.30	18.36	10.26
C33 H45 N6 P S	588.319	2.772	20	5.35	4.78	5.59	5.65	4.68	5.63	23.34	18.12	35.12
C30 H49 N P2 S	517.3039	2.179	9	1.99	0.81	1.90	2.19	0.77	1.79	23.37	30.87	33.56

C24 H60 N9 O3 P	553.4557	3.202	10	2.55	2.58	2.95	2.74	2.63	2.96	23.47	13.73	13.91
C47 H77 N O7	767.5685	4.601	12	7.32	6.53	7.36	7.37	6.40	7.62	23.47	46.15	45.97
C61 H101 N3 P2 S	969.7195	9.624	15	4.22	4.11	4.46	4.21	4.19	4.43	23.49	17.42	8.38
C15 H5 N5 O13 P2 S	556.908	3.132	5	3.35	3.20	3.52	3.53	3.17	3.50	23.49	4.60	35.84
C60 H92 N7 O2 P	973.7042	3.704	7	5.36	3.59	5.33	5.39	3.67	5.47	23.65	17.44	33.64
C28 H58 N2 O	438.4544	3.866	7	1.22	0.33	0.70	1.05	0.04	0.84	23.65	41.48	17.09
C47 H95 N O2 P2 S2	831.6277	3.24	4	4.48	4.09	4.53	4.62	4.15	4.52	23.66	8.36	23.23
C57 H121 N10 O11 P S	1184.867	3.461	8	2.33	2.46	2.56	2.54	2.45	2.57	23.67	3.90	19.27
C39 H84 N9 O P3	787.6013	3.256	6	3.44	3.13	3.39	3.66	3.17	3.47	23.69	9.40	30.61
C43 H75 O10 P	782.507	5.21	15	1.21	1.42	1.15	1.30	1.45	1.13	23.73	22.08	7.57
C67 H140 N9 O14 P3	1387.973	3.375	2	2.89	2.77	3.07	3.18	2.80	3.12	23.78	4.89	19.66
C49 H94 N3 O8 P S	915.6505	3.023	15	1.31	1.29	1.74	1.85	1.28	1.78	23.79	1.23	20.58
C32 H53 N10 P3 S	702.3411	3.481	10	5.28	3.71	5.78	5.55	3.76	5.93	23.85	31.32	47.22
C19 H47 N7 O2	405.3809	2.785	15	2.28	1.01	2.27	2.18	1.23	2.17	23.88	28.74	43.21
C42 H68 S	604.5038	7.607	7	1.36	0.51	1.56	1.22	0.42	1.44	23.88	30.21	30.75
C84 H179 N9 O16 S5	1730.207	3.269	8	2.85	2.51	2.89	3.06	2.56	2.90	23.93	12.15	21.46
C82 H146 O3 P2	1241.074	7.754	4	3.25	2.07	3.32	3.16	2.30	3.62	23.98	40.67	37.76
C67 H142 N9 O5 P3 S2	1309.978	3.22	4	1.97	1.76	1.94	1.88	1.83	1.93	23.98	8.86	1.87
C35 H78 N10	638.6402	8.072	16	1.26	1.38	1.34	1.24	1.41	1.23	23.99	49.58	15.46
C37 H77 N3 O2	595.6008	5.532	15	2.07	1.76	2.31	2.09	1.61	2.21	24.01	22.94	12.55
C28 H70 N9 P3 S	657.4667	2.548	8	2.34	2.36	2.32	2.24	2.33	2.01	24.02	17.57	44.29
C32 H68 N2 O	496.5327	5.923	12	1.21	0.06	1.09	1.19	0.18	1.14	24.09	46.66	8.35
C21 H43 N O	325.3339	2.357	24	1.68	0.14	0.46	2.18	0.06	0.47	24.11	41.92	48.60
C54 H108 N2 O8	912.8108	11.489	16	9.92	8.87	9.82	9.79	8.82	10.13	24.15	7.32	39.19
C22 H39 N	317.3075	5.131	9	1.33	0.16	1.15	1.16	0.04	1.11	24.19	23.65	9.15
C42 H80 N5 O7 P	797.5796	11.31	22	3.36	3.37	3.58	2.71	3.42	3.65	24.24	25.20	11.00

C33 H61 N8 O P	616.4728	4.977	18	1.51	0.41	1.04	1.40	0.47	1.04	24.24	45.41	7.87
C75 H159 N10 O18 P3	1581.106	3.313	21	3.52	3.42	3.67	3.76	3.36	3.73	24.27	8.32	16.87
C36 H73 N	519.5736	5.698	15	1.72	0.70	1.61	1.72	0.33	1.54	24.31	48.60	16.14
C28 H60 N9 P S	585.4451	2.58	7	2.92	2.08	3.01	3.19	2.04	3.20	24.34	14.41	39.19
C15 H24 N2	232.1933	0.923	20	1.91	0.78	2.01	1.86	0.84	2.25	24.37	23.08	49.51
C25 H51 N O	381.3963	6.081	6	2.28	1.13	2.26	2.16	1.18	2.23	24.45	39.88	10.20
C12 H32 N5 O P	293.2351	2.056	28	1.60	1.67	1.04	1.71	1.40	0.97	24.49	40.27	21.98
C33 H48 O S	492.3426	3.304	10	1.08	0.63	0.91	1.26	0.56	1.01	24.51	18.42	21.07
C32 H65 N	463.5114	4.213	19	1.60	0.24	1.22	1.48	0.16	1.18	24.52	49.45	20.33
C22 H40 O	320.3073	3.908	9	1.24	1.10	1.25	1.18	1.41	1.29	24.54	34.58	5.72
C18 H34 N2	278.2716	2.592	6	1.74	0.36	1.17	1.52	0.27	1.12	24.54	12.73	20.66
C61 H79 N7 O2	941.629	2.554	6	2.77	2.51	2.69	3.01	2.54	2.83	24.56	6.78	19.09
C51 H102 N3 O9 P S	963.7076	3.181	6	3.82	3.61	3.96	3.94	3.61	3.93	24.57	0.51	27.06
C40 H84 Cl N3 O11	817.5787	5.169	28	4.82	4.79	4.93	5.21	4.83	4.90	24.58	6.97	4.90
C87 H139 N3 O5 P2	1368.02	3.258	3	2.36	2.07	2.16	2.24	2.15	2.17	24.61	10.72	6.63
C52 H109 N6 O P S2	928.7848	11.49	19	6.09	4.93	6.00	5.92	4.88	6.32	24.67	14.72	42.89
C36 H67 N	513.5272	4.327	20	1.37	0.11	0.91	1.37	0.04	0.63	24.77	32.97	40.78
C18 H48 N9 P	421.3762	3.24	19	1.21	1.40	2.05	1.40	1.43	1.77	24.78	5.73	46.45
C26 H51 N5 O3 S	513.369	2.677	21	3.71	3.46	3.44	3.77	3.39	3.55	24.88	19.67	18.82
C63 H130 N6 O11 S2	1210.922	3.116	14	1.80	1.64	1.69	1.75	1.71	1.70	24.88	10.89	6.56
C19 H7 N7 O17 S	636.9623	3.437	7	3.32	3.26	3.34	3.53	3.26	3.42	24.90	6.02	23.38
C33 H42 S	470.3006	3.351	15	3.11	2.58	3.63	3.49	2.39	3.59	24.93	24.67	34.21
C38 H73 O10 P	720.4929	4.85	25	4.40	4.02	4.27	4.57	3.77	4.12	24.94	49.17	27.39
C52 H101 N7 O12	1015.75	3.461	14	7.62	5.74	7.44	7.50	5.66	7.53	24.96	31.79	25.31
C39 H63 N O6	641.4642	1.765	23	6.33	5.42	5.82	6.34	5.12	5.83	25.05	46.89	11.12
C36 H56 N9 P S2	709.386	2.789	5	4.45	3.74	4.72	4.67	3.86	4.99	25.14	41.40	48.38

	C8 H15 N O3	173.1047	1.946	18	1.62	0.63	1.21	1.55	0.72	1.42	25.20	15.80	33.17
	C38 H70 N2 O P2	632.4984	5.394	13	1.42	0.85	1.63	1.36	0.82	1.64	25.21	21.07	36.14
	C15 H39 N8 P	362.3026	2.767	7	4.27	3.24	4.75	4.23	3.33	4.54	25.23	14.76	48.79
	C46 H87 N10 O8 P3	1000.592	3.492	6	8.70	7.29	8.51	8.47	6.99	8.74	25.23	46.26	27.98
	C59 H121 N4 O13 P S	1156.839	3.121	2	2.80	2.46	2.72	2.89	2.50	2.83	25.31	3.97	27.78
	C13 H37 N10 O P	380.2897	2.744	20	1.17	0.55	1.93	1.59	0.73	1.86	25.35	35.62	9.92
	C31 H51 O9 P	598.3293	2.627	3	5.74	5.69	6.35	6.00	5.87	6.14	25.38	27.81	31.75
	C16 H22 O4	278.1513	2.445	5	1.89	1.82	1.96	2.02	1.92	1.83	25.38	21.87	30.68
	C31 H59 N S	477.4392	3.03	10	4.68	3.60	4.83	4.47	3.68	4.82	25.40	22.55	45.19
	C34 H76 N10	624.6246	7.894	7	3.99	3.12	4.40	3.94	3.10	4.26	25.41	48.65	32.29
	C27 H48 S	404.3496	3.281	18	1.71	1.80	1.85	1.66	1.78	1.87	25.43	9.18	27.30
	C41 H87 N3 O6	717.66	8.265	22	1.77	1.67	1.87	2.11	1.58	1.84	25.45	38.36	7.40
	C68 H130 N6 O17 S	1334.922	2.625	7	4.89	4.93	4.82	5.01	4.80	4.90	25.50	17.62	14.31
	C57 H101 N8 O5 P	1008.763	3.571	3	2.97	2.97	3.15	3.29	3.00	3.10	25.54	3.39	21.12
	C22 H50 N6 O16	654.3269	3.065	9	4.74	3.20	4.72	4.58	3.26	4.96	25.56	20.70	45.60
	C49 H80 N O10 P	873.5484	4.446	14	3.51	3.27	3.23	3.32	3.35	3.30	25.57	13.90	10.24
	C38 H82 N9 O2 P3	789.5806	2.756	8	2.91	2.16	3.18	3.15	2.17	3.27	25.57	2.64	36.43
	C13 H23 N O	209.1776	3.103	10	2.34	2.23	2.58	2.41	2.03	2.60	25.64	40.49	3.23
	C41 H57 N O6	659.4175	2.772	4	7.99	7.44	8.31	8.21	7.39	8.36	25.64	19.38	43.85
	C10 H23 N O9	301.1365	2.452	26	2.68	3.02	2.64	2.84	3.02	2.71	25.66	3.91	18.31
	C20 H52 N9 O3 P	497.3924	2.592	9	3.47	2.60	3.50	3.51	2.46	3.69	25.67	24.10	21.70
	C14 H27 N O3	257.1986	1.985	16	3.14	3.00	2.60	3.07	3.00	2.63	25.71	15.76	21.88
	C42 H75 O8 P	738.5175	4.6	11	2.95	2.31	2.99	3.20	2.20	3.28	25.76	20.15	39.04
	C21 H40 O3	340.2975	2.5	22	2.12	0.85	2.30	2.40	0.91	2.32	25.77	10.77	41.59
	C22 H41 N O	335.3181	3.504	13	3.09	3.01	3.03	3.02	3.22	3.05	25.77	24.91	17.11
	C59 H127 N10 O11 P3	1244.89	3.09	3	2.56	2.31	2.68	2.73	2.32	2.77	25.86	9.20	26.49

C19 H48 N8 O4 S	484.3503	0.768	18	3.28	2.50	3.10	3.42	2.66	3.03	25.88	35.33	10.51
C34 H71 N3 O S2	601.5038	4.854	6	1.36	0.80	1.03	1.13	0.87	0.96	25.89	10.48	10.41
C38 H51 N O6	617.3705	2.772	4	11.37	10.74	11.60	11.54	10.69	11.69	25.91	14.94	46.71
C57 H117 N4 O12 P S	1112.813	3.13	5	3.49	3.19	3.54	3.58	3.20	3.56	25.91	1.63	34.86
C43 H89 N O	635.694	11.868	14	0.97	0.95	0.40	1.04	0.58	0.35	25.94	40.38	23.65
C15 H20 O5	280.1304	1.701	9	12.10	12.05	12.32	12.27	11.78	12.21	25.95	46.82	26.65
C73 H155 N10 O17 P3	1537.079	3.326	3	3.29	3.08	3.45	3.50	3.05	3.46	25.96	5.43	16.82
C38 H51 P3	600.3191	2.772	16	4.41	3.68	4.73	4.51	3.63	4.72	25.96	7.62	44.81
C15 H29 N O2	255.2192	3.57	8	2.31	2.12	2.15	2.15	2.12	2.14	26.01	6.72	6.97
C13 H18	174.1406	3.119	12	1.65	1.48	1.65	1.33	1.48	1.56	26.02	12.73	24.20
C46 H82 N O8 P	807.5761	4.861	6	3.65	3.64	3.63	3.45	3.88	3.45	26.02	28.89	23.76
C34 H72 N8 O P2 S	702.4997	3.376	4	2.68	2.59	2.87	2.94	2.62	2.92	26.06	4.07	18.71
C32 H76 N9 O8 P	745.5542	2.763	3	3.60	2.81	3.93	3.77	2.84	4.01	26.06	4.98	38.81
C59 H79 N4 O3 P S	954.5615	3.583	12	1.65	0.42	1.82	1.74	0.50	2.14	26.12	22.89	48.22
C36 H24 N3 O13 P3	799.0519	2.997	13	3.10	2.78	3.25	3.47	2.85	3.33	26.12	9.93	22.93
C78 H166 N9 O17 P3 S	1626.133	3.296	5	2.91	2.72	3.19	3.03	2.68	3.19	26.13	5.53	13.38
C21 H46 N O P S2	423.2748	3.153	23	3.04	2.93	3.06	2.92	2.89	3.08	26.16	11.23	13.04
C29 H68 N9 O6 P	669.5021	3.076	15	1.89	1.65	1.98	1.88	1.67	1.86	26.18	5.51	20.24
C69 H132 N6 O15 S	1316.947	3.412	2	2.67	2.82	2.99	3.10	2.83	3.04	26.21	0.54	18.42
C32 H72 N10 O S	644.56	3.945	6	1.19	0.26	1.03	1.24	0.44	1.06	26.22	36.42	7.60
C20 H37 N O4	355.2717	3.233	12	2.44	2.09	2.18	2.43	2.14	2.12	26.27	16.06	8.76
C39 H53 N O6	631.3862	2.772	4	11.29	10.62	11.54	11.42	10.60	11.63	26.32	16.26	49.87
C68 H135 N O17 P2	1299.921	3.414	2	2.76	2.87	3.05	3.18	2.88	3.10	26.32	0.55	18.81
C49 H110 N9 O15 P	1095.786	3.132	3	3.53	3.22	3.58	3.61	3.21	3.59	26.34	2.57	33.22
C18 H38 O4	318.2764	2.787	7	2.75	2.00	3.22	2.89	2.00	3.12	26.37	5.53	33.81
C67 H128 N6 O15 S	1288.916	3.076	4	2.90	2.61	3.10	3.06	2.62	3.13	26.44	4.73	28.67

	C60 H117 N4 O6 P3 S	1114.791	2.652	8	4.18	3.83	4.14	4.29	3.84	4.08	26.46	2.01	21.28
	C59 H118 N3 O13 P S	1139.812	3.117	2	2.98	2.63	2.91	3.07	2.65	3.02	26.48	4.66	28.65
	C42 H90 N9 O2 P3	845.6435	2.833	14	2.79	2.48	2.71	2.58	2.46	2.70	26.49	4.17	7.43
	C18 H39 N O	285.3024	5.167	19	1.52	0.01	1.21	1.52	0.17	1.15	26.50	38.09	19.59
	C24 H43 Cl N4 O2	454.3067	1.3	9	4.44	2.53	3.41	4.63	2.62	3.43	26.50	39.24	17.48
	C39 H78 N5 O3 P3 S2	821.4737	3.798	15	1.42	0.07	0.61	1.07	0.11	0.75	26.51	35.32	18.01
	C69 H126 N7 O P3 S	1193.896	3.118	10	1.83	1.75	1.78	1.81	1.80	1.79	26.52	8.29	5.05
	C22 H52 N9 P	473.4079	2.514	20	4.51	2.80	4.42	4.81	2.81	4.46	26.56	7.78	15.29
	C18 H40 N5 O3 P	405.285	3.101	13	3.63	3.28	3.44	3.62	3.23	3.35	26.57	7.79	20.16
	C65 H123 N5 O12 P2	1227.864	3.09	3	2.66	2.41	2.80	2.84	2.42	2.88	26.63	9.93	26.79
	C27 H59 N9 O6	605.4607	3.12	2	1.45	1.34	1.48	1.35	1.36	1.46	26.64	7.73	6.70
	C59 H89 N3 O4	903.6854	3.617	4	3.02	2.78	3.03	3.23	2.83	3.09	26.65	6.43	19.92
	C20 H39 N O2	325.2979	2.959	14	1.98	0.87	2.03	1.84	0.88	1.92	26.71	31.38	33.49
	C34 H59 N7 O5 P2 S	739.3799	3.045	5	1.59	1.49	1.87	1.50	1.88	1.94	26.71	41.84	16.64
	C69 H141 N4 O18 P S	1376.969	3.051	4	3.22	3.10	3.47	3.47	3.09	3.57	26.74	3.02	25.21
	C41 H73 N4 O3 P S	732.5106	3.062	4	2.62	2.28	2.77	2.81	2.33	2.84	26.75	6.52	29.75
	C81 H156 N3 O14 P3 S	1520.052	3.327	2	3.16	2.93	3.31	3.37	2.92	3.33	26.80	5.25	16.96
	C39 H90 N9 O10 P	875.6544	3.222	4	4.28	3.94	4.25	4.30	3.94	4.30	26.81	10.16	23.55
	C47 H106 N9 O14 P	1051.76	3.146	2	2.87	2.71	3.08	3.06	2.72	3.08	26.81	1.89	27.82
	C25 H61 N10 O10 P S	724.406	3.057	14	4.42	3.20	4.63	4.27	3.49	4.81	26.83	35.75	45.01
	C28 H62 N6 O3 P2	592.434	3.495	7	2.24	2.47	2.56	2.60	2.48	2.53	26.83	2.16	18.18
	C19 H41 N O	299.3182	5.701	7	1.80	0.12	1.11	1.60	0.17	1.16	26.85	34.66	12.93
	C65 H130 N3 O16 P S	1271.89	3.076	4	2.95	2.64	3.15	3.12	2.66	3.19	26.85	4.80	29.19
	C87 H137 N10 O5 P S	1465.022	3.032	6	2.70	2.42	2.86	2.95	2.43	2.93	26.88	5.96	32.16
	C44 H65 N O6	703.4784	3.063	3	2.03	0.72	1.92	1.79	0.53	2.12	26.97	31.75	22.79
	C41 H88 N9 O P3	815.6324	3.684	6	3.33	3.07	3.32	3.48	3.09	3.39	27.00	3.07	14.17

C47 H97 N3 O10 P2 S	957.6371	3.905	18	4.07	3.29	3.93	3.84	3.31	4.11	27.04	25.40	40.18
C55 H111 N O5 P2 S2	991.737	3.563	3	3.07	3.03	3.26	3.36	3.03	3.22	27.05	0.57	21.34
C36 H71 N O	533.5532	7.95	21	0.89	0.28	1.06	1.22	0.31	1.06	27.06	48.78	7.00
C83 H157 N9 O14 P2 S	1598.104	3.003	15	2.63	2.28	2.83	2.94	2.33	2.92	27.08	9.23	20.21
C29 H54 O6 S	530.363	3.529	28	2.08	0.86	1.58	2.10	0.89	1.54	27.14	35.01	24.95
C34 H76 N5 P	585.5823	8.41	9	1.03	0.95	0.55	1.07	0.56	0.51	27.18	46.34	32.68
C51 H79 N9 O3 S	897.6031	2.562	8	3.76	3.48	3.71	3.83	3.40	3.66	27.20	10.92	14.60
C55 H113 N4 O11 P S	1068.786	3.15	3	2.68	2.53	2.91	2.90	2.54	2.90	27.25	1.63	28.65
C11 H25 N8 O4 P S	396.1457	1.852	24	3.32	2.80	3.46	3.49	2.84	3.29	27.29	4.64	26.79
C18 H45 N10 O P	448.3523	3.408	11	2.50	2.39	2.42	2.32	2.39	2.30	27.31	1.88	16.11
C32 H72 N9 O P S	661.5333	6.821	8	4.65	4.38	5.19	4.72	4.17	5.01	27.34	38.65	33.69
C57 H120 N9 O10 P3	1183.838	3.103	2	3.12	2.90	3.19	3.32	2.93	3.28	27.44	4.38	29.64
C24 H53 N9 O5	547.419	3.021	6	1.50	1.37	1.49	1.36	1.39	1.54	27.45	6.77	7.37
C24 H49 N O	367.3809	5.856	4	1.51	0.60	2.10	1.42	0.61	1.87	27.46	38.48	31.10
C64 H107 N6 O13 P S	1230.735	4.459	15	2.59	1.25	2.57	2.59	1.50	2.84	27.49	29.33	42.64
C28 H26 O3	410.1877	2.283	9	3.04	2.45	2.85	3.62	2.32	2.94	27.52	24.04	22.49
C30 H59 N9 O P2	623.4342	2.633	7	5.08	4.99	4.95	5.35	4.92	4.94	27.53	24.83	18.56
C40 H79 N5 O9	773.5862	3.088	10	2.64	2.02	2.69	2.69	1.90	2.71	27.56	22.18	26.03
C40 H81 N O3	623.621	7.89	24	3.73	2.59	4.25	3.79	2.91	4.15	27.59	35.52	30.04
C33 H78 N9 O7 P	743.5752	3.278	5	2.83	2.53	2.65	2.81	2.54	2.74	27.59	10.50	14.27
C38 H79 N3 O	593.6219	8.065	19	2.39	0.71	1.79	2.50	1.05	1.74	27.60	42.80	43.75
C21 H41 N	307.3234	4.836	4	2.49	1.48	2.90	2.42	1.57	2.72	27.61	30.87	33.74
C69 H124 N3 O P3 S2	1167.841	3.464	4	2.61	2.71	2.85	2.81	2.68	2.80	27.63	4.20	21.30
C48 H79 N O7	781.5852	4.16	10	3.58	2.89	3.78	3.74	2.77	3.96	27.65	49.09	48.85
C69 H147 N10 O15 P3	1449.026	3.358	3	3.27	3.05	3.38	3.40	3.07	3.43	27.76	2.56	21.21
C19 H43 N7 O12	561.2956	2.604	8	2.38	1.35	2.40	2.41	1.61	2.68	27.80	34.14	46.14

C58 H116 N3 O10 P S	1077.812	3.022	7	2.87	2.57	2.75	2.81	2.63	2.78	27.80	11.50	6.38
C17 H34 N6 O2	354.2741	2.874	13	2.75	1.40	2.89	2.69	1.72	3.02	27.85	40.76	35.08
C47 H70 N7 O P	779.5386	2.653	7	3.35	2.94	3.33	3.27	2.92	3.36	27.87	10.62	13.51
C9 H9 O3 P	196.0293	5.125	19	1.12	0.39	0.95	1.17	0.55	1.28	27.93	22.08	36.52
C33 H66 N10 O P2	680.4867	3.391	4	2.94	2.81	3.00	3.11	2.79	3.08	27.95	3.26	21.04
C56 H86 O3 S	838.6289	4.385	4	4.55	4.28	4.45	4.17	4.18	4.43	27.95	28.85	4.95
C12 H35 N10 O6 P	446.2488	1.744	15	13.90	13.56	13.84	13.45	13.42	13.87	27.95	49.96	20.53
C49 H91 N5 O3 P2	859.6593	3.649	8	2.67	2.37	2.74	2.81	2.37	2.74	27.96	12.97	16.39
C19 H39 N3 O4	373.295	2.796	14	1.05	1.36	1.01	1.10	1.44	0.94	27.98	12.11	16.57
C22 H45 N O	339.3497	4.834	4	2.64	1.67	3.10	2.57	1.76	2.91	28.00	30.92	34.56
C45 H79 N8 O3 P S	842.5736	5.628	19	7.15	6.43	6.70	6.95	6.44	6.69	28.04	14.23	3.15
C30 H66 N8 O2 P2	632.4797	3.166	4	2.11	1.91	2.03	1.98	2.03	2.10	28.16	18.20	22.89
C36 H54 S	518.3967	2.979	8	2.77	2.56	2.69	2.69	2.61	2.66	28.18	10.17	9.13
C47 H100 N9 O4 P3	947.7111	3.587	4	2.84	2.60	2.81	2.95	2.64	2.92	28.19	6.07	20.76
C45 H54 N3 O3 P	715.3932	3.337	8	2.91	1.55	2.87	2.77	1.75	3.13	28.20	23.08	48.24
C23 H43 N3 O6	457.3139	2.559	11	3.10	2.68	3.02	3.33	2.70	2.99	28.27	10.21	18.89
C41 H65 N O7	683.4754	4.493	9	3.76	2.92	3.79	3.67	2.76	4.06	28.27	47.18	49.13
C54 H91 N O7	865.6763	3.858	17	2.30	2.40	2.29	2.40	2.42	2.30	28.32	13.98	10.71
C16 H40 Cl N8 O P	426.2756	1.305	15	3.70	2.03	2.90	4.14	2.10	3.09	28.34	39.91	34.00
C38 H79 N O	565.6155	3.715	15	0.92	0.91	1.20	1.15	1.40	1.20	28.35	47.26	8.85
C63 H122 N6 O11 P2	1200.865	3.104	2	3.10	2.91	3.19	3.33	2.96	3.27	28.37	5.35	29.88
C26 H51 N3 O2 S2	501.3403	2.55	12	3.43	2.99	3.44	3.53	3.00	3.32	28.38	23.30	31.30
C77 H136 O13 S2	1332.943	3.064	4	3.07	2.87	3.30	3.22	2.89	3.32	28.40	3.22	27.73
C5 H11 N4 O2 P	190.0627	2.44	10	3.27	3.22	3.37	3.35	3.37	3.40	28.42	26.53	11.45
C31 H59 N O S	493.4336	2.748	16	3.59	2.80	4.38	3.67	2.86	4.12	28.44	14.53	46.45
C40 H75 N4 P S	674.5455	8.114	11	3.40	2.28	3.55	3.43	2.20	3.80	28.50	40.82	40.95

C69 H144 N9 O15 P3	1432	3.357	3	3.23	3.02	3.36	3.38	3.04	3.40	28.53	2.48	21.28
C71 H107 N3 O P2	1079.789	3.521	3	2.94	2.92	2.99	3.10	2.96	3.01	28.56	6.04	19.50
C40 H80 N4 O12	808.5792	5.621	6	3.75	4.61	4.21	3.59	4.29	3.94	28.57	46.73	34.57
C78 H144 N10 O15 S	1493.053	3.342	20	3.75	3.47	3.71	3.86	3.49	3.88	28.58	6.86	21.89
C13 H37 N9 O2 P2	413.2563	2.249	17	1.50	0.68	0.92	1.50	0.92	0.96	28.59	35.99	12.57
C23 H36	312.281	11.259	20	2.95	3.24	3.01	2.73	3.28	3.03	28.63	10.56	20.17
C35 H77 N10 O3 P	716.5924	8.406	19	2.26	1.97	2.00	2.05	2.07	1.95	28.69	15.75	26.63
C39 H84 N9 P3	771.6061	3.715	3	2.76	2.58	2.94	3.01	2.58	2.91	28.70	2.52	16.17
C82 H147 N3 O15 P2	1476.028	3.343	19	3.66	3.38	3.62	3.77	3.39	3.79	28.73	6.75	22.02
C48 H91 N P2	743.663	8.027	13	3.10	0.67	2.78	2.95	0.43	3.06	28.74	39.12	38.48
C37 H74 N6 O3	650.5843	8.019	2	2.89	2.44	3.05	2.77	2.79	3.11	28.76	45.43	30.41
C36 H73 N2 O9 P	708.5028	3.074	6	3.65	3.06	3.73	3.61	3.01	3.87	28.77	11.96	26.11
C18 H29 N	259.2296	2.237	10	1.42	0.42	0.61	1.31	0.22	0.76	28.79	34.91	17.96
C51 H101 N5 O14	1007.734	3.162	6	3.84	3.48	3.85	3.91	3.50	3.91	28.93	4.50	25.69
C30 H72 N9 O7 P S	733.4995	2.607	9	4.46	4.42	4.36	5.02	4.42	4.36	28.95	32.66	25.29
C41 H94 N9 O11 P	919.6814	3.202	7	3.79	3.42	3.85	3.87	3.47	3.81	29.00	6.51	27.92
C22 H44 N2 O	352.3448	2.53	22	1.70	1.24	1.83	1.60	1.24	1.86	29.01	35.10	7.98
C41 H79 N O14	809.5503	2.571	4	2.35	1.88	2.22	2.46	1.92	2.28	29.04	6.19	13.71
C40 H63 N O7	669.4598	3.946	6	4.15	3.27	4.19	4.14	3.23	4.43	29.08	44.60	48.80
C59 H122 N9 O12 P S	1211.867	3.447	5	2.93	2.83	3.03	3.16	2.85	2.99	29.08	7.97	19.83
C16 H30 O4	286.2138	3.213	20	1.57	1.24	1.37	1.49	1.35	1.41	29.08	14.12	7.88
C19 H39 Cl O6	398.2441	1.308	10	2.62	0.73	1.61	3.07	0.85	1.66	29.12	43.09	36.04
C63 H119 N5 O8 P2	1135.854	3.069	3	1.52	1.40	1.56	1.43	1.40	1.53	29.15	11.87	3.86
C12 H23 N O2	213.1724	3.219	22	1.50	0.87	1.58	1.59	0.72	1.57	29.17	39.74	12.06
C18 H20 O3	284.1409	2.227	7	1.76	0.09	0.91	1.53	0.02	1.04	29.17	33.53	18.07
C36 H84 N9 O10 P	833.6072	2.747	5	3.18	2.12	3.06	3.14	2.13	3.23	29.20	1.49	41.66

C51 H104 N6 O14	1024.761	3.157	7	3.83	3.46	3.85	3.92	3.49	3.92	29.34	4.20	27.21
C19 H40 O4	332.2921	2.884	11	3.10	2.02	3.29	3.13	2.12	3.45	29.42	28.86	22.83
C37 H73 N O6	627.5431	7.541	17	1.55	1.42	0.81	1.57	1.25	0.79	29.43	24.93	42.18
C6 H13 N4 O2 P	204.0783	2.445	9	3.10	3.07	3.19	3.18	3.14	3.27	29.45	15.38	10.74
C20 H45 N9 O5	491.3558	2.69	11	3.12	2.51	3.02	3.02	2.54	3.18	29.45	12.28	23.06
C62 H104 N6 O S	980.7991	11.49	21	4.05	2.83	4.09	3.92	2.75	4.49	29.54	29.75	41.65
C20 H41 N O4	359.3031	2.27	12	1.89	0.70	1.06	2.14	0.58	1.06	29.56	26.08	3.23
C31 H71 N10 O7 P	726.5261	4.162	14	2.79	1.97	2.85	2.84	1.86	3.12	29.60	39.45	47.74
C31 H48 N3 O11 P	669.3013	3.062	6	2.58	2.45	3.13	2.39	2.65	3.09	29.65	34.83	30.57
C32 H57 P S	504.3919	4.399	22	2.02	2.53	2.26	2.39	2.61	2.18	29.68	21.48	22.32
C21 H41 N4 O P S	428.2741	1.326	12	4.66	2.56	3.47	4.73	2.76	3.47	29.72	36.10	41.35
C9 H6 N6 O18 P2	547.9211	3.022	8	1.32	1.25	1.28	1.14	1.21	1.29	29.74	7.84	6.20
C32 H46 N4 O2	518.3604	4.164	15	2.23	1.43	2.40	2.27	1.32	2.65	29.77	32.34	48.74
C62 H126 N2 O12 P2	1152.879	3.069	5	2.95	2.93	3.06	2.88	2.93	3.05	29.83	12.18	3.62
C67 H144 N10 O15 P2 S	1423.001	3.039	14	3.29	2.99	3.14	3.34	2.96	3.31	29.83	11.42	27.24
C71 H126 N7 O13 P	1315.916	3.063	4	3.11	2.88	3.33	3.26	2.90	3.35	29.95	3.21	28.23
C76 H139 Br N O7 P3	1349.896	3.445	14	1.63	0.94	1.36	1.34	0.88	1.46	29.99	12.12	32.68
C75 H120 N4 P2 S2	1202.843	2.641	11	3.87	3.67	3.92	4.00	3.67	3.89	29.99	11.71	9.88
C15 H22 O	218.1666	2.316	15	1.80	0.09	0.84	1.46	0.13	0.81	30.00	44.25	6.43
C79 H157 N7 O18 P2	1554.105	3.327	20	1.95	1.64	2.25	1.83	1.69	2.20	30.06	6.42	16.60
C22 H46 N7 O P S	487.3213	3.221	15	1.57	0.43	1.49	1.37	0.61	1.32	30.15	21.89	23.59
C69 H147 N10 O14 P S3	1467.001	2.602	8	3.92	3.88	3.96	4.42	3.83	3.90	30.17	29.63	13.73
C30 H72 N9 O8 P	717.5238	2.563	8	3.20	2.09	2.89	3.15	2.14	3.14	30.20	6.61	33.73
C26 H52 N8 O5	556.4061	3.134	3	3.43	3.29	3.58	3.60	3.26	3.62	30.21	4.61	30.68
C50 H81 O10 P	872.5528	5.599	19	3.36	3.27	3.83	3.64	3.47	3.83	30.22	32.97	7.26
C22 H46 N2 O	354.3603	3.896	8	1.63	1.46	1.58	1.55	1.69	1.60	30.23	29.03	5.76

C45 H73 N O7	739.5381	3.949	6	5.22	4.54	5.45	5.44	4.43	5.66	30.26	48.54	48.74
C11 H21 N O2	199.1566	1.007	10	1.94	0.61	2.21	1.60	0.90	1.92	30.35	35.45	39.22
C33 H65 O10 P	652.4334	3.946	2	4.30	3.29	4.24	4.17	3.26	4.50	30.38	42.64	48.63
C23 H48 N2 O2	384.371	2.533	17	2.32	1.57	2.40	2.20	1.67	2.44	30.41	29.58	4.64
C67 H139 N5 O10 S3	1269.968	3.162	5	2.36	2.22	2.18	2.19	2.23	2.18	30.44	10.81	2.73
C42 H83 N O7	713.616	8.011	25	2.61	2.12	2.71	2.40	2.32	2.75	30.47	44.92	44.72
C47 H71 N O6	745.5245	3.341	2	3.29	3.00	3.36	3.44	3.05	3.48	30.48	7.83	20.17
C18 H40 N3 O6 P	425.267	2.053	4	2.39	1.33	2.25	2.24	1.39	2.26	30.49	46.66	6.46
C22 H54 N10 P2	520.399	2.051	12	1.78	0.44	0.48	1.64	0.40	0.60	30.57	17.80	27.73
C60 H115 N	849.9027	13.769	2	2.16	0.50	1.67	1.99	0.80	1.63	30.57	43.90	6.42
C83 H163 N4 O16 P3 S	1597.1	2.998	17	3.16	2.93	3.41	3.38	2.89	3.37	30.58	7.61	12.81
C39 H90 N10 O14	922.6634	2.742	24	3.14	2.15	3.37	3.32	2.16	3.35	30.68	33.06	17.92
C35 H71 N O2	537.548	8.098	17	2.16	0.42	2.27	2.09	0.90	2.30	30.71	49.10	13.13
C30 H45 N O6	515.3244	2.128	18	7.94	5.64	7.74	7.60	5.65	7.65	30.72	45.27	26.64
C18 H42 N6 O4	406.3288	2.755	17	4.74	3.88	5.03	4.61	3.88	4.99	30.81	2.07	46.76
C24 H48 N2 O	380.3761	2.483	12	1.04	0.58	0.72	1.00	0.16	0.73	30.84	44.80	16.68
C18 H24 O2	272.1771	2.38	16	1.44	0.46	1.09	1.35	0.13	1.07	30.84	44.07	11.08
C61 H95 N O6	937.712	3.206	11	2.12	1.83	2.25	2.05	1.78	2.09	30.85	6.97	47.00
C38 H60 N9 P	673.4742	3.382	7	2.47	2.13	2.59	2.83	2.17	2.78	31.08	8.84	21.56
C28 H57 N3 O9	579.4085	2.645	14	3.09	2.87	2.79	3.22	2.73	2.82	31.08	18.33	25.86
C47 H103 N10 O4 P3	964.7374	3.596	5	2.75	2.57	2.80	2.80	2.61	2.84	31.09	9.95	20.57
C31 H74 N9 O8 P	731.5389	2.267	13	1.61	1.32	2.17	2.19	1.20	2.35	31.12	16.09	30.30
C22 H45 N3 O6	447.3294	2.738	13	2.77	2.32	3.71	3.42	2.28	3.85	31.15	19.18	28.29
C23 H52 N6 O P2	490.3669	3.179	8	3.49	3.16	3.48	3.56	3.01	3.42	31.22	28.03	41.98
C33 H77 N10 O P3 S	754.5239	3.021	6	3.75	3.46	4.16	3.99	3.51	4.12	31.26	12.00	31.98
C51 H109 N10 O7 P S	1036.795	2.98	5	3.57	3.43	3.49	3.47	3.42	3.50	31.29	2.69	6.24

Formula												
C24 H47 N O	365.3654	4.578	9	2.68	2.49	2.64	2.70	2.76	2.63	31.29	37.21	9.82
C40 H71 O8 P	710.4867	4.163	7	3.93	3.24	4.01	4.17	3.35	4.11	31.50	19.36	38.58
C58 H109 N O6	915.8215	11.486	19	4.35	3.29	4.24	4.11	3.20	4.58	31.64	17.74	38.03
C31 H62 N3 O P S	555.4344	2.47	7	1.02	0.48	1.40	1.41	0.62	1.66	31.75	45.71	46.32
C34 H75 N10 O6 P	750.5589	3.947	11	3.88	3.25	3.83	3.88	3.24	4.15	31.75	47.09	45.55
C68 H144 N8 O14 P2 S2	1422.973	2.612	22	4.90	4.53	4.57	5.16	4.57	4.67	31.81	26.95	16.25
C17 H36 N6 O4	388.2816	1.309	12	3.92	1.92	2.76	4.11	2.06	2.95	31.82	36.97	33.26
C26 H57 N5 O5	519.4338	5.887	15	2.14	2.72	2.41	2.18	2.38	2.39	31.84	46.20	11.69
C19 H37 N O2	311.2818	2.639	7	2.02	0.91	1.71	2.19	1.01	1.64	31.88	28.75	13.61
C41 H71 O8 P	722.4867	4.167	10	1.96	1.36	1.74	2.09	1.60	2.03	31.99	49.11	41.65
C21 H42 O4	358.3077	7.753	7	3.71	2.38	3.86	3.47	2.30	3.90	32.11	48.03	36.42
C36 H80 N5 P	613.613	8.834	5	2.77	0.90	1.95	2.51	1.10	2.10	32.14	46.67	29.40
C21 H37 Cl N4 O2	412.2598	1.295	12	5.19	3.17	4.08	5.37	3.32	4.21	32.24	45.36	39.27
C51 H108 N5 O13 P	1029.768	3.635	12	3.14	0.72	2.73	2.95	0.84	2.93	32.24	40.03	25.59
C53 H113 N10 O9 P S	1096.815	3.528	3	2.47	2.55	2.45	2.68	2.60	2.55	32.30	5.72	18.52
C18 H38 N2 O8	410.2637	1.309	12	5.68	3.64	4.50	5.86	3.79	4.65	32.30	36.47	36.53
C26 H58 N6 O3 P2	564.4028	2.861	17	2.13	1.97	2.66	2.27	2.29	2.62	32.36	34.15	44.56
C27 H61 N8 O P S	576.4396	3.069	3	2.79	3.04	3.08	2.79	2.95	3.06	32.37	14.42	7.14
C16 H31 N	237.245	1.294	7	1.43	1.39	0.43	1.13	0.92	0.24	32.42	49.85	27.27
C32 H40 N8 O	552.334	4.078	7	3.59	2.03	3.06	3.46	2.37	3.08	32.52	39.15	5.94
C46 H97 N7 O9 P2 S	985.6549	2.53	9	3.02	2.71	3.00	3.25	2.72	2.92	32.53	8.73	25.50
C45 H77 O8 P	776.5372	3.012	4	4.22	4.11	4.51	4.54	4.09	4.71	32.55	7.83	21.52
C90 H162 N10 O13 P2 S	1685.151	2.979	11	2.39	2.07	2.56	2.38	2.37	2.72	32.61	32.04	30.87
C23 H56 N9 O5 P	569.4143	2.563	17	0.91	0.91	0.83	1.27	0.85	0.77	32.68	9.64	24.17
C19 H41 N O2	315.3133	2.308	20	2.58	1.37	2.44	2.36	1.44	2.70	32.75	29.98	32.37
C29 H55 N S	449.4074	2.752	9	4.90	3.76	5.14	4.79	3.79	4.98	32.84	2.80	33.62

Formula	Mass											
C10 H23 N3 O5	265.1649	3.119	10	3.46	3.09	3.34	3.17	3.06	3.22	32.87	7.59	21.45
C35 H61 N3 O S3	635.3975	2.749	22	0.84	0.12	1.33	1.15	0.16	1.08	32.98	7.05	33.32
C59 H110 N5 O8 P	1047.809	4.864	7	3.92	1.77	3.46	3.81	1.94	3.78	33.14	30.53	38.32
C28 H56 Cl P3	520.327	0.779	13	3.29	2.59	3.25	3.35	2.82	3.22	33.22	32.90	15.83
C73 H155 N10 O18 P3	1553.074	3.009	4	2.92	2.60	3.06	3.08	2.59	3.21	33.24	7.92	19.29
C43 H69 N O7	711.5071	3.627	7	1.82	1.26	1.97	1.97	1.29	2.21	33.53	36.68	41.14
C20 H52 N9 O4 P	513.3874	2.262	23	2.01	1.23	2.82	2.70	1.28	2.94	33.54	42.87	43.09
C34 H49 N5 O4 P2	653.3233	3.061	10	5.44	4.00	5.35	5.12	4.05	5.73	33.55	10.28	47.57
C65 H138 N10 O10 P2 S2	1344.952	3.397	8	1.79	1.84	1.76	2.27	1.83	1.99	33.59	5.01	27.58
C41 H78 N O10 P	775.5367	2.995	4	2.79	2.47	3.10	3.01	2.48	3.18	33.68	7.32	20.08
C13 H20 N2 O6	300.1334	2.44	19	3.11	3.05	2.90	3.07	3.02	3.00	33.73	20.35	11.23
C16 H31 N O2	269.2349	3.113	13	2.39	1.94	2.01	2.31	1.95	1.92	33.75	19.51	26.38
C39 H70 N O8 P	711.4872	2.624	8	4.77	4.51	4.47	5.05	4.53	4.59	33.76	18.68	17.36
C37 H75 N O5	613.5645	2.578	14	0.76	1.36	0.32	1.22	1.32	0.03	33.80	5.77	48.69
C73 H143 N9 O18 S	1466.027	3.036	4	3.59	3.22	3.72	3.67	3.20	3.74	33.92	4.23	26.80
C70 H139 N O18 P2	1343.947	3.394	4	3.00	2.83	3.01	3.08	2.80	3.08	34.05	4.07	20.60
C26 H53 N	379.4173	3.199	11	1.51	0.17	1.18	1.42	0.34	1.27	34.21	39.17	12.92
C47 H75 N O7	765.5531	4.884	28	1.04	0.69	1.46	1.37	0.45	1.65	34.22	46.53	37.71
C57 H107 N5 O6 P2	1019.769	2.972	4	2.82	2.60	2.67	2.64	2.62	2.74	34.25	4.10	13.25
C40 H79 N O6	669.5902	6.481	23	2.26	1.39	2.38	2.24	1.23	2.26	34.38	29.42	32.53
C72 H110 N4 O12	1222.812	2.362	16	2.94	3.06	2.65	3.32	2.75	2.68	34.38	44.80	30.22
C71 H151 N10 O17 P3	1509.049	3.019	3	3.58	3.49	3.93	3.92	3.30	4.03	34.51	29.24	32.42
C42 H83 N O8 P2	791.5605	2.406	22	2.73	2.06	3.00	2.84	1.98	2.91	34.72	15.48	19.72
C20 H48 N5 P	389.3652	3.045	8	1.41	0.52	1.14	1.32	0.08	1.17	34.73	48.97	4.15
C16 H34 N O7 P	383.2081	1.282	10	0.78	0.97	0.35	1.16	1.13	0.25	34.81	49.32	42.98

C47 H87 N4 P S	770.6381	3.134	21	3.83	3.24	3.65	3.83	3.27	3.72	34.94	22.57	8.70
C18 H30 O2	278.224	2.328	12	1.48	0.78	0.95	1.30	0.75	1.07	34.96	7.10	33.64
C73 H133 N8 O13 P	1360.973	3.394	4	2.96	2.79	2.98	3.05	2.76	3.04	34.99	4.00	20.47
C55 H100 N2 O7	900.7535	11.222	14	4.65	3.07	4.80	4.43	3.09	5.04	35.01	18.53	47.69
C18 H35 N	265.2767	2.289	13	2.42	0.57	2.03	2.15	0.73	1.93	35.14	46.70	19.57
C45 H73 N O7	739.5381	4.599	19	2.11	1.77	1.89	2.13	1.70	2.15	35.17	33.85	37.29
C28 H58 N2 O2	454.4494	2.977	18	1.40	1.81	0.55	1.43	1.71	0.92	35.18	29.18	38.82
C36 H77 N10 O8 P	808.5654	4.39	15	2.95	2.22	2.90	2.53	2.24	2.84	35.22	38.43	11.10
C10 H7 N O3	189.0422	2.444	12	2.10	2.11	2.18	2.07	2.24	2.17	35.28	28.45	17.33
C30 H60 N9 O9 P S	753.3957	3.045	2	2.21	2.07	2.37	1.96	2.40	2.48	35.36	36.21	29.83
C21 H44 N2 O	340.3447	3.945	6	1.35	1.40	1.31	1.39	1.41	1.37	35.42	9.35	20.10
C12 H24 N5 P	269.1773	2.355	7	2.70	1.84	2.46	2.31	2.10	2.48	35.48	33.94	20.58
C27 H54 N6 O7	574.4049	2.803	12	3.59	2.60	3.86	3.23	2.41	3.81	35.49	24.60	43.99
C32 H61 O3 P3	586.3842	3.933	15	3.60	2.52	3.37	3.86	2.47	3.57	35.49	22.00	27.98
C17 H42 N10 O4 P2	512.2855	3.363	22	2.42	1.04	2.69	2.84	0.92	2.76	35.63	39.93	36.83
C57 H108 N6 O4	940.8432	11.752	17	3.79	2.98	3.70	3.50	3.28	3.99	35.69	40.49	37.21
C22 H58 N9 O P3	557.3956	2.652	20	4.71	4.48	4.59	4.90	4.51	4.65	35.72	8.99	19.91
C60 H124 N10 O15 S	1256.897	3.435	14	2.61	2.77	3.02	3.26	2.88	3.07	35.75	13.70	32.59
C8 H21 N4 P	204.1512	2.091	4	2.73	0.63	1.40	2.38	0.90	1.38	36.05	35.73	11.43
C9 H21 N10 O9 P3 S	538.0425	3.004	22	2.00	1.69	1.83	2.24	1.72	2.10	36.07	16.35	43.81
C37 H73 N O5 P2	673.498	2.568	8	3.59	2.60	3.41	3.65	2.57	3.72	36.09	4.19	33.67
C21 H40 O4	356.2919	4.387	12	1.87	1.44	1.70	1.35	1.52	1.72	36.15	15.49	4.65
C46 H67 N O8	761.4857	2.818	10	5.87	4.62	5.51	5.60	4.65	5.85	36.20	46.63	49.41
C23 H42 Cl N3 S	427.2788	1.325	11	1.34	1.11	0.08	1.46	0.76	0.32	36.23	38.09	32.36
C26 H61 N10 O2 P	576.4727	7.31	24	1.47	1.54	1.38	1.30	1.70	1.41	36.28	28.56	8.17
C20 H43 N3 O4	389.3262	3.096	18	1.21	0.24	1.82	1.12	0.04	1.70	36.28	34.50	21.04

C29 H55 N O S	465.4026	3.256	11	2.71	2.36	2.93	2.83	2.46	2.80	36.59	12.73	28.07
C37 H58 P2	564.4024	3.94	12	3.02	1.88	3.09	3.41	1.87	3.32	36.61	19.40	42.84
C59 H120 N5 O P3 S2	1071.815	4.348	13	1.87	0.56	1.57	1.85	0.50	1.70	36.63	23.90	34.82
C46 H75 N O7	753.5533	4.599	16	3.32	2.53	3.15	3.01	2.24	3.25	36.68	45.72	26.78
C22 H52 N5 P	417.3968	3.153	4	1.46	0.09	1.62	1.47	0.22	1.49	36.73	32.98	23.00
C35 H63 O10 P	674.4155	3.944	17	5.35	3.98	5.13	4.91	4.06	5.45	36.76	34.99	48.76
C24 H47 O7 P	478.3077	3.118	11	3.19	2.33	3.41	3.71	2.17	3.39	36.86	34.28	10.06
C24 H42 N4 O3	434.3247	1.492	21	4.59	3.23	4.15	4.76	3.36	4.20	36.99	30.23	16.36
C41 H57 N O6	659.4177	2.97	16	3.03	2.66	3.37	2.93	2.47	3.54	37.17	28.01	47.75
C52 H110 N5 O13 P	1043.783	3.823	11	2.04	0.87	2.51	2.55	0.87	2.59	37.22	7.08	20.87
C36 H35 N5	537.2872	2.318	20	3.89	2.95	3.56	3.85	2.91	3.90	37.25	42.78	49.84
C41 H81 N O5	667.6107	8.026	2	3.71	3.15	3.93	3.55	3.38	3.99	37.34	34.24	34.59
C24 H48 O7	448.3403	1.474	20	5.03	4.66	4.95	5.75	4.57	4.94	37.43	15.82	34.22
C18 H42 N5 O P	375.3109	2.999	15	2.37	1.61	1.37	1.91	1.67	1.34	37.51	28.61	26.36
C20 H32 N9 O2 P	461.2401	1.681	23	8.50	8.05	8.49	8.27	8.44	8.40	37.57	40.74	19.09
C59 H94 N3 O6 P	971.6881	3.599	7	2.97	0.51	2.93	3.00	0.59	3.23	37.66	36.48	42.23
C48 H69 N O6	755.5143	2.601	9	3.13	2.62	2.71	3.20	2.62	2.67	37.71	37.14	9.20
C28 H61 N9 O9	667.4605	2.624	23	4.62	4.45	4.49	4.76	4.51	4.48	37.82	16.38	14.83
C37 H73 O8 P	676.5036	6.471	12	2.31	0.78	2.61	2.05	1.02	2.24	37.95	31.82	49.61
C24 H57 N9 O8 P2 S	693.3554	2.791	19	1.93	1.32	2.39	2.16	1.47	2.63	37.96	39.25	41.19
C41 H54 N2	574.4264	3.124	8	2.70	1.00	1.99	2.31	1.30	2.05	38.05	35.42	7.21
C39 H80 N2 O6 P2	734.5477	3.092	19	5.35	3.40	5.28	4.90	3.39	5.46	38.25	21.12	36.90
C18 H43 N9 O4	449.3435	1.493	6	3.69	2.91	3.05	4.15	2.80	3.19	38.49	31.08	16.76
C21 H32 Cl N3 O3	409.2123	1.922	19	2.17	1.45	2.09	2.35	1.50	2.02	38.59	29.25	20.82
C12 H35 N10 O6 P	446.2488	1.343	20	4.56	4.07	4.76	4.79	4.20	4.79	38.71	40.58	45.47
C22 H53 N7 O5	495.4133	2.732	9	2.13	0.78	2.24	1.72	0.87	2.20	39.00	22.36	23.82

233

C28 H59 N O S	457.4316	2.755	13	1.71	1.88	1.84	1.80	1.74	1.79	39.03	36.11	10.83
C16 H33 N O3	287.2454	1.595	21	3.61	3.46	3.53	4.84	3.14	3.49	39.15	42.38	13.27
C19 H36 O3	312.2659	7.752	3	2.87	1.77	3.05	2.58	1.63	2.97	39.17	38.54	43.48
C16 H30 O3	270.2191	3.124	22	2.93	2.28	2.54	2.70	2.38	2.68	39.19	14.53	16.18
C23 H13 N2 O18 P S	667.9622	2.616	15	4.22	4.07	3.79	4.29	4.00	3.84	39.23	11.32	13.83
C13 H36 N7 O2 P	353.267	0.795	19	2.00	1.80	2.79	1.65	1.77	2.68	39.32	28.32	47.66
C24 H49 N3 O2	411.3824	3.02	18	1.80	1.03	1.23	1.55	1.32	1.45	39.41	43.41	36.49
C43 H52 O5 P2	710.328	3.043	5	2.76	2.48	2.79	2.85	2.54	2.98	39.43	8.69	26.72
C14 H26 O2	226.1927	1.87	22	2.94	0.63	0.59	2.42	0.98	0.89	39.52	37.83	32.40
C64 H100 N O P S	961.7267	2.929	16	2.19	2.36	2.07	1.71	2.35	2.15	39.56	2.70	22.98
C19 H48 N7 O4 P	469.3503	3.369	13	5.81	3.84	5.90	6.21	4.00	5.80	39.85	21.59	34.08
C19 H32	260.2497	11.261	23	2.19	2.30	2.38	2.03	2.23	2.32	40.01	12.97	28.13
C50 H75 N O6	785.5586	2.764	16	0.53	0.10	0.27	1.50	0.12	0.44	40.04	10.29	34.17
C18 H41 N9 O S	431.3143	2.323	10	1.75	1.01	1.42	1.42	0.98	1.43	40.34	11.73	5.29
C80 H171 N10 O15 P3 S2	1669.158	3.284	15	3.56	3.25	3.69	3.50	3.22	3.71	40.61	5.32	15.58
C13 H25 N O3	243.1832	3.203	18	2.25	1.84	1.99	2.11	1.90	1.94	40.64	23.65	6.97
C31 H50 N8 O8 S	694.35	2.791	17	2.38	1.74	2.76	2.76	1.91	3.11	40.71	41.19	42.64
C48 H76 N5 O3 P	801.5692	2.603	14	1.08	0.22	0.84	1.11	0.16	0.81	40.86	17.19	29.73
C19 H40 N4 O13	532.257	1.985	22	2.93	1.51	2.50	3.24	1.52	2.37	40.95	0.77	33.48
C22 H51 Cl N6	434.3844	2.599	9	2.53	1.17	2.22	2.36	1.16	2.47	41.05	25.76	30.77
C11 H30 N10 O6	398.2365	1.459	11	3.84	3.01	3.61	4.76	2.99	3.87	41.06	34.02	29.11
C17 H32 N2 O2 P2	358.1942	1.297	22	2.58	1.95	2.42	2.25	1.83	2.43	41.20	25.92	5.49
C18 H17 N8 O3 P3 S	518.0354	3.326	7	1.67	1.31	1.85	1.69	1.29	1.88	41.26	5.39	20.50
C16 H44 N9 O P	409.3398	2.611	4	1.56	0.67	1.49	1.58	0.69	1.82	41.39	14.24	35.18
C19 H26 N9 O17 P3 S	777.0382	3.007	7	3.00	2.62	3.22	3.13	2.64	3.30	41.45	8.95	17.87

	C11 H14 O	162.1042	1.249	2	2.30	0.87	0.24	2.03	0.86	0.13	41.49	38.51	16.51
	C20 H41 N O3	343.3083	2.629	7	3.10	2.52	2.61	3.39	2.37	2.57	41.59	30.88	10.51
	C27 H43 N3 O2 S	473.3059	3.229	10	1.61	0.74	0.67	1.23	0.66	0.83	41.66	15.60	27.35
	C45 H96 N9 O3 P3	903.6848	2.887	11	2.43	2.17	2.43	1.90	2.22	2.42	41.70	11.96	5.55
	C7 H6 N8 O S	250.0389	2.712	15	1.94	1.95	2.03	1.77	1.81	1.80	41.95	30.81	34.24
	C30 H55 N5	485.4438	4.387	8	3.77	3.12	3.55	3.21	2.97	3.51	42.03	49.12	5.55
	C51 H105 N O	747.8194	12.39	12	0.48	0.79	0.55	1.06	0.37	0.50	42.14	46.62	27.04
	C9 H20 N O4 P	237.1124	1.023	13	3.22	1.73	3.52	2.66	2.01	3.24	42.16	37.48	49.72
	C43 H83 N O4	677.6314	8.083	11	1.01	1.36	1.67	1.10	1.14	1.58	42.19	28.16	21.66
	C33 H71 N6 O P	598.5399	0.897	23	4.50	4.74	5.22	3.79	4.72	5.11	42.33	30.21	28.01
	C12 H22 N8 O P2	356.139	1.969	25	1.99	1.73	2.40	2.88	1.64	2.39	42.36	26.73	16.84
	C77 H148 N9 O14 P S2	1518.033	1.449	14	1.69	0.30	0.98	1.82	0.43	1.12	42.71	21.26	19.32
	C25 H49 N O3	411.3705	2.741	21	2.04	1.88	1.67	1.91	2.04	1.75	43.14	24.09	20.00
	C38 H85 N6 O4 P S	752.6079	3.11	16	3.50	2.12	3.33	3.61	2.18	3.69	43.33	23.57	39.79
	C29 H58 N6 O8 P2	680.3786	3.588	21	3.12	1.16	2.77	2.65	1.11	2.79	43.61	32.11	35.98
	C13 H24 O3	228.1721	3.115	14	1.26	1.32	0.99	1.03	1.23	1.02	43.70	12.58	24.16
	C22 H28 O4	356.1972	1.306	22	4.53	3.65	4.38	4.19	3.64	4.34	44.10	20.46	5.95
	C25 H49 N O4	427.3658	2.671	11	1.71	0.89	1.15	1.98	0.64	1.34	44.12	34.20	23.70
	C72 H133 N7 O8	1224.022	9.629	9	6.93	6.95	6.77	6.26	6.99	6.43	44.16	12.85	44.93
	C25 H49 N O3	411.3708	4.738	18	1.13	0.22	1.31	1.13	0.23	1.13	44.47	45.30	35.56
	C34 H50 N4 O9 S	690.3322	2.776	15	0.22	0.10	0.95	2.04	0.09	0.65	44.71	10.94	44.47
	C16 H32 O4	288.2297	2.058	4	0.99	0.54	0.73	1.45	0.45	0.58	44.85	35.51	19.30
	C18 H37 N2 O4 P	376.2488	1.527	17	3.78	3.00	3.56	3.53	3.01	3.74	44.85	18.78	24.66
	C20 H39 N O4	357.2874	2.713	21	1.64	0.49	1.71	1.70	0.36	1.53	44.93	31.84	40.34
	C15 H19 N10 P	370.1549	2.325	8	4.25	3.55	4.09	4.46	3.58	4.22	44.95	14.61	18.65
	C12 H29 N6 O4 P S	384.1708	2.531	11	4.65	4.10	4.68	4.94	4.13	4.67	44.97	11.46	22.39

C15 H36 Cl N8 O2 P	426.2391	1.922	25	1.30	0.90	1.32	1.50	0.80	1.40	44.98	29.31	12.64
C74 H136 N10 O14 S	1420.996	3.042	4	3.19	2.71	3.31	3.04	2.67	3.44	45.20	5.68	28.56
C48 H77 N O7	779.5709	3.524	22	1.83	1.94	1.17	1.71	1.77	1.28	45.26	31.71	30.45
C38 H77 N7 O3 S	711.5815	3.087	12	3.97	2.69	4.43	3.88	2.57	4.50	45.46	25.21	41.90
C5 H14 N O4 P	183.0657	2.651	21	1.46	1.78	1.86	1.41	1.53	1.67	45.63	33.01	38.36
C37 H73 O8 P	676.5038	6.826	19	2.31	0.75	2.84	2.24	0.98	2.73	45.64	41.03	30.91
C45 H79 N O6	729.5921	3.102	21	3.14	1.48	3.23	2.77	1.45	3.66	45.94	15.67	49.82
C19 H36 O2	296.2707	2.649	21	1.03	1.17	0.71	1.40	1.25	0.80	46.00	24.02	33.58
C35 H63 N O15	737.4174	3.054	8	4.80	3.44	4.95	4.58	3.49	4.98	46.42	12.87	49.07
C28 H59 N4 P S	514.4175	2.529	13	3.32	3.26	3.37	3.92	3.24	3.53	46.60	12.09	19.66
C67 H134 N3 O13 P S	1251.938	3.164	5	2.06	1.86	1.83	1.78	1.88	1.87	46.75	8.22	5.17
C9 H21 N4 P	216.151	3.012	15	1.64	0.42	0.49	1.18	0.24	0.40	46.79	41.76	15.95
C24 H47 Cl N4	426.349	2.751	11	3.13	2.43	3.04	2.29	2.53	3.17	47.01	11.84	27.29
C9 H18 N2 O8	282.1073	0.893	16	0.08	0.18	0.06	1.02	0.18	0.24	47.31	22.54	48.47
C17 H25 N3 O2	303.1939	1.06	22	1.91	0.21	1.29	2.04	0.43	1.17	47.40	42.71	45.63
C22 H54 N6 O3 P2	512.3724	2.062	6	1.64	0.21	0.86	1.21	0.14	0.88	47.43	40.28	17.47
C23 H50 N10 O4	530.4003	4.575	5	1.71	0.97	2.08	1.85	1.19	1.89	47.44	32.69	33.21
C28 H55 N O4	469.4125	3.822	24	1.62	1.48	1.34	1.64	1.48	1.37	47.66	11.34	23.75
C30 H68 N9 P S	617.5049	4.576	7	1.84	1.31	2.14	1.87	1.28	1.97	47.80	26.77	35.97
C14 H37 N7 O5 S	415.2597	2.331	14	1.89	1.02	1.89	2.30	1.21	1.88	47.98	34.86	5.87
C56 H123 N8 O2 P	970.9508	7.986	22	1.24	1.14	1.17	1.14	1.28	1.09	48.01	28.48	14.07
C41 H84 N4 O4	696.6503	3.915	19	5.86	5.57	5.68	5.52	5.77	5.62	48.30	32.90	8.27
C31 H61 O4 P	528.4329	2.525	10	4.24	3.87	4.16	4.72	3.90	4.15	48.31	3.69	32.95
C27 H42 N5 O3 P S	547.2771	1.345	20	1.39	0.31	0.37	1.71	0.17	0.18	48.43	23.74	41.23
C36 H75 N	521.589	5.34	22	3.89	3.51	3.87	4.08	3.64	3.68	48.57	17.96	27.05
C36 H71 N3 O	561.5597	4.205	10	1.70	1.12	1.56	1.50	1.16	1.86	48.83	6.70	31.90

	C78 H163 N10 O16 P S	1559.171	3.42	20	1.86	1.63	1.81	1.50	1.66	2.01	49.21	21.99	42.95
	C82 H132 N5 O5 P3	1359.945	3.059	8	2.24	1.86	2.33	2.45	1.87	2.46	49.40	9.80	46.16

Table A.5: Lipidomics results of CFTR-SMALPs and analysis results. The abbreviation FC is the fold change. These features determined at a confidence level of 5 with identification of the retention time (RT) only.

Name	Formula	Molecular Weight	RT [min]	RSD QC Areas [%]	Ave. E1	Ave. E2	Ave. E3	Med. E1	Med. E2	Med. E3	CV of FC E1	CV of FC E2	CV of FC E3
		774.0836	5.635	6	9.90	10.00	9.88	9.91	9.98	9.88	0.21	5.61	0.88
		885.8559	9.625	6	4.85	4.69	4.76	4.83	4.67	4.75	0.35	5.76	1.48
		3058.397	5.619	7	5.84	5.72	5.85	5.88	5.86	5.85	0.73	18.28	2.34
		736.6315	5.176	4	9.81	9.83	9.79	9.76	9.72	9.79	0.78	15.99	9.16
		563.5463	5.205	4	7.19	7.16	7.21	7.16	7.12	7.17	0.86	6.40	6.50
		470.3271	2.754	10	3.49	3.44	3.53	3.54	3.53	3.54	0.88	14.03	8.94
		872.8436	9.621	8	3.77	3.61	3.71	3.79	3.64	3.71	0.93	5.91	5.47
		811.6595	5.626	22	4.69	4.72	4.65	4.61	4.66	4.67	1.22	8.35	4.48
		1997.926	11.244	5	7.57	7.27	7.55	7.56	7.63	7.54	1.25	49.16	2.56
		489.465	3.563	6	2.94	2.79	2.77	2.89	2.77	2.80	1.27	9.47	14.18
		1523.179	5.679	8	3.94	3.93	4.03	3.96	4.09	4.00	1.32	25.36	8.03
		638.6514	6.649	2	2.02	1.56	1.99	2.04	1.63	1.94	1.33	12.68	7.15
		1528.195	5.62	4	6.77	6.69	6.77	6.79	6.75	6.75	1.36	11.68	3.51
		871.8395	9.626	6	5.53	5.41	5.48	5.53	5.38	5.49	1.40	5.28	4.38
		2301.778	5.619	10	7.11	7.10	6.95	7.12	7.16	7.06	1.43	18.01	22.40
		812.7653	9.616	3	9.66	9.62	9.67	9.63	9.62	9.65	1.50	4.42	4.48
		1635.517	9.629	3	6.65	6.63	6.66	6.64	6.63	6.64	1.52	6.23	2.91
		1648.52	9.625	3	7.20	7.12	7.18	7.22	7.16	7.18	1.64	8.40	1.05
		1647.517	9.625	3	8.65	8.57	8.60	8.66	8.59	8.60	1.64	8.27	0.97
		187.5182	5.614	2	2.77	2.86	2.76	2.78	2.78	2.78	1.68	11.56	4.25

		527.3855	2.644	3	8.10	7.99	8.02	8.04	8.02	8.03	1.69	5.56	3.10
		755.6765	10.548	7	6.49	6.31	6.49	6.49	6.27	6.49	1.70	14.75	2.72
		662.6038	5.379	7	2.77	2.83	2.76	2.77	2.78	2.76	1.73	20.65	0.96
		753.667	10.55	8	5.99	5.82	5.99	5.97	5.77	5.98	1.75	8.96	3.47
		1992.904	11.25	5	10.07	9.71	10.04	10.08	10.03	10.03	1.78	48.54	2.41
		466.3243	4.381	3	3.36	3.34	3.31	3.30	3.38	3.30	1.84	5.01	5.26
		1026.991	11.249	3	8.71	8.65	8.68	8.72	8.63	8.67	1.92	2.84	2.52
		525.383	2.645	3	9.71	9.59	9.61	9.66	9.58	9.60	1.95	5.95	2.99
		994.9601	3.513	13	1.69	1.47	1.83	1.71	1.50	1.72	2.06	5.91	19.42
		3056.39	5.621	8	7.09	7.01	7.11	7.15	7.09	7.12	2.09	14.38	3.61
		1507.216	5.622	4	7.93	8.08	7.94	7.94	7.93	7.95	2.10	18.72	1.47
		1020.885	2.305	9	1.97	1.20	1.96	1.92	1.04	1.99	2.11	35.68	4.04
		368.473	11.263	9	1.76	2.26	1.82	1.92	2.09	2.02	2.19	28.55	33.48
		440.3219	2.631	18	4.44	3.62	4.45	4.31	3.59	4.06	2.21	14.04	43.50
		884.8524	10.884	14	3.24	3.33	3.42	3.35	3.32	3.41	2.23	14.93	7.43
		898.7283	9.19	20	4.46	3.95	4.39	4.49	4.08	4.39	2.24	29.16	3.42
		827.7848	9.625	5	13.16	12.93	13.10	13.13	12.95	13.09	2.26	7.68	0.68
		898.8674	9.622	3	10.96	10.75	10.94	10.98	10.74	10.94	2.34	7.36	1.44
		1724.07	1.486	17	1.77	0.97	1.47	1.74	0.96	1.48	2.41	26.81	23.19
		1502.176	5.192	18	3.21	3.07	3.17	3.19	2.99	3.19	2.45	11.87	7.20
		529.3951	2.575	18	8.12	8.02	8.00	8.01	8.02	8.00	2.48	9.22	3.08
		392.2836	3.401	7	3.42	3.39	3.37	3.42	3.40	3.36	2.55	20.91	15.81
		899.8708	9.623	2	9.61	9.41	9.60	9.63	9.41	9.60	2.56	6.63	2.04
		892.7071	9.621	4	4.53	5.00	4.32	4.47	4.66	4.39	2.56	37.62	11.09
		440.8237	2.656	21	1.93	1.00	2.18	2.02	0.96	1.92	2.58	5.60	35.25
		808.7614	9.649	13	3.91	3.92	3.55	3.79	3.91	3.54	2.62	7.51	10.49

		826.7783	9.627	5	8.93	8.71	8.91	8.93	8.77	8.92	2.64	6.92	2.19
		898.8672	9.806	15	4.27	4.20	4.28	4.33	4.35	4.24	2.69	40.81	4.29
		739.6437	5.173	3	7.28	7.28	7.25	7.22	7.15	7.18	2.71	15.25	10.01
		746.5287	3.525	15	1.80	1.58	2.00	1.79	1.56	1.92	2.72	1.90	20.96
		913.8866	9.624	3	8.55	8.31	8.53	8.57	8.30	8.51	2.76	4.85	3.71
		854.8048	9.625	14	5.25	5.08	5.07	5.21	4.87	5.18	2.77	28.51	21.01
		525.3769	2.647	9	4.08	4.09	4.10	4.03	4.15	4.11	2.84	7.34	5.94
		839.7085	5.62	24	4.69	4.98	4.86	4.70	5.00	4.86	2.90	8.30	4.96
		624.6358	6.647	20	1.70	1.28	1.59	1.76	1.41	1.57	2.92	17.64	7.29
		717.7713	11.486	4	1.55	0.17	0.96	1.60	0.34	0.94	2.95	36.97	6.55
		251.2608	2.307	21	1.88	1.26	1.86	1.84	1.32	1.84	2.99	38.52	4.68
		884.8517	9.625	4	6.14	6.02	6.09	6.12	6.02	6.09	3.08	2.08	1.28
		805.8358	7.849	15	2.33	2.55	2.42	2.34	2.53	2.39	3.22	3.00	7.08
		1525.686	5.617	13	5.74	5.66	5.69	5.78	5.78	5.70	3.33	18.16	5.39
		652.6668	7.352	4	1.09	0.60	0.99	1.08	0.64	0.95	3.35	8.54	9.88
		1983.919	11.256	8	6.99	6.97	6.98	6.94	7.00	6.94	3.41	4.79	6.57
		832.801	9.623	3	5.83	5.60	5.77	5.83	5.58	5.74	3.48	3.69	3.65
		3054.383	5.62	9	7.13	6.99	7.15	7.19	7.14	7.15	3.50	22.18	0.88
		1901.991	5.607	23	4.06	4.03	4.07	4.14	4.16	4.12	3.52	21.85	8.10
		825.7578	9.62	4	10.11	10.08	10.16	10.10	10.08	10.16	3.54	6.58	1.72
		757.6737	10.545	7	4.54	4.28	4.55	4.48	4.29	4.54	3.63	5.66	6.05
		773.2444	5.388	16	2.27	2.36	2.28	2.33	2.35	2.29	3.63	8.08	2.78
		756.5369	5.204	2	6.87	6.80	6.81	6.85	6.77	6.79	3.69	5.07	2.32
		1504.204	5.613	4	9.85	10.01	9.85	9.85	9.82	9.88	3.69	23.30	3.61
		206.5645	9.623	9	2.34	1.87	2.18	2.30	1.92	2.20	3.71	10.85	3.49
		1506.213	5.62	4	9.36	9.50	9.36	9.36	9.30	9.39	3.77	24.04	2.93

		736.5578	5.208	4	4.72	4.76	4.75	4.67	4.70	4.72	3.81	10.02	6.03
		1900.988	5.612	18	4.40	4.55	3.95	4.48	4.57	3.78	3.81	9.50	23.46
		1641.557	9.625	14	8.41	8.18	8.42	8.41	8.22	8.43	3.84	5.55	3.24
		187.2688	5.615	8	1.45	1.47	1.31	1.37	1.25	1.32	3.96	25.00	4.05
		1024.981	11.25	5	6.99	7.50	7.57	7.00	7.01	7.07	4.09	49.33	48.15
		2304.787	5.612	9	5.08	5.09	5.10	5.17	5.21	5.07	4.11	19.22	3.76
		1901.489	5.611	27	4.56	4.62	4.48	4.76	4.80	4.56	4.12	31.48	20.26
		541.1992	2.316	17	2.34	1.69	2.45	2.29	1.78	2.34	4.14	31.71	17.29
		374.3883	2.681	11	3.74	3.50	3.53	3.80	3.42	3.53	4.14	9.97	2.83
		1529.198	5.622	4	5.76	5.79	5.73	5.78	5.75	5.76	4.17	5.74	3.64
		1150.385	5.614	19	4.54	4.51	4.41	4.61	4.47	4.37	4.17	7.68	6.05
		903.7369	9.551	8	2.84	3.08	2.94	2.87	2.85	2.95	4.21	33.73	2.85
		791.8203	7.846	10	4.07	4.20	4.08	4.01	4.22	4.11	4.22	4.35	3.80
		557.4136	2.265	9	1.29	0.24	1.17	1.42	0.26	1.10	4.22	23.22	39.33
		573.4575	2.75	10	3.71	3.50	3.30	3.55	3.49	3.24	4.25	5.83	9.74
		424.2851	2.7	6	3.13	2.84	3.10	3.07	2.86	3.12	4.30	3.67	7.09
		484.3484	2.661	5	9.41	9.50	9.53	9.44	9.52	9.55	4.32	3.58	2.04
		323.3181	2.751	22	1.52	1.63	1.23	1.52	1.58	1.23	4.37	49.43	32.36
		552.479	3.935	8	3.16	2.95	3.15	3.12	2.93	3.08	4.40	8.76	10.46
		1519.067	5.201	14	2.31	2.41	2.31	2.30	2.27	2.29	4.48	23.93	9.93
		484.3392	2.661	8	5.12	5.10	5.19	5.15	5.06	5.22	4.51	8.25	10.42
		630.4833	5.462	9	3.23	3.43	3.21	3.24	3.44	3.17	4.52	11.64	5.35
		1338.273	11.249	6	10.84	10.63	10.80	10.82	10.84	10.80	4.54	32.16	3.17
		560.3898	2.674	12	2.00	1.85	2.21	1.91	1.70	2.30	4.62	17.39	23.45
		1472.193	5.196	14	3.00	2.89	3.03	2.98	2.70	3.02	4.68	29.77	18.11
		587.5441	7.384	8	3.56	2.93	3.55	3.58	2.97	3.50	4.69	19.12	9.28

		2302.781	5.62	16	6.76	6.78	6.75	6.82	6.87	6.75	4.72	16.56	1.09
		832.738	9.64	4	5.83	6.15	5.75	5.88	5.88	5.77	4.82	33.90	10.91
		711.5615	5.889	3	5.49	5.39	5.52	5.45	5.40	5.57	4.87	3.60	6.25
		2281.803	5.616	18	4.83	4.81	4.76	4.89	4.97	4.77	4.96	25.65	1.17
		1642.561	9.62	5	7.25	7.05	7.26	7.25	7.11	7.29	5.00	8.07	5.18
		837.7548	9.631	7	3.30	3.29	3.16	3.31	3.30	3.22	5.00	3.37	38.66
		1471.191	5.2	7	2.43	2.55	2.49	2.47	2.16	2.43	5.01	46.99	13.96
		510.4423	2.323	15	1.72	1.00	1.73	1.73	0.74	1.74	5.05	35.39	5.50
		920.3038	7.763	9	2.28	2.14	2.39	2.29	2.23	2.40	5.07	10.93	8.83
		187.5196	5.618	3	2.06	2.03	1.92	2.00	1.90	1.92	5.17	19.22	0.14
		993.3223	7.883	8	4.99	4.95	5.02	5.05	4.99	5.02	5.18	7.04	4.95
		299.2455	1.467	25	2.03	0.69	1.26	1.68	0.56	1.21	5.27	21.56	14.94
		366.3282	8.075	14	1.15	0.56	1.19	1.04	0.74	1.29	5.35	43.51	13.93
		1054.29	7.79	12	1.04	0.99	1.13	1.01	0.93	1.03	5.40	14.08	14.61
		1638.542	9.626	6	4.76	4.53	4.72	4.78	4.61	4.72	5.43	11.31	1.23
		3060.404	5.62	6	4.26	4.02	4.25	4.33	4.07	4.25	5.46	12.39	10.02
		868.809	9.62	6	4.63	4.42	4.59	4.60	4.48	4.60	5.53	20.62	0.69
		838.5827	5.665	24	6.60	6.54	6.66	6.55	6.49	6.65	5.59	7.49	8.43
		536.6063	7.127	3	1.46	0.07	1.16	1.55	0.11	1.39	5.60	45.57	29.75
		410.4313	5.927	11	1.28	0.13	1.00	1.30	0.24	1.08	5.62	42.45	21.48
		807.5669	4.831	4	2.56	2.76	2.44	2.52	2.53	2.44	5.62	28.54	0.80
		284.2904	2.314	15	1.90	1.19	1.91	1.91	0.91	1.92	5.67	35.49	5.78
		1027.678	9.627	22	4.30	4.40	4.36	4.24	4.43	4.41	5.72	7.94	11.33
		1198.087	7.31	7	4.71	5.03	4.67	4.69	4.71	4.63	5.72	42.75	8.10
		1510.227	5.611	17	3.84	3.52	3.74	3.69	3.43	3.81	5.75	13.14	11.65
		757.5343	5.208	2	7.67	7.63	7.67	7.61	7.63	7.69	5.79	0.44	2.53

		2303.786	5.613	13	6.93	6.88	6.91	7.05	6.99	6.93	5.82	17.16	2.94
		568.5327	9.628	7	3.16	2.89	3.23	3.22	2.83	3.20	5.89	8.84	5.55
		494.32	2.746	9	4.16	3.99	4.36	4.14	3.99	4.32	5.91	5.87	8.03
		1894.289	1.481	19	2.17	1.37	1.91	2.16	1.34	1.92	6.06	24.92	24.24
		1643.564	9.624	8	5.97	5.68	5.87	6.02	5.72	5.88	6.08	7.52	2.69
		996.9496	3.376	15	2.37	2.48	2.53	2.48	2.50	2.52	6.12	9.34	4.59
		3718.417	1.555	16	3.68	2.95	3.47	3.56	3.26	3.51	6.16	49.97	14.26
		820.5448	5.224	3	6.20	6.26	6.08	6.20	6.07	6.10	6.23	23.20	3.88
		440.2339	1.588	19	3.94	3.23	3.75	3.84	3.54	3.79	6.24	49.77	14.31
		1500.088	5.227	19	4.23	4.10	4.17	4.13	3.99	4.19	6.24	13.34	12.51
		441.3119	2.711	12	3.67	3.62	3.71	3.56	3.57	3.68	6.25	8.48	4.94
		539.1703	3.912	14	1.95	1.71	1.79	1.77	1.66	1.84	6.25	29.82	10.05
		3055.387	5.617	17	5.38	5.32	5.39	5.35	5.46	5.35	6.31	19.14	5.24
		843.0178	5.239	10	3.26	3.57	3.12	3.28	3.31	3.16	6.34	29.30	6.22
		1344.368	1.474	14	2.05	1.34	1.83	2.07	1.39	1.83	6.37	32.12	22.50
		700.5189	3.34	21	1.99	2.44	2.11	2.26	2.40	2.27	6.43	5.21	23.60
		940.9144	9.627	22	3.55	3.11	3.52	3.46	3.09	3.62	6.43	10.90	13.58
		1650.527	9.628	3	3.37	3.42	3.50	3.38	3.54	3.46	6.49	15.27	7.77
		757.6164	5.623	15	3.30	3.60	3.35	3.35	3.58	3.38	6.56	8.39	8.61
		1225.026	9.679	14	6.75	7.21	6.84	6.80	7.09	6.83	6.67	21.81	2.52
		706.7674	10.033	11	1.12	0.49	0.86	1.20	0.60	0.84	6.69	27.66	10.96
		326.3372	2.366	23	1.36	0.61	1.45	1.36	0.77	1.49	6.75	41.01	7.25
		206.5661	9.619	13	1.11	0.93	0.98	1.16	1.03	1.03	6.86	14.01	6.68
		478.3845	5.792	23	1.36	0.70	1.52	1.28	0.48	1.64	6.94	38.30	29.05
		478.4497	3.079	6	1.29	0.56	0.53	1.33	0.77	0.58	6.94	45.31	36.16
		514.3759	2.447	21	3.36	2.97	3.32	3.27	2.87	3.34	6.95	15.79	3.26

		1246.828	1.449	20	1.49	0.60	1.24	1.42	0.51	1.16	6.97	16.02	12.32
		1644.567	9.625	6	3.70	3.37	3.58	3.71	3.34	3.59	6.98	3.96	3.64
		485.3383	2.663	6	4.83	4.98	5.00	4.92	5.03	4.99	7.01	11.31	1.53
		573.3133	1.449	4	1.60	0.76	1.35	1.55	0.69	1.30	7.06	17.63	7.64
		916.6678	4.385	11	4.12	4.08	4.11	4.12	4.03	4.17	7.16	17.75	11.10
		790.5601	5.622	10	6.11	6.15	6.16	6.19	6.09	6.16	7.18	11.42	1.64
		950.7536	8.087	18	1.22	0.61	1.34	1.12	0.77	1.40	7.32	30.15	12.65
		821.6098	5.669	17	3.62	3.43	3.74	3.67	3.60	3.86	7.32	26.91	24.02
		1850.195	1.572	26	3.92	3.12	3.68	3.77	3.33	3.69	7.37	42.45	15.86
		624.5619	11.253	22	2.60	3.18	2.89	2.69	3.11	2.82	7.41	10.55	17.82
		806.481	1.587	25	3.55	2.84	3.85	3.44	3.09	3.39	7.48	48.41	46.69
		375.3706	4.194	14	2.15	2.18	2.16	2.20	2.18	2.11	7.51	1.41	5.96
		526.3793	2.648	12	3.87	3.69	3.80	3.71	3.72	3.80	7.57	3.94	4.23
		506.3221	2.648	3	6.32	6.41	6.50	6.39	6.39	6.48	7.59	3.71	6.44
		591.6506	7.28	4	2.98	1.68	2.40	3.05	1.41	2.50	7.59	40.85	21.27
		3716.417	1.562	21	3.73	2.98	3.51	3.58	3.25	3.55	7.62	46.75	15.14
		481.5488	5.321	6	1.79	0.54	1.57	1.77	0.38	1.61	7.70	49.83	11.29
		424.4466	6.345	8	1.09	0.16	0.85	1.05	0.07	0.91	7.80	36.49	16.77
		835.7501	9.623	5	8.21	8.15	8.25	8.22	8.13	8.30	7.85	3.81	7.24
		597.3228	2.621	15	3.60	3.13	3.34	3.44	3.09	3.26	7.87	4.92	9.27
		805.6671	7.353	20	1.20	1.77	1.10	1.23	1.43	1.14	7.89	39.18	5.64
		868.8215	9.629	22	3.74	3.47	3.83	3.68	3.44	3.69	7.90	19.10	27.02
		3012.172	5.212	11	2.03	1.78	1.82	1.99	1.84	1.77	8.09	12.08	16.09
		677.6798	11.256	7	1.83	1.93	2.11	1.72	1.97	2.14	8.09	10.90	8.55
		757.5725	5.204	20	4.47	4.64	4.54	4.47	4.31	4.60	8.11	36.51	7.20
		658.6465	11.246	7	5.38	5.28	5.42	5.37	5.31	5.41	8.14	16.54	2.40

		550.588	5.017	5	2.30	0.97	2.04	2.28	0.70	1.96	8.16	39.99	10.31
		922.7192	8.038	24	1.25	0.56	1.34	1.16	0.70	1.26	8.21	32.92	14.39
		1177.862	5.623	8	5.35	5.12	5.23	5.39	5.33	5.22	8.28	28.29	1.80
		834.6036	5.13	10	3.05	3.17	3.00	2.94	3.04	2.91	8.31	16.99	12.02
		1178.365	5.623	15	5.57	5.38	5.49	5.62	5.66	5.48	8.36	37.59	4.78
		1720.01	1.525	25	3.92	3.12	3.70	3.76	3.29	3.75	8.41	38.26	17.12
		706.5159	8.033	19	3.48	2.86	3.39	3.33	3.01	3.54	8.41	41.84	30.23
		2280.799	5.618	12	5.72	5.67	5.64	5.67	5.76	5.70	8.42	10.76	7.14
		843.8072	9.623	5	6.43	6.36	6.54	6.42	6.30	6.53	8.45	8.03	1.92
		366.3856	6.625	7	2.15	0.95	1.81	2.16	1.03	1.81	8.46	30.99	5.24
		443.2888	1.449	26	2.80	1.24	1.36	2.71	1.40	1.26	8.47	46.49	23.54
		1202.329	7.964	9	2.22	1.87	2.36	2.16	2.06	2.27	8.48	44.95	12.43
		762.5278	5.21	13	2.99	2.75	2.91	2.89	2.76	2.93	8.51	1.59	2.04
		1998.929	11.244	8	5.86	5.62	5.93	5.95	5.96	5.94	8.55	43.99	2.32
		216.1873	11.258	19	3.21	3.41	3.28	3.22	3.27	3.17	8.55	22.28	20.53
		524.24	1.724	26	9.33	8.94	9.29	9.24	9.06	9.33	8.56	48.99	31.48
		296.2905	1.915	20	1.48	0.57	1.43	1.36	0.60	1.62	8.57	11.75	37.78
		463.3423	3.394	15	4.01	3.39	3.90	3.85	3.41	3.96	8.59	5.96	13.98
		530.4782	5.537	9	1.79	1.20	1.73	1.64	1.26	1.70	8.66	11.45	4.89
		568.5328	5.214	13	3.19	3.28	3.17	3.12	3.34	3.19	8.68	7.14	3.88
		1292.378	7.745	30	1.88	1.54	1.92	1.92	1.52	1.98	8.69	12.32	8.65
		425.3163	2.749	16	4.46	3.70	4.92	4.16	3.66	4.80	8.84	5.66	41.17
		756.6799	10.547	6	4.13	3.88	4.06	4.07	3.89	4.09	8.86	15.05	15.14
		675.7247	10.565	6	1.63	0.02	1.45	1.76	0.44	1.60	8.89	47.76	22.24
		627.1755	1.824	19	3.75	3.53	3.79	3.79	3.64	4.00	8.92	15.37	28.45
		608.5258	7.314	9	3.86	3.95	3.76	3.82	3.81	3.75	9.05	37.18	2.93

		808.5793	4.856	5	2.31	2.47	2.15	2.20	2.27	2.17	9.08	27.41	12.01
		3810.001	5.618	20	3.78	4.02	3.95	3.93	4.03	3.94	9.13	5.97	11.75
		609.1759	5.688	14	1.96	2.11	2.27	2.01	2.10	2.29	9.15	10.00	7.70
		945.6222	3.532	10	1.11	0.80	1.05	1.06	0.88	0.97	9.17	15.96	12.77
		814.7751	9.386	11	2.95	2.74	2.92	2.98	2.73	2.92	9.27	1.76	1.21
		1499.193	8.066	12	1.11	0.54	1.22	1.06	0.76	1.35	9.44	37.83	16.85
		702.4513	1.74	17	6.42	5.19	5.83	5.95	5.51	5.93	9.50	49.71	13.05
		1317.295	11.254	10	6.28	6.19	6.32	6.25	6.36	6.31	9.51	22.33	1.55
		846.5212	5.228	22	2.65	3.19	2.73	2.72	3.23	2.65	9.51	28.32	17.67
		549.3671	2.644	8	4.65	4.47	4.43	4.52	4.47	4.56	9.55	0.22	16.14
		510.2474	3.514	28	3.98	3.83	3.90	3.88	4.14	4.01	9.63	43.23	22.84
		1152.73	1.469	12	1.62	0.92	1.43	1.59	0.91	1.41	9.65	38.13	19.63
		994.9604	6.8	7	1.31	0.30	0.97	1.43	0.39	0.98	9.67	34.47	11.89
		675.6728	11.254	9	8.82	8.89	8.90	8.84	8.93	8.89	9.69	10.29	5.76
		427.3768	2.675	10	3.30	2.92	2.88	3.14	2.92	2.92	9.70	22.47	7.98
		800.5752	4.838	2	2.95	3.24	2.70	2.85	2.81	2.79	9.71	45.44	17.05
		2450.811	3.597	11	3.03	3.21	3.06	3.26	3.16	3.05	9.73	11.22	12.63
		1579.505	1.471	21	2.06	1.21	1.79	1.95	1.07	1.83	9.82	17.26	27.68
		241.2763	3.374	13	1.83	1.67	1.97	1.77	1.60	1.93	9.85	24.91	21.00
		816.9386	3.592	19	3.25	3.42	3.27	3.47	3.42	3.26	9.92	2.56	13.74
		1028.683	9.618	8	2.83	2.83	2.92	2.84	2.82	2.93	9.93	4.74	4.15
		587.3087	2.79	24	1.12	0.47	1.23	0.95	0.36	1.17	10.04	15.60	37.76
		2306.46	1.518	26	2.20	1.07	1.85	2.01	0.93	1.79	10.09	19.06	8.41
		994.7624	3.881	16	3.91	3.92	4.08	3.89	3.81	4.10	10.11	13.08	2.88
		440.4051	3.586	16	1.69	1.51	1.75	1.71	1.50	1.78	10.19	4.99	4.26
		2299.502	1.555	24	4.09	3.30	3.85	3.92	3.53	3.91	10.19	41.27	16.62

		2279.795	5.618	27	5.78	5.53	5.70	5.61	5.56	5.65	10.24	7.00	5.29
		535.1578	4.989	7	1.18	1.27	1.36	1.24	1.25	1.35	10.27	5.65	1.55
		1649.523	9.623	12	5.60	5.63	5.81	5.77	5.61	5.77	10.28	7.58	7.04
		1246.836	5.16	28	3.61	3.70	3.60	3.50	3.64	3.50	10.29	35.09	21.11
		507.3525	3.475	19	5.35	2.66	5.37	5.59	2.20	5.40	10.29	46.57	30.05
		739.5908	5.215	7	3.97	4.05	3.91	3.86	3.92	3.90	10.39	16.49	2.66
		399.4066	3.948	17	2.38	2.06	2.16	2.09	1.94	2.21	10.41	17.81	14.67
		2282.806	5.628	22	4.89	4.95	4.99	4.96	5.04	4.96	10.42	14.98	3.75
		312.3575	2.81	4	1.56	1.52	1.42	1.66	1.48	1.44	10.52	8.16	21.78
		1216.618	1.467	25	2.14	1.22	1.86	2.00	1.17	1.90	10.57	21.56	28.16
		437.189	3.074	20	1.93	1.07	2.31	1.84	1.36	2.21	10.59	44.16	11.59
		1330.302	11.25	24	9.73	8.93	9.76	9.73	8.75	9.76	10.64	37.00	6.02
		1163.653	9.624	20	2.76	3.25	3.06	2.86	3.31	2.90	10.70	9.05	19.55
		960.7032	8.575	12	1.03	0.82	0.96	1.13	0.89	0.94	10.72	19.20	3.51
		515.3503	2.791	26	3.74	2.03	3.42	3.86	1.97	3.44	10.73	27.34	33.14
		833.2306	7.396	13	2.34	2.28	2.44	2.39	2.32	2.53	10.74	9.19	13.63
		559.4418	2.748	7	4.10	4.01	3.73	3.76	4.03	3.76	10.81	12.79	17.45
		618.4307	2.793	22	1.93	0.72	2.63	2.04	0.70	2.50	10.83	39.21	38.12
		756.5487	5.256	18	4.42	4.64	4.42	4.36	4.55	4.42	10.84	13.50	2.89
		545.3616	1.692	9	7.94	7.37	7.84	7.85	7.10	7.84	10.91	46.34	2.52
		758.2136	7.162	27	3.74	3.62	3.79	3.85	3.53	3.86	10.97	13.97	9.33
		446.3749	3.386	9	4.25	3.30	3.94	4.01	3.18	4.08	11.05	16.11	22.92
		451.3138	2.315	2	1.33	0.56	1.41	1.34	0.38	1.40	11.05	40.95	5.10
		158.1092	11.261	16	2.68	3.07	2.51	2.64	3.14	2.60	11.16	8.74	11.73
		1549.049	5.198	15	4.49	4.35	4.54	4.52	4.48	4.52	11.20	22.47	7.65
		562.3961	3.288	11	1.95	1.34	1.92	1.79	1.34	1.89	11.26	9.53	10.77

		797.4412	1.447	17	1.30	0.59	1.08	1.19	0.61	1.09	11.26	29.54	13.16
		594.6505	11.294	8	1.68	0.53	1.46	1.96	0.46	1.44	11.28	43.34	21.36
		1109.638	3.518	4	6.12	3.82	5.92	6.04	3.75	5.71	11.32	16.56	29.87
		866.6479	3.575	20	1.98	2.10	1.59	2.32	2.12	1.57	11.38	7.79	8.94
		781.5704	3.438	11	4.04	4.49	3.63	3.91	4.37	3.75	11.41	23.84	41.54
		1646.513	9.625	4	9.44	9.28	9.36	9.62	9.31	9.35	11.42	6.84	1.44
		634.6818	10.759	11	1.90	0.62	1.87	2.10	0.35	1.83	11.42	33.25	18.02
		2851.844	1.539	24	4.51	3.63	4.30	4.43	3.79	4.34	11.52	41.39	13.28
		2305.791	5.614	22	3.57	3.65	3.60	3.82	3.74	3.58	11.62	20.02	10.40
		1218.352	5.688	22	1.67	1.77	2.03	1.74	1.82	1.96	11.86	17.74	9.82
		751.3263	1.937	12	2.30	1.57	2.30	2.19	1.82	2.36	11.95	36.36	26.23
		351.1446	1.508	19	2.37	1.58	2.21	2.17	1.40	1.94	11.95	38.73	29.22
		429.3814	3.504	11	2.67	2.47	3.04	3.18	2.18	2.97	12.10	40.48	27.55
		1110.884	3.507	18	7.58	7.38	7.79	7.80	7.52	7.62	12.12	45.42	26.54
		995.3019	7.291	10	2.75	2.92	2.84	2.67	2.91	2.89	12.12	2.58	11.56
		819.7898	3.39	22	2.35	0.88	2.28	2.34	1.11	2.18	12.18	39.74	11.75
		506.2542	1.614	24	3.69	3.03	3.55	3.64	3.34	3.63	12.28	45.34	14.78
		454.2885	3.412	10	2.69	2.80	2.68	2.79	2.84	2.69	12.31	8.68	5.04
		1487.117	5.2	15	2.93	2.94	2.91	2.83	2.99	2.89	12.32	18.71	3.63
		1876.852	5.789	12	2.65	1.84	2.85	2.59	1.86	2.99	12.34	28.60	39.08
		539.1699	7.755	21	1.39	0.24	1.68	1.28	0.56	1.57	12.36	47.33	22.67
		1095.666	9.626	20	2.99	3.05	2.99	2.95	3.13	3.00	12.42	20.40	1.64
		959.6906	8.3	11	1.28	1.37	1.79	1.33	1.34	1.62	12.48	20.78	26.90
		764.5969	5.642	11	6.71	6.60	6.58	6.58	6.63	6.56	12.49	3.85	9.40
		610.5722	7.691	10	1.10	0.37	1.07	0.98	0.31	1.16	12.50	29.57	22.73
		3811.006	5.613	17	3.50	3.24	3.49	3.76	3.29	3.54	12.62	15.63	11.97

		466.4939	3.58	15	1.11	0.17	1.24	1.22	0.09	1.37	12.74	32.17	22.70
		665.7245	8.614	11	1.13	0.19	0.73	1.34	0.51	0.78	12.77	47.81	20.39
		1416.009	6.052	11	1.15	0.14	0.73	1.24	0.05	0.78	12.84	43.66	14.37
		720.6459	8.054	18	1.00	0.63	1.14	1.09	0.76	1.14	12.85	28.21	14.86
		3057.395	5.62	15	4.74	4.68	4.66	4.89	4.81	4.67	12.91	20.53	3.41
		2566.894	3.703	15	1.76	1.59	2.14	1.94	1.80	2.05	12.98	30.67	18.50
		550.5879	4.78	7	4.38	2.68	4.22	4.10	2.25	4.23	13.00	49.23	4.91
		474.2801	1.347	14	1.71	1.07	1.48	1.60	0.95	1.52	13.00	20.50	42.37
		557.2616	3.914	19	1.65	1.44	1.66	1.85	1.42	1.74	13.04	3.33	10.62
		881.7893	11.226	11	5.84	5.02	6.25	5.83	4.69	5.98	13.16	43.16	46.24
		841.7877	7.624	16	2.40	2.19	2.35	2.53	2.21	2.33	13.23	4.61	6.22
		1331.308	11.246	7	8.36	8.21	8.45	8.28	8.40	8.45	13.34	25.58	2.05
		1014.736	2.651	15	2.43	2.60	2.70	2.57	2.72	2.68	13.39	21.44	8.36
		621.0969	3.248	17	1.70	1.68	1.94	1.53	1.72	1.83	13.53	6.02	29.55
		221.1066	2.314	24	2.53	1.34	2.15	2.14	1.31	2.15	13.54	37.77	2.89
		421.3397	2.793	7	2.17	1.75	2.21	2.13	1.75	2.14	13.57	9.36	10.63
		1672.111	5.628	26	2.58	2.48	2.65	2.66	2.47	2.57	13.57	13.36	13.03
		602.5453	7.754	14	2.09	1.94	2.03	1.98	1.90	2.14	13.58	20.45	34.26
		1526.185	5.617	7	7.31	6.95	7.21	7.57	7.01	7.20	13.58	23.75	22.72
		1178.866	5.623	22	4.84	4.51	4.74	4.63	4.65	4.73	13.61	19.44	7.67
		393.3964	6.868	14	2.05	0.50	1.74	2.15	0.13	1.81	13.68	38.29	16.69
		1016.713	3.477	15	7.81	6.77	7.94	7.78	6.80	7.98	13.72	29.27	30.82
		1054.795	3.548	25	3.07	2.54	3.29	2.81	2.48	3.42	13.75	9.95	17.62
		1129.306	7.918	21	2.51	2.52	2.71	2.42	2.54	2.72	13.78	5.48	3.34
		313.2609	2.624	24	2.40	2.06	1.82	2.34	1.96	1.99	13.87	14.38	43.51
		383.3396	3.135	9	1.80	1.83	1.93	1.71	1.80	1.95	13.98	5.93	5.99

		495.5646	5.473	4	1.53	0.14	1.29	1.65	0.11	1.25	14.09	45.50	7.82
		436.312	1.5	15	2.03	1.44	1.87	2.11	1.45	1.96	14.16	11.73	17.56
		715.6453	8.264	10	2.23	2.29	2.44	2.35	2.36	2.43	14.17	10.74	6.66
		506.4163	4.384	10	2.05	1.93	1.80	1.92	1.93	1.74	14.18	4.51	11.70
		447.225	1.479	16	1.81	1.13	1.55	1.60	1.22	1.61	14.28	27.24	12.31
		1113.902	9.65	20	3.77	4.03	3.83	3.70	3.79	3.82	14.29	27.32	1.74
		384.4154	8.188	6	2.44	1.04	2.25	2.57	0.86	2.25	14.31	43.37	13.35
		829.2311	9.643	22	2.62	2.09	2.05	2.48	2.06	2.07	14.31	24.58	6.64
		577.4287	2.704	15	2.06	1.69	1.41	1.69	1.68	1.50	14.33	11.50	34.17
		337.2974	3.289	18	1.81	0.28	1.50	1.75	0.17	1.40	14.36	20.64	13.28
		214.1717	11.257	19	3.96	4.22	4.13	3.95	4.11	4.08	14.41	19.31	8.97
		3100.108	5.215	16	2.57	2.50	2.70	2.51	2.75	2.70	14.44	33.00	7.76
		670.5931	8.102	22	2.70	1.90	2.92	2.85	1.45	2.60	14.45	44.70	44.49
		1494.122	5.247	8	1.70	1.62	1.76	1.65	1.44	1.81	14.71	23.73	15.48
		736.6879	11.272	13	2.96	3.33	3.00	2.84	3.23	3.10	14.74	26.87	13.61
		738.6405	5.177	2	9.22	9.23	9.17	9.16	9.10	9.12	14.84	15.01	8.62
		3034.407	5.619	24	4.83	4.60	4.79	4.68	4.73	4.81	14.84	21.63	10.65
		434.2871	2.314	2	1.19	0.49	1.30	1.25	0.28	1.28	14.91	39.17	5.03
		2507.849	3.654	12	1.76	2.24	1.93	2.04	2.19	1.93	14.97	7.36	22.28
		1365.89	3.486	3	8.33	7.35	8.59	8.39	7.33	8.46	15.15	15.36	29.06
		1141.844	3.498	6	2.66	2.39	2.68	2.67	2.36	2.67	15.18	5.45	23.86
		1383.901	3.485	4	8.58	7.60	8.84	8.65	7.57	8.70	15.35	14.26	28.76
		738.5387	4.892	10	2.96	2.10	3.26	3.00	2.06	2.99	15.38	26.48	45.31
		772.5941	5.172	11	2.27	2.97	2.37	2.45	2.85	2.61	15.45	32.11	30.92
		1037.707	9.624	26	3.87	3.81	3.92	3.92	3.91	3.89	15.64	13.48	9.53
		902.8801	9.626	8	2.80	2.58	2.88	2.86	2.53	3.01	15.80	13.51	21.82

		395.2883	1.495	6	1.26	0.48	0.90	1.50	0.42	0.94	15.84	12.30	12.80
		368.5357	3.475	29	3.64	3.39	3.28	3.37	3.52	3.05	15.86	27.99	32.64
		696.6547	11.254	14	3.72	3.95	3.73	3.67	3.96	3.67	15.94	4.21	9.95
		644.2819	1.478	17	2.00	1.29	1.77	1.76	1.26	1.85	16.14	16.19	15.90
		959.9227	11.22	9	3.26	1.96	3.55	3.30	1.85	3.35	16.19	14.95	46.68
		509.3918	2.776	17	1.91	2.04	2.20	2.12	2.04	2.15	16.20	6.10	9.80
		3113.345	5.619	21	3.91	3.65	3.91	3.86	3.89	3.94	16.21	42.59	8.03
		1010.771	3.572	13	3.13	3.09	3.08	3.06	2.98	3.03	16.22	13.81	10.27
		517.2668	1.785	26	6.06	5.14	5.86	5.97	5.36	5.90	16.25	39.20	15.63
		796.9205	3.547	16	2.88	2.97	2.82	2.71	2.92	2.73	16.27	7.12	10.19
		1523.155	5.192	22	3.00	2.68	2.87	2.97	2.97	2.86	16.38	37.71	4.06
		1144.788	1.486	15	2.24	1.29	1.92	2.22	1.08	1.92	16.43	34.82	26.40
		901.1191	3.251	14	1.87	1.16	1.80	1.90	1.15	1.75	16.44	1.84	11.53
		877.8362	11.225	3	5.95	5.05	6.25	5.93	4.64	6.06	16.46	43.47	46.19
		349.3188	2.778	23	3.23	3.05	3.69	2.97	3.04	3.63	16.47	30.21	30.81
		836.753	9.628	15	6.10	5.85	6.01	5.94	5.81	6.00	16.53	7.41	1.51
		722.4102	3.102	8	1.32	0.30	1.08	1.56	0.24	0.87	16.63	37.79	26.99
		340.1854	1.292	5	1.64	0.72	1.42	1.78	0.63	1.47	16.75	29.07	10.60
		652.2344	1.924	16	2.40	1.65	2.35	2.23	1.95	2.46	16.95	41.72	23.96
		587.4391	2.871	24	2.84	2.50	3.37	3.12	2.61	3.04	17.07	26.07	36.76
		663.5485	6.378	19	3.97	2.91	3.80	4.07	2.89	4.09	17.27	49.60	44.99
		1802.239	3.244	16	2.12	1.42	2.06	2.15	1.41	2.00	17.29	2.44	11.21
		340.3527	3.904	10	2.18	0.81	1.81	2.30	0.69	1.80	17.43	36.99	22.83
		964.9219	11.497	10	3.40	2.45	3.77	3.46	2.51	3.47	17.53	11.15	35.88
		1874.848	5.791	10	4.37	3.60	4.61	4.41	3.61	4.60	17.67	18.59	30.93
		500.1936	2.271	12	1.53	0.80	1.48	1.48	0.49	1.52	17.71	36.90	6.68

		776.0914	5.623	19	4.04	4.07	4.18	3.98	4.10	4.22	17.74	14.25	10.82
		633.5324	6.638	11	1.73	1.79	1.76	1.57	1.46	1.66	17.76	40.92	46.06
		2431.777	3.592	11	1.90	1.88	1.96	2.06	1.78	2.02	17.84	18.83	18.74
		780.087	3.425	15	1.58	1.71	1.72	1.50	1.59	1.65	17.99	15.33	18.65
		1471.026	2.654	12	3.31	2.92	3.25	3.30	2.91	3.28	18.01	9.91	11.90
		350.3176	2.777	18	1.03	1.16	1.03	0.79	1.26	0.74	18.04	38.57	39.01
		429.3566	3.115	25	3.53	3.09	3.41	3.33	2.97	3.43	18.12	21.15	15.49
		606.4215	3.245	6	3.62	2.94	3.62	3.20	2.98	3.47	18.17	12.63	25.07
		856.8202	10.236	15	2.48	2.44	2.49	2.58	2.33	2.49	18.21	36.39	6.19
		898.8534	5.987	11	2.24	1.75	2.09	2.33	1.68	2.21	18.29	21.02	33.73
		678.6188	11.257	13	1.77	1.51	1.99	1.61	1.63	1.85	18.35	14.86	28.66
		635.9724	2.789	5	7.34	6.86	7.86	7.36	6.79	7.55	18.63	32.44	43.99
		445.3396	2.825	21	1.23	0.19	1.20	1.48	0.14	1.03	18.64	18.03	30.66
		2437.786	3.524	20	1.68	1.27	2.53	1.67	1.19	2.62	18.65	10.00	37.91
		592.6351	9.952	8	1.75	0.21	1.52	1.55	0.15	1.51	18.84	49.79	5.93
		1774.234	3.258	14	1.80	1.39	1.98	1.82	1.46	1.94	18.88	22.30	5.93
		491.8575	2.685	19	3.48	2.72	3.64	3.54	2.81	3.58	18.90	42.09	22.88
		346.3288	2.758	9	4.11	3.82	4.00	3.89	3.83	4.06	19.10	7.40	8.72
		692.7516	9.05	6	1.18	0.05	0.70	1.26	0.25	0.66	19.16	47.74	20.29
		303.2923	2.624	7	1.46	0.31	1.09	1.45	0.35	1.12	19.17	38.54	16.13
		751.5498	4.895	6	5.06	4.30	5.36	5.02	4.17	5.12	19.21	21.94	44.74
		1823.157	5.634	19	2.36	2.49	2.49	2.09	2.59	2.45	19.22	14.22	19.93
		877.6335	2.738	7	2.95	2.16	3.10	2.66	2.00	2.83	19.23	22.26	34.85
		1582.108	3.309	2	3.11	2.68	3.13	2.95	2.75	3.08	19.26	9.80	11.14
		1819.264	3.246	12	1.53	0.98	1.32	1.62	0.95	1.07	19.26	10.90	27.32
		783.5679	4.923	16	1.61	1.31	1.73	1.78	1.62	1.74	19.40	47.04	11.23

		522.5564	7.889	10	1.16	0.63	0.72	1.01	1.13	0.71	19.41	48.41	7.74
		1729.179	2.974	9	2.13	1.77	2.02	2.11	1.80	1.90	19.41	18.58	26.66
		460.8572	3.626	8	2.95	2.51	2.83	2.57	2.50	2.77	19.51	10.03	10.02
		761.5835	4.885	7	7.59	6.77	7.84	7.51	6.69	7.58	19.52	23.10	44.31
		426.4179	2.747	18	3.41	2.99	3.57	3.47	2.99	3.52	19.55	29.92	6.35
		363.3343	3.06	12	2.35	1.62	2.66	2.48	1.64	2.62	19.64	6.05	34.58
		493.3332	1.478	16	1.78	0.79	1.81	1.47	0.91	1.74	19.85	16.52	49.15
		250.1773	0.99	6	2.18	1.48	1.67	1.92	1.79	1.52	19.96	41.67	20.97
		904.865	11.489	5	7.70	6.70	8.09	7.85	6.54	7.72	20.09	20.84	41.52
		2623.933	3.755	18	2.03	1.99	1.99	1.89	1.99	1.98	20.11	3.39	1.81
		434.3367	4.063	10	2.31	2.45	2.34	2.31	2.41	2.39	20.34	10.68	30.25
		712.677	8.081	20	3.26	2.76	3.20	3.18	2.77	3.20	20.36	34.63	8.41
		1160.138	8.045	18	4.64	2.78	4.12	4.52	2.43	4.09	20.36	47.85	32.81
		905.8671	11.497	2	7.92	6.87	8.31	8.07	6.80	7.91	20.41	14.88	41.63
		514.3776	2.711	13	1.51	1.53	1.93	1.70	1.54	1.95	20.47	3.07	13.75
		340.3529	5.482	4	2.48	1.22	2.16	2.64	1.29	2.17	20.50	29.16	19.33
		1733.299	3.578	21	2.52	2.66	2.48	2.83	2.64	2.48	20.53	25.97	5.66
		415.3615	1.691	21	5.84	5.26	5.81	5.92	5.47	5.60	20.56	27.31	23.70
		689.7407	10.659	6	1.18	0.13	0.88	1.33	0.31	0.93	20.64	43.26	11.38
		382.3072	2.777	28	3.38	2.08	3.53	3.19	2.24	3.44	20.67	46.61	12.50
		2200.616	3.404	13	2.75	2.62	2.40	2.62	2.65	2.48	20.88	10.18	11.62
		913.6121	3.596	14	1.63	0.33	1.69	1.48	0.06	1.65	20.89	43.66	12.62
		842.6241	2.765	6	4.83	3.85	4.74	4.62	3.89	4.69	20.93	5.21	39.05
		368.3844	6.602	4	1.38	0.34	1.11	1.50	0.34	1.10	21.04	25.47	9.51
		778.5904	4.886	4	5.75	4.99	6.06	5.75	4.93	5.80	21.12	29.21	44.29
		506.4099	1.473	13	2.42	1.99	2.07	2.18	2.00	2.04	21.30	27.18	33.62

		548.9097	3.545	14	2.86	2.77	2.71	2.58	2.69	2.77	21.31	14.04	22.40
		1990.963	11.248	14	7.61	7.61	7.81	7.61	7.80	7.82	21.44	32.34	5.79
		404.292	3.59	14	1.36	0.96	1.21	1.39	0.86	1.15	21.44	14.51	12.12
		1991.967	11.25	11	6.95	6.95	7.11	6.94	7.16	7.13	21.49	32.23	3.31
		335.303	2.74	14	2.54	1.84	2.80	2.46	1.80	3.01	21.50	12.99	36.48
		970.7702	11.49	9	5.57	4.35	5.86	5.63	4.33	5.61	21.63	4.40	44.38
		306.2857	1.837	17	6.40	6.54	6.33	6.32	6.48	6.31	21.64	12.91	15.27
		1421.998	3.074	11	3.67	2.98	4.03	3.84	3.13	3.89	21.66	20.81	31.03
		842.8045	9.628	15	7.09	7.41	7.58	7.43	7.40	7.56	21.68	7.74	3.81
		508.6923	3.023	13	2.60	1.96	2.63	2.23	1.96	2.63	21.88	6.27	38.99
		679.358	3.462	25	8.75	7.99	8.94	8.57	8.02	8.90	21.91	38.85	50.21
		497.4224	7.232	18	1.92	0.06	1.52	1.91	0.14	1.46	22.00	39.55	19.45
		535.3175	2.274	21	1.37	0.51	1.30	1.41	0.21	1.23	22.01	40.25	21.95
		1818.263	3.247	7	3.16	2.58	3.22	2.92	2.58	3.04	22.19	17.86	22.70
		547.7211	3.309	5	2.46	2.00	2.36	2.09	1.96	2.37	22.20	13.73	11.70
		1950.34	3.213	13	1.28	0.80	1.29	1.43	0.79	1.19	22.33	9.31	26.80
		867.1498	3.575	16	2.64	2.56	2.67	2.52	2.79	2.68	22.35	32.89	21.38
		603.5703	7.318	8	2.76	2.75	2.61	2.61	2.83	2.63	22.37	11.50	4.14
		339.3297	3.677	5	1.40	0.12	1.05	1.37	0.21	0.99	22.53	35.72	13.20
		379.3808	3.393	21	2.38	2.03	2.18	2.37	2.13	2.03	22.53	24.10	23.52
		310.3232	4.506	2	1.37	0.14	1.15	1.50	0.13	1.17	22.59	34.03	18.93
		937.6935	9.627	15	3.68	3.66	3.90	3.69	3.58	3.92	22.72	16.79	8.14
		787.7883	9.717	16	1.08	0.07	0.12	1.05	0.13	0.12	22.75	13.40	9.99
		965.6864	2.698	10	3.65	3.20	3.51	3.31	3.25	3.58	22.79	11.15	16.20
		725.5962	3.075	17	6.47	4.91	7.07	6.75	4.97	7.02	22.84	8.80	23.52
		1670.16	3.283	8	2.96	2.53	3.02	2.86	2.51	2.93	22.91	8.33	14.11

		2681.975	3.804	16	2.10	2.04	2.44	1.98	2.07	2.66	22.92	13.13	30.65
		1583.111	3.31	3	2.73	2.14	2.61	2.28	2.10	2.50	23.07	4.60	16.02
		301.1364	3.237	12	3.04	2.83	2.77	3.10	2.85	2.76	23.11	11.80	3.87
		774.4915	1.463	12	1.15	0.55	0.17	0.71	0.55	0.06	23.24	25.66	27.33
		473.3836	3.504	30	4.20	4.06	3.90	4.00	4.20	4.10	23.24	19.26	31.17
		675.6715	3.908	6	1.64	1.76	1.59	1.61	1.45	1.55	23.38	34.86	6.48
		562.0611	3.279	6	1.28	0.85	1.33	1.22	0.94	1.28	23.51	11.48	20.48
		797.2547	3.547	28	1.83	1.93	1.71	1.44	1.72	1.71	23.59	35.06	10.89
		1453.051	0.779	7	3.56	2.68	3.07	3.35	2.45	3.10	23.64	39.09	5.47
		1025.763	3.161	7	4.15	3.70	4.13	4.05	3.67	4.15	23.69	9.96	29.40
		1538.083	3.323	4	3.73	3.31	3.77	3.57	3.34	3.68	23.71	4.23	15.74
		690.4103	7.953	25	1.09	1.04	0.80	1.26	0.96	0.70	23.84	30.42	12.97
		660.4211	2.771	9	6.85	5.98	6.97	6.60	6.06	6.98	23.99	18.03	47.46
		621.6784	7.683	20	1.72	0.70	1.42	1.59	0.36	1.59	24.15	36.06	34.42
		763.5972	3.506	15	9.49	9.43	9.60	9.59	9.41	9.58	24.17	4.95	7.43
		1520.187	5.668	11	1.07	3.03	1.52	0.71	3.00	1.70	24.27	13.29	45.49
		1027.75	3.45	26	2.56	1.76	2.64	2.56	1.73	2.54	24.38	11.62	30.96
		501.8426	2.547	14	2.90	2.65	2.34	2.66	2.67	2.22	24.43	20.74	25.87
		395.2855	1.509	10	1.98	1.32	1.86	1.91	1.26	1.99	24.45	7.73	17.73
		331.3236	2.875	26	1.31	0.18	1.38	1.00	0.27	1.48	24.54	29.46	48.38
		224.2135	2.835	25	1.09	0.47	0.22	1.07	0.37	0.37	24.58	14.79	29.90
		326.3369	5.06	4	1.78	0.47	1.57	1.93	0.14	1.59	24.63	34.39	17.24
		567.7266	2.976	21	2.07	2.34	2.72	1.81	2.35	2.84	24.70	4.93	35.62
		535.3819	2.656	13	3.83	3.25	3.52	3.29	3.31	3.51	24.74	10.67	19.08
		1992.97	11.246	17	5.78	5.87	5.77	5.76	6.07	5.86	24.78	28.01	14.36
		330.3126	3.551	8	2.07	2.09	2.19	1.94	2.16	2.09	24.83	9.41	35.23

		367.2848	2.258	9	3.40	2.65	2.66	3.58	2.73	2.52	24.89	36.89	21.26
		435.3282	1.477	17	3.59	2.74	2.89	3.45	2.78	3.01	24.91	8.36	16.67
		503.6945	3.339	15	2.15	1.40	2.11	1.78	1.38	2.23	24.94	7.90	31.13
		769.5358	1.522	12	5.57	3.31	4.75	5.18	3.31	4.41	25.02	12.10	37.63
		1617.508	3.532	23	1.75	2.38	1.96	1.89	2.44	2.03	25.03	8.16	33.92
		579.9089	2.643	9	3.89	3.28	3.42	3.70	3.24	3.44	25.05	9.61	8.25
		1158.817	2.644	8	3.66	3.14	3.30	3.13	3.08	3.33	25.14	7.52	16.50
		593.6204	8.057	17	2.02	0.84	1.32	1.94	0.84	1.35	25.15	43.23	40.43
		1543.427	11.23	12	4.96	3.72	5.26	4.99	3.70	4.91	25.17	19.43	47.77
		579.6229	4.487	14	1.14	0.57	0.95	1.09	0.74	0.93	25.18	43.29	43.59
		1366.948	4.49	10	3.84	2.96	4.25	3.94	3.05	4.03	25.33	40.39	49.04
		689.4738	2.617	4	4.43	3.95	3.94	4.20	4.01	3.82	25.62	21.66	17.81
		1510.052	3.025	7	4.13	3.64	4.11	3.88	3.59	4.02	25.63	10.55	26.03
		213.1724	2.758	16	1.00	1.54	1.13	0.86	1.59	1.07	25.63	21.64	18.82
		842.5761	2.984	20	2.89	2.59	3.19	2.83	2.72	3.05	25.67	18.05	29.66
		889.7361	4.397	18	1.24	0.16	2.18	1.47	0.12	2.12	25.84	35.29	34.31
		805.6177	4.838	4	2.91	2.24	3.24	2.89	2.15	3.10	25.84	23.49	43.44
		474.2799	1.678	7	7.27	7.13	7.12	7.13	7.11	7.09	25.91	32.63	6.20
		393.4175	5.587	21	1.85	0.55	1.81	2.01	0.27	2.12	25.92	44.92	40.16
		751.067	3.363	13	2.66	2.70	2.76	2.90	2.73	2.76	25.94	5.53	5.00
		994.9103	3.578	20	1.04	1.24	0.71	1.10	0.81	0.72	25.97	48.00	6.22
		307.3232	2.34	17	2.25	0.90	1.71	2.32	0.81	1.72	26.10	36.56	3.16
		568.5332	7.309	18	2.26	2.25	1.82	2.16	2.35	1.77	26.18	17.58	8.35
		1643.162	3.3	13	2.73	2.25	2.70	2.23	2.32	2.71	26.45	18.13	9.21
		622.4453	3.108	1	2.67	2.23	2.75	2.65	2.20	2.68	26.53	5.36	26.69
		845.6315	2.911	21	1.68	2.05	2.16	2.48	1.90	2.17	26.65	20.58	10.00

		425.4228	2.959	25	1.62	1.30	0.79	1.63	1.36	0.95	26.68	8.70	39.24
		623.9363	2.634	8	4.53	4.03	3.90	4.02	4.04	3.91	26.95	23.71	22.42
		420.4435	2.995	19	1.12	0.39	1.20	1.24	0.58	1.17	26.97	25.87	4.41
		495.8686	3.562	4	3.36	2.98	3.26	3.10	2.99	3.29	27.05	3.24	21.49
		982.7256	9.267	26	2.77	1.86	2.22	2.50	1.89	2.25	27.08	9.00	23.21
		1714.186	3.275	10	1.14	0.66	1.17	1.09	0.58	1.12	27.11	8.75	10.41
		503.3596	3.34	8	3.25	2.67	3.24	2.85	2.71	3.37	27.31	8.35	22.73
		523.7017	3.004	14	2.37	2.01	2.24	2.44	2.12	1.94	27.36	16.52	34.66
		1550.051	5.205	22	2.89	2.96	2.75	2.75	3.20	2.96	27.68	32.93	27.41
		721.6492	8.084	3	3.75	3.85	3.98	4.02	3.88	4.16	27.82	30.98	30.86
		490.8689	3.181	5	3.51	3.06	3.47	3.46	3.12	3.53	27.92	9.52	26.97
		547.4443	3.841	19	1.91	1.54	1.76	1.65	1.52	1.68	28.05	10.86	10.99
		942.7382	11.224	18	3.61	1.56	3.86	3.44	1.44	3.52	28.09	37.20	49.39
		1215.744	5.402	18	2.06	1.48	2.41	2.23	1.34	2.56	28.54	25.80	34.20
		553.0514	2.982	11	2.74	2.10	2.82	2.17	2.08	2.69	28.62	5.78	16.94
		468.8553	3.201	12	2.27	1.95	2.30	2.33	1.93	2.44	28.95	3.37	46.42
		342.3321	3.678	18	1.86	0.59	1.74	1.86	0.53	1.69	29.00	47.35	6.67
		355.3638	3.915	19	2.24	2.42	2.43	2.13	2.24	2.41	29.01	32.57	7.22
		374.3388	3.522	17	3.94	3.93	3.86	4.11	3.97	3.98	29.11	18.12	27.44
		1043.013	11.251	17	3.67	3.36	2.95	3.64	3.22	2.83	29.26	16.17	18.94
		783.5909	4.892	21	4.40	3.61	4.89	4.44	3.64	4.52	29.59	40.10	44.92
		408.2658	3.063	17	1.23	0.55	0.93	1.24	0.47	0.89	29.62	17.69	20.21
		700.2423	3.471	23	4.23	2.68	5.14	4.01	2.55	5.11	29.74	33.62	49.84
		677.6785	3.908	11	2.04	2.23	2.03	2.06	1.87	2.02	29.74	37.78	8.85
		955.587	3.331	17	2.57	1.35	2.82	2.20	1.20	2.57	29.77	19.80	47.16
		601.4212	2.637	7	3.99	3.36	3.63	3.82	3.39	3.63	30.14	17.94	24.19

		437.3193	3.718	12	2.39	0.92	2.58	2.49	1.07	2.45	30.16	44.46	34.48
		996.7857	11.485	18	3.10	1.78	3.60	3.32	1.93	3.25	30.72	21.02	39.71
		1511.024	2.621	17	4.31	3.64	3.67	3.88	3.74	3.60	30.93	34.35	11.07
		508.3079	3.695	3	2.11	0.77	1.92	2.24	0.33	1.96	31.15	45.72	7.33
		673.6634	11.254	3	5.43	5.70	5.71	5.60	5.72	5.75	31.34	2.97	6.64
		387.3859	2.925	14	2.54	2.11	2.26	2.06	2.16	2.45	31.36	5.95	24.37
		661.5319	6.513	11	5.60	4.97	5.89	5.72	5.06	5.97	31.62	35.89	48.86
		1642.13	2.995	11	1.58	0.92	1.56	0.99	0.95	1.33	31.70	4.80	27.52
		1378.976	3.042	9	2.02	1.73	2.03	1.52	1.71	2.03	31.89	7.32	33.39
		1377.974	3.052	6	3.85	3.50	3.96	3.64	3.50	3.90	31.97	0.50	24.79
		586.3675	3.539	20	1.70	2.46	2.11	2.07	2.14	2.17	32.03	45.24	35.71
		296.2321	2.816	13	2.45	2.13	2.82	2.82	2.23	2.81	32.10	21.91	0.86
		454.4208	7.09	20	1.59	1.34	1.19	1.55	1.16	1.07	32.22	30.30	41.50
		707.4985	3.072	3	3.22	2.73	3.35	3.19	2.73	3.18	32.36	8.69	28.54
		997.7892	11.49	21	3.10	1.77	3.54	3.36	1.83	3.27	32.38	17.97	33.62
		529.3676	3.529	24	1.70	0.50	1.08	1.67	0.47	1.08	32.69	47.01	16.32
		1335.924	2.628	10	4.24	3.91	3.81	3.84	4.02	3.72	32.76	15.36	12.20
		374.3025	2.352	21	2.52	1.13	2.16	2.14	1.21	2.27	32.80	40.99	14.61
		787.789	9.441	3	1.80	0.51	1.48	2.09	0.32	1.54	33.07	47.14	11.38
		576.9414	3.07	7	1.61	1.70	1.80	1.75	1.69	1.89	33.13	11.45	13.46
		413.2074	1.464	23	3.67	2.73	3.11	3.87	2.48	3.12	33.20	29.29	24.89
		389.2671	1.793	16	2.07	1.39	1.57	1.90	1.44	1.60	33.43	9.09	7.03
		359.3547	2.697	11	2.67	2.09	2.53	2.04	1.98	2.46	33.57	12.84	46.80
		692.6506	7.817	16	1.09	0.76	1.65	1.29	0.77	1.53	33.65	20.01	30.31
		1197.753	5.136	25	2.14	1.99	2.46	2.42	1.78	2.64	33.73	36.53	41.14
		706.7663	9.312	8	1.07	0.22	1.02	1.59	0.02	0.78	33.90	43.71	26.18

		502.2748	1.66	20	6.09	6.46	5.89	5.96	6.40	5.77	34.13	26.21	20.01
		712.0009	3.05	13	1.93	1.26	2.16	1.77	1.36	1.90	34.45	21.86	32.17
		523.3533	2.533	11	3.19	2.78	2.57	3.20	2.73	2.66	34.50	6.33	30.97
		476.4079	2.306	18	1.13	0.67	0.99	1.73	0.70	1.05	35.17	43.34	14.91
		680.3343	2.791	12	1.28	0.32	1.98	0.83	0.04	1.91	35.22	32.97	31.23
		1143.784	1.452	22	2.02	0.69	1.60	1.70	0.55	1.22	35.45	17.19	39.30
		725.4345	3.46	24	2.85	1.91	2.61	2.74	1.63	2.41	35.72	30.42	32.22
		1203.846	2.65	8	4.19	3.93	4.10	4.04	3.92	4.08	35.97	16.89	18.39
		601.923	2.662	8	4.17	3.91	4.08	4.02	3.91	4.06	36.09	16.75	18.34
		1009.711	2.648	5	3.31	2.69	2.90	2.55	2.71	2.85	36.22	6.09	30.10
		162.1405	11.257	18	3.08	2.89	3.14	3.20	2.91	3.09	36.91	23.67	27.02
		423.2977	2.701	6	6.37	5.64	5.91	6.24	5.72	5.82	36.93	18.96	21.82
		1846.266	3.241	13	1.52	1.32	1.56	1.58	1.44	1.64	36.94	18.65	48.18
		689.4881	3.054	18	1.83	1.28	1.84	1.17	1.30	1.94	36.95	4.12	26.63
		1758.213	3.257	7	1.43	1.13	1.52	1.41	1.13	1.46	38.23	9.12	11.94
		599.5433	0.863	7	3.03	2.74	3.53	3.13	2.63	3.45	38.84	40.77	16.97
		827.7726	4.379	19	1.06	0.12	0.19	0.43	0.05	0.01	38.99	12.72	23.57
		904.7422	9.615	17	1.03	1.50	2.24	0.99	1.48	2.38	39.40	36.16	47.82
		326.2927	2.835	10	1.57	1.03	1.93	1.84	0.99	2.17	39.63	10.61	34.42
		710.999	3.042	6	2.79	2.46	2.96	2.71	2.42	2.78	39.76	8.87	25.08
		431.0656	1.592	30	5.53	4.97	5.69	5.08	4.93	5.71	40.01	40.08	44.44
		2359.736	5.622	18	4.41	4.37	4.41	4.20	4.30	4.20	40.26	17.86	30.48
		514.4167	2.362	19	4.47	2.99	3.29	3.47	2.95	3.30	40.84	29.04	19.92
		545.3667	2.532	14	2.52	1.72	2.24	2.54	1.75	2.28	40.91	27.45	12.51
		518.3692	3.333	12	1.90	1.50	2.06	1.88	1.53	1.96	41.15	5.44	20.48
		754.6117	6.304	29	2.50	2.60	2.19	2.49	2.62	2.11	41.35	15.89	18.20

		1509.094	5.112	5	4.35	5.21	5.46	4.56	5.12	5.75	41.78	13.29	37.98
		1498.405	8.518	10	3.15	2.44	3.05	2.70	2.37	3.35	42.08	18.67	48.88
		2361.741	5.621	24	5.20	4.64	4.49	4.44	4.53	4.22	42.63	26.53	44.64
		626.1074	8.083	22	1.53	0.73	0.91	1.37	0.66	0.91	45.50	21.18	10.84
		512.3595	3.427	18	1.91	0.38	2.12	1.91	0.29	2.08	45.56	13.47	18.79
		978.5478	5.636	19	2.38	3.12	2.78	3.10	3.18	3.02	45.95	19.99	35.46
		489.3923	2.717	13	1.91	0.07	0.58	1.24	0.09	0.48	47.06	8.37	28.84
		1584.116	3.316	7	1.64	1.16	1.68	1.63	1.19	1.58	48.73	11.59	31.21
		428.2678	3.536	13	1.45	0.80	1.35	2.14	0.56	1.31	48.80	46.46	20.08
		1845.261	3.238	13	2.40	1.84	2.42	2.30	1.82	2.27	48.87	6.91	22.71
		411.1811	2.312	18	4.78	3.48	4.13	4.40	3.55	3.77	49.23	28.67	37.88
		859.6442	3.53	15	1.62	0.81	1.16	2.02	0.50	0.86	49.74	40.09	40.79

REFERENCES

1.   McLean, M. A., Gregory, M. C., and Sligar, S. G. (2018) Nanodiscs: A Controlled Bilayer Surface for the Study of Membrane Proteins. *Annual Review of Biophysics* **47**, 107-124

2.   Overington, J. P., Al-Lazikani, B., and Hopkins, A. L. (2006) How many drug targets are there? *Nat Rev Drug Discov* **5**, 993-996

3.   Dean, M., and Annilo, T. (2005) EVOLUTION OF THE ATP-BINDING CASSETTE (ABC) TRANSPORTER SUPERFAMILY IN VERTEBRATES. *Annual Review of Genomics and Human Genetics* **6**, 123-142

4.   Tarling, E. J., Vallim, T. Q. D. A., and Edwards, P. A. (2013) Role of ABC transporters in lipid transport and human disease. **24**, 342-350

5.   Vasiliou, V., Vasiliou, K., and Nebert, D. W. (2008) Human ATP-binding cassette (ABC) transporter family. *Human Genomics* **3**, 281

6.   Jones, P. M., and George, A. M. (2004) The ABC transporter structure and mechanism: perspectives on recent research. *Cellular and Molecular Life Sciences (CMLS)* **61**, 682-699

7.   Dawson, R. J. P., and Locher, K. P. (2006) Structure of a bacterial multidrug ABC transporter. *Nature* **443**, 180-185

8.   Hollenstein, K., Dawson, R. J., and Locher, K. P. (2007) Structure and mechanism of ABC transporter proteins. *Current Opinion in Structural Biology* **17**, 412-418

9.   Dawson, R. J. P., and Locher, K. P. (2007) Structure of the multidrug ABC transporter Sav1866 fromStaphylococcus aureusin complex with AMP-PNP. *FEBS Letters* **581**, 935-938

10.   Hopfner, K.-P., Karcher, A., Shin, D. S., Craig, L., Arthur, L. M., Carney, J. P., and Tainer, J. A. (2000) Structural Biology of Rad50 ATPase. **101**, 789-800

11.   Smith, P. C., Karpowich, N., Millen, L., Moody, J. E., Rosen, J., Thomas, P. J., and Hunt, J. F. (2002) ATP Binding to the Motor Domain from an ABC Transporter Drives Formation of a Nucleotide Sandwich Dimer. *Molecular Cell* **10**, 139-149

12.   Chen, J., Lu, G., Lin, J., Davidson, A. L., and Quiocho, F. A. (2003) A Tweezers-like Motion of the ATP-Binding Cassette Dimer in an ABC Transport Cycle. **12**, 651-661

13. Gerber, S., Comellas-Bigler, M., Goetz, B. A., and Locher, K. P. (2008) Structural Basis of Trans-Inhibition in a Molybdate/Tungstate ABC Transporter. *Science* **321**, 246-250

14. Hohl, M., Briand, C., Grütter, M. G., and Seeger, M. A. (2012) Crystal structure of a heterodimeric ABC transporter in its inward-facing conformation. **19**, 395-402

15. Abele, R., and Tampé, R. (2009) Peptide trafficking and translocation across membranes in cellular signaling and self-defense strategies. **21**, 508-515

16. Prieß, M., Göddeke, H., Groenhof, G., and Schäfer, L. V. (2018) Molecular Mechanism of ATP Hydrolysis in an ABC Transporter. *ACS Central Science*

17. Locher, K. P. (2016) Mechanistic diversity in ATP-binding cassette (ABC) transporters. *Nature Structural & Molecular Biology* **23**, 487-493

18. Schmitt, L. (2002) Structure and mechanism of ABC transporters. **12**, 754-760

19. Zaitseva, J., Jenewein, S., Jumpertz, T., Holland, I. B., and Schmitt, L. (2005) H662 is the linchpin of ATP hydrolysis in the nucleotide-binding domain of the ABC transporter HlyB. **24**, 1901-1910

20. Jardetzky, O. (1966) Simple Allosteric Model for Membrane Pumps. *Nature* **211**, 969-970

21. (1995) The catalytic cycle of P-glycoprotein. *FEBS Letters* **377**, 285-289

22. Van Veen, H. W. (2000) The homodimeric ATP-binding cassette transporter LmrA mediates multidrug transport by an alternating two-site (two-cylinder engine) mechanism. **19**, 2503-2514

23. Khare, D., Oldham, M. L., Orelle, C., Davidson, A. L., and Chen, J. (2009) Alternating Access in Maltose Transporter Mediated by Rigid-Body Rotations. *Molecular Cell* **33**, 528-536

24. Oldham, M. L., Khare, D., Quiocho, F. A., Davidson, A. L., and Chen, J. (2007) Crystal structure of a catalytic intermediate of the maltose transporter. *Nature* **450**, 515-521

25. Oldham, M. L., Davidson, A. L., and Chen, J. (2008) Structural insights into ABC transporter mechanism. *Current Opinion in Structural Biology* **18**, 726-733

26. Zou, P., and McHaourab, H. S. (2009) Alternating Access of the Putative Substrate-Binding Chamber in the ABC Transporter MsbA. **393**, 574-585

27. Davidson, A. L., and Chen, J. (2004) ATP-Binding Cassette Transporters in Bacteria. *Annual Review of Biochemistry* **73**, 241-268

28. Delannoy, S., Urbatsch, I. L., Tombline, G., Senior, A. E., and Vogel, P. D. (2005) Nucleotide Binding to the Multidrug Resistance P-Glycoprotein as Studied by ESR Spectroscopy. *Biochemistry* **44**, 14010-14019

29. Van Der Does, C., and Tampé, R. (2004) How do ABC transporters drive transport? **385**

30. Higgins, C. F., and Linton, K. J. (2004) The ATP switch model for ABC transporters. *Nature Structural & Molecular Biology* **11**, 918-926

31. George, A. M., and Jones, P. M. (2012) Perspectives on the structure–function of ABC transporters: The Switch and Constant Contact Models. *Progress in Biophysics and Molecular Biology* **109**, 95-107

32. Aller, S. G., Yu, J., Ward, A., Weng, Y., Chittaboina, S., Zhuo, R., Harrell, P. M., Trinh, Y. T., Zhang, Q., Urbatsch, I. L., and Chang, G. (2009) Structure of P-Glycoprotein Reveals a Molecular Basis for Poly-Specific Drug Binding. *Science* **323**, 1718-1722

33. Jones, P. M., O'Mara, M. L., and George, A. M. (2009) ABC transporters: a riddle wrapped in a mystery inside an enigma. **34**, 520-531

34. Loo, T. W., Bartlett, M. C., and Clarke, D. M. (2010) Human P-glycoprotein is active when the two halves are clamped together in the closed conformation. **395**, 436-440

35. Sauna, Z. E., Kim, I.-W., Nandigama, K., Kopp, S., Chiba, P., and Ambudkar, S. V. (2007) Catalytic Cycle of ATP Hydrolysis by P-Glycoprotein: Evidence for Formation of the E·S Reaction Intermediate with ATP-γ-S, a Nonhydrolyzable Analogue of ATP †. **46**, 13787-13799

36. Siarheyeva, A., Liu, R., and Sharom, F. J. (2010) Characterization of an Asymmetric Occluded State of P-glycoprotein with Two Bound Nucleotides: IMPLICATIONS FOR CATALYSIS. **285**, 7575-7586

37. Ford, R. C., and Beis, K. (2019) Learning the ABCs one at a time: structure and mechanism of ABC transporters. *Biochemical Society Transactions* **47**, 23-36

38. Riordan, J., Rommens, J., Kerem, B., Alon, N., Rozmahel, R., Grzelczak, Z., Zielenski, J., Lok, S., Plavsic, N., Chou, J., and al., e. (1989) Identification of the cystic fibrosis gene: cloning and characterization of complementary DNA. *Science* **245**, 1066-1073

39. Hrycyna, C. A., Airan, L. E., Germann, U. A., Ambudkar, S. V., Pastan, I., and Gottesman, M. M. (1998) Structural Flexibility of the Linker Region of Human P-Glycoprotein Permits ATP Hydrolysis and Drug Transport †. **37**, 13660-13673

40. Qian, H., Zhao, X., Cao, P., Lei, J., Yan, N., and Gong, X. (2017) Structure of the Human Lipid Exporter ABCA1. *Cell* **169**, 1228-1239.e1210

41. Baker, J. M. R., Hudson, R. P., Kanelis, V., Choy, W.-Y., Thibodeau, P. H., Thomas, P. J., and Forman-Kay, J. D. (2007) CFTR regulatory region interacts with NBD1 predominantly via multiple transient helices. **14**, 738-745

42. Hwang, T. C. (1993) Functionally distinct phospho-forms underlie incremental activation of protein kinase-regulated Cl- conductance in mammalian heart. **101**, 629-650

43. Drumm, M., Wilkinson, D., Smit, L., Worrell, R., Strong, T., Frizzell, R., Dawson, D., and Collins, F. (1991) Chloride conductance expressed by delta F508 and other mutant CFTRs in Xenopus oocytes. *Science* **254**, 1797-1799

44. O'Riordan, C. R., Lachapelle, A. L., Marshall, J., Higgins, E. A., and Cheng, S. H. (2000) Characterization of the oligosaccharide structures associated with the cystic fibrosis transmembrane conductance regulator. **10**, 1225-1233

45. Hall, R. A., Ostedgaard, L. S., Premont, R. T., Blitzer, J. T., Rahman, N., Welsh, M. J., and Lefkowitz, R. J. (1998) A C-terminal motif found in the 2-adrenergic receptor, P2Y1 receptor and cystic fibrosis transmembrane conductance regulator determines binding to the Na+/H+ exchanger regulatory factor family of PDZ proteins. **95**, 8496-8501

46. Short, D. B., Trotter, K. W., Reczek, D., Kreda, S. M., Bretscher, A., Boucher, R. C., Stutts, M. J., and Milgram, S. L. (1998) An Apical PDZ Protein Anchors the Cystic Fibrosis Transmembrane Conductance Regulator to the Cytoskeleton. **273**, 19797-19801

47. Wang, S., Raab, R. W., Schatz, P. J., Guggino, W. B., and Li, M. (1998) Peptide binding consensus of the NHE-RF-PDZ1 domain matches the C-terminal sequence of cystic fibrosis transmembrane conductance regulator (CFTR). **427**, 103-108

48. Zhang, Z., and Chen, J. (2016) Atomic Structure of the Cystic Fibrosis Transmembrane Conductance Regulator. *Cell* **167**, 1586-1597.e1589

49. Li, N., Wu, J.-X., Ding, D., Cheng, J., Gao, N., and Chen, L. (2017) Structure of a Pancreatic ATP-Sensitive Potassium Channel. **168**, 101-110.e110

50. Johnson, Z. L., and Chen, J. (2017) Structural Basis of Substrate Recognition by the Multidrug Resistance Protein MRP1. *Cell* **168**, 1075-1085.e1079

51. Martin, G. M., Yoshioka, C., Rex, E. A., Fay, J. F., Xie, Q., Whorton, M. R., Chen, J. Z., and Shyng, S.-L. (2017) Cryo-EM structure of the ATP-sensitive potassium channel illuminates mechanisms of assembly and gating. *Elife* **6**, e24149

52.	Peters, K., Qi, J., Johnson, J., Watkins, S., and R, F. (2001) Role of snare proteins in CFTR and ENaC trafficking. **443**, S65-S69

53.	Naren, A. P., Quick, M. W., Collawn, J. F., Nelson, D. J., and Kirk, K. L. (1998) Syntaxin 1A inhibits CFTR chloride channels by means of domain-specific protein-protein interactions. **95**, 10972-10977

54.	Lu, Y., Xiong, X., Helm, A., Kimani, K., Bragin, A., and Skach, W. R. (1998) Co- and Posttranslational Translocation Mechanisms Direct Cystic Fibrosis Transmembrane Conductance Regulator N Terminus Transmembrane Assembly. **273**, 568-576

55.	Carveth, K., Buck, T., Anthony, V., and Skach, W. R. (2002) Cooperativity and Flexibility of Cystic Fibrosis Transmembrane Conductance Regulator Transmembrane Segments Participate in Membrane Localization of a Charged Residue. **277**, 39507-39514

56.	Kleizen, B., van Vlijmen, T., de Jonge, H. R., and Braakman, I. (2005) Folding of CFTR is predominantly cotranslational. *Mol Cell* **20**, 277-287

57.	Khushoo, A., Yang, Z., Arthur, and William. (2011) Ligand-Driven Vectorial Folding of Ribosome-Bound Human CFTR NBD1. **41**, 682-692

58.	Kim, S. J., and Skach, W. R. (2012) Mechanisms of CFTR Folding at the Endoplasmic Reticulum. **3**

59.	Xiong, X., Bragin, A., Widdicombe, J. H., Cohn, J., and Skach, W. R. (1997) Structural cues involved in endoplasmic reticulum degradation of G85E and G91R mutant cystic fibrosis transmembrane conductance regulator. **100**, 1079-1088

60.	Du, K., and Lukacs, G. L. (2009) Cooperative Assembly and Misfolding of CFTR Domains In Vivo. **20**, 1903-1915

61.	Pitonzo, D., Yang, Z., Matsumura, Y., Johnson, A. E., and Skach, W. R. (2009) Sequence-specific retention and regulated integration of a nascent membrane protein by the endoplasmic reticulum Sec61 translocon. *Mol Biol Cell* **20**, 685-698

62.	Enquist, K., Fransson, M., Boekel, C., Bengtsson, I., Geiger, K., Lang, L., Pettersson, A., Johansson, S., von Heijne, G., and Nilsson, I. (2009) Membrane-integration characteristics of two ABC transporters, CFTR and P-glycoprotein. *J Mol Biol* **387**, 1153-1164

63.	Farinha, C. M., and Canato, S. (2017) From the endoplasmic reticulum to the plasma membrane: mechanisms of CFTR folding and trafficking. *Cellular and Molecular Life Sciences* **74**, 39-55

64. Meacham, G. C., Lu, Z., King, S., Sorscher, E., Tousson, A., and Cyr, D. M. (1999) The Hdj-2/Hsc70 chaperone pair facilitates early steps in CFTR biogenesis. *EMBO J* **18**, 1492-1505

65. Oberdorf, J., Pitonzo, D., and Skach, W. R. (2005) An energy-dependent maturation step is required for release of the cystic fibrosis transmembrane conductance regulator from early endoplasmic reticulum biosynthetic machinery. *J Biol Chem* **280**, 38193-38202

66. Farinha, C. M., Nogueira, P., Mendes, F., Penque, D., and Amaral, M. D. (2002) The human DnaJ homologue (Hdj)-1/heat-shock protein (Hsp) 40 co-chaperone is required for the in vivo stabilization of the cystic fibrosis transmembrane conductance regulator by Hsp70. *Biochem J* **366**, 797-806

67. Roxo-Rosa, M., Xu, Z., Schmidt, A., Neto, M., Cai, Z., Soares, C. M., Sheppard, D. N., and Amaral, M. D. (2006) Revertant mutants G550E and 4RK rescue cystic fibrosis mutants in the first nucleotide-binding domain of CFTR by different mechanisms. *Proc Natl Acad Sci U S A* **103**, 17891-17896

68. Yang, Y., Janich, S., Cohn, J. A., and Wilson, J. M. (1993) The common variant of cystic fibrosis transmembrane conductance regulator is recognized by hsp70 and degraded in a pre-Golgi nonlysosomal compartment. *Proc Natl Acad Sci U S A* **90**, 9480-9484

69. Loo, M. A., Jensen, T. J., Cui, L., Hou, Y., Chang, X. B., and Riordan, J. R. (1998) Perturbation of Hsp90 interaction with nascent CFTR prevents its maturation and accelerates its degradation by the proteasome. *EMBO J* **17**, 6879-6887

70. Younger, J. M., Ren, H. Y., Chen, L., Fan, C. Y., Fields, A., Patterson, C., and Cyr, D. M. (2004) A foldable CFTR{Delta}F508 biogenic intermediate accumulates upon inhibition of the Hsc70-CHIP E3 ubiquitin ligase. *J Cell Biol* **167**, 1075-1085

71. Grove, D. E., Fan, C. Y., Ren, H. Y., and Cyr, D. M. (2011) The endoplasmic reticulum-associated Hsp40 DNAJB12 and Hsc70 cooperate to facilitate RMA1 E3-dependent degradation of nascent CFTRDeltaF508. *Mol Biol Cell* **22**, 301-314

72. Matsumura, Y., Sakai, J., and Skach, W. R. (2013) Endoplasmic reticulum protein quality control is determined by cooperative interactions between Hsp/c70 protein and the CHIP E3 ligase. *J Biol Chem* **288**, 31069-31079

73. Patrick, A. E., Karamyshev, A. L., Millen, L., and Thomas, P. J. (2011) Alteration of CFTR transmembrane span integration by disease-causing mutations. *Mol Biol Cell* **22**, 4461-4471

74. Pind, S., Riordan, J. R., and Williams, D. B. (1994) Participation of the endoplasmic reticulum chaperone calnexin (p88, IP90) in the biogenesis of the

cystic fibrosis transmembrane conductance regulator. *J Biol Chem* **269**, 12784-12788

75. Harada, K., Okiyoneda, T., Hashimoto, Y., Ueno, K., Nakamura, K., Yamahira, K., Sugahara, T., Shuto, T., Wada, I., Suico, M. A., and Kai, H. (2006) Calreticulin negatively regulates the cell surface expression of cystic fibrosis transmembrane conductance regulator. *J Biol Chem* **281**, 12841-12848

76. Rosser, M. F., Grove, D. E., Chen, L., and Cyr, D. M. (2008) Assembly and misassembly of cystic fibrosis transmembrane conductance regulator: folding defects caused by deletion of F508 occur before and after the calnexin-dependent association of membrane spanning domain (MSD) 1 and MSD2. *Mol Biol Cell* **19**, 4570-4579

77. Hammond, C., Braakman, I., and Helenius, A. (1994) Role of N-linked oligosaccharide recognition, glucose trimming, and calnexin in glycoprotein folding and quality control. *Proc Natl Acad Sci U S A* **91**, 913-917

78. Michelsen, K., Yuan, H., and Schwappach, B. (2005) Hide and run. Arginine-based endoplasmic-reticulum-sorting motifs in the assembly of heteromultimeric membrane proteins. *EMBO Rep* **6**, 717-722

79. Santos, J. D., Canato, S., Carvalho, A. S., Botelho, H. M., Aloria, K., Amaral, M. D., Matthiesen, R., Falcao, A. O., and Farinha, C. M. (2019) Folding Status Is Determinant over Traffic-Competence in Defining CFTR Interactors in the Endoplasmic Reticulum. *Cells* **8**, 353

80. Wang, X., Matteson, J., An, Y., Moyer, B., Yoo, J. S., Bannykh, S., Wilson, I. A., Riordan, J. R., and Balch, W. E. (2004) COPII-dependent export of cystic fibrosis transmembrane conductance regulator from the ER uses a di-acidic exit code. *J Cell Biol* **167**, 65-74

81. Nishimura, N., and Balch, W. E. (1997) A di-acidic signal required for selective export from the endoplasmic reticulum. *Science* **277**, 556-558

82. Farinha, Carlos M., King-Underwood, J., Sousa, M., Correia, Ana R., Henriques, Bárbara J., Roxo-Rosa, M., Da Paula, Ana C., Williams, J., Hirst, S., Gomes, Cláudio M., and Amaral, Margarida D. (2013) Revertants, Low Temperature, and Correctors Reveal the Mechanism of F508del-CFTR Rescue by VX-809 and Suggest Multiple Agents for Full Correction. *Chemistry & Biology* **20**, 943-955

83. Amaral, M. D., Farinha, C. M., Matos, P., and Botelho, H. M. (2016) Investigating Alternative Transport of Integral Plasma Membrane Proteins from the ER to the Golgi: Lessons from the Cystic Fibrosis Transmembrane Conductance Regulator (CFTR). *Methods Mol Biol* **1459**, 105-126

84. Grieve, A. G., and Rabouille, C. (2011) Golgi bypass: skirting around the heart of classical secretion. *Cold Spring Harb Perspect Biol* **3**

85.   Bannykh, S. I., Bannykh, G. I., Fish, K. N., Moyer, B. D., Riordan, J. R., and Balch, W. E. (2000) Traffic pattern of cystic fibrosis transmembrane regulator through the early exocytic pathway. *Traffic* **1**, 852-870

86.   Hu, W., Howard, M., and Lukacs, G. L. (2001) Multiple endocytic signals in the C-terminal tail of the cystic fibrosis transmembrane conductance regulator. *Biochem J* **354**, 561-572

87.   Peter, K., Varga, K., Bebok, Z., McNicholas-Bevensee, C. M., Schwiebert, L., Sorscher, E. J., Schwiebert, E. M., and Collawn, J. F. (2002) Ablation of internalization signals in the carboxyl-terminal tail of the cystic fibrosis transmembrane conductance regulator enhances cell surface expression. *J Biol Chem* **277**, 49952-49957

88.   Gentzsch, M., Aleksandrov, A., Aleksandrov, L., and Riordan, J. R. (2002) Functional analysis of the C-terminal boundary of the second nucleotide binding domain of the cystic fibrosis transmembrane conductance regulator and structural implications. *Biochem J* **366**, 541-548

89.   Weixel, K. M., and Bradbury, N. A. (2000) The carboxyl terminus of the cystic fibrosis transmembrane conductance regulator binds to AP-2 clathrin adaptors. *J Biol Chem* **275**, 3655-3660

90.   Swiatecka-Urban, A., Brown, A., Moreau-Marquis, S., Renuka, J., Coutermarsh, B., Barnaby, R., Karlson, K. H., Flotte, T. R., Fukuda, M., Langford, G. M., and Stanton, B. A. (2005) The short apical membrane half-life of rescued {Delta}F508-cystic fibrosis transmembrane conductance regulator (CFTR) results from accelerated endocytosis of {Delta}F508-CFTR in polarized human airway epithelial cells. *J Biol Chem* **280**, 36762-36772

91.   Short, D. B., Trotter, K. W., Reczek, D., Kreda, S. M., Bretscher, A., Boucher, R. C., Stutts, M. J., and Milgram, S. L. (1998) An apical PDZ protein anchors the cystic fibrosis transmembrane conductance regulator to the cytoskeleton. *J Biol Chem* **273**, 19797-19801

92.   Hall, R. A., Ostedgaard, L. S., Premont, R. T., Blitzer, J. T., Rahman, N., Welsh, M. J., and Lefkowitz, R. J. (1998) A C-terminal motif found in the beta2-adrenergic receptor, P2Y1 receptor and cystic fibrosis transmembrane conductance regulator determines binding to the Na+/H+ exchanger regulatory factor family of PDZ proteins. *Proc Natl Acad Sci U S A* **95**, 8496-8501

93.   Wang, S., Raab, R. W., Schatz, P. J., Guggino, W. B., and Li, M. (1998) Peptide binding consensus of the NHE-RF-PDZ1 domain matches the C-terminal sequence of cystic fibrosis transmembrane conductance regulator (CFTR). *FEBS Lett* **427**, 103-108

94.   Ranganathan, R., and Ross, E. M. (1997) PDZ domain proteins: scaffolds for signaling complexes. *Curr Biol* **7**, R770-773

95.   Cushing, P. R., Fellows, A., Villone, D., Boisguerin, P., and Madden, D. R. (2008) The relative binding affinities of PDZ partners for CFTR: a biochemical basis for efficient endocytic recycling. *Biochemistry* **47**, 10084-10098

96.   Guggino, W. B., and Stanton, B. A. (2006) New insights into cystic fibrosis: molecular switches that regulate CFTR. *Nat Rev Mol Cell Biol* **7**, 426-436

97.   Sun, F., Hug, M. J., Lewarchik, C. M., Yun, C. H., Bradbury, N. A., and Frizzell, R. A. (2000) E3KARP mediates the association of ezrin and protein kinase A with the cystic fibrosis transmembrane conductance regulator in airway cells. *J Biol Chem* **275**, 29539-29546

98.   Haggie, P. M., Kim, J. K., Lukacs, G. L., and Verkman, A. S. (2006) Tracking of quantum dot-labeled CFTR shows near immobilization by C-terminal PDZ interactions. *Mol Biol Cell* **17**, 4937-4945

99.   Anderson, M. P., Gregory, R. J., Thompson, S., Souza, D. W., Paul, S., Mulligan, R. C., Smith, A. E., and Welsh, M. J. (1991) Demonstration that CFTR is a Chloride Channel by Alteration of its Anion Selectivity. *Science* **253**, 202-205

100.   Anderson, M. P., Rich, D. P., Gregory, R. J., Smith, A. E., and Welsh, M. J. (1991) Generation of cAMP-activated chloride currents by expression of CFTR. *Science (New York, N.Y.)* **251**, 679-682

101.   Bear, C. E., Duguay, F., Naismith, A. L., Kartner, N., Hanrahan, J. W., and Riordan, J. R. (1991) Cl- channel activity in Xenopus oocytes expressing the cystic fibrosis gene. *The Journal of biological chemistry* **266**, 19142-19145

102.   Tabcharani, J. A., Chang, X.-B., Riordan, J. R., and Hanrahan, J. W. (1991) Phosphorylation-regulated CI– channel in CHO cells stably expressing the cystic fibrosis gene. **352**, 628-631

103.   Rich, D. P., Gregory, R. J., Anderson, M. P., Manavalan, P., Smith, A. E., and Welsh, M. J. (1991) Effect of deleting the R domain on CFTR-generated chloride channels. *Science* **253**, 205

104.   Berger, H. A., Anderson, M. P., Gregory, R. J., Thompson, S., Howard, P. W., Maurer, R. A., Mulligan, R., Smith, A. E., and Welsh, M. J. (1991) Identification and regulation of the cystic fibrosis transmembrane conductance regulator-generated chloride channel. **88**, 1422-1431

105.   Chang, X. B., Tabcharani, J. A., Hou, Y. X., Jensen, T. J., Kartner, N., Alon, N., Hanrahan, J. W., and Riordan, J. R. (1993) Protein kinase A (PKA) still activates CFTR chloride channel after mutagenesis of all 10 PKA consensus phosphorylation sites. *Journal of Biological Chemistry* **268**, 11304-11311

106. Cheng, S. H., Rich, D. P., Marshall, J., Gregory, R. J., Welsh, M. J., and Smith, A. E. (1991) Phosphorylation of the R domain by cAMP-dependent protein kinase regulates the CFTR chloride channel. *Cell* **66**, 1027-1036

107. Hwang, T. C., Nagel, G., Nairn, A. C., and Gadsby, D. C. (1994) Regulation of the gating of cystic fibrosis transmembrane conductance regulator C1 channels by phosphorylation and ATP hydrolysis. **91**, 4698-4702

108. Winter, M. C., and Welsh, M. J. (1997) Stimulation of CFTR activity by its phosphorylated R domain. *Nature* **389**, 294-296

109. Anderson, M. P., Berger, H. A., Rich, D. P., Gregory, R. J., Smith, A. E., and Welsh, M. J. (1991) Nucleoside triphosphates are required to open the CFTR chloride channel. *Cell* **67**, 775

110. Baukrowitz, T., Hwang, T.-C., Nairn, A. C., and Gadsby, D. C. (1994) Coupling of CFTR Cl− channel gating to an ATP hydrolysis cycle. *Neuron* **12**, 473-482

111. Carson, M. R., Travis, S. M., and Welsh, M. J. (1995) The Two Nucleotide-binding Domains of Cystic Fibrosis Transmembrane Conductance Regulator (CFTR) Have Distinct Functions in Controlling Channel Activity. *Journal of Biological Chemistry* **270**, 1711-1717

112. Gunderson, K. L., and Kopito, R. R. (1995) Conformational states of CFTR associated with channel gating: The role of ATP binding and hydrolysis. **82**, 231-239

113. Ko, Y. H., and Pedersen, P. L. (1995) The First Nucleotide Binding Fold of the Cystic Fibrosis Transmembrane Conductance Regulator Can Function as an Active ATPase. **270**, 22093-22096

114. Li, C., Ramjeesingh, M., Wang, W., Garami, E., Hewryk, M., Lee, D., Rommens, J. M., Galley, K., and Bear, C. E. (1996) ATPase Activity of the Cystic Fibrosis Transmembrane Conductance Regulator. *Journal of Biological Chemistry* **271**, 28463-28468

115. Tabcharani, J. A., Seibert, F. S., Chang, X. B., Dulhanty, A. M., Mathews, C., Hanrahan, J. W., and Riordan, J. R. (1995) cAMP-dependent Protein Kinase-mediated Phosphorylation of Cystic Fibrosis Transmembrane Conductance Regulator Residue Ser-753 and Its Role in Channel Activation. **270**, 2158-2162

116. Picciotto, M. R., Cohn, J. A., Bertuzzi, G., Greengard, P., and Nairn, A. C. (1992) Phosphorylation of the cystic fibrosis transmembrane conductance regulator. *Journal of Biological Chemistry* **267**, 12742-12752

117. Jia, Y., Mathews, C. J., and Hanrahan, J. W. (1997) Phosphorylation by Protein Kinase C Is Required For Acute Activation of Cystic Fibrosis Transmembrane Conductance Regulator by Protein Kinase A. **272**, 4978-4984

118. Wilkinson, D. J., Strong, T. V., Mansoura, M. K., Wood, D. L., Smith, S. S., Collins, F. S., and Dawson, D. C. (1997) CFTR activation: additive effects of stimulatory and inhibitory phosphorylation sites in the R domain. *American Journal of Physiology-Lung Cellular and Molecular Physiology* **273**, L127-L133

119. Vais, H., Zhang, R., and Reenstra, W. W. (2004) Dibasic phosphorylation sites in the R domain of CFTR have stimulatory and inhibitory effects on channel activation. **287**, C737-C745

120. Csanady, L. (2005) Preferential Phosphorylation of R-domain Serine 768 Dampens Activation of CFTR Channels by PKA. **125**, 171-186

121. Hegedűs, T., Aleksandrov, A., Mengos, A., Cui, L., Jensen, T. J., and Riordan, J. R. (2009) Role of individual R domain phosphorylation sites in CFTR regulation by protein kinase A. **1788**, 1341-1349

122. Rich, D. P., Berger, H. A., Cheng, S. H., Travis, S. M., Saxena, M., Smith, A. E., and Welsh, M. J. (1993) Regulation of the cystic fibrosis transmembrane conductance regulator Cl- channel by negative charge in the R domain. *Journal of Biological Chemistry* **268**, 20259-20267

123. Seibert, F. S., Chang, X. B., Aleksandrov, A. A., Clarke, D. M., Hanrahan, J. W., and Riordan, J. R. (1999) Influence of phosphorylation by protein kinase A on CFTR at the cell surface and endoplasmic reticulum. **1461**, 275-283

124. Sheppard, D. N., and Welsh, M. J. (1999) Structure and Function of the CFTR Chloride Channel. *Physiological Reviews* **79**, S23-S45

125. Ma, J., Zhao, J., Drumm, M. L., Xie, J., and Davis, P. B. (1997) Function of the R Domain in the Cystic Fibrosis Transmembrane Conductance Regulator Chloride Channel. **272**, 28133-28141

126. Liu, F., Zhang, Z., Csanády, L., Gadsby, D. C., and Chen, J. (2017) Molecular Structure of the Human CFTR Ion Channel. *Cell* **169**, 85-95.e88

127. Zhang, Z., Liu, F., and Chen, J. (2017) Conformational Changes of CFTR upon Phosphorylation and ATP Binding. *Cell* **170**, 483-491.e488

128. Zhang, Z., Liu, F., and Chen, J. (2018) Molecular structure of the ATP-bound, phosphorylated human CFTR. *Proceedings of the National Academy of Sciences* **115**, 12757-12762

129. Jih, K. Y., and Hwang, T. C. (2012) Nonequilibrium Gating of CFTR on an Equilibrium Theme. **27**, 351-361

130. Rahman, K. S., Cui, G., Harvey, S. C., and McCarty, N. A. (2013) Modeling the Conformational Changes Underlying Channel Opening in CFTR. **8**, e74574

131. Randak, C., Neth, P., Auerswald, E. A., Eckerskorn, C., Assfalg-Machleidt, I., and Machleidt, W. (1997) A recombinant polypeptide model of the second nucleotide-binding fold of the cystic fibrosis transmembrane conductance regulator functions as an active ATPase, GTPase and adenylate kinase. *FEBS Letters* **410**, 180-186

132. Bear, C. E., Li, C., Kartner, N., Bridges, R. J., Jensen, T. J., Ramjeesingh, M., and Riordan, J. R. (1992) Purification and functional reconstitution of the cystic fibrosis transmembrane conductance regulator (CFTR). *Cell* **68**, 809-818

133. Hildebrandt, E., Zhang, Q., Cant, N., Ding, H., Dai, Q., Peng, L., Fu, Y., Delucas, L. J., Ford, R., Kappes, J. C., and Urbatsch, I. L. (2014) A survey of detergents for the purification of stable, active human cystic fibrosis transmembrane conductance regulator (CFTR). **1838**, 2825-2837

134. Hildebrandt, E., Khazanov, N., Kappes, J. C., Dai, Q., Senderowitz, H., and Urbatsch, I. L. (2017) Specific stabilization of CFTR by phosphatidylserine. **1859**, 289-293

135. Linsdell, P., Tabcharani, J. A., Rommens, J. M., Hou, Y. X., Chang, X. B., Tsui, L. C., Riordan, J. R., and Hanrahan, J. W. (1997) Permeability of wild-type and mutant cystic fibrosis transmembrane conductance regulator chloride channels to polyatomic anions. *The Journal of general physiology* **110**, 355-364

136. Bridges, R. J. (2012) Mechanisms of Bicarbonate Secretion: Lessons from the Airways. *Cold Spring Harbor Perspectives in Medicine* **2**

137. Linsdell, P., and Hanrahan, J. W. (1998) Glutathione permeability of CFTR. *American Journal of Physiology-Cell Physiology* **275**, C323-C326

138. Frizzell, R. A., and Hanrahan, J. W. (2012) Physiology of Epithelial Chloride and Fluid Secretion. *Cold Spring Harbor Perspectives in Medicine* **2**, a009563-a009563

139. Norimatsu, Y., Ivetac, A., Alexander, C., Kirkham, J., O'Donnell, N., Dawson, D. C., and Sansom, M. S. P. (2012) Cystic Fibrosis Transmembrane Conductance Regulator: A Molecular Model Defines the Architecture of the Anion Conduction Path and Locates a "Bottleneck" in the Pore. **51**, 2199-2212

140. Tabcharani, J. A., Low, W., Elie, D., and Hanrahan, J. W. (1990) Low-conductance chloride channel activated by cAMP in the epithelial cell line T 84. **270**, 157-164

141. Tabcharani, J. A. (1997) Halide Permeation in Wild-Type and Mutant Cystic Fibrosis Transmembrane Conductance Regulator Chloride Channels. **110**, 341-354

142. McCarty, N. A. (1993) Voltage-dependent block of the cystic fibrosis transmembrane conductance regulator Cl- channel by two closely related arylaminobenzoates. **102**, 1-23

143. Tao, T., Xie, J., Drumm, M. L., Zhao, J., Davis, P. B., and Ma, J. (1996) Slow conversions among subconductance states of cystic fibrosis transmembrane conductance regulator chloride channel. **70**, 743-753

144. Cui, G., Song, B., Turki, H. W., and McCarty, N. A. (2012) Differential contribution of TM6 and TM12 to the pore of CFTR identified by three sulfonylurea-based blockers. **463**, 405-418

145. Zhang, Z. R., Cui, G., Liu, X., Song, B., Dawson, D. C., and McCarty, N. A. (2005) Determination of the Functional Unit of the Cystic Fibrosis Transmembrane Conductance Regulator Chloride Channel: ONE POLYPEPTIDE FORMS ONE PORE. **280**, 458-468

146. Cui, G., Zhang, Z.-R., O'Brien, A. R. W., Song, B., and McCarty, N. A. (2008) Mutations at Arginine 352 Alter the Pore Architecture of CFTR. **222**, 91-106

147. Cotten, J. F., and Welsh, M. J. (1999) Cystic Fibrosis-associated Mutations at Arginine 347 Alter the Pore Architecture of CFTR: EVIDENCE FOR DISRUPTION OF A SALT BRIDGE. **274**, 5429-5435

148. Cui, G., Freeman, C. S., Knotts, T., Prince, C. Z., Kuang, C., and McCarty, N. A. (2013) Two Salt Bridges Differentially Contribute to the Maintenance of Cystic Fibrosis Transmembrane Conductance Regulator (CFTR) Channel Function. **288**, 20758-20767

149. Harrington, M. A., and Kopito, R. R. (2002) Cysteine Residues in the Nucleotide Binding Domains Regulate the Conductance State of CFTR Channels. **82**, 1278-1292

150. McCarty, N. A. (2000) Permeation through the CFTR chloride channel. *Journal of Experimental Biology* **203**, 1947-1962

151. Linsdell, P. (2014) Functional architecture of the CFTR chloride channel. **31**, 1-16

152. McCarty, N. A., and Zhang, Z.-R. (2001) Identification of a region of strong discrimination in the pore of CFTR. *American Journal of Physiology-Lung Cellular and Molecular Physiology* **281**, L852-L867

153. De Boeck, K., Zolin, A., Cuppens, H., Olesen, H. V., and Viviani, L. (2014) The relative frequency of CFTR mutation classes in European patients with cystic fibrosis. *Journal of Cystic Fibrosis* **13**, 403-409

154. Solomon, G. M., Marshall, S. G., Ramsey, B. W., and Rowe, S. M. (2015) Breakthrough therapies: Cystic fibrosis (CF) potentiators and correctors. *Pediatric Pulmonology* **50**, S3-S13

155. Veit, G., Avramescu, R. G., Chiang, A. N., Houck, S. A., Cai, Z., Peters, K. W., Hong, J. S., Pollard, H. B., Guggino, W. B., Balch, W. E., Skach, W. R., Cutting, G. R., Frizzell, R. A., Sheppard, D. N., Cyr, D. M., Sorscher, E. J., Brodsky, J. L., and Lukacs, G. L. (2016) From CFTR biology toward combinatorial pharmacotherapy: expanded classification of cystic fibrosis mutations. *Molecular Biology of the Cell* **27**, 424-433

156. Rosenberg, M. F., Kamis, A. B., Aleksandrov, L. A., Ford, R. C., and Riordan, J. R. (2004) Purification and Crystallization of the Cystic Fibrosis Transmembrane Conductance Regulator (CFTR). **279**, 39051-39057

157. Rosenberg, M. F., O'Ryan, L. P., Hughes, G., Zhao, Z., Aleksandrov, L. A., Riordan, J. R., and Ford, R. C. (2011) The Cystic Fibrosis Transmembrane Conductance Regulator (CFTR): THREE-DIMENSIONAL STRUCTURE AND LOCALIZATION OF A CHANNEL GATE. **286**, 42647-42654

158. Li, J., Jaimes, K. F., and Aller, S. G. (2014) Refined structures of mouse P-glycoprotein. **23**, 34-46

159. Serohijos, A. W. R., Hegedus, T., Aleksandrov, A. A., He, L., Cui, L., Dokholyan, N. V., and Riordan, J. R. (2008) Phenylalanine-508 mediates a cytoplasmic-membrane domain contact in the CFTR 3D structure crucial to assembly and channel function. **105**, 3256-3261

160. Mornon, J. P., Lehn, P., and Callebaut, I. (2008) Atomic model of human cystic fibrosis transmembrane conductance regulator: Membrane-spanning domains and coupling interfaces. **65**, 2594-2612

161. Mornon, J.-P., Lehn, P., and Callebaut, I. (2009) Molecular models of the open and closed states of the whole human CFTR protein. **66**, 3469-3486

162. Corradi, V., Vergani, P., and Tieleman, D. P. (2015) Cystic Fibrosis Transmembrane Conductance Regulator (CFTR). **290**, 22891-22906

163. Furukawa-Hagiya, T., Furuta, T., Chiba, S., Sohma, Y., and Sakurai, M. (2013) The Power Stroke Driven by ATP Binding in CFTR As Studied by Molecular Dynamics Simulations. **117**, 83-93

164. Dalton, J., Kalid, O., Schushan, M., Ben-Tal, N., and Villà-Freixa, J. (2012) New Model of Cystic Fibrosis Transmembrane Conductance Regulator Proposes Active Channel-like Conformation. **52**, 1842-1853

165. Mornon, J.-P., Hoffmann, B., Jonic, S., Lehn, P., and Callebaut, I. (2015) Full-open and closed CFTR channels, with lateral tunnels from the cytoplasm and an

alternative position of the F508 region, as revealed by molecular dynamics. **72**, 1377-1403

166. Strickland, K. M., Stock, G., Cui, G., Hwang, H., Infield, D. T., Schmidt-Krey, I., McCarty, N. A., and Gumbart, J. C. (2019) ATP-Dependent Signaling in Simulations of a Revised Model of Cystic Fibrosis Transmembrane Conductance Regulator (CFTR). *The Journal of Physical Chemistry B* **123**, 3177-3188

167. Corradi, V., Gu, R.-X., Vergani, P., and Tieleman, D. P. (2018) Structure of Transmembrane Helix 8 and Possible Membrane Defects in CFTR. *Biophysical Journal* **114**, 1751-1754

168. Negoda, A., Hogan, M. S., Cowley, E. A., and Linsdell, P. (2019) Contribution of the eighth transmembrane segment to the function of the CFTR chloride channel pore. *Cellular and Molecular Life Sciences*

169. Farkas, B., Tordai, H., Padányi, R., Tordai, A., Gera, J., Paragi, G., and Hegedűs, T. (2019) Discovering the chloride pathway in the CFTR channel. *Cellular and Molecular Life Sciences*

170. Liu, F., Zhang, Z., Levit, A., Levring, J., Touhara, K. K., Shoichet, B. K., and Chen, J. (2019) Structural identification of a hotspot on CFTR for potentiation. *Science* **364**, 1184-1188

171. Fay, J. F., Aleksandrov, L. A., Jensen, T. J., Cui, L. L., Kousouros, J. N., He, L., Aleksandrov, A. A., Gingerich, D. S., Riordan, J. R., and Chen, J. Z. (2018) Cryo-EM Visualization of an Active High Open Probability CFTR Anion Channel. *Biochemistry* **57**, 6234-6246

172. Vorobiev, S. M., Wang, C., Yang, Z., Clarke, O. B., Jiang, F., Aleksandrov, A., Fu, Z., Grassucci, R. A., Wu, S., and Mezzell, A. (2019) THERMODYNAMIC ENGINEERING ENABLES DETERMINATION OF NEAR-ATOMIC RESOLUTION CRYO-EM STRUCTURES OF HUMAN F508DEL-CFTR IN DIVERSE CONFORMATIONAL STATES. In *PEDIATRIC PULMONOLOGY* Vol. 54 pp. S81-S82, WILEY 111 RIVER ST, HOBOKEN 07030-5774, NJ USA

173. Seddon, A. M., Curnow, P., and Booth, P. J. (2004) Membrane proteins, lipids and detergents: not just a soap opera. *Biochim Biophys Acta* **1666**, 105-117

174. Pollock, N. L., Lee, S. C., Patel, J. H., Gulamhussein, A. A., and Rothnie, A. J. (2018) Structure and function of membrane proteins encapsulated in a polymer-bound lipid bilayer. *Biochimica et Biophysica Acta (BBA) - Biomembranes* **1860**, 809-817

175. Bogdanov, M., Mileykovskaya, E., and Dowhan, W. (2008) Lipids in the Assembly of Membrane Proteins and Organization of Protein Supercomplexes: Implications for Lipid-linked Disorders. pp. 197-239, Springer Netherlands

176. Saliba, A.-E., Vonkova, I., and Gavin, A.-C. (2015) The systematic analysis of protein–lipid interactions comes of age. *Nature Reviews Molecular Cell Biology* **16**, 753-761

177. Contreras, F. X., Ernst, A. M., Wieland, F., and Brugger, B. (2011) Specificity of Intramembrane Protein-Lipid Interactions. *Cold Spring Harbor Perspectives in Biology* **3**, a004705-a004705

178. Popot, J. L. (2010) Amphipols, nanodiscs, and fluorinated surfactants: three nonconventional approaches to studying membrane proteins in aqueous solutions. *Annu Rev Biochem* **79**, 737-775

179. Denisov, I. G., and Sligar, S. G. (2017) Nanodiscs in Membrane Biochemistry and Biophysics. *Chemical Reviews* **117**, 4669-4713

180. Overduin, M., and Esmaili, M. (2019) Native Nanodiscs and the Convergence of Lipidomics, Metabolomics, Interactomics and Proteomics. *Applied Sciences* **9**, 1230

181. Ravula, T., Hardin, N. Z., and Ramamoorthy, A. (2019) Polymer nanodiscs: Advantages and limitations. *Chemistry and Physics of Lipids* **219**, 45-49

182. Bayburt, T. H., Carlson, J. W., and Sligar, S. G. (1998) Reconstitution and imaging of a membrane protein in a nanometer-size phospholipid bilayer. *J Struct Biol* **123**, 37-44

183. Bayburt, T. H., Grinkova, Y. V., and Sligar, S. G. (2002) Self-Assembly of Discoidal Phospholipid Bilayer Nanoparticles with Membrane Scaffold Proteins. *Nano Letters* **2**, 853-856

184. Denisov, I. G., Grinkova, Y. V., Lazarides, A. A., and Sligar, S. G. (2004) Directed self-assembly of monodisperse phospholipid bilayer Nanodiscs with controlled size. *J Am Chem Soc* **126**, 3477-3487

185. Grinkova, Y. V., Denisov, I. G., and Sligar, S. G. (2010) Engineering extended membrane scaffold proteins for self-assembly of soluble nanoscale lipid bilayers. *Protein Eng Des Sel* **23**, 843-848

186. Hagn, F., Etzkorn, M., Raschle, T., and Wagner, G. (2013) Optimized Phospholipid Bilayer Nanodiscs Facilitate High-Resolution Structure Determination of Membrane Proteins. **135**, 1919-1925

187. Inagaki, S., Ghirlando, R., and Grisshammer, R. (2013) Biophysical characterization of membrane proteins in nanodiscs. *Methods* **59**, 287-300

188. Rouck, J. E., Krapf, J. E., Roy, J., Huff, H. C., and Das, A. (2017) Recent advances in nanodisc technology for membrane protein studies (2012-2017). *FEBS Lett* **591**, 2057-2088

189. Civjan, N. R., Bayburt, T. H., Schuler, M. A., and Sligar, S. G. (2003) Direct solubilization of heterologously expressed membrane proteins by incorporation into nanoscale lipid bilayers. *BioTechniques* **35**, 556-563

190. Yeh, V., Lee, T.-Y., Chen, C.-W., Kuo, P.-C., Shiue, J., Chu, L.-K., and Yu, T.-Y. (2018) Highly Efficient Transfer of 7TM Membrane Protein from Native Membrane to Covalently Circularized Nanodisc. *Scientific Reports* **8**, 13501

191. Dörr, J. M., Koorengevel, M. C., Schäfer, M., Prokofyev, A. V., Scheidelaar, S., Van Der Cruijsen, E. A. W., Dafforn, T. R., Baldus, M., and Killian, J. A. (2014) Detergent-free isolation, characterization, and functional reconstitution of a tetrameric K + channel: The power of native nanodiscs. **111**, 18607-18612

192. Knowles, T. J., Finka, R., Smith, C., Lin, Y.-P., Dafforn, T., and Overduin, M. (2009) Membrane Proteins Solubilized Intact in Lipid Containing Nanoparticles Bounded by Styrene Maleic Acid Copolymer. *Journal of the American Chemical Society* **131**, 7484-7485

193. Orwick, M. C., Judge, P. J., Procek, J., Lindholm, L., Graziadei, A., Engel, A., Gröbner, G., and Watts, A. (2012) Detergent-Free Formation and Physicochemical Characterization of Nanosized Lipid-Polymer Complexes: Lipodisq. **51**, 4653-4657

194. Dörr, J. M., Scheidelaar, S., Koorengevel, M. C., Dominguez, J. J., Schäfer, M., Van Walree, C. A., and Killian, J. A. (2016) The styrene–maleic acid copolymer: a versatile tool in membrane research. *European Biophysics Journal* **45**, 3-21

195. Xue, M., Cheng, L., Faustino, I., Guo, W., and Marrink, S. J. (2018) Molecular Mechanism of Lipid Nanodisc Formation by Styrene Maleic Acid Copolymers. *Biophysical Journal*

196. Scheidelaar, S., Martijn, Cornelius, Juan, Jonas, and J. (2016) Effect of Polymer Composition and pH on Membrane Solubilization by Styrene-Maleic Acid Copolymers. *Biophysical Journal* **111**, 1974-1986

197. Lee, S. C., Knowles, T. J., Postis, V. L. G., Jamshad, M., Parslow, R. A., Lin, Y.-P., Goldman, A., Sridhar, P., Overduin, M., Muench, S. P., and Dafforn, T. R. (2016) A method for detergent-free isolation of membrane proteins in their local lipid environment. *Nature Protocols* **11**, 1149-1162

198. Scheidelaar, S., Martijn, Juan, Johannes, Breukink, E., and J. (2015) Molecular Model for the Solubilization of Membranes into Nanodisks by Styrene Maleic Acid Copolymers. *Biophysical Journal* **108**, 279-290

199. Dominguez Pardo, J. J., Dörr, J. M., Iyer, A., Cox, R. C., Scheidelaar, S., Koorengevel, M. C., Subramaniam, V., and Killian, J. A. (2016) Solubilization of lipids and lipid phases by the styrene–maleic acid copolymer.

276

200. Teo, A. C. K., Lee, S. C., Pollock, N. L., Stroud, Z., Hall, S., Thakker, A., Pitt, A. R., Dafforn, T. R., Spickett, C. M., and Roper, D. I. (2019) Analysis of SMALP co-extracted phospholipids shows distinct membrane environments for three classes of bacterial membrane protein. *Scientific Reports* **9**

201. Fiori, M. C., Jiang, Y., Altenberg, G. A., and Liang, H. (2017) Polymer-encased nanodiscs with improved buffer compatibility. *Scientific Reports* **7**

202. Oluwole, A. O., Danielczak, B., Meister, A., Babalola, J. O., Vargas, C., and Keller, S. (2017) Solubilization of Membrane Proteins into Functional Lipid-Bilayer Nanodiscs Using a Diisobutylene/Maleic Acid Copolymer. *Angewandte Chemie International Edition* **56**, 1919-1924

203. Hall, S. C. L., Tognoloni, C., Charlton, J., Bragginton, É. C., Rothnie, A. J., Sridhar, P., Wheatley, M., Knowles, T. J., Arnold, T., Edler, K. J., and Dafforn, T. R. (2018) An acid-compatible co-polymer for the solubilization of membranes and proteins into lipid bilayer-containing nanoparticles. *Nanoscale* **10**, 10609-10619

204. Ravula, T., Hardin, N. Z., Ramadugu, S. K., Cox, S. J., and Ramamoorthy, A. (2018) Formation of pH-Resistant Monodispersed Polymer-Lipid Nanodiscs. *Angew Chem Int Ed Engl* **57**, 1342-1345

205. Lindhoud, S., Carvalho, V., Pronk, J. W., and Aubin-Tam, M.-E. (2016) SMA-SH: Modified Styrene–Maleic Acid Copolymer for Functionalization of Lipid Nanodiscs. *Biomacromolecules* **17**, 1516-1522

206. Schmidt, V., and Sturgis, J. N. (2018) Modifying styrene-maleic acid co-polymer for studying lipid nanodiscs. *Biochimica et Biophysica Acta (BBA) - Biomembranes* **1860**, 777-783

207. Sosnay, P. R., Siklosi, K. R., Van Goor, F., Kaniecki, K., Yu, H., Sharma, N., Ramalho, A. S., Amaral, M. D., Dorfman, R., Zielenski, J., Masica, D. L., Karchin, R., Millen, L., Thomas, P. J., Patrinos, G. P., Corey, M., Lewis, M. H., Rommens, J. M., Castellani, C., Penland, C. M., and Cutting, G. R. (2013) Defining the disease liability of variants in the cystic fibrosis transmembrane conductance regulator gene. **45**, 1160-1167

208. Kartner, N., Hanrahan, J. W., Jensen, T. J., Naismith, A. L., Sun, S., Ackerley, C. A., Reyes, E. F., Tsui, L.-C., Rommens, J. M., Bear, C. E., and Riordan, J. R. (1991) Expression of the cystic fibrosis gene in non-epithelial invertebrate cells produces a regulated anion conductance. *Cell* **64**, 681-691

209. Hyde, S. C., Emsley, P., Hartshorn, M. J., Mimmack, M. M., Gileadi, U., Pearce, S. R., Gallagher, M. P., Gill, D. R., Hubbard, R. E., and Higgins, C. F. (1990) Structural model of ATP-binding proteing associated with cystic fibrosis, multidrug resistance and bacterial transport. **346**, 362-365

210. Rees, D. C., Johnson, E., and Lewinson, O. (2009) ABC transporters: the power to change. *Nature Reviews Molecular Cell Biology* **10**, 218-227

211. Wang, W., and Linsdell, P. (2012) Alternating Access to the Transmembrane Domain of the ATP-binding Cassette Protein Cystic Fibrosis Transmembrane Conductance Regulator (ABCC7). **287**, 10156-10165

212. Ter Beek, J., Guskov, A., and Slotboom, D. J. (2014) Structural diversity of ABC transporters. *The Journal of General Physiology* **143**, 419-435

213. Denning, G. M., Anderson, M. P., Amara, J. F., Marshall, J., Smith, A. E., and Welsh, M. J. (1992) Processing of mutant cystic fibrosis transmembrane conductance regulator is temperature-sensitive. *Nature* **358**, 761-764

214. Dalemans, W., Barbry, P., Champigny, G., Jallat, S., Jallat, S., Dott, K., Dreyer, D., Crystal, R. G., Pavirani, A., Lecocq, J.-P., and Lazdunski, M. (1991) Altered chloride ion channel kinetics associated with the ΔF508 cystic fibrosis mutation. **354**, 526-528

215. Csanády, L. (2017) CFTR gating: Invisible transitions made visible. jgp.201711777

216. Choudhury, H. G., Tong, Z., Mathavan, I., Li, Y., Iwata, S., Zirah, S., Rebuffat, S., Van Veen, H. W., and Beis, K. (2014) Structure of an antibacterial peptide ATP-binding cassette transporter in a novel outward occluded state. **111**, 9145-9150

217. Trabuco, L. G., Villa, E., Mitra, K., Frank, J., and Schulten, K. (2008) Flexible Fitting of Atomic Structures into Electron Microscopy Maps Using Molecular Dynamics. *Structure* **16**, 673-683

218. Šali, A., and Blundell, T. L. (1993) Comparative Protein Modelling by Satisfaction of Spatial Restraints. *Journal of Molecular Biology* **234**, 779-815

219. Trabuco, L. G., Schreiner, E., Gumbart, J., Hsin, J., Villa, E., and Schulten, K. (2011) Applications of the molecular dynamics flexible fitting method. **173**, 420-427

220. Wriggers, W. (2012) Conventions and workflows for using Situs. **68**, 344-351

221. Phillips, J. C., Braun, R., Wang, W., Gumbart, J., Tajkhorshid, E., Villa, E., Chipot, C., Skeel, R. D., Kalé, L., and Schulten, K. (2005) Scalable molecular dynamics with NAMD. *Journal of Computational Chemistry* **26**, 1781-1802

222. Chan, K.-Y., Gumbart, J., McGreevy, R., Jean, B, and Schulten, K. (2011) Symmetry-Restrained Flexible Fitting for Symmetric EM Maps. **19**, 1211-1218

223. Simhaev, L., McCarty, N. A., Ford, R. C., and Senderowitz, H. (2017) Molecular Dynamics Flexible Fitting Simulations Identify New Models of the Closed State of the Cystic Fibrosis Transmembrane Conductance Regulator Protein. *Journal of Chemical Information and Modeling* **57**, 1932-1946

224. Atwell, S., Brouillette, C. G., Conners, K., Emtage, S., Gheyi, T., Guggino, W. B., Hendle, J., Hunt, J. F., Lewis, H. A., Lu, F., Protasevich, I. I., Rodgers, L. A., Romero, R., Wasserman, S. R., Weber, P. C., Wetmore, D., Zhang, F. F., and Zhao, X. (2010) Structures of a minimal human CFTR first nucleotide-binding domain as a monomer, head-to-tail homodimer, and pathogenic mutant. **23**, 375-384

225. Haffke, M., Menzel, A., Carius, Y., Jahn, D., and Heinz, D. W. (2010) Structures of the nucleotide-binding domain of the human ABCB6 transporter and its complexes with nucleotides. **66**, 979-987

226. Humphrey, W., Dalke, A., and Schulten, K. (1996) VMD: Visual molecular dynamics. *Journal of Molecular Graphics* **14**, 33-38

227. Pastor, R. W., and Mackerell, A. D. (2011) Development of the CHARMM Force Field for Lipids. **2**, 1526-1532

228. Best, R. B., Zhu, X., Shim, J., Lopes, P. E. M., Mittal, J., Feig, M., and Mackerell, A. D. (2012) Optimization of the Additive CHARMM All-Atom Protein Force Field Targeting Improved Sampling of the Backbone ϕ, ψ and Side-Chain χ1 and χ2 Dihedral Angles. *Journal of Chemical Theory and Computation* **8**, 3257-3273

229. Denning, E. J., Priyakumar, U. D., Nilsson, L., and Mackerell, A. D. (2011) Impact of 2′-hydroxyl sampling on the conformational properties of RNA: Update of the CHARMM all-atom additive force field for RNA. *Journal of Computational Chemistry* **32**, 1929-1943

230. Jorgensen, W. L., Chandrasekhar, J., Madura, J. D., Impey, R. W., and Klein, M. L. (1983) Comparison of simple potential functions for simulating liquid water. *The Journal of Chemical Physics* **79**, 926-935

231. Darden, T., York, D., and Pedersen, L. (1993) Particle mesh Ewald: An N·log(N) method for Ewald sums in large systems. *The Journal of Chemical Physics* **98**, 10089-10092

232. Gumbart, J., and Schulten, K. (2006) Molecular Dynamics Studies of the Archaeal Translocon. **90**, 2356-2367

233. Smart, O. S., Neduvelil, J. G., Wang, X., Wallace, B. A., and Sansom, M. S. P. (1996) HOLE: A program for the analysis of the pore dimensions of ion channel structural models. **14**, 354-360

234. Michaud-Agrawal, N., Denning, E. J., Woolf, T. B., and Beckstein, O. (2011) MDAnalysis: a toolkit for the analysis of molecular dynamics simulations. *Journal of computational chemistry* **32**, 2319-2327

235. Wang, W., Roessler, B. C., and Kirk, K. L. (2014) An Electrostatic Interaction at the Tetrahelix Bundle Promotes Phosphorylation-dependent Cystic Fibrosis Transmembrane Conductance Regulator (CFTR) Channel Opening. *Journal of Biological Chemistry* **289**, 30364-30378

236. Mense, M., Vergani, P., White, D. M., Altberg, G., Nairn, A. C., and Gadsby, D. C. (2006) In vivo phosphorylation of CFTR promotes formation of a nucleotide-binding domain heterodimer. *The EMBO Journal* **25**, 4728-4739

237. Csanady, L. (2004) Functional Roles of Nonconserved Structural Segments in CFTR's NH2-terminal Nucleotide Binding Domain. **125**, 43-55

238. Travis, S. M. (1995) The Two Nucleotide-binding Domains of Cystic Fibrosis Transmembrane Conductance Regulator (CFTR) Have Distinct Functions in Controlling Channel Activity. **270**, 1711-1717

239. Szollosi, A., Muallem, D. R., Csanady, L., and Vergani, P. (2011) Mutant cycles at CFTR's non-canonical ATP-binding site support little interface separation during gating. **137**, 549-562

240. Tsai, M. F., Li, M., and Hwang, T. C. (2010) Stable ATP binding mediated by a partial NBD dimer of the CFTR chloride channel. **135**, 399-414

241. Vergani, P., Lockless, S. W., Nairn, A. C., and Gadsby, D. C. (2005) CFTR channel opening by ATP-driven tight dimerization of its nucleotide-binding domains. **433**, 876-880

242. Chaves, L. A. P., and Gadsby, D. C. (2015) Cysteine accessibility probes timing and extent of NBD separation along the dimer interface in gating CFTR channels. **145**, 261-283

243. Szöllősi, D., Szakács, G., Chiba, P., and Stockner, T. (2018) Dissecting the Forces that Dominate Dimerization of the Nucleotide Binding Domains of ABCB1. *Biophysical Journal* **114**, 331-342

244. Vergani, P. (2002) On the Mechanism of MgATP-dependent Gating of CFTR Cl-Channels. **121**, 17-36

245. Berger, A. L., Ikuma, M., and Welsh, M. J. (2005) Normal gating of CFTR requires ATP binding to both nucleotide-binding domains and hydrolysis at the second nucleotide-binding domain. **102**, 455-460

246. Li, J., Shaikh, S. A., Enkavi, G., Wen, P. C., Huang, Z., and Tajkhorshid, E. (2013) Transient formation of water-conducting states in membrane transporters. **110**, 7696-7701

247. Norimatsu, Y., Ivetac, A., Alexander, C., O'Donnell, N., Frye, L., Sansom, M. S. P., and Dawson, D. C. (2012) Locating a Plausible Binding Site for an Open-Channel Blocker, GlyH-101, in the Pore of the Cystic Fibrosis Transmembrane Conductance Regulator. **82**, 1042-1055

248. Infield, D. T., Cui, G., Kuang, C., and McCarty, N. A. (2016) Positioning of extracellular loop 1 affects pore gating of the cystic fibrosis transmembrane conductance regulator. *Am J Physiol Lung Cell Mol Physiol* **310**, L403-L414

249. St-Pierre, J.-F., Bunker, A., Róg, T., Karttunen, M., and Mousseau, N. (2012) Molecular Dynamics Simulations of the Bacterial ABC Transporter SAV1866 in the Closed Form. *The Journal of Physical Chemistry B* **116**, 2934-2942

250. Moradi, M., and Tajkhorshid, E. (2013) Mechanistic picture for conformational transition of a membrane transporter at atomic resolution. **110**, 18916-18921

251. Cui, G., Rahman, K. S., Infield, D. T., Kuang, C., Prince, C. Z., and McCarty, N. A. (2014) Three charged amino acids in extracellular loop 1 are involved in maintaining the outer pore architecture of CFTR. *The Journal of General Physiology* **144**, 159-179

252. Alexander, C., Ivetac, A., Liu, X., Norimatsu, Y., Serrano, J. R., Landstrom, A., Sansom, M., and Dawson, D. C. (2009) Cystic Fibrosis Transmembrane Conductance Regulator: Using Differential Reactivity toward Channel-Permeant and Channel-Impermeant Thiol-Reactive Probes To Test a Molecular Model for the Pore. **48**, 10078-10088

253. Linsdell, P. (1996) Disease-associated Mutations in the Fourth Cytoplasmic Loop of Cystic Fibrosis Transmembrane Conductance Regulator Compromise Biosynthetic Processing and Chloride Channel Activity. **271**, 15139-15145

254. Dalmas, O., Orelle, C., Foucher, A.-E., Geourjon, C., Crouzy, S., Di Pietro, A., and Jault, J.-M. (2005) The Q-loop Disengages from the First Intracellular Loop during the Catalytic Cycle of the Multidrug ABC Transporter BmrA. *Journal of Biological Chemistry* **280**, 36857-36864

255. Chong, P. A., Farber, P. J., Vernon, R. M., Hudson, R. P., Mittermaier, A. K., and Forman-Kay, J. D. (2015) Deletion of Phenylalanine 508 in the First Nucleotide-binding Domain of the Cystic Fibrosis Transmembrane Conductance Regulator Increases Conformational Exchange and Inhibits Dimerization. **290**, 22862-22878

256. He, L., Aleksandrov, A. A., Serohijos, A. W. R., Hegedus, T., Aleksandrov, L. A., Cui, L., Dokholyan, N. V., and Riordan, J. R. (2008) Multiple Membrane-Cytoplasmic Domain Contacts in the Cystic Fibrosis Transmembrane

Conductance Regulator (CFTR) Mediate Regulation of Channel Gating. **283**, 26383-26390

257. Cui, G., Hong, J., Chung-Davidson, Y.-W., Infield, D., Xu, X., Li, J., Simhaev, L., Khazanov, N., Stauffer, B., Imhoff, B., Cottrill, K., Blalock, J. E., Li, W., Senderowitz, H., Sorscher, E., McCarty, N. A., and Gaggar, A. (2019) An Ancient CFTR Ortholog Informs Molecular Evolution in ABC Transporters. *Developmental Cell* **51**, 421-430.e423

258. Galián, C., Manon, F., Dezi, M., Torres, C., Ebel, C., Lévy, D., and Jault, J.-M. (2011) Optimized Purification of a Heterodimeric ABC Transporter in a Highly Stable Form Amenable to 2-D Crystallization. **6**, e19677

259. Infed, N., Hanekop, N., Driessen, A. J. M., Smits, S. H. J., and Schmitt, L. (2011) Influence of detergents on the activity of the ABC transporter LmrA. *Biochimica et Biophysica Acta (BBA) - Biomembranes* **1808**, 2313-2321

260. Ellinger, P., Kluth, M., Stindt, J., Smits, S. H. J., and Schmitt, L. (2013) Detergent Screening and Purification of the Human Liver ABC Transporters BSEP (ABCB11) and MDR3 (ABCB4) Expressed in the Yeast Pichia pastoris. *PLoS ONE* **8**, e60620

261. Xu, J., Sun, H., Huang, G., Liu, G., Li, Z., Yang, H., Jin, L., Cui, X., Shi, L., Ma, T., Kameyama, A., and Dong, W. (2019) A fixation method for the optimisation of western blotting. *Scientific Reports* **9**, 6649

262. Alam, A., Kowal, J., Broude, E., Roninson, I., and Locher, K. P. (2019) Structural insight into substrate and inhibitor discrimination by human P-glycoprotein. *Science* **363**, 753-756

263. Taylor, N. M. I., Manolaridis, I., Jackson, S. M., Kowal, J., Stahlberg, H., and Locher, K. P. (2017) Structure of the human multidrug transporter ABCG2. *Nature* **546**, 504

264. Sonoda, Y., Cameron, A., Newstead, S., Omote, H., Moriyama, Y., Kasahara, M., Iwata, S., and Drew, D. (2010) Tricks of the trade used to accelerate high-resolution structure determination of membrane proteins. *FEBS Letters* **584**, 2539-2547

265. Hanson, M. A., Cherezov, V., Griffith, M. T., Roth, C. B., Jaakola, V.-P., Chien, E. Y. T., Velasquez, J., Kuhn, P., and Stevens, R. C. (2008) A Specific Cholesterol Binding Site Is Established by the 2.8 Å Structure of the Human β2-Adrenergic Receptor. *Structure* **16**, 897-905

266. Lichty, J. J., Malecki, J. L., Agnew, H. D., Michelson-Horowitz, D. J., and Tan, S. (2005) Comparison of affinity tags for protein purification. *Protein Expression and Purification* **41**, 98-105

267. Bao, H., Dalal, K., Wang, V., Rouiller, I., and Duong, F. (2013) The maltose ABC transporter: Action of membrane lipids on the transporter stability, coupling and ATPase activity. **1828**, 1723-1730

268. Dang, S., Feng, S., Tien, J., Peters, C. J., Bulkley, D., Lolicato, M., Zhao, J., Zuberbühler, K., Ye, W., Qi, L., Chen, T., Craik, C. S., Jan, Y. N., Minor, D. L., Jr., Cheng, Y., and Jan, L. Y. (2017) Cryo-EM structures of the TMEM16A calcium-activated chloride channel. *Nature* **552**, 426-429

269. Tang, G., Peng, L., Baldwin, P. R., Mann, D. S., Jiang, W., Rees, I., and Ludtke, S. J. (2007) EMAN2: An extensible image processing suite for electron microscopy. *Journal of Structural Biology* **157**, 38-46

270. Mindell, J. A., and Grigorieff, N. (2003) Accurate determination of local defocus and specimen tilt in electron microscopy. *Journal of Structural Biology* **142**, 334-347

271. Gao, Y., Cao, E., Julius, D., and Cheng, Y. (2016) TRPV1 structures in nanodiscs reveal mechanisms of ligand and lipid action. *Nature* **534**, 347-351

272. Zhou, M., Morgner, N., Barrera, N. P., Politis, A., Isaacson, S. C., Matak-Vinkovic, D., Murata, T., Bernal, R. A., Stock, D., and Robinson, C. V. (2011) Mass Spectrometry of Intact V-Type ATPases Reveals Bound Lipids and the Effects of Nucleotide Binding. **334**, 380-385

273. Gupta, K., Li, J., Liko, I., Gault, J., Bechara, C., Wu, D., Hopper, J. T. S., Giles, K., Benesch, J. L. P., and Robinson, C. V. (2018) Identifying key membrane protein lipid interactions using mass spectrometry. *Nature protocols* **13**, 1106-1120

274. Abu-Arish, A., Pandzic, E., Goepp, J., Matthes, E., John, and Paul. (2015) Cholesterol Modulates CFTR Confinement in the Plasma Membrane of Primary Epithelial Cells. **109**, 85-94

275. Schymanski, E. L., Jeon, J., Gulde, R., Fenner, K., Ruff, M., Singer, H. P., and Hollender, J. (2014) Identifying Small Molecules via High Resolution Mass Spectrometry: Communicating Confidence. *Environmental Science & Technology* **48**, 2097-2098

276. Lange, Y., Echevarria, F., and Steck, T. L. (1991) Movement of zymosterol, a precursor of cholesterol, among three membranes in human fibroblasts. *Journal of Biological Chemistry* **266**, 21439-21443

277. Jenkins, B., West, J., and Koulman, A. (2015) A Review of Odd-Chain Fatty Acid Metabolism and the Role of Pentadecanoic Acid (C15:0) and Heptadecanoic Acid (C17:0) in Health and Disease. *Molecules* **20**, 2425-2444

278. Cui, G., Stauffer, B. B., Imhoff, B. R., Rab, A., Hong, J. S., Sorscher, E. J., and McCarty, N. A. (2019) VX-770-mediated potentiation of numerous human CFTR disease mutants is influenced by phosphorylation level. *Scientific Reports* **9**

279. Andréll, J., and Tate, C. G. (2013) Overexpression of membrane proteins in mammalian cells for structural studies. *Molecular Membrane Biology* **30**, 52-63

280. Cheung, R. C. F., Wong, J. H., and Ng, T. B. (2012) Immobilized metal ion affinity chromatography: a review on its applications. *Applied Microbiology and Biotechnology* **96**, 1411-1420

281. Wood, D. W. (2014) New trends and affinity tag designs for recombinant protein purification. *Current Opinion in Structural Biology* **26**, 54-61

282. Blanksby, S. J., and Mitchell, T. W. (2010) Advances in Mass Spectrometry for Lipidomics. *Annual Review of Analytical Chemistry* **3**, 433-465